EPA U.S. Environmental Protection Agency
Office of Research and Development
Industrial Environmental Research Laboratory
Research Triangle Park, North Carolina 27711

EPA-600/7-78-009
January 1978

# PARTICULATE SAMPLING SUPPORT: 1977 Annual Report

Interagency
Energy-Environment
Research and Development
Program Report

## RESEARCH REPORTING SERIES

Research reports of the Office of Research and Development, U.S. Environmental Protection Agency, have been grouped into nine series. These nine broad categories were established to facilitate further development and application of environmental technology. Elimination of traditional grouping was consciously planned to foster technology transfer and a maximum interface in related fields. The nine series are:

1. Environmental Health Effects Research
2. Environmental Protection Technology
3. Ecological Research
4. Environmental Monitoring
5. Socioeconomic Environmental Studies
6. Scientific and Technical Assessment Reports (STAR)
7. Interagency Energy-Environment Research and Development
8. "Special" Reports
9. Miscellaneous Reports

This report has been assigned to the INTERAGENCY ENERGY-ENVIRONMENT RESEARCH AND DEVELOPMENT series. Reports in this series result from the effort funded under the 17-agency Federal Energy/Environment Research and Development Program. These studies relate to EPA's mission to protect the public health and welfare from adverse effects of pollutants associated with energy systems. The goal of the Program is to assure the rapid development of domestic energy supplies in an environmentally-compatible manner by providing the necessary environmental data and control technology. Investigations include analyses of the transport of energy-related pollutants and their health and ecological effects; assessments of, and development of, control technologies for energy systems; and integrated assessments of a wide range of energy-related environmental issues.

## EPA REVIEW NOTICE

This report has been reviewed by the participating Federal Agencies, and approved for publication. Approval does not signify that the contents necessarily reflect the views and policies of the Government, nor does mention of trade names or commercial products constitute endorsement or recommendation for use.

This document is available to the public through the National Technical Information Service, Springfield, Virginia 22161.

EPA-600/7-78-009
January 1978

# PARTICULATE SAMPLING SUPPORT: 1977 Annual Report

by

K.M. Cushing, William Farthing, L.G. Felix,
J.D. McCain, and W.B. Smith

Southern Research Institute
2000 Ninth Avenue, South
Birmingham, Alabama 35205

Contract No. 68-02-2131
Program Element No. EHE624

EPA Project Officer: D. Bruce Harris

Industrial Environmental Research Laboratory
Office of Energy, Minerals, and Industry
Research Triangle Park, N.C. 27711

Prepared for

U.S. ENVIRONMENTAL PROTECTION AGENCY
Office of Research and Development
Washington, D.C. 20460

TABLE OF CONTENTS


| | Page |
|---|---|
| Introduction | 1 |
| Executive Summary | 3 |
| Technical Summary | 9 |
| Task Category - Cascade Impactors | |
| Technical Directive No. 10101 - Cascade Impactor Computer Data Reduction | 9 |
| Technical Directive No. 10201 - HP-65/HP-25 Source Sampling Programs | 22 |
| Technical Directive No. 10301 - Non-Ideal Cascade Impactor Behavior | 24 |
| Technical Directive No. 10401 - Cascade Impactor Sampling of Charged Particles | 42 |
| Technical Directive No. 10501 - Cascade Impactor Substrate Media Study | 90 |
| Technical Directive No. 20101 - Calibration and Evaluation of Commercial Impactors | 94 |
| Technical Directive No. 20201 - Soviet Impactor-Cyclone Calibration | 115 |
| Task Category - Cyclones | |
| Technical Directive No. 10602 - Develop and Evaluate Five Stage Series Cyclone System | 124 |
| Technical Directive No. 20302 - Calibration of the Source Assessment Sampling System Cyclones | 128 |
| Technical Directive No. 20402 - Recalibration of the Three SASS Cyclones | 132 |
| Technical Directive No. 20502 - High Temperature Recalibration and Modification of SASS Cyclones | 138 |

Page

Technical Directive No. 21002 - Calibration of SASS Cyclones for HERL ..... 140

Task Category - E.S.P. Back-Up
Technical Directive No. 10703 - Develop an E.S.P. Back-Up for Sampling Systems ..... 151

Task Category - Guidelines, Manuals
Technical Directive No. 10804 - Guideline for Particulate Sampling and Annotated Bibliography. 153

Technical Directive No. 10904 - Technical Manual on Particulate Sampling ..... 153

Technical Directive No. 20604 - Procedures Manual for Electrostatic Precipitator Evaluation ..... 154

Task Category - Review of Documents
Technical Directive No. 20705 - Review Documents and Reports Furnished by EPA ..... 155

Task Category - Consulting Services
Technical Directive No. 20806 - Participate in U.S.A. - Soviet Information Exchange Program ... 156

Technical Directive No. 20906 - EPA/IERL/PMB Booth Exhibit at the 1977 APCA Meeting ..... 156

Task Category - Advanced Concepts - Mass and Size
Technical Directive No. 11007 - Evaluation of a PILLS IV Particle Sizing Instrument ..... 159

References ..... 160

## LIST OF FIGURES AND TABLES


| Figure No. | | Page |
|---|---|---|
| 1 | - Cumulative mass loading versus particle diameter for an individual impactor run..... | 11 |
| 2 | - Differential mass concentration (dM/dlogD) versus particle diameter..... | 12 |
| 3 | - Cumulative mass loading versus particle diameter for eight individual impactor runs made on the same source..... | 13 |
| 4 | - Differential mass concentration (dM/dlogD) versus particle diameter for eight individual impactor runs made on the same source..... | 14 |
| 5 | - Differential number concentration (dN/dlogD) versus particle diameter for eight individual impactor runs made on the same source..... | 15 |
| 6 | - Cumulative mass concentration versus particle diameter averaged for a set of runs..... | 16 |
| 7 | - Percent of mass concentration (cumulative percent) versus particle diameter averaged for a set of runs..... | 17 |
| 8 | - Differential mass concentration (dM/dlogD) versus particle diameter averaged for a set of runs..... | 18 |
| 9 | - Differential number concentration (dN/dlogD) versus particle diameter averaged for a set of runs..... | 19 |
| 10 | - Penetration-efficiency versus particle diameter for a number of inlet and outlet impactor runs at a particular control device..... | 20 |
| 11 | - Penetration-efficiency versus particle diameter for a number of inlet and outlet impactor runs at a particular control device..... | 21 |
| 12 | - HP-65 and HP-25 Programmable Calculator Source Measurement Booklets..... | 25 |

Figure No. Page


13 - Composite of calibration data for the Andersen impactor--stages 2 through 7..... 29

14 - An illustration of the four modeled stage collection efficiency curves of a typical stage of the Andersen impactor..... 30

15 - Recovered size distributions on a cumulative percentage basis from the Brink impactor models for σg = 2.0 and MMD's of 1.5, 4.5, 13.5, and 27 μm..... 32

16 - Recovered size distributions on a cumulative percentage basis from the Brink impactor models as shown in Figure 15 with the backup filter catches omitted from the analysis..... 33

17 - Recovered size distributions on a cumulative percentage basis from the Brink impactor models for σg = 3.0 and MMD's of 1.5, 4.5, 13.5 and 27 μm (backup filter included in the analysis).. 34

18 - Recovered size distributions on a cumulative percentage basis for the Andersen impactor for σg = 2.0 and MMD's of 1.5, 4.5, and 13.5 μm. 35

19 - Recovered size distributions on a differential basis from the Brink impactor models for MMD's of 4.5 and 27 μm and σg's of 2 and 3..... 37

20 - Recovered size distributions on a differential basis from the Andersen impactor models for MMD's of 1.5 and 13.5 μm and σg's of 2 and 3..... 38

21 - Charged particle generator orifice region with the parallel plates for charge measurement..... 45

22 - Schematic of the charged particle generator and sampling arrangement..... 46

23 - Particle Charge Versus Charging Voltage as Determined by Methods I-IV.

24 - Particle Charge Versus Charging Voltage..... 54

25 - Control sampling run using MRI-Model 1502 Impactor with no charge..... 56

Figure No. Page


26 - Sampling charged particles using MRI-Model 1502 Impactor with no grounding wire--high particle charge..... 57

27 - Sampling charged particles using MRI-Model 1502 Impactor with grounding wire--high particle charge..... 58

28 - Sampling charge-neutralized particles using MRI-Model 1502 Impactor with neutralizer at Nozzle - $n_p = 4 \times 10^4$..... 59

29 - Sampling charge-neutralized particles using MRI-Model 1502 Impactor with Nozzle Losses Corrected... 60

30 - Sampling charged particles using MRI-Model 1502 Impactor with grounding-wire moderate particle charge..... 61

31 - Sampling charge-neutralized particles using MRI-Model 1502 Impactor with neutralizer at Nozzle - $n_p = 2.4 \times 10^3$ ..... 62

32 - Sampling charged particles using MRI-Model 1502 Impactor with grounding wire - moderate particle charge..... 63

33 - Sampling charge-neutralized particles using U. of W. Mark III Impactor with charge neutralizer at Nozzle - $n_p = 4 \times 10^4$..... 64

34 - Sampling charged particles using U. of W. Mark III Impactor with no grounding wire - high particle charge..... 65

35 - Sampling charged particles using U. of W. Mark III Impactor with grounding wire - high particle charge..... 66

36 - Sampling charged particles using U. of W. Mark III Impactor with grounding wire - moderate particle charge..... 67

37 - Sampling charge - neutralized particles using Andersen Mark III Stack Sampler with neutralizer at Nozzle - $n_p = 7 \times 10^3$..... 68

Figure No. Page


38 - Sampling charged particles using Andersen Mark III Stack Sampler with grounding wire - moderate particle charge..... 69

39 - Sampling charged particles using Andersen Mark III Stack Sampler with grounding wire - moderate particle charge..... 70

40 - Photographs of deposition patterns of ammonium fluorescein particles in MRI-Model 1502 Impactor.... 74

41 - Photographs of deposition patterns of ammonium fluorescein particles in MRI-Model 1502 Impactor.... 75

42 - Photographs of deposition patterns of ammonium fluorescein particles in Andersen Mark III Stack Sampler..... 76

43 - Photographs of deposition patterns of ammonium fluorescein particles in Andersen Mark III Stack Sampler..... 77

44 - Photographs of deposition patterns of ammonium fluorescein particles in Andersen Mark III Stack Sampler..... 78

45 - Sampling charged particles using MRI-Model 1502 Impactor with plexiglass jet plates, 2J, 3J, and 4J..... 79

46 - Reference curve (solid) giving collection efficiency as a function of $\sqrt{\psi}$ for the Andersen Stack Sampler and neutral particles..... 81

47 - Efficiency versus $\sqrt{\psi}$ of stages in Andersen Stack Sampler for neutral particles (solid curve) and moderately charged particles (dashed curve)..... 83

48 - Reference curve (solid) giving collection efficiency as a function of $\sqrt{\psi}$ for the MRI-Model 1502 Impactor and neutral particles..... 84

49 - Efficiency versus $\sqrt{\psi}$ of stages in MRI-Model 1502 Impactor for neutral (solid curve), moderately charged (dashed curve), and highly charged particles..... 85

Figure No. Page


50 - Reference curve (solid) giving collection efficiency as a function of the $\sqrt{\psi}$ for the U. of W. Mark III Impactor and neutral particles..... 86

51 - Efficiency versus $\sqrt{\psi}$ of stages in the U. of W. Mark III Impactor for neutral (solid curve), moderately charged (dashed curve), and highly charged particles..... 87

52 - Flow chart for acid wash treatment of glass fiber filter material..... 95

53 - Theoretical impactor efficiency curves for rectangular and round impactors showing the effect of jet-to-plate distance S, Reynolds number Re, and throat length T..... 100

54 - Schematic representation of the Vibrating Orifice Aerosol Generator..... 101

55 - PSL calibration system for high and low flowrate impactor..... 103

56 - Total wall loss vs. Particle diameter..... 105

57 - Collection efficiency vs. $\sqrt{\psi}$ . Andersen Mark III Stack Sampler with glass fiber collection substrates..... 106

58 - Collection efficiency vs. $\sqrt{\psi}$ . Brink Model BMS-11 Cascade Impactor with glass fiber collection substrates..... 107

59 - Collection efficiency vs. $\sqrt{\psi}$ . Brink Model BMS-11 Cascade Impactor with greased collection plates..... 108

60 - Collection efficiency vs. $\sqrt{\psi}$ . MRI Model 1502 Inertial Cascade Impactor with greased collection plates..... 109

61 - Collection efficiency vs. $\sqrt{\psi}$ . Sierra Model 226 Source Cascade Impactor with glass fiber collection substrates..... 110

62 - Collection efficiency vs. $\sqrt{\psi}$ . Sierra Model 226 Source Cascade Impactor with glass fiber collection substrates..... 111

Figure No. Page


63 - Collection efficiency vs. $\sqrt{\psi}$ . University of Washington Mark III Source Test Cascade Impactor with greased collection plates..... 112

64 - Soviet 14-Stage Cascade Impactor..... 116

65 - Soviet 3-Stage Impactor/Cyclone..... 116

66 - Collection efficiency vs. Particle diameter. Soviet 3-Stage Impactor/Cyclone..... 118

67 - Collection efficiency vs. Particle diameter. Soviet 12-Stage Cascade Impactor. Data shown for the first nine stages from 2-20 microns... 119

68 - Collection efficiency vs. Particle diameter. Soviet 12-Stage Cascade Impactor. Data shown in combined form in the configuration for field measurements..... 120

69 - Collection efficiency vs. Particle diameter. Soviet 14-Stage Cascade Impactor (Small Cut-points)..... 122

70 - Collection efficiency vs. Particle diameter. Soviet 14-Stage Cascade Impactor (Large Cut-points)..... 123

71 - Five Stage Series Cyclone System..... 125

72 - Laboratory calibration for the Five Stage Series Cyclone System..... 126

73 - Collection efficiency vs. Particle diameter. Large SASS Cyclone..... 129

74 - Collection efficiency vs. Particle diameter. Middle SASS Cyclone..... 130

75 - Collection efficiency vs. Particle diameter. Small SASS Cyclone..... 131

76 - SASS cyclone cut points..... 133

77 - Collection efficiency vs. Particle diameter. Large SASS Cyclone..... 135

78 - Collection efficiency vs. Particle diameter. Unmodified Middle SASS Cyclone..... 136

79 - Collection efficiency vs. Particle diameter. Modified Middle SASS Cyclone..... 137

Figure No. Page


80 - Collection Efficiency - Temperature Relationship..... 142

81 - $D_{50}$ -Viscosity Relationship..... 143

82 - Collection Efficiency - Particle Density Relationship..... 144

83 - Collection Efficiency at 400°F, 4 SCFM..... 145

84 - Exxon SASS Cyclones..... 148

85 - A sketch of the electrostatic precipitator design..... 152


Table No.


1 - Tentative Project Schedule, Contract No. 68-02-2131..... 4

2 - Outputs From Scheduled Tasks, Contract No. 68-02-2131..... 8

3 - Simulation Conditions of the Modeled Impactor Performance..... 27

4 - Percent Errors in $\Delta M/\Delta \log D$, Andersen Impactor..... 39

5 - Percent Errors in $\Delta M/\Delta \log D$, Brink Impactor..... 40

6 - Percentage of Trial Cases in Which Recovered Value of ($\Delta M/\Delta \log D$) is Within the Indicated Factor of the True Value..... 41

7 - Average Values and Standard Deviations of Charging Parameters Observed by Reischl, et al[12]..... 48

8 - Grouping of Surfaces for the Efficiency of Each Stage..... 88

9 - Cascade Impactor Calibration Study--Operational Parameters..... 97

Table No. Page

10 - Laboratory Calibration of the Five Stage Series Cyclones - Values of $D_{50}$ cut points (in micrometers) for various conditions of sample flow, temperature, and particle density..... 127

11 - Five-Stage Cyclone Calibration Data..... 141

# INTRODUCTION

The scope of the research, development, and support to be done for the EPA under this contract encompasses every aspect of particulate sampling in gaseous process and effluent streams. Specific objectives which have been identified and given priority in the technical work plan are:

1. Identify current and future requirements for particulate sampling - the nature of the particles (shape, volatility, concentration, size distribution, charge, etc.), the sampling conditions (temperature, pressure, entrained fluids, etc.), and the goals of the sampling programs (control device evaluation, health effects, etc.).

2. Design prototype high and low flow rate impactors which incorporate all that we have learned about their fundamental behavior and operational problems. Continue research on the non-ideal or unmodelled behavior of impactors. Investigate problems in using impactors on nonroutine process streams (wet, hot, high pressure).

3. Evaluate cyclone systems for particle sizing. Develop a theory for calculating cyclone $D_{50}$'s at stack conditions. Consider alternatives to filter backups on high flow rate systems.

4. Study alternatives to impactors and cyclones for particle sizing. Possibilities are optical, electrical, or hybrid systems. Concentrate on devices which offer the possibility of real time, automatic, sampling and analysis.

5. Study and evaluate mass monitors. Again the emphasis should be on new systems with high flow rates or automatic features.

6. Study methods of Quality Assurance in sampling and calibration programs.

7. Generate and review documents on particulate sampling and continually update our bibliography and literature survey.

8. Continue to study and evaluate new ideas, techniques, and instruments for particulate sampling.

9. Attend and organize meetings and symposia on particulate sampling.

10. Provide consulting and support to EPA programs.

Considerable progress has been made in research related to inertial particle sizing techniques, and less emphasis will be placed on the development and operation of such devices after the current tasks have been completed. An exception will be the special problems of sampling with inertial devices in high temperature, high pressure process streams.

A second area of special interest is the development of an advanced technique (perhaps optical) to obtain particle size information in real time. We are starting now to develop the necessary background to initiate a research program to develop or improve instruments for real-time, instack sampling.

There are two main sections in the remainder of this report. The Executive Summary is a review of the work accomplished to date, and also outlines our projected schedule for the remainder of the contract. The Technical Summary contains a description of the Technical Directives issued to date under this contract. The scope of work for each task is presented, followed by a summary of the work accomplished to date on each task.

## EXECUTIVE SUMMARY

Under this Term Level of Effort contract, Southern Research Institute is working toward the completion of several relatively small tasks, generally less than 2000 man-hours, rather than one single goal encompassing the total number of contracted man-hours. The Project Officer at his discretion issues Technical Directives which specify the scope of the tasks to be performed and the level of effort. The current tasks are grouped under eight Task Categories. These categories are indicated in Table I, the Tentative Project Schedule, which outlines our areas of research and the status of each task. Our projected schedule for some future tasks is also shown.

Through the end of June, twenty Technical Directives had been issued; twelve tasks have been completed, and eight tasks are still in progress. Of these twenty tasks, seven come under the Task Category of Cascade Impactors, five under Cyclones, one under E.S.P. Back-Up, three under Guidelines and Manuals, one under Review of Documents, two under Consulting Services, and one under Advanced Concepts - Mass and Size. Tasks numbers beginning with a 1 (10000) are categorized as research and development projects, and those beginning with a 2 (20000) are categorized as support service projects. At present the 20 Technical Directives are split evenly between these two categories. A brief Status Report on each task is given below.

### Task Category - Cascade Impactors

Cascade Impactor Computer Data Reduction (10101) - This task is still active. A report including computer program listings will be issued in several months. It will be applicable to the Andersen Mark III, Brink, MRI Model 1502, and University of Washington Mark III cascade impactors.

HP-65, HP-25 Calculator Programs For Source Sampling (10201) - This task has been completed. Two reports have been issued, each containing twenty-two programs to facilitate source sampling measurement calculations: "HP-65 Programmable Pocket Calculator Applied To Air Pollution Measurement Studies: Stationary Sources," EPA-600/8-76-002 (October 1976), and "HP-25 Programmable Pocket Calculator Applied To Air Pollution Measurement Studies: Stationary Sources," EPA-600/7-77-058 (June 1977).

Non-Ideal Cascade Impactor Behavior (10301) - This task has been completed. Non-ideal behavior of both the Andersen Mark III and Brink impactors was studied. The results were presented at the 1977 APCA Meeting in Toronto, Canada.

*Table 1. Tentative Project Schedule, Contract No. 68-02-2131*

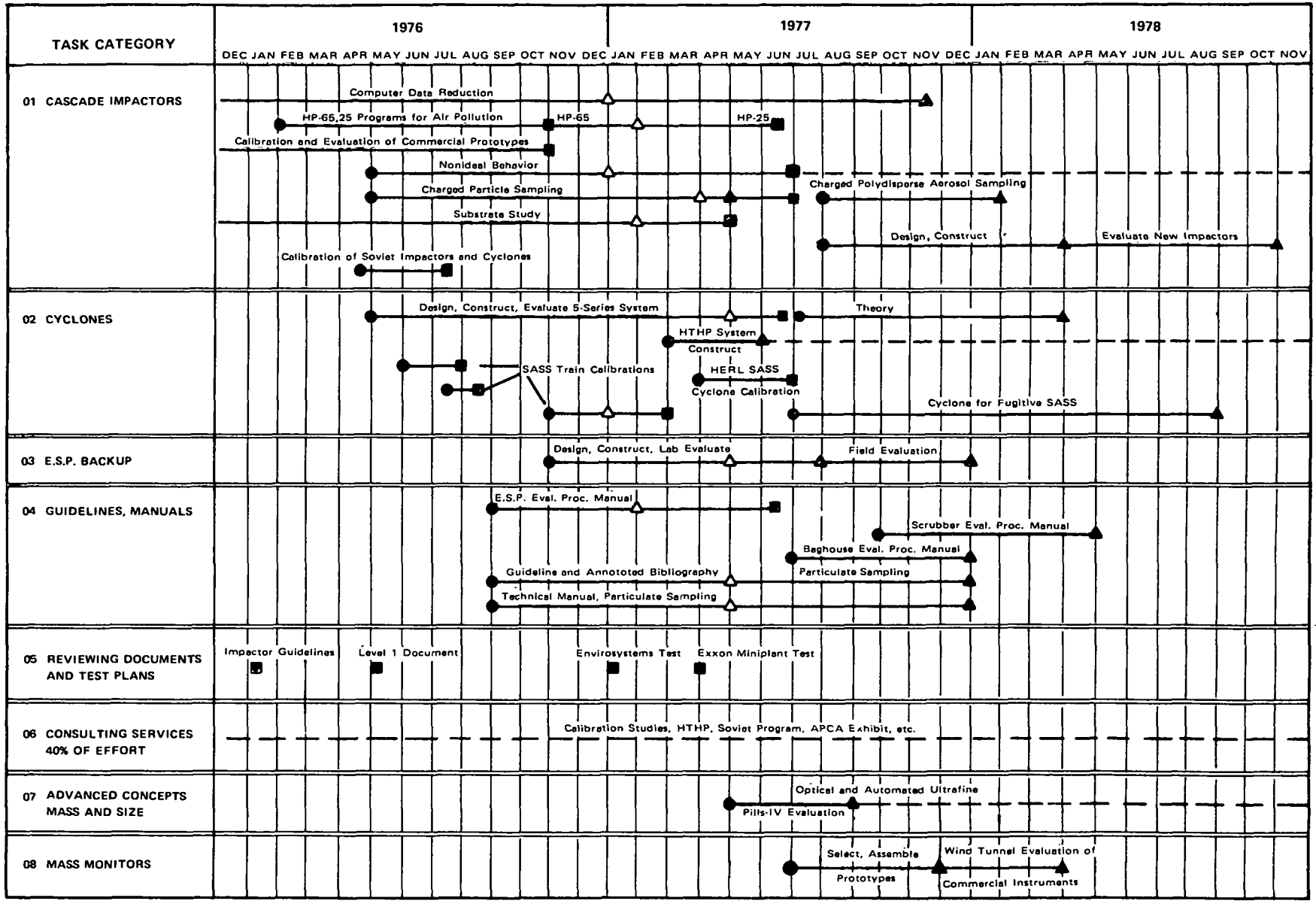


KEY: ● TASK INITIATED, △ ESTIMATED COMPLETION DATE, ▲ LATEST ESTIMATE, ■ TASK COMPLETED
— — — LIKELY CONTINUATION

Cascade Impactor Sampling of Charged Particles (10401) - This task is still active. A final report is being written which describes the results of sampling two and five micrometer diameter particles charged to levels near and much greater than those normally found in electrostatic precipitation control devices.

Cascade Impactor Substrate Media Study (10501) - This task has been completed. A final report has been published which presents the results of a laboratory and field evaluation of over twenty greases and six types of glass fiber substrate media. The title of this report is "Inertial Cascade Impactor Substrate Media For Flue Gas Sampling," EPA-600/7-77-060 (June 1977).

Calibration and Evaluation of Commercial Impactors (20101) - This task has been completed. A report has been written discussing the calibration of the Andersen Mark III, Brink, MRI Model 1502, Sierra Model 226, and University of Washington Mark III Cascade Impactors. This document is entitled "Particulate Sizing Techniques For Control Device Evaluation: Cascade Impactor Calibrations," EPA-600/2-76-280 (October 1976).

Soviet Impactor-Cyclone Calibrations (20201) - This task has been completed. Using monodisperse aerosols, two 14-stage, multiple hole, Soviet impactors, one twelve-stage Soviet impactor, and one three-stage Soviet impactor-cyclone were calibrated.

## Task Category - Cyclones

Develop and Evaluate Five-Stage Series Cyclone (10602) - This task is still active. A final report is being written. It will describe the design and development of this cyclone system, as well as the results of calibration at several combinations of flow rate, particle density, and gas stream temperature.

Calibration of the Aerotherm SASS Cyclones (20302) - This task has been completed. The three SASS cyclones were calibrated at 4 ACFM and 3 ACFM using ammonium fluorescein and polystyrene latex particles under laboratory conditions.

Recalibration of Aerotherm SASS Cyclones (20402) - This task has been completed. The three SASS cyclones were calibrated at 400°F and 4 SCFM. The results were not acceptable due to problems with the physical integrity of the calibration aerosol.

High Temperature Recalibration and Modification of the SASS Cyclones (20502) - This task has been completed. Using a new calibration aerosol, the "three micrometer" cut point SASS cyclone was calibrated at 400°F and 4 SCFM. A modification was made to obtain a $D_{50}$ closer to 3 micrometers.

Exxon-SASS Cyclone Calibration (21002) - This task has been completed. The middle ("three micrometer") cyclone of the Source Assessment Sampling System used by Exxon Research Laboratory at a coal-fired power plant in Kentucky was calibrated at 450°F and 13 ACFM.

Task Category - E.S.P. Back-up

Develop ESP Back-Up To Replace Conventional Filter (10703) - This task is still active. Under this task an electrostatic precipitator is being designed to replace the normal glass fiber back up filters in high volume sampling systems. The prototype is currently being evaluated.

Task Category - Guidelines and Manuals

Generate a Guideline Report and Annotated Bibliography on Particulate Sampling (10804) - This task is still active. This guideline document will be a concise survey of the methods and instruments used in sampling effluent gaseous process streams for particulate matter.

Technical Manual on Particulate Sampling Instrumentation and Techniques (10904) - This task is still active. This comprehensive document will be a technical survey of the methods and instruments used in sampling effluent gaseous process streams for particulate matter.

Procedures Manual For ESP Evaluation (20604) - This task has been completed. A report has been published which describes the methods and instrumentation necessary to completely evaluate the performance of an electrostatic precipitator. Topics discussed include ESP operation, mass sampling, particle sizing, resistivity measurements, gas analysis, and test plan development. The title of this report is "Procedures Manual For Electrostatic Precipitator Evaluation," EPA-600/2-77-059 (June 1977).

Task Category - Review of Documents

Review Documents Furnished by EPA (20705) - This task has been completed. Under this task the IERL/PMB Cascade Impactor Guidelines, the TRW Level 1 Assessment Report, and the GCA Sampling Protocol To Minimize Errors were reviewed and comments sent to the Project Officer.

Task Category - Consulting Services

USA-Soviet Information Exchange Program (20806) - This task has been completed. Sampling equipment and personnel were sent to the Soviet Union to participate in tests at a scrubber on a metallurgical process plant.

EPA/IERL 1977 APCA Exhibit Booth (20906) - This task has been completed. Southern Research coordinated the planning for an exhibit booth at the 1977 APCA meeting in Toronto, Canada. Four thousand EPA sponsored research publications were distributed and several pieces of hardware were displayed.

Task Category - Advanced Concepts (Mass and Size)

Evaluation of the PILLS-IV (11007) - This task is still active. Under this task a complete detailed evaluation of the theory and operation of the PILLS-IV particle sizing instrument will be performed.

Several new topics for research and development and support services are tentatively scheduled during the latter part of 1977. These include (1) Procedures Manual For Fabric Filter Evaluation, (2) Evaluation of Commercial and Prototype Mass Monitors, (3) 1978 Particulate Sampling Technology Symposium; and (4) Cyclone For Fugitive Assessment Sampling Train.

Specific outputs from the tasks issued to date are shown in Table II.

*Table II. Outputs From Scheduled Tasks, Contract No. 68-02-2131*

| | |
|---|---|
| **01-CASCADE IMPACTORS** | |
| Computer Data Reduction | Program Report, November, 1977. |
| HP-65, 25 Programs | Handbooks, June, 1977. |
| Non-ideal Impactor Behavior | Paper, APCA, June, 1977<br>Paper, Env. Sci. & Tech., April, 1978 |
| Charged Particle Sampling | Special Report, Recommendations, Oct. 1977.<br>(Also input to Non-ideal Model) |
| Substrate Study | Substrate Report, June, 1977. |
| Design, Construct, Evaluate New Impactors. | Prototypes, Drawings, May, 1978.<br>Report on Evaluation, June, 1978. |
| **02-CYCLONES** | |
| Develop and Evaluate 5-series System. | Prototype, Evaluation, June, 1977.<br>Better Theory, March, 1978. |
| Develop and Evaluate HTHP System | Prototype, June, 1977.<br>Continuing Evaluation. |
| **03-E.S.P. BACKUP** | Prototype, Theoretical Analysis, Calibration, December, 1977. |
| **04-GUIDELINES AND MANUALS** | E.S.P. Evaluation Procedures Manual, June, 1977.<br>Baghouse Evaluation Procedures Manual, December, 1977,<br>Guidelines and Annotated Bibliography on Particle Sampling, December, 1977.<br>Technical Manual on Particulate Sampling, December, 1977. |
| **06-CONSULTING SERVICES** | |
| APCA Exhibit, Prototype Evaluation | Information Transfer, June, 1977. |
| KLD | Special Reports, Suggestions |
| TRW | |
| HTHP | Procedures Manuals, Improved Theory. |
| SYMPOSIUM | May, 1978. |
| **07-ADVANCED SYSTEMS-MASS AND SIZE** | |
| **OPTICAL SYSTEMS** | Review of State-of-Art, Recommendations, 1977.<br>Periodic reports of laboratory research. |
| | Evaluation of PILLS--IV, October, 1977. |
| Automated System and Data Analysis (0.01-2.0 μm) | Schedule at Project Officer Discretion.<br>No sooner than December, 1977. |
| **08-MASS MONITORS** | Special Report on Evaluation-Comparison April, 1978. |

## TECHNICAL SUMMARY

In this section a detailed report on work accomplished under each task is presented. The twenty tasks are organized according to the seven task categories.

### Task Category - Cascade Impactors

### Cascade Impactor Computer Data Reduction (Technical Directive Number 10101)

Description of Task:

The purpose of this task is to improve the accuracy and efficiency of cascade impactor data reduction. This will be accomplished in four parts.

1. A computer program will be written to calculate all of the necessary variables (gas viscosity, particle mean free path, slip correction factors, etc.) in order to obtain cascade impactor cut points. Also this program will be able to incorporate calibration constants for each impactor stage. Initially, this program will be written for the Andersen Mark III, the Brink, the MRI Model 1502, and the University of Washington Mark III impactors.

2. A curve fitting routine will be developed which can be used to fit the experimental data from individual impactor runs.

3. A statistical routine will be written to manipulate the fitted curves and to calculate differential size distributions and fractional efficiency curves, all with confidence limits.

4. A final report will be written documenting the entire program.

Summary of Progress:

Parts 1, 2, and 3 are complete. A series of computer programs have been written which constitute a cascade impactor data

reduction package. These programs calculate stage cut points, cumulative mass distributions and differential mass and number size distributions (dM/dlogD and dN/dlogD). A modified spline curve fitting procedure is incorporated into this particle-size package so that individual cumulative mass distributions can be fitted and groups of impactor run data averaged. Inlet and outlet distributions for particulate control devices are used to calculate fractional efficiency and penetration curves with 50 or 90 percent confidence intervals. Graphs which can be produced by the computer and plotter include cumulative mass vs. particle size, dM/dlogD, dN/dlogD and fractional efficiency-penetration curves. The efficiency-penetration curves can be plotted on log-log or log probability axes.

Figures 1 through 11 illustrate most of the various graphical outputs which the impactor computer data reduction program provides. All data are plotted with particle diameter in micrometers as the abscissa. Data can be reduced and graphed versus Stokes diameter or aerodynamic particle diameter. All the following figures show Stokes diameter.

Figures 1 and 2 show data for a single impactor run. Figure 1 is a cumulative mass loading plot and Figure 2 is the derivative with respect to log (particle diameter) of the cumulative mass loading curve, the dM/dlogD plot. Data, derived manually from impactor stage weights, are shown along with results from the computer generated curve fit. In Figure 1 the curve fit is drawn as a solid curve and in Figure 2 the derivative of this fit with respect to log (particle diameter) is plotted as an x where calculated.

Figures 3 through 5 are computer graphs where the data for eight individual impactor runs are plotted on each graph. Each run is identified by a particular plotting symbol. Scatter in the data can be clearly seen. Cumulative mass loading, dM/dlogD and dN/dlogD (differential number concentration) data are shown. No curve fits are drawn.

Figures 6 through 11 show typical results for several impactor runs which have been averaged together with outliers identified and discarded. Such data as these rely on curve fits to make such averaging possible. Fifty percent confidence intervals are shown. Figures 6 through 9 show cumulative mass loading, cumulative percent, dM/dlogD, and dN/dlogD averaged results, respectively. Figures 10 and 11 are penetration-efficiency curves (for a fictitious control device) which may be presented in two formats, a log probability grid or a log-log grid.

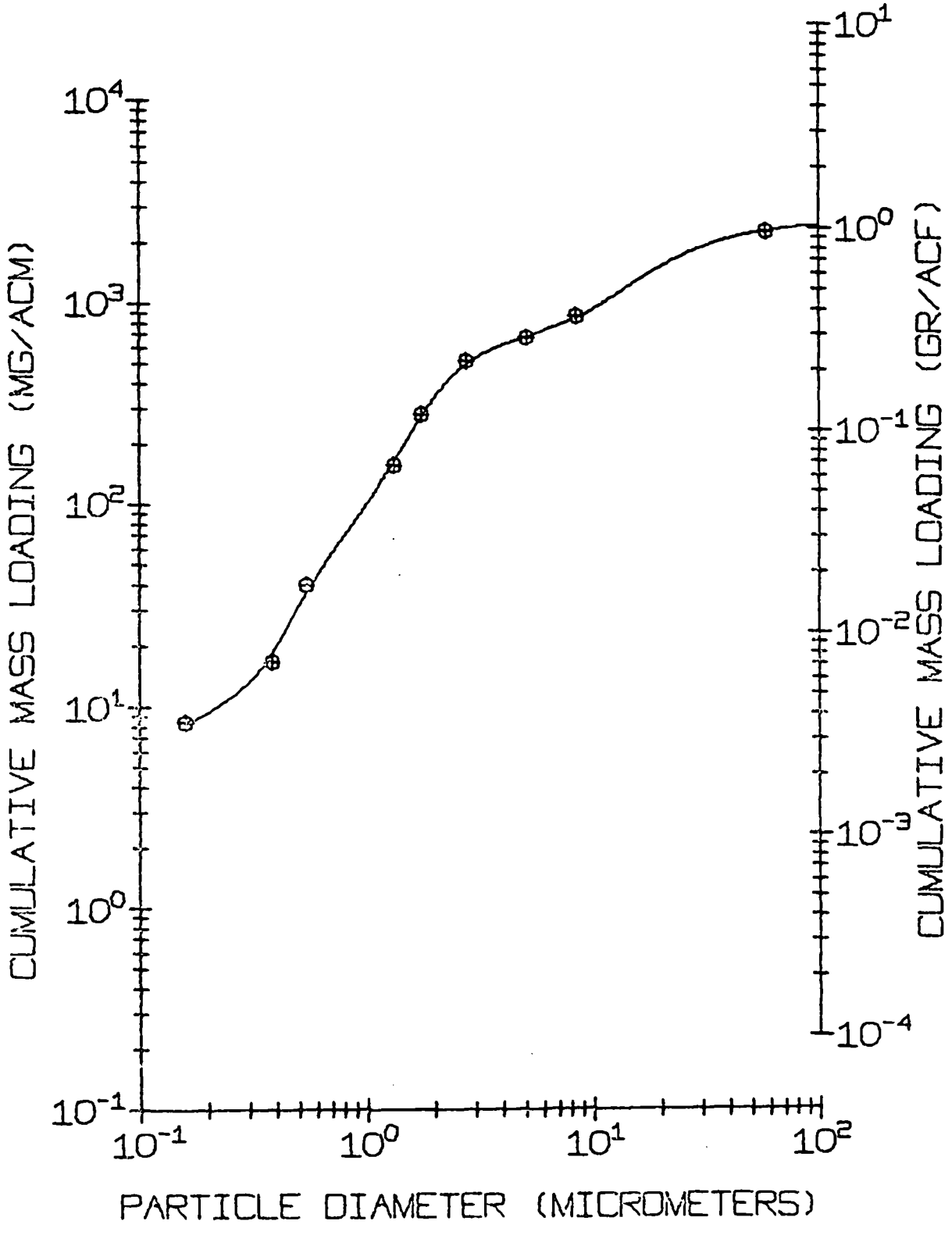


*Figure 1. Cumulative mass loading versus particle diameter for an individual impactor run. Data generated from stage weights are shown as circles with crosses. The computer generated curve fit is shown as a solid curve.*

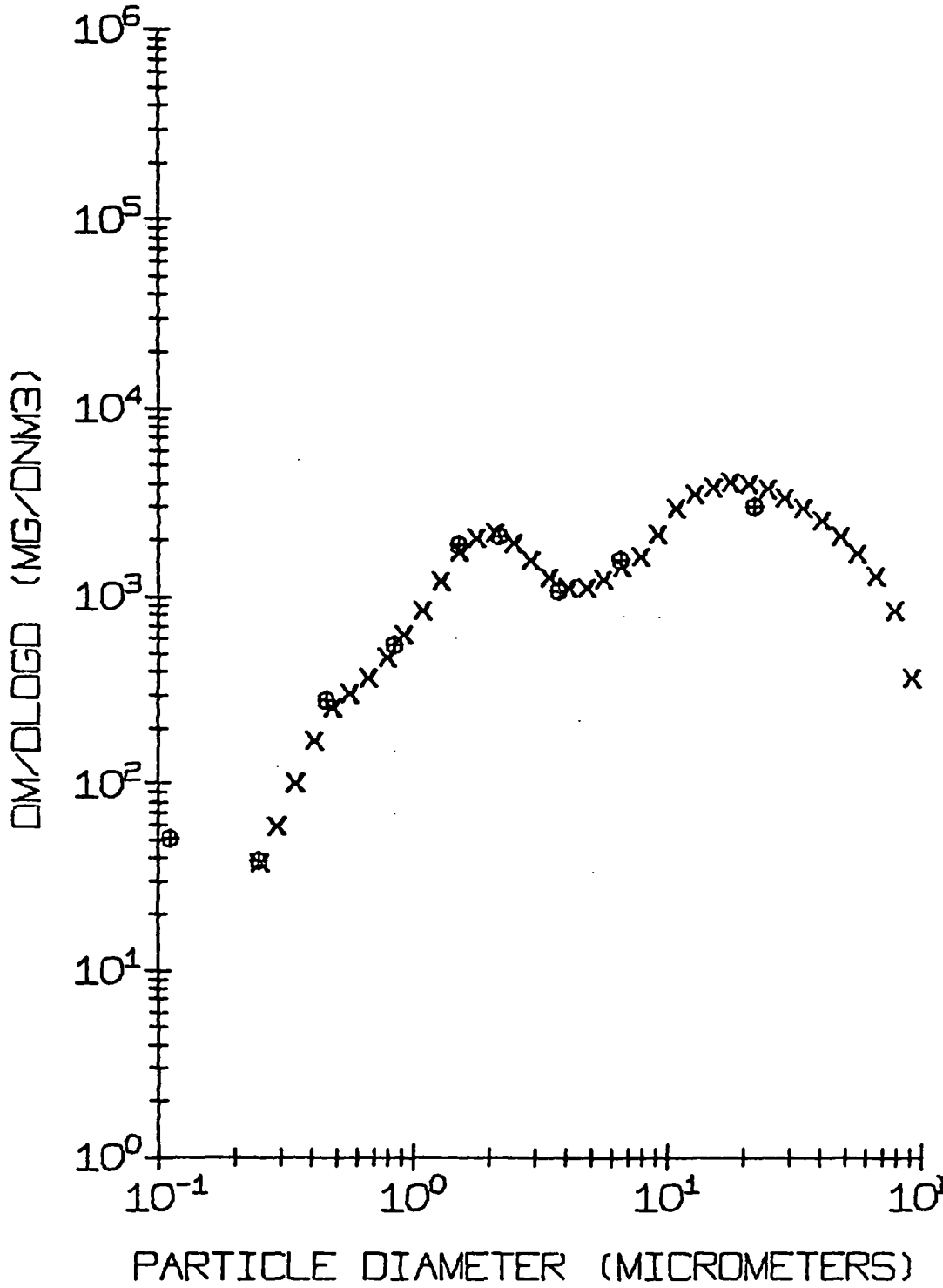


*Figure 2. Differential mass concentration(dM/dlogD) versus particle diameter. Data generated from stage weights are shown as circles with crosses. The derivative with respect to log(particle diameter) of the curve fit to the cumulative mass concentration(Figure 1.) is plotted with an X where calculated.*

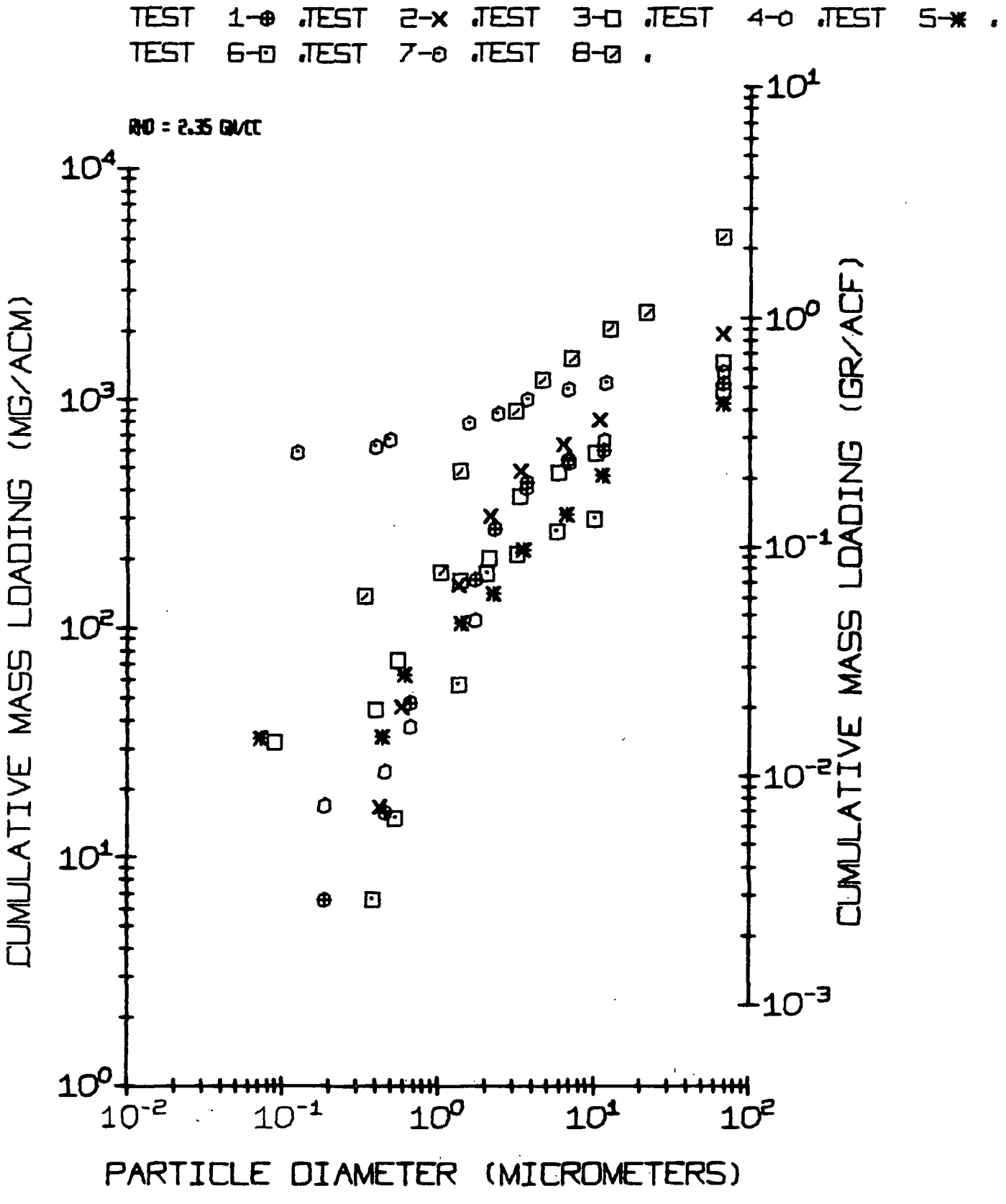


*Figure 3. Cumulative mass loading versus particle diameter for eight individual impactor runs made on the same source. Only data derived from individual stage weights are shown.*

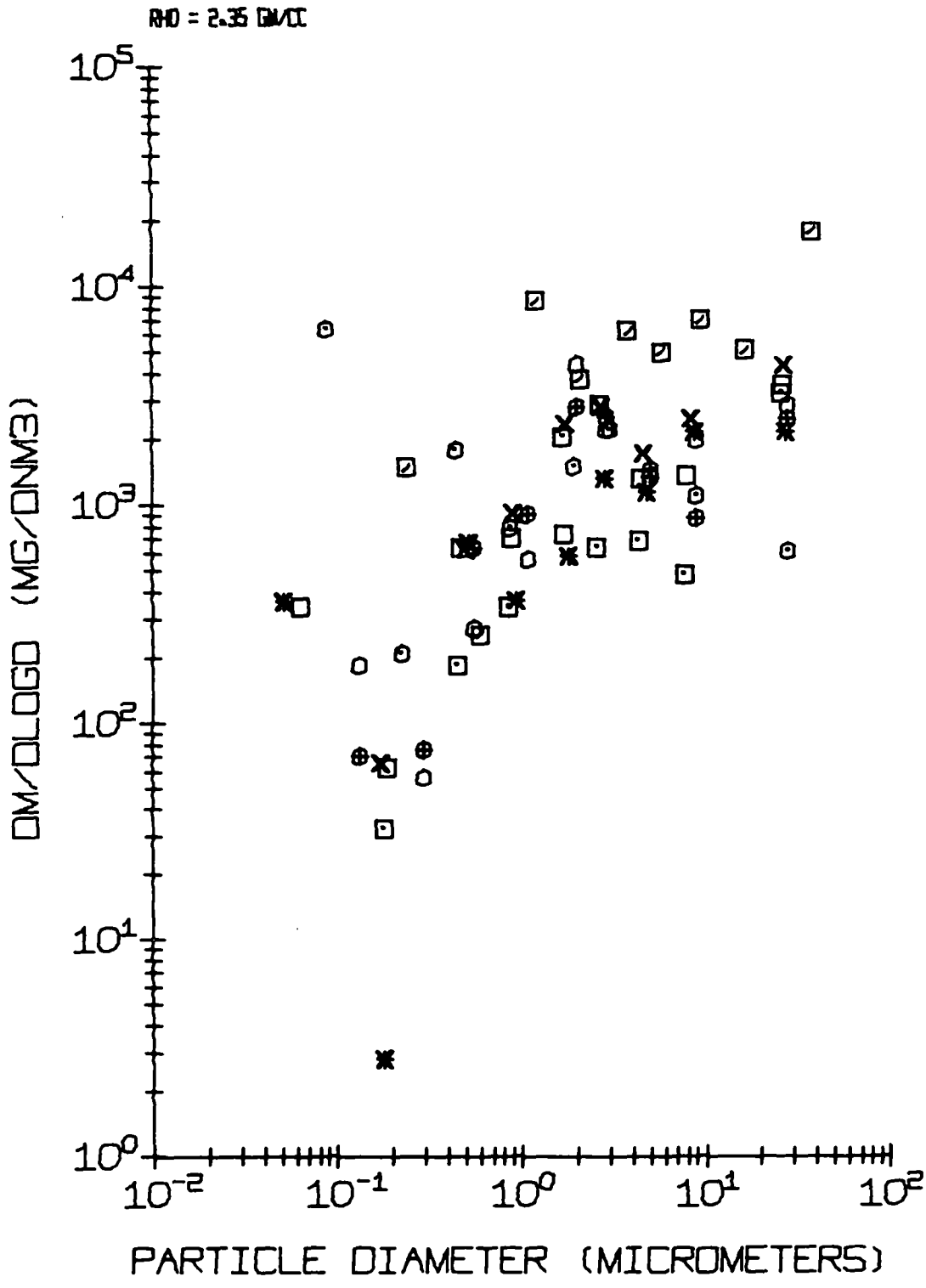


*Figure 4. Differential mass concentration(dM/dlogD) versus particle diameter for eight individual impactor runs made on the same source. Only data derived from individual stage weights are shown.*

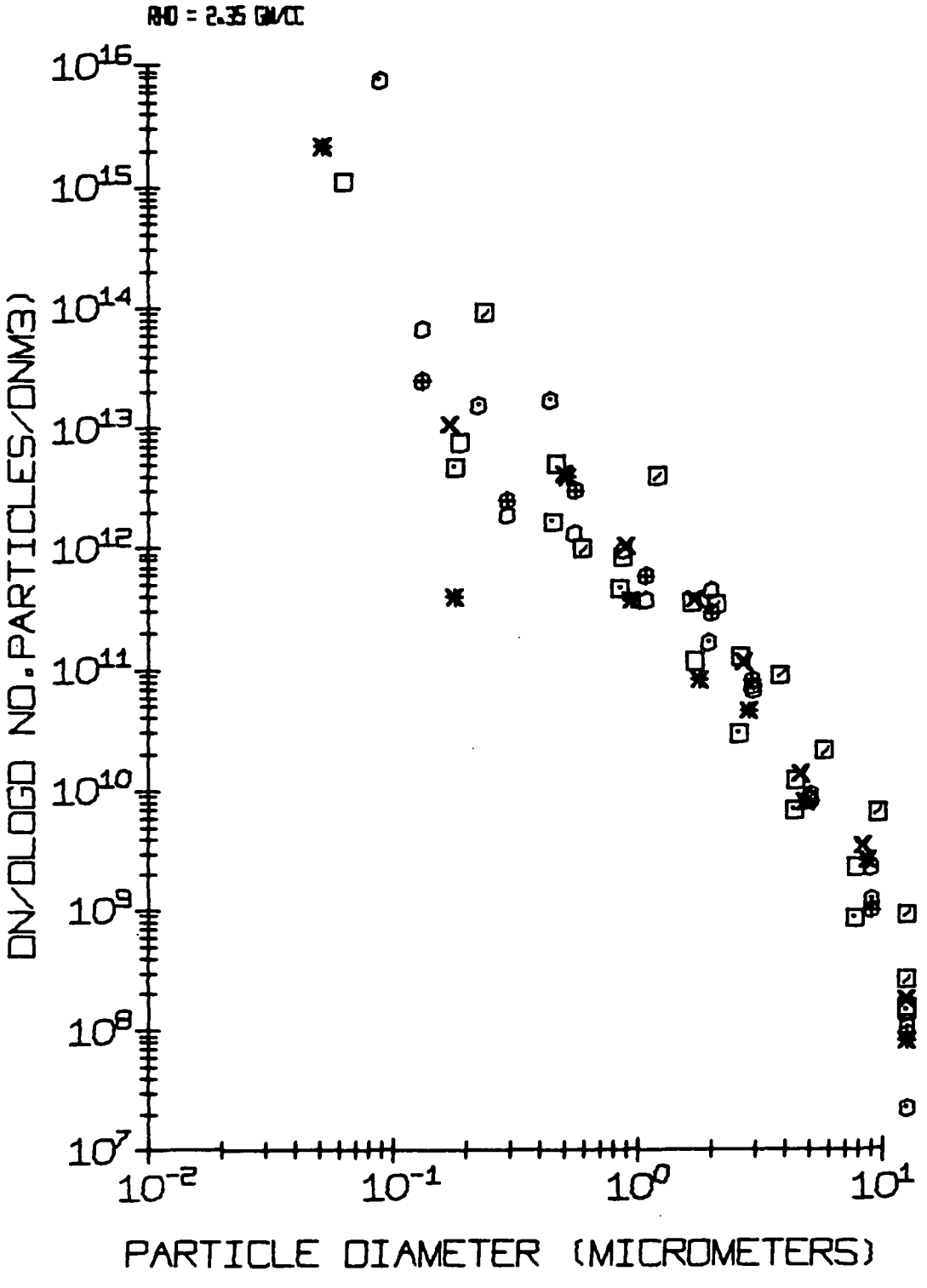


*Figure 5. Differential number concentration(dN/dlogD) versus particle diameter for eight individual impactor runs made on the same source. Only data derived from individual stage weights are shown.*

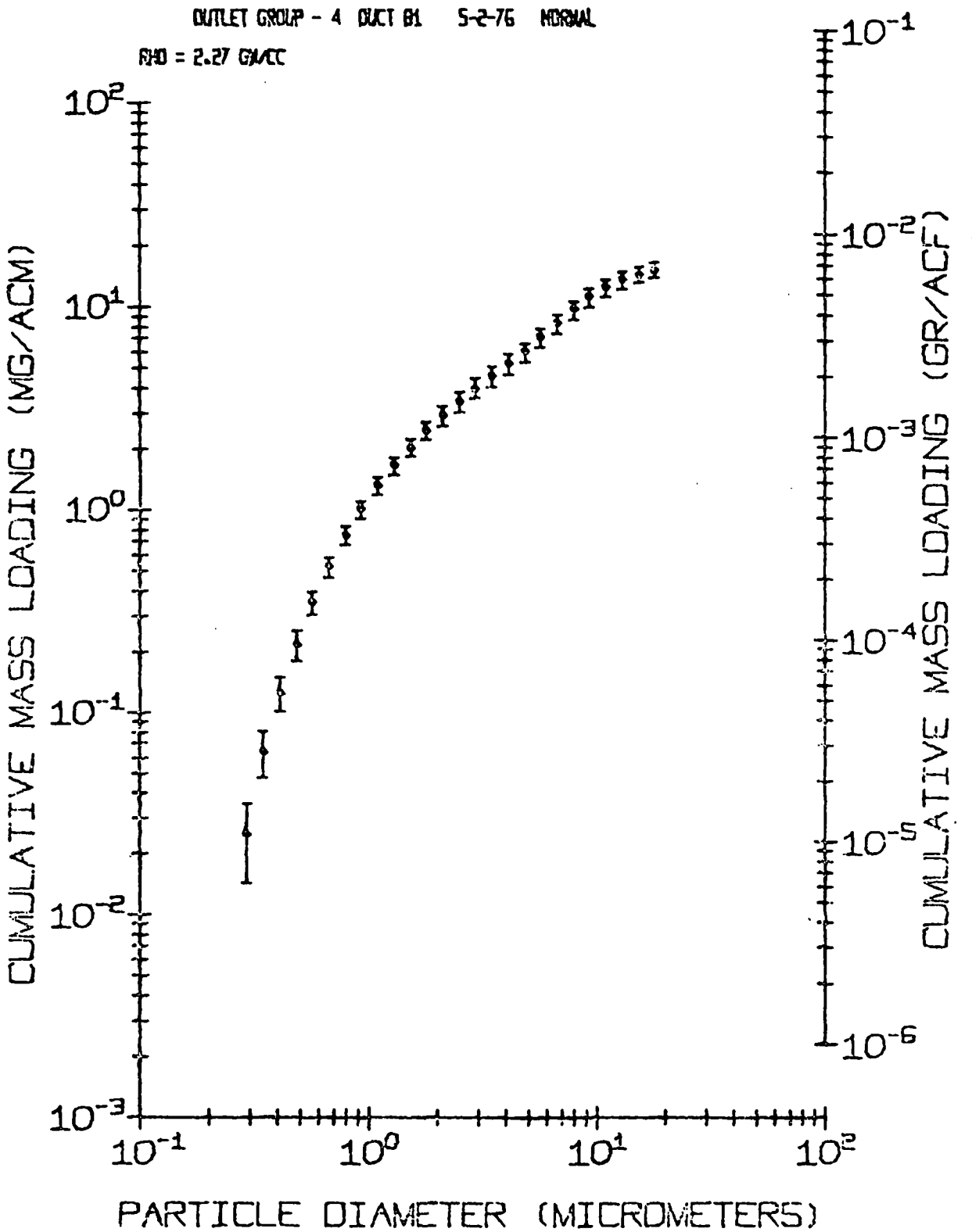


*Figure 6. Cumulative mass concentration versus particle diameter averaged for a set of runs. Fifty percent confidence intervals are shown.*

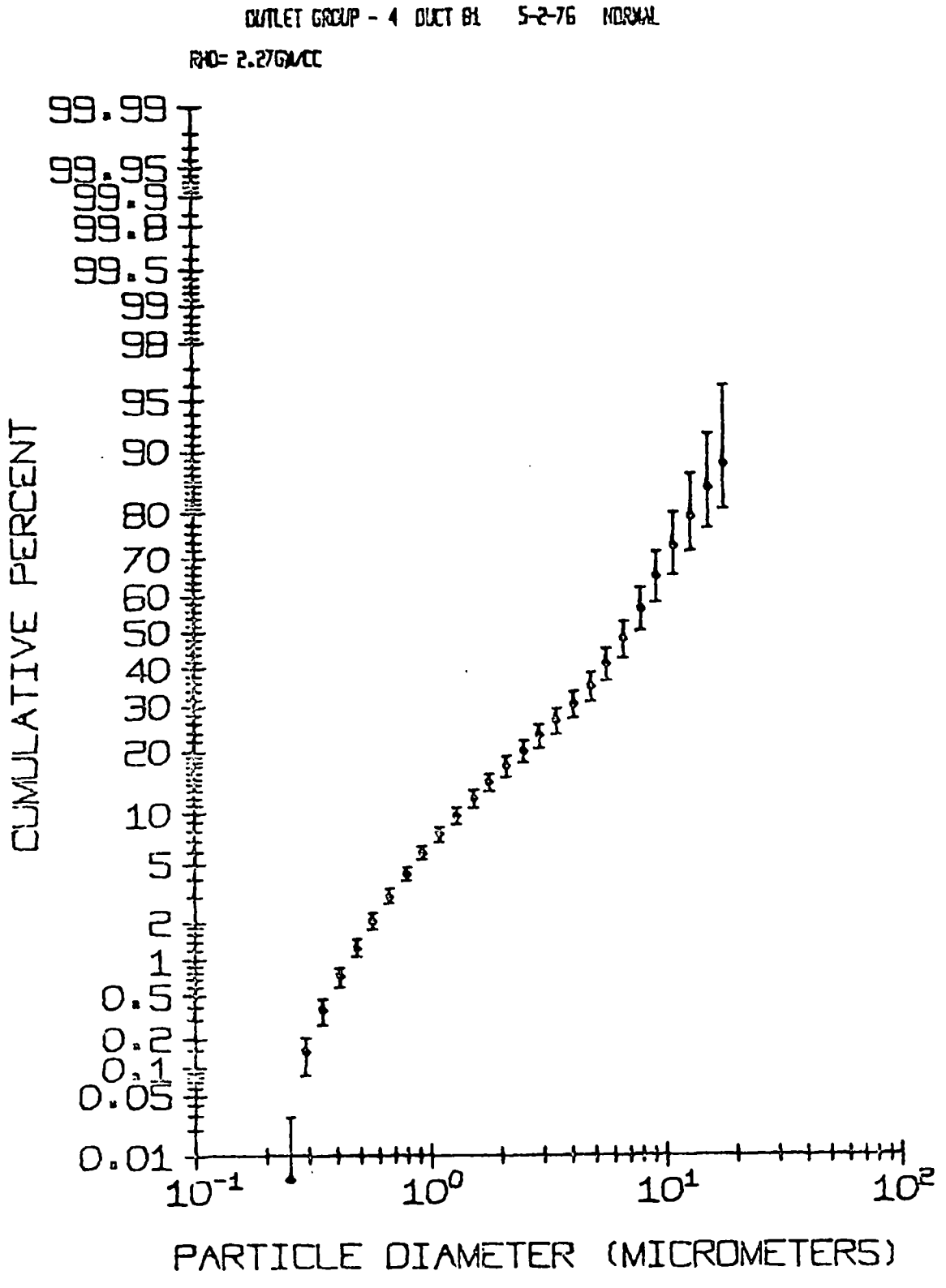


*Figure 7. Percent of mass concentration(cumulative percent) versus particle diameter averaged for a set of runs. Fifty percent confidence intervals are shown.*

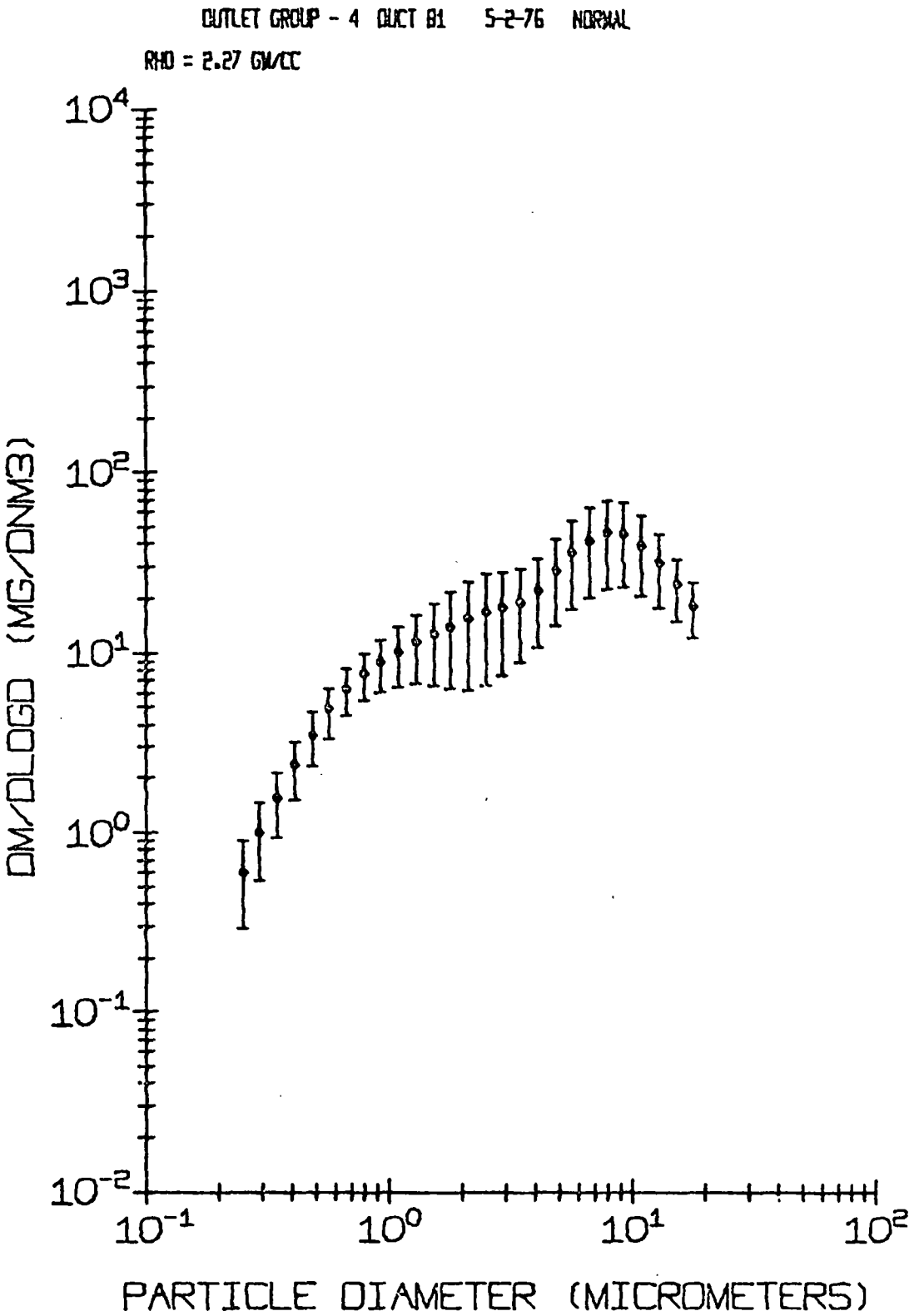


*Figure 8. Differential mass concentration(dM/dlogD) versus particle diameter averaged for a set of runs. Fifty percent confidence intervals are shown.*

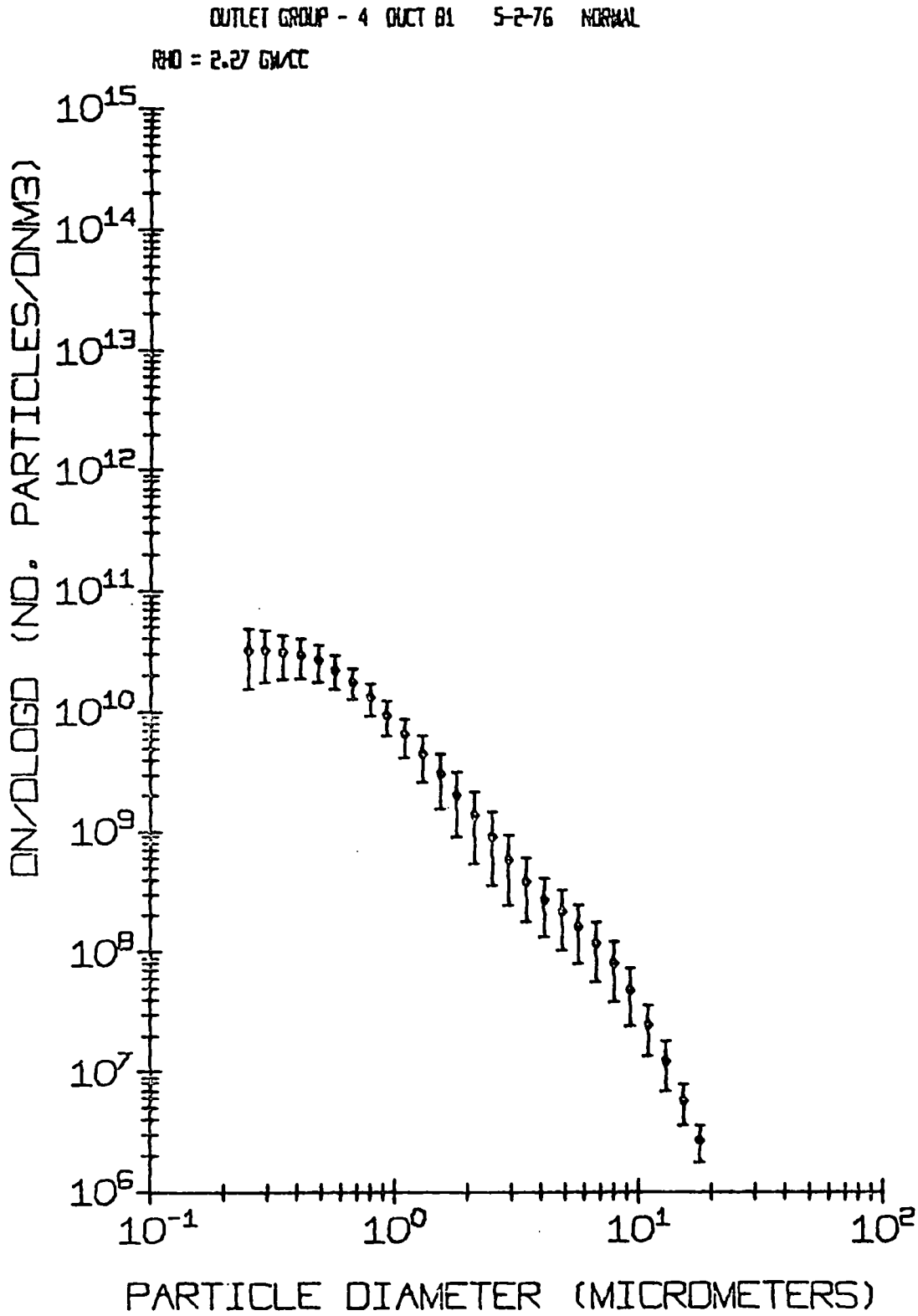


*Figure 9. Differential number concentration(dN/dlogD) versus particle diameter averaged for a set of runs. Fifty percent confidence intervals are shown.*

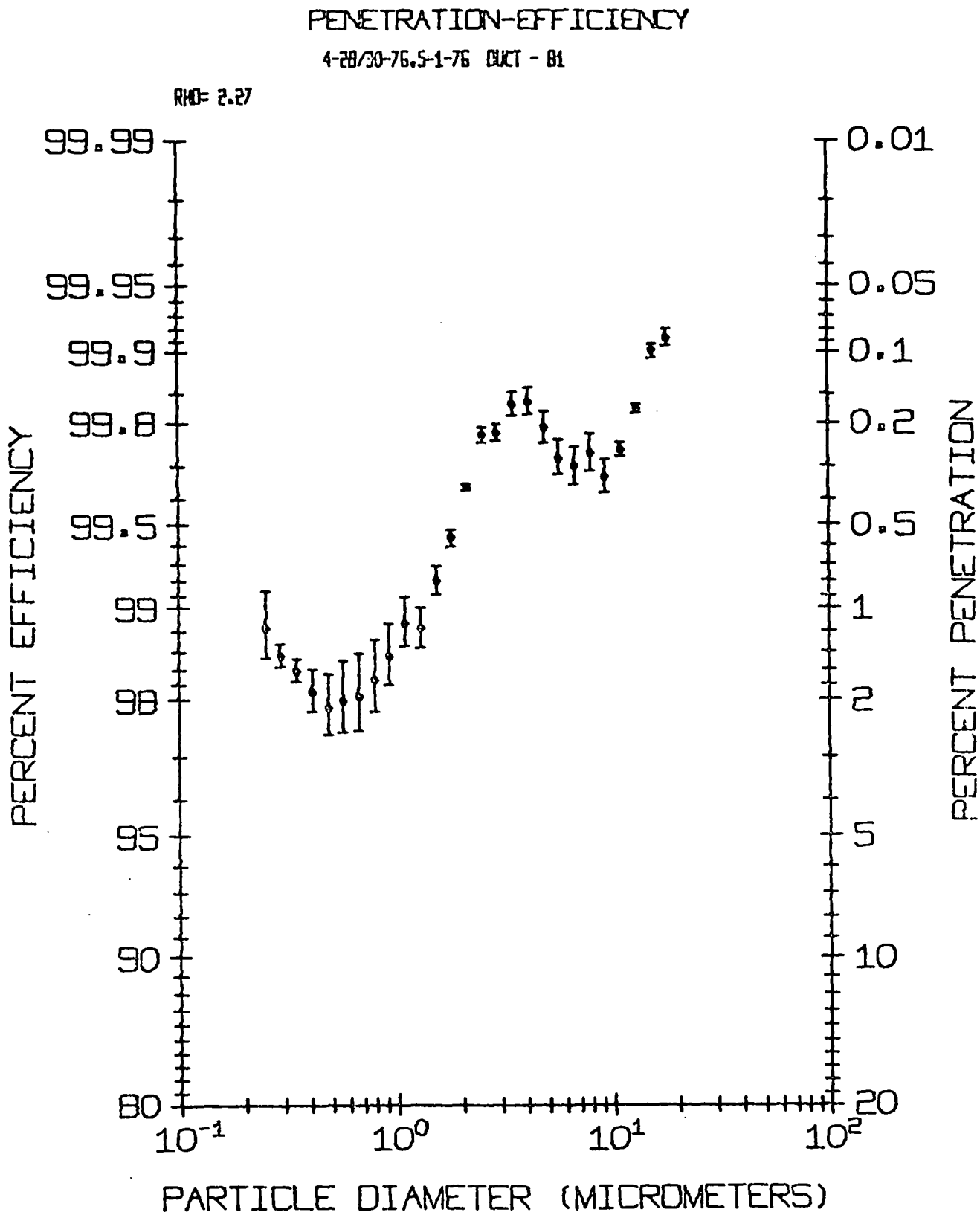


*Figure 10. Penetration--efficiency versus particle diameter for a number of inlet and outlet impactor runs at a particular control device. Log--probability grid. Fifty percent confidence intervals are shown.*

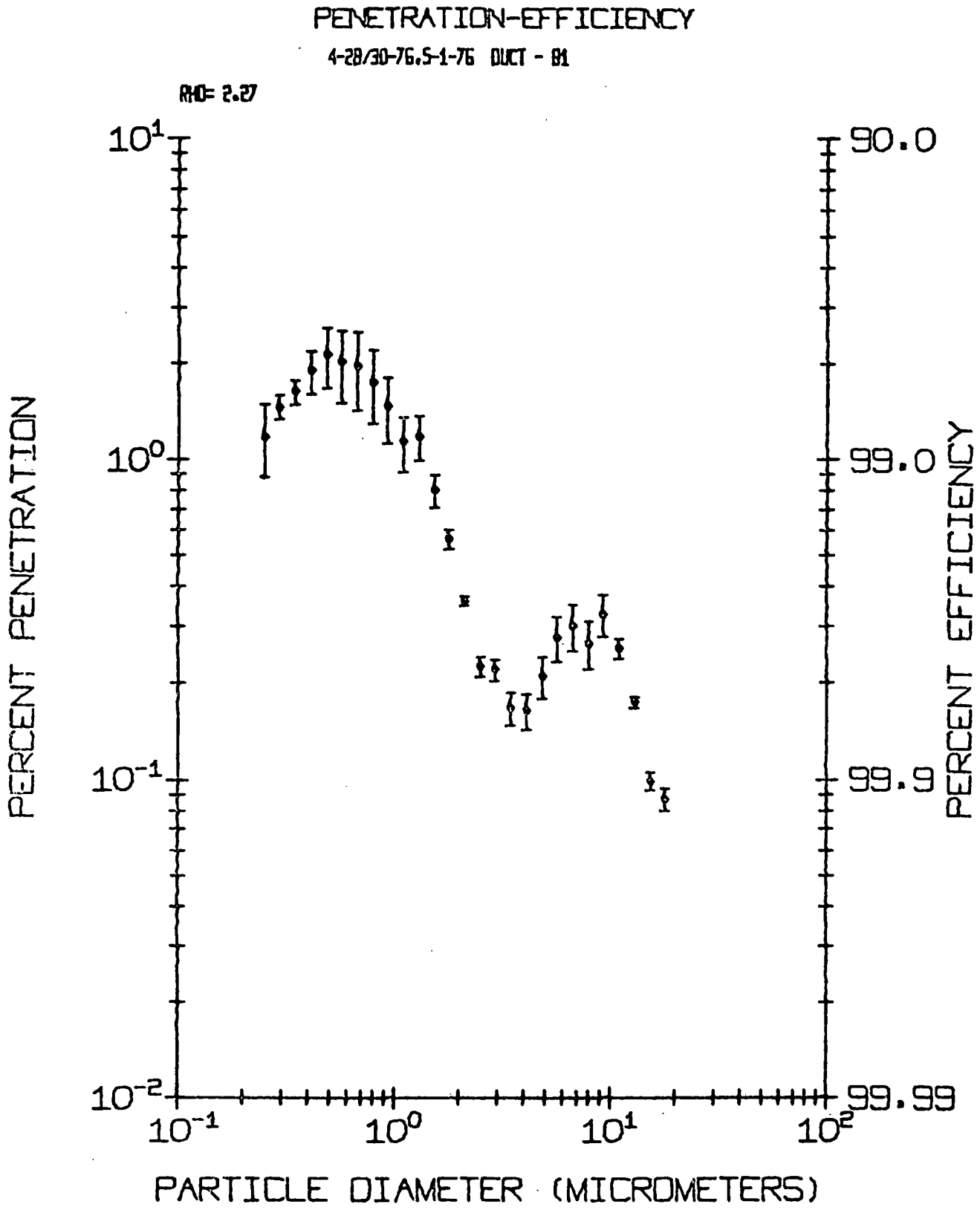


*Figure 11. Penetration--efficiency versus particle diameter for a number of inlet and outlet impactor runs at a particular control device. Log--log grid. Fifty percent confidence intervals are shown.*

Ordinate and abscissa maximum and minimum values can be fixed or data regulated. If any point lies beyond an axis limit on a non-data regulated graph, it is plotted with the correct ordinate or abscissa value slightly beyond the axis it exceeds.

Part 4 of the program to develop a computer data reduction package is currently underway and documentation is proceeding. The program has been placed into a "version 1" status based on the work of Parts 1, 2, and 3. A future version is anticipated which will be more automated and will accommodate any impactor.

## HP-65/HP-25 Source Sampling Programs (Technical Directive Number 10201)

Description of Task:

A library of programs to facilitate calculations associated with source sampling were compiled for the Hewlett-Packard HP-65 and HP-25 Pocket Programmable Calculators. This library contains EPA Reference Methods 1-8, cascade impactor programs, and others which the Project Officer selected. Two documents were published in two formats—a normal 8½"x11" and a special 5"x7" spiral bound version for field use.

Summary of Progress:

Twenty-two programs for air pollution measurement studies have been written for both the Hewlett-Packard HP-65 and HP-25 Pocket Programmable Calculators. Each program includes a general description, formulas used in the problem solution, a numerical example, user instructions, and a program listing.

A list of the calculator programs follows.

APol-01 Method 1 - Sample and Velocity Traverses for Stationary Sources

APol-02 Method 2 - Determination of Stack Gas Velocity and Volumetric Flow Rate (Type S Pitot Tube)

APol-03 Method 3 - Gas Analysis for Carbon Dioxide, Excess Air, and Dry Molecular Weight

APol-04 Method 4 - Determination of Moisture in Stack Gases

APol-05 Method 5 - Determination of Particulate Emissions from Stationary Sources

APol-06 Method 6 - Determination of Sulfur Dioxide Emissions from Stationary Sources

APol-07 Method 7 - Determination of Nitrogen Oxide Emissions from Stationary Sources

APol-08 Method 8 - Determination of Sulfuric Acid Mist and Sulfur Dioxide Emissions from Stationary Sources

APol-09 Cascade Impactor Operation

APol-10 Impactor Flow Rate Given Orifice $\Delta H$

APol-11 Impactor Flow Rate, Given Gas Velocity and Nozzle Diameter

APol-12 Impactor Sampling Time to Collect 50 Milligrams

APol-13 Impactor Flow Rate, Sample Volume, Mass Loading

APol-14 Impactor Stage $D_{50}$

APol-15 $\sqrt{\Psi}$ Calculation - Round Jets

APol-16 $\sqrt{\Psi}$ Calculation - Rectangular Slots

APol-17 Cumulative Concentration vs $D_{50}$ and $\Delta M/\Delta \log D$ vs Geometric Mean Diameter

APol-18 Mean, Standard Deviation, 90/95% Confidence Interval, Mean ± CI

APol-19 Resistivity and Electric Field Strength

APol-20 Channel Concentrations for the KLD Droplet Measuring Device (1-600 μm) DC-1

APol-21 Aerotherm High Volume Stack Sampler; Stack Velocity, Nozzle Diameter, Isokinetic $\Delta H$

APol-22 Flame Photometric Detector Calibration by Permeation Tube Technique

Both of the program documents were published in two formats. The first of these was the normal 8½"x11" bound version; the second was a special, 5"x7" spiral bound version with plastic laminated covers. The HP-65 document was published under the

title: HP-65 Programmable Pocket Calculator Applied To Air Pollution Measurement Studies: Stationary Sources. (EPA-600/8-76-002) (NTIS-PB 264284/$5.50). The HP-25 document was published under the title: HP-25 Programmable Pocket Calculator Applied To Air Pollution Measurement Studies: Stationary Sources. (EPA-600/7-77-058). A photograph of the two spiral bound booklets is shown in Figure 12.

## Non-Ideal Cascade Impactor Behavior
## (Technical Directive Number 10301)

### Description of Task:

The purpose of this task was to theoretically investigate the effect of non-ideal cascade impactor behavior on field test data. The feasibility of compensating for non-ideal behavior during data reduction was investigated. In addition, studies were made to determine the "ultimate" accuracy of size distributions measured with impactors, given this non-ideal behavior.

### Summary of Progress:

Cascade impactors have become commonly used measurement devices for the determination of size distributions of particulate matter emissions from industrial sources. Data obtained with impactors are used to characterize emissions from sources, to determine the performance of particulate control devices, and in the selection and design of control devices for specific sources.

Data provided by impactors are of relatively low resolution and do not permit the exact reconstruction of the size distribution of the aerosol being sampled, even over the limited range of sizes normally covered by most impactors (approximately 0.5 to 10 μm). However, little has been done to estimate the magnitude of the uncertainties, or errors, which are inherent in the method insofar as they relate to industrial source emission measurements and determinations of fractional collection efficiencies of control devices. The study described here was one with the specific goals of estimating the effects of two non-ideal operating characteristics of impactors on the data obtained with them. These two non-idealities are (1) the lack of step function stage collection characteristics and (2) particle bounce. Several authors[1,2,3] have proposed various deconvolution procedures which, when applied to impactor data, would to a large degree, correct for the effect of the finite slopes of the stage collection efficiency curves. However,

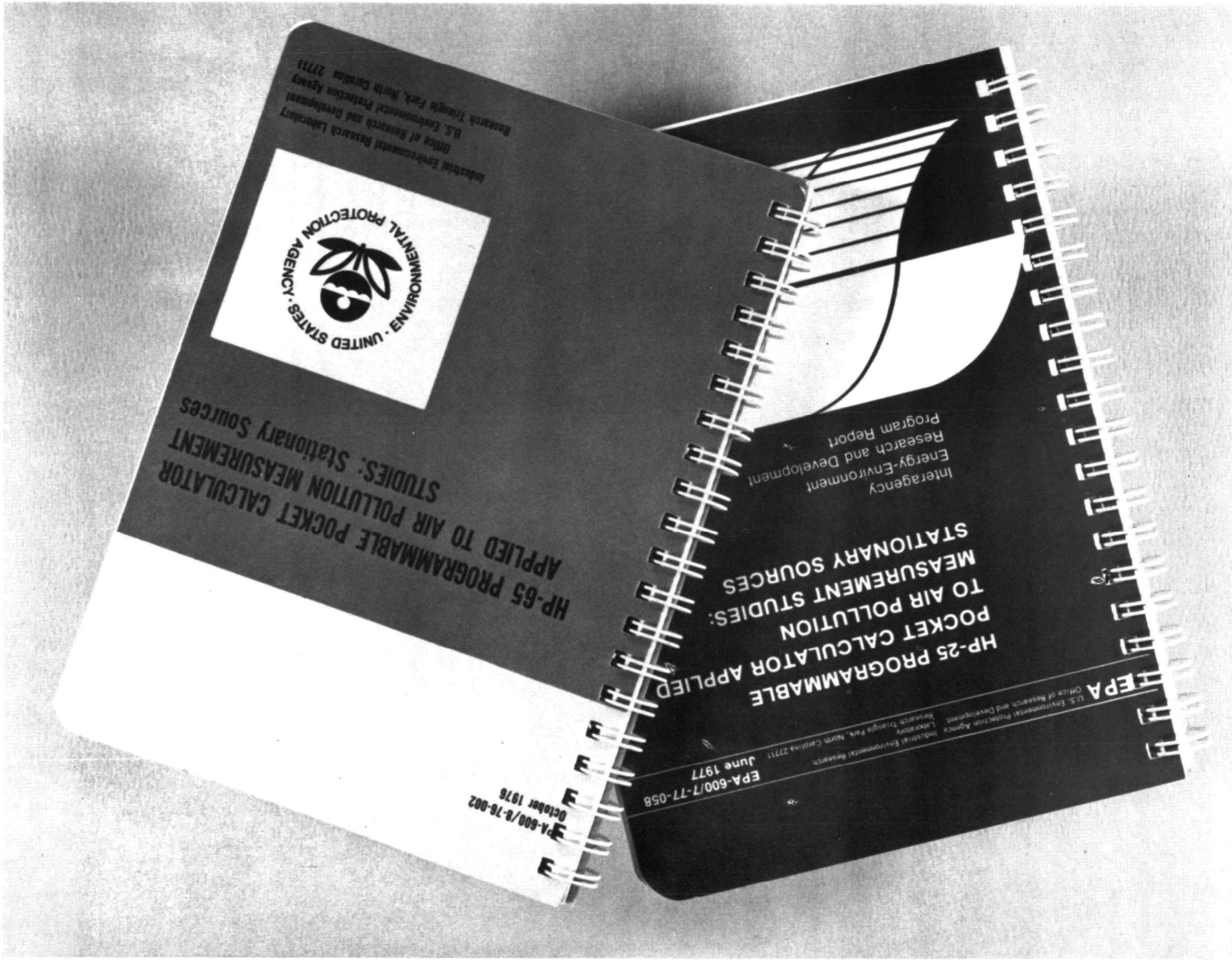


*Figure 12. HP--65 and HP--25 Programmable Calculator Source Measurement Booklets.*

little use has been made of these procedures, primarily because noise in the data frequently results in oscillatory solutions with large negative values. In any case, little quantitative information regarding the magnitude of the errors introduced by the lack of sharp size cuts in impactors commonly used for stack sampling has been published. The magnitude of errors introduced by particle bounce has not previously been quantified although the existence of such errors has been described in the literature.[4,5,6,7]

## Technical Procedures

The approach used in this study was the development of a computer model of cascade impactor performance. The model was based on actual impactor performance as measured in a calibration study of commercially available cascade impactors for stack sampling. A total of four simulation models were used for both a Brink impactor in a commonly used modified configuration for stack sampling and an Andersen Mark III stack sampler. The use of glass fiber collection substrates was assumed for both impactors. Both grease and glass fiber substrates are commonly used for sampling at temperatures below 150°C (300°F) but no satisfactory greases have been found for use at temperatures over 150°C. Therefore, glass fiber substrates must usually be used for collection substrates at elevated temperatures.

The first model for each impactor was one having ideal collection characteristics, i.e., step functions from 0% to 100% collection at the stage $D_{50}$'s. (The stage $D_{50}$ is that particle diameter at which the stage has a collection efficiency of 50%. The $D_{50}$ is generally used as the characteristic cut off diameter for particles collected by the stage.) This model was used as a performance standard against which the remaining three models could be compared and also provided a basis for checking the program.

The assumed operating conditions and resulting cut sizes ($D_{50}$'s) of the two impactors modeled in the study are given in Table III. The models of the Brink impactor included a cyclone precollector which was assumed to have the same performance characteristics in all three of the simulations other than that of the "IDEAL Brink." The cylone performance was based on calibration data for a cyclone in common use with the Brink impactor modified for stack sampling. This cyclone has a collection efficiency of 100% for particles larger than about 20 μm.

Table III. Simulation Conditions of the Modeled Impactor Performance

| | Brink | Andersen |
|---|---|---|
| Temperature, °C (°F) | 177 (350) | 177 (350) |
| Gas composition | Std. air | Std. air |
| Particle density, $gm/cm^3$ | 2.27 | 2.27 |
| Flowrate, alpm (acfm) | 1.13 (0.040) | 17.0 (0.600) |
| Barometric Pressure, mm Hg | 749 | 749 |
| Stage/$D_{50}$ (μm) | | |
| 1 | 9.60[1] | 7.84 |
| 2 | 6.18[2] | 7.40 |
| 3 | 3.39 | 4.44 |
| 4 | 1.85 | 2.87 |
| 5 | 1.23 | 1.58 |
| 6 | 0.905 | 0.855 |
| 7 | 0.589 | 0.449 |
| 8 | 0.198[2] | 0.200 |

1. Stage 1 is a cyclone precollector.

2. Stages 2 and 8 are part of the modifications to the impactor.

The second model for each impactor used the actual calibration data for each stage. In this model the stage collection efficiencies increased monotonically with increasing Stokes' numbers (increasing particle size) to a maximum value of about 90% to 95%. The efficiencies then decreased for larger Stokes' numbers to a value of 35% to 40% and remained constant thereafter. A composite of the calibration data for stages two (2) through seven (7) of the Andersen impactor, which illustrates the behavior described above, is shown in Figure 13. Data for States 1 and 8 were offset from the tight grouping of the data for the remaining stages and hence were omitted in Figure 13 for purposes of clarity in illustrating the behavior trends of the stage efficiency curves. The data for the Brink impactor exhibited similar trends. This model, Model 2, is called the "Normal Bounce" model.

The third model was identical to the second except that the rollover and decline in efficiency for larger Stokes' numbers was ignored. Instead, the efficiencies were assumed to smoothly increase to 100% and remain at that value for increasingly larger Stokes' numbers. This is called the "No Bounce" model. The fourth model was also identical to Model 2 with the exception that the collection efficiencies were assumed to drop rapidly to a value of 2% for Stokes' numbers larger than that at which the collection efficiency reached a peak in the calibration data. This model was termed the "Extreme Bounce" model.

The use of the same basic collection efficiency curves for the "No Bounce", "Normal Bounce", and "Extreme Bounce" models for particle sizes smaller than those for which the collection efficiencies were maximal in the calibration data is probably a realistic representation of the actual performance of the impactors in collecting various types of particles. Rao[5] found that impactor collection characteristics for dry solid particles and oil particles were virtually identical when glass fiber substrates were used for Stokes' numbers smaller than those at which the peak efficiency was reached for the dry solid particles. Beyond this point he found that oil particles were collected with efficiencies which increased to 100% with increasing Stokes' number while the efficiencies declined for the dry particles as a result of bounce. Figure 14 shows an example of the four modeled collection efficiency characteristics of one stage of the Andersen impactor.

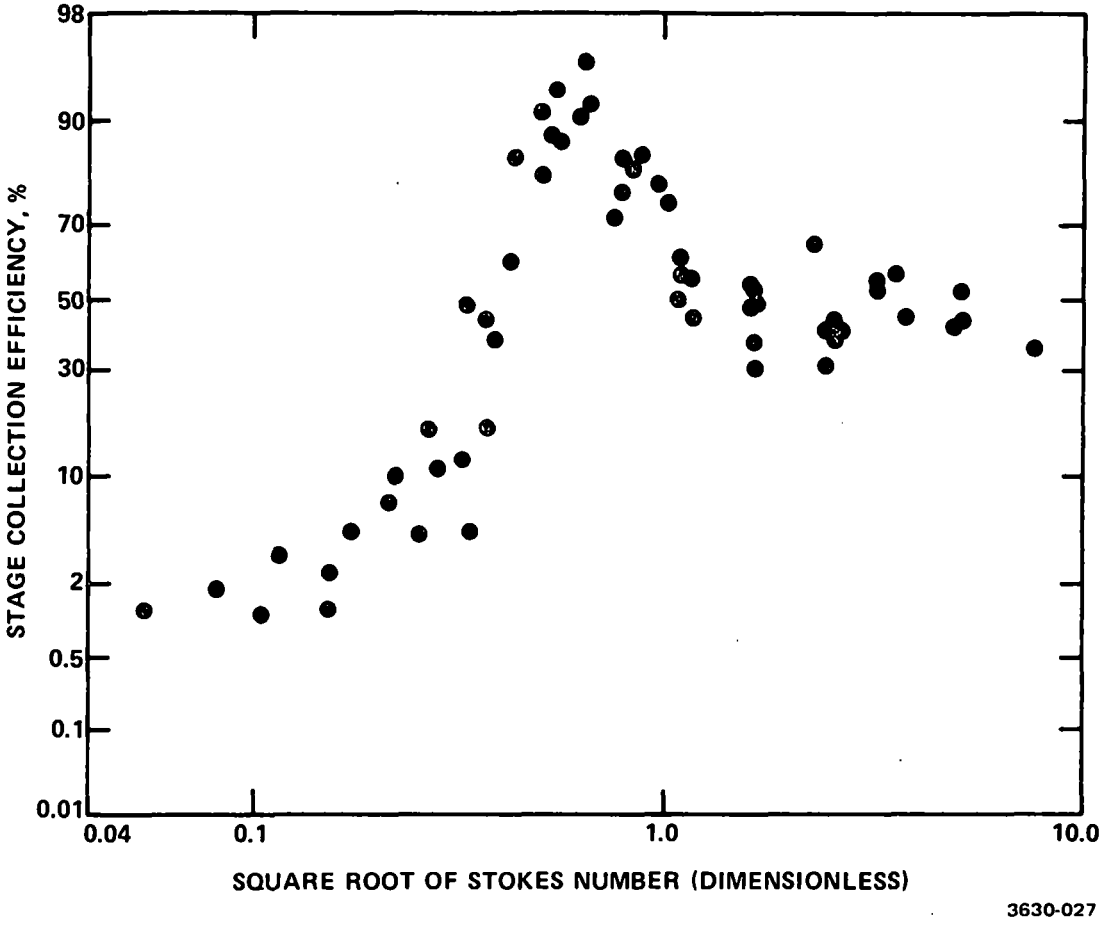


*Figure 13. Composite of calibration data for the Andersen impactor-stages 2 through 7.*

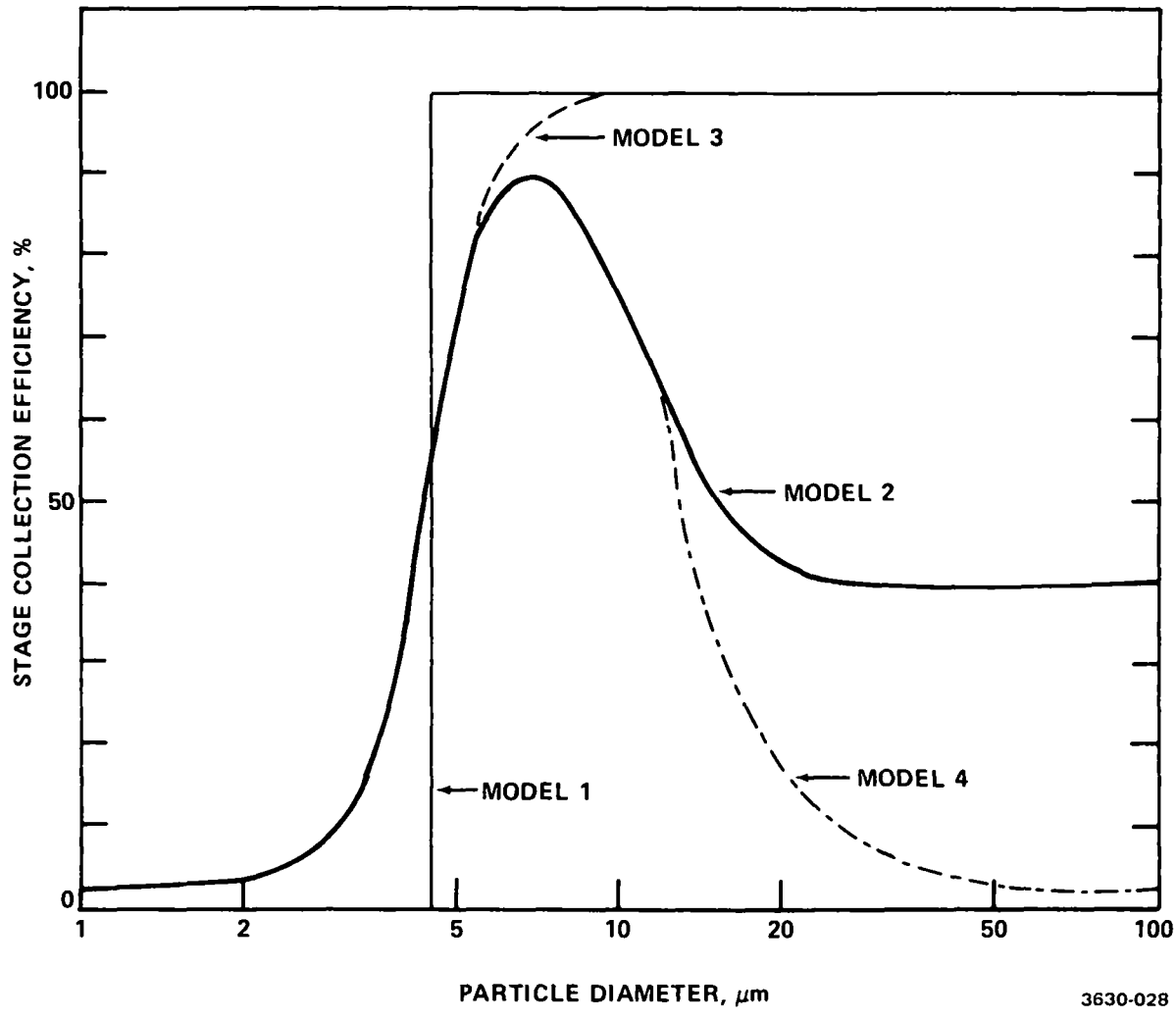


*Figure 14. An illustration of the four modeled stage collection efficiency curves of a typical stage of the Anderson impactor. Model 1 is the ideal behavior model, model 2 is the normal bounce model, model 3 is the no bounce model, and model 4 is the extreme bounce model.*

## Results and Discussion

The performance of each model of the two impactors was evaluated for aerosols having log-normal size distributions with mass median diameters (MMD) of 1.5, 2.6, 4.5, 7.8, 13.5, and 27 micrometers and geometric standard deviations, $\sigma_g$, of 2, 3 and 4. Representative results are presented in this report.

Figures 15 through 18 show typical results for the two impactors in a cumulative percentage presentation. It is evident from all four of these figures that particle bounce severely distorts the size distributions, especially for aerosols having large mass median diameters. Figures 15 and 16 show the results of the simulations for the same impactor and size distributions, the difference between the two being the omission of the back-up filter catch in presenting the results in Figure 16. Comparison of Figures 15 and 16 indicate that omitting the back-up filter in calculating the cumulative percentages greatly reduces the distortion resulting from bounce. Comparison of Figures 15 and 16 shows that increasing the width of the input size distribution (increasing $\sigma_g$ reduces the distortion caused by bounce although the distortion remains appreciable for the extreme bounce models at large MMD's.

Figure 18 shows the results from the Andersen models corresponding to three of the four cases for the Brink Model shown in Figure 16. Note that the deviations from the input distribution resulting from bounce are more severe in the Andersen results than in the Brink. This difference in the severity of the distortions apparently results from the cyclone precollector on the Brink which removes most of the larger particles that are responsible for raising the apparent percentages of fines in the recovered size distributions.

It should also be noted that the relative errors in mass median diameters become increasingly large as the MMD of the input aerosol decreases. The recovered MMD's were found to be systematically large for test aerosol MMD's below 10 μm. The values of $\sigma_g$ were also systematically high with larger relative errors at the lower values of $\sigma_g$, as would be expected because of the low resolution afforded by impactors.

In many cases (e.g., control device fractional collection efficiency studies) the slope of the size distribution curve, expressed in mass concentration units, is the quantity of greatest interest. The most common manner of presentation of this slope is the form dM/dlogD (units of mass concentration). The quantity dM/dlogD is often approximated directly from the impactor data, stage by stage, as $\Delta m_i/\Delta \log D_i$, where

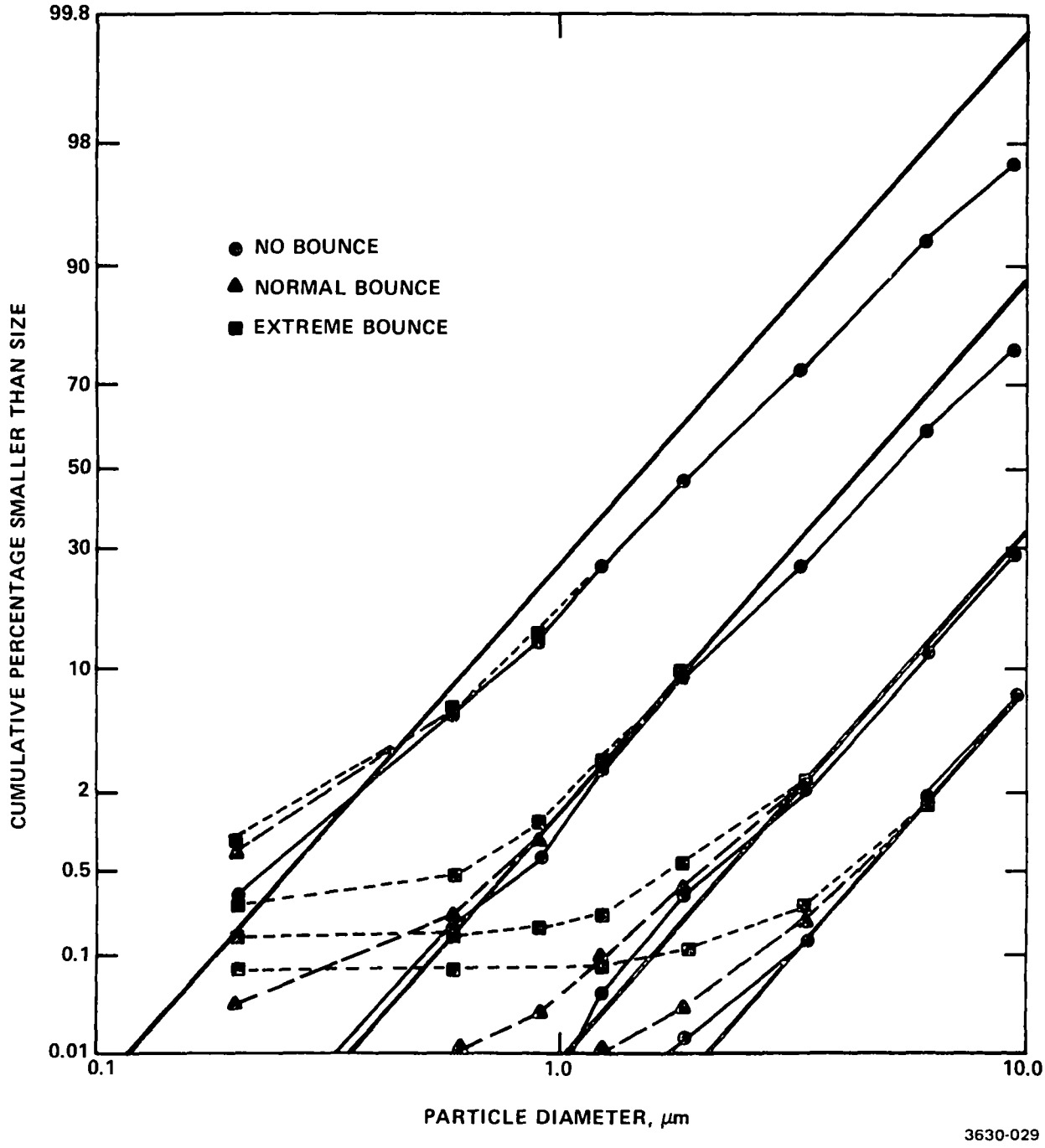


*Figure 15. Recovered size distributions on a cumulative percentage basis from the Brink impactor models for $\sigma g$ = 2.0 and MMD's of 1.5, 4.5, 13.5, and 27 μm. The bold lines represent the input distributions.*

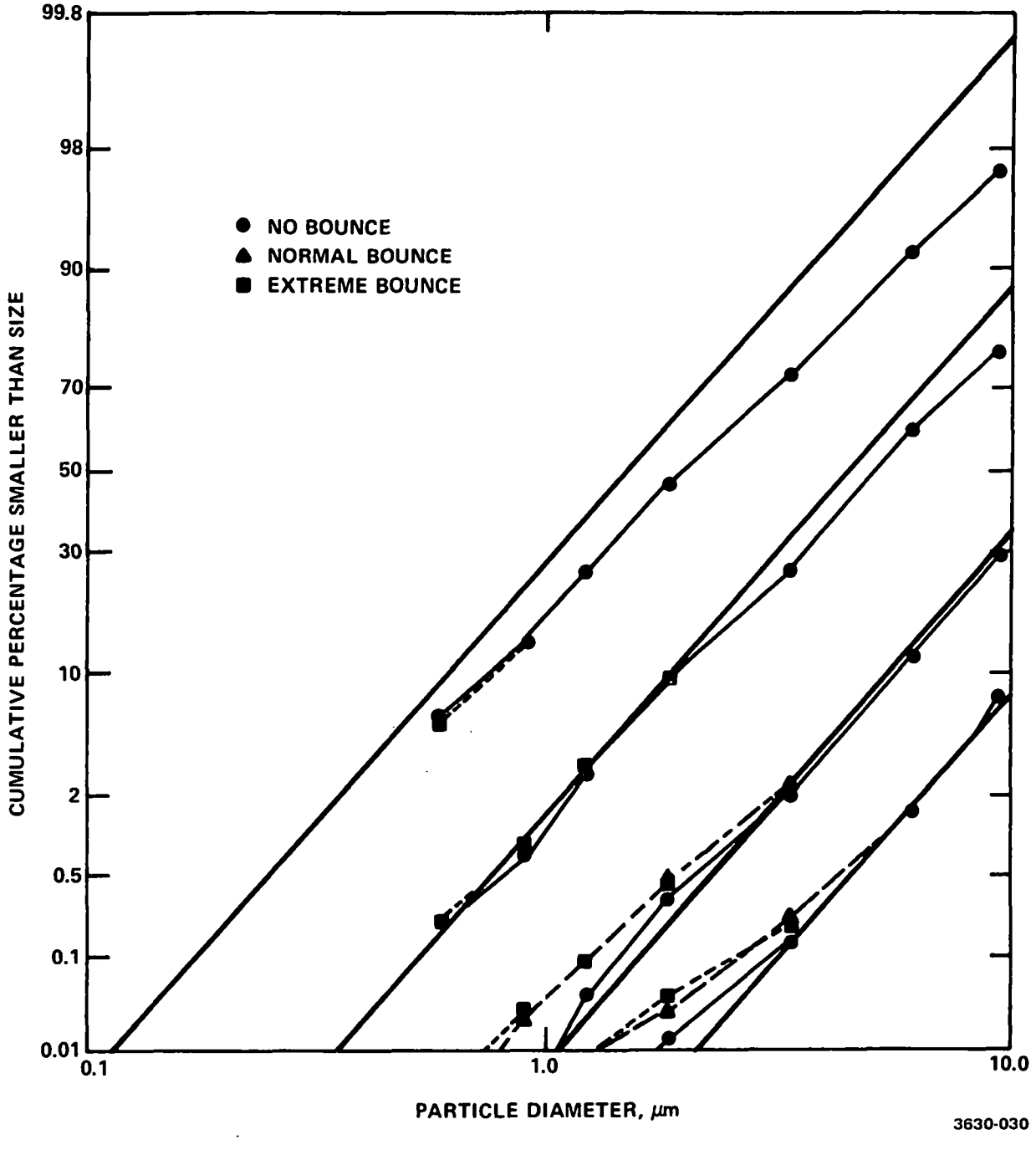


*Figure 16. Recovered size distributions on a cumulative percentage basis from the Brink impactor models as shown in Figure 15 with the backup filter catches omitted from the analysis. The bold lines represent the input distributions.*

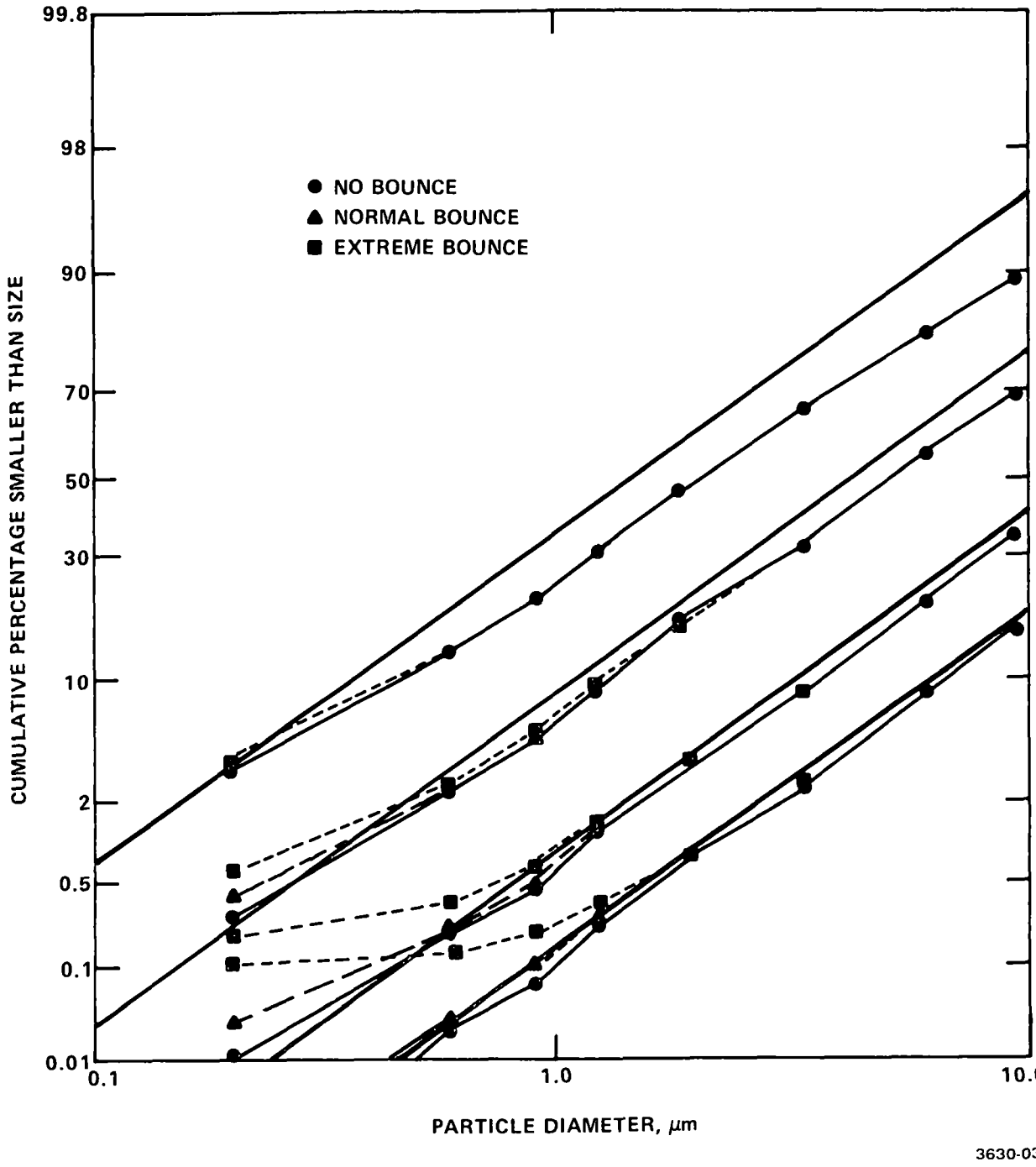


*Figure 17. Recovered size distributions on a cumulative percentage basis from the Brink impactor models for $\sigma g$ = 3.0 and MMD's of 1.5, 4.5, 13.5 and 27 μm (backup filter included in the analysis). The bold lines represent the input distributions.*

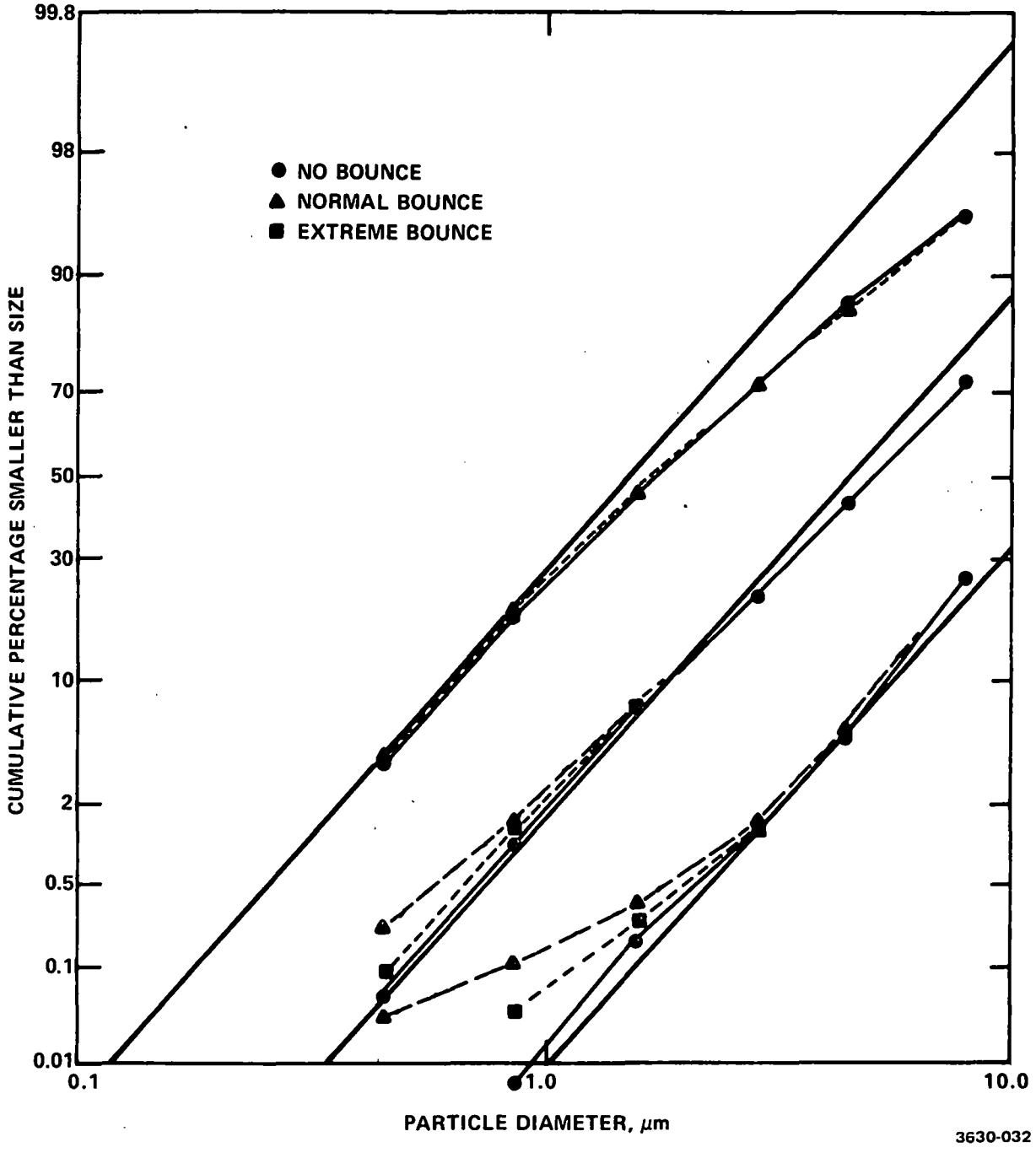


*Figure 18. Recovered size distributions on a cumulative percentage basis for the Andersen impactor for σg = 2.0 and MMD's of 1.5, 4.5, and 13.5 μm. The backup filter was excluded from analysis in the results shown. The bold lines represent the input distributions.*

$m_i$ = mass concentration of particles retained by the $i^{th}$ stage

$$\text{and} \quad \Delta \log D_i = \log \frac{(D_{50})_{i-1}}{(D_{50})_i} .$$

The particle diameter is then taken to be the geometric mean of $(D_{50})_i$ and $(D_{50})_{i-1}$ or

$$\bar{D}_g = \sqrt{(D_{50})_i \times (D_{50})_{i-1}}$$

Figures 19 and 20 illustrate recovered size distributions presented in such a manner, together with the input distributions, for representative sets of Brink and Andersen results. The results for the "extreme bounce" case are not shown in Figures 19 and 20 but the values in those cases generally fall between the "no bounce" and "normal bounce" cases except for the back-up filters, for which the values were much higher in the "extreme bounce" case than in the other two cases. Except for the finest size fractions, represented by the back-up filter catches, and the fine fraction tails of the low $\sigma_g$ distributions, the agreement between the recovered values of $(\Delta M/\Delta \log D)_i$ generally lie reasonably close to the input distributions. However, errors of up to ±35% are not infrequent.

Tables IV and V show the errors, expressed as percentages, in the recovered values of $(\Delta m/\Delta \log D)_i$ for several cases for each of the two impactors. (For the purpose of calculating log D and $\bar{D}$ for the filter catches, it was assumed that the diameter range covered by the filter was $(D_{50})_8$ down to $\frac{1}{2}(D_{50})_8$.

Although no results for $\sigma_g = 4$ have been shown, the agreement between the recovered size distributions and the input distributions was progressively better as $\sigma_g$ increased and was quite good in all cases for $\sigma_g = 4$ with the exception of back-up filter catches when bounce was present.

Table VI shows the percentages of cases in which the recovered values $(\Delta m/\Delta \log D)_i$ lay within factors of 1.2, 1.5, and 2 of the true value. From these results it appears that the concentrations of fine particles as measured with impactors can seldom be taken to be known better than to within a factor much smaller than 1.5 unless the particles are known to be adhesive or an effective adhesive coating can be applied to the substrates.

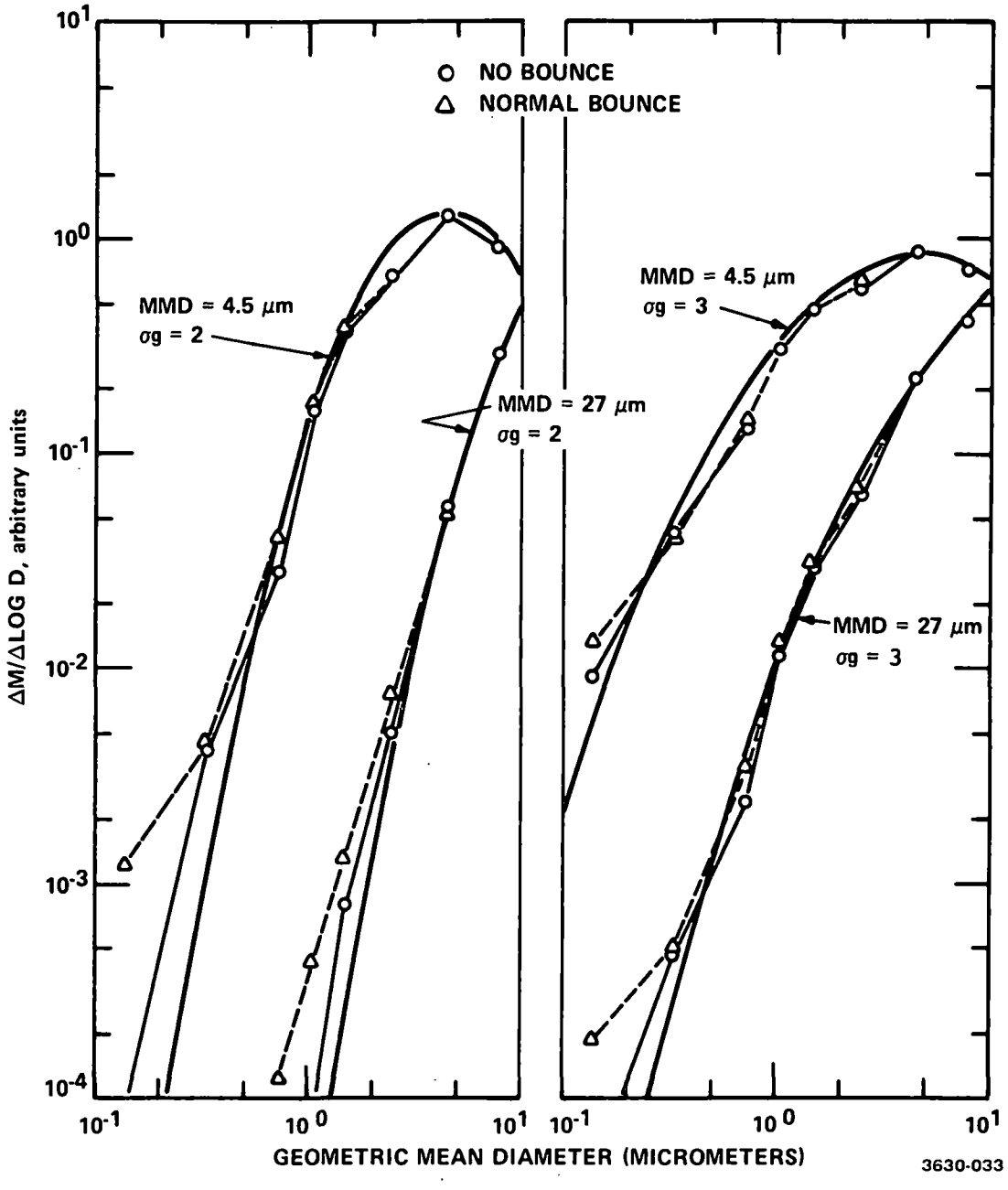


*Figure 19. Recovered size distributions on a differential basis from the Brink impactor models for MMD's of 4.5 and 27 μm and σg's of 2 and 3. The bold curves represent the input distributions.*

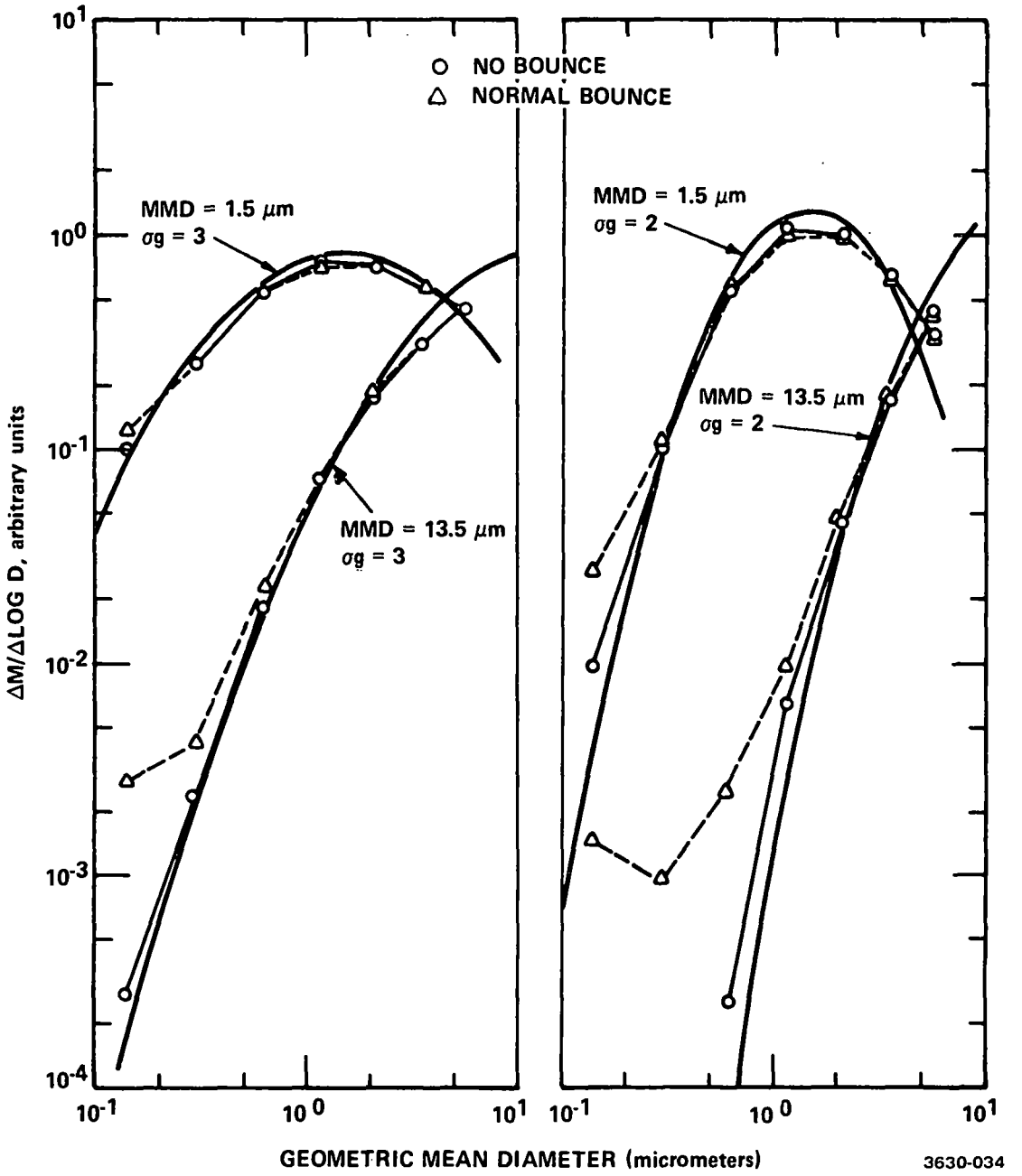


*Figure 20. Recovered size distributions on a differential basis from the Andersen impactor models for MMD's of 1.5 and 13.5 μm and σg's of 2 and 3. The bold curves represent the input distributions.*

Table IV. Percent Errors in $\Delta M/\Delta \log D$, Andersen Impactor

| | No Bounce | | | | | |
|---|---|---|---|---|---|---|
| $\sigma_g$ = | 2 | | | 3 | | |
| MMD: | 1.5 | 4.5 | 13.5 | 1.5 | 4.5 | 13.5 |
| Stage/Error | | | | | | |
| F | 144 | | | 22 | 38 | |
| 8 | 9 | | | -14 | -5 | |
| 7 | -8 | 56 | | -11 | -4 | |
| 6 | -18 | 13 | | -10 | -8 | 4 |
| 5 | -14 | -19 | 18 | -12 | -17 | -24 |
| 4 | 6 | -26 | -20 | -7 | -21 | -25 |
| 3 | | -19 | -30 | 10 | -15 | 0 |
| 2 | | -23 | -28 | 9 | -22 | -24 |
| | Normal Bounce | | | | | |
| F | 568 | 121000 | | 44 | 173 | 1720 |
| 8 | 22 | 920 | | -12 | 8 | 103 |
| 7 | -6 | 111 | | -11 | 1 | 37 |
| 6 | -20 | 9 | 293 | -12 | -11 | 4 |
| 5 | -16 | -18 | 39 | -12 | -16 | -11 |
| 4 | 5 | -27 | -17 | -7 | -21 | -24 |
| 3 | | -20 | -30 | 9 | -16 | -25 |

NOTE: Values are omitted for stages for which the collected mass would be too small to be detected in field sampling programs.

Table V. Percent Errors in $\Delta M/\Delta \log D$, Brink Impactor

| | No Bounce | | | | | | | |
|---|---|---|---|---|---|---|---|---|
| $\sigma_g$ = | 2 | | | | 3 | | | |
| MMD: | 1.5 | 4.5 | 13.5 | 27 | 1.5 | 4.5 | 13.5 | 27 |
| Stage/Error | | | | | | | | |
| F | 220 | | | | 24 | 53 | | |
| 6 | -6 | 220 | | | -37 | -21 | 13 | |
| 5 | -43 | -35 | | | -32 | -39 | -40 | -37 |
| 4 | -19 | 3 | | | -9 | -12 | -5 | 4 |
| 3 | -15 | -3 | 84 | | -4 | -9 | -3 | 8 |
| 2 | -1 | -10 | -8 | 33 | 4 | -20 | -23 | -22 |
| 1 | 88 | -14 | -15 | 7 | 34 | -3 | -14 | -14 |
| | Bounce | | | | | | | |
| F | 550 | | | | 41 | 123 | | |
| 6 | -10 | 238 | | | -39 | -24 | 12 | |
| 5 | -40 | -8 | | | -29 | -33 | -26 | -10 |
| 4 | -20 | 10 | | | -10 | -12 | 0 | 17 |
| 3 | -16 | -4 | 107 | | -4 | -10 | -3 | 10 |
| 2 | -1 | -28 | 7 | 100 | 4 | -18 | -20 | -16 |
| 1 | 86 | -15 | -18 | 3 | 33 | -4 | -16 | -17 |

NOTE: Values are omitted for stages for which the collected mass would be too small to be detected in field sampling programs.

Table VI. Percentage of Trial Cases in Which Recovered Value of ($\Delta M/\Delta \log D$) is Within the Indicated Factor of the True Value

| | Andersen | | | | Brink | | |
|---|---|---|---|---|---|---|---|
| Factor: | 1.2 | 1.5 | 2.0 | Factor: | 1.2 | 1.5 | 2.0 |
| Stage/Percent of cases | | | | Stage/Percent of cases | | | |
| F | 0 | 31 | 38 | F | 0 | 33 | 56 |
| 8 | 57 | 71 | 79 | 6 | 35 | 59 | 82 |
| 7 | 65 | 76 | 82 | 5 | 11 | 47 | 100 |
| 6 | 65 | 80 | 90 | 4 | 80 | 95 | 100 |
| 5 | 75 | 100 | 100 | 3 | 74 | 91 | 91 |
| 4 | 30 | 100 | 100 | 2 | 42 | 96 | 100 |
| 3 | 40 | 90 | 90 | 1 | 71 | 72 | 100 |
| 2 | (30) | (90) | (90) | | | | |

Andersen table covers all cases with
MMD = 1.5, 2.6, 4.5, 7.8, 13.5 and
$\sigma_g$ = 2, 3
for both normal bounce and no bounce

Brink table covers all cases with with
MMD = 1.5, 2.6, 4.5, 7.8, 13.5, 27, and
$\sigma_g$ = 2, 3
for both normal bounce and no bounce

There is some evidence,[8,9] although it is not conclusive, that the use of adhesive coatings (greases) on the substrates may become ineffective as the particulate deposits build up under the impactor jets. This would result in the same type of errors due to particle bounce resulting in back-up filter contamination by oversize particles with greased substrates as has been shown to occur with glass fiber substrates.

### Conclusions and Recommendations

From the evidence presented here, it is suggested that back-up filter catches generally should be omitted from data presentation when dry, non-sticky particulates are sampled. Exceptions should be made only if the MMD is smaller than about 2.5 μm. In addition it is suggested that cyclone precollectors having $D_{50}$'s somewhat larger than the first impaction stage $D_{50}$ be used whenever a non-sticky particulate is sampled. The use of such cyclones tends to greatly reduce errors due to particle bounce.

The results of this study were reported at the 1977 Air Pollution Control Association Annual Meeting in Toronto, Ontario, as Paper No. 77-35.3, entitled "Non-Ideal Behavior in Cascade Impactors."

## Cascade Impactor Sampling of Charged Particles (Technical Directive Number 10401)

Description of Task:

The purpose of this task is to investigate the errors introduced in particle-size measurements when sampling charged particles with cascade impactors. One aspect of this study is to sample charged aerosols with and without charge neutralizers situated at the impactor nozzle. If it is found necessary to employ a charge netralizer for in-stack sampling, then a collaborative effort will be planned with manufacturers to develop the needed device.

Summary of Progress:

### Introduction

The purpose of this study is to identify the effects of particle charge upon cascade impactor behavior and to evaluate methods of eliminating the effects, if they are significant.

To accomplish this goal a charged particle generator of monodisperse, uniformly charged particles was developed and calibrated. Then cascade impactor sampling of these aerosols was carried out under a variety of conditions. The parameters

varied from run to run include particle charge, particle size (2 μm and 5 μm diameters), electrical grounding of the impactor, and the use of a charge neutralizer. The impactors investigated in this study were

1. Andersen Mark III Stack Sampler (Andersen)
   Andersen 2000, Inc.
   Atlanta, GA 30320

2. MRI Model 1502 Inertial Cascade Impactor (MRI)
   Meteorology Research, Inc.
   Altadena, CA 91001

3. University of Washington Mark III Source Test Cascade Impactor
   (U. of W.)
   Pollution Control Systems, Inc.
   Renton, Washington 98055

The laboratory sampling phase of the project has been completed and analysis of the data is proceeding. Current results and conclusions are presented in this report. Further analyses to be performed are described in the last section.

The main area where the charge on particles is of interest is for the case of flyash exiting an electrostatic precipitator (ESP). For large particles (>2 μm in dia.) and common ESP operating conditions, the upper limit of charge is that of saturation in field charging. For a typical field strength ($4 \times 10^3$ volts/cm), $n_p$, the number of charges per particle, is given by

$$n_p = 834\ a_p^2 \qquad (1)$$

where $a_p$ is the particle radius in micrometers.[10] This means that for particles with a 5 μm diameter $n_p$ is approximately 5600 and for a 2 μm diameter is approximately 900.

In this study a monodisperse aerosol was produced with a Vibrating Orifice Aerosol Generator (VOAG). Ammonium fluorescein droplets were charged, dried, and then sampled with a cascade impactor. The collection efficiencies of the various impactor surfaces were then found by washing each surface individually with an ammonium hydroxide solution and measuring the optical absorbance of the wash to find the total mass on each surface. This procedure is similar to that of Cushing, et al.[11]

In this discussion, the method of charging particles and measuring the charge is described first, then impactor data and conclusions are presented.

## Particle Charging

The induction method of charging droplets produced with a VOAG was introduced by Reischl, et al.[12] The region of droplet formation of a VOAG is depicted in Figure 21, with the entire aerosol system shown in Figure 22. Ammonium fluorescein solution is pumped through an orifice mounted on a piezoelectric ceramic. Due to the applied voltage of frequency f, the crystal oscillates, producing mechanical vibrations of the liquid jet formed at the orifice. This causes the jet to become detached and form droplets at regular intervals. Droplet formation occurs at a height L above the orifice. The solvent, ammonia water, evaporates and leaves spherical particles of the solute, ammonium fluorescein. The particle radius $a_p$ is then given by

$$a_p = \left[\frac{3F_{sy}C'}{4\pi f}\right]^{1/3} \tag{2}$$

where $F_{sy}$ is the liquid flowrate in ml per second and C' is the solute concentration. In this study f was always set at 65 $kH_z$ and $F_{sy}$ at 0.201 ml per minute. If the liquid conducts, then charge can be induced upon the droplet during its formation by applying an electric field. The expression for the induced charge per droplet $n_p$ given by Reischl, et al[12] for a highly conducting liquid is

$$n_p = n_{p_o} - \frac{4\pi\varepsilon_0 a_d}{e} \frac{L\alpha}{H} V_c \tag{3}$$

where $a_d$ = droplet radius = $\left(\frac{3F_{sy}}{4\pi f}\right)^{1/3}$,

H = height of top electrode plate above the orifice,

$V_c$ = applied voltage,

e = elementary unit of charge,

$\varepsilon_0$ = dielectric constant of free space,

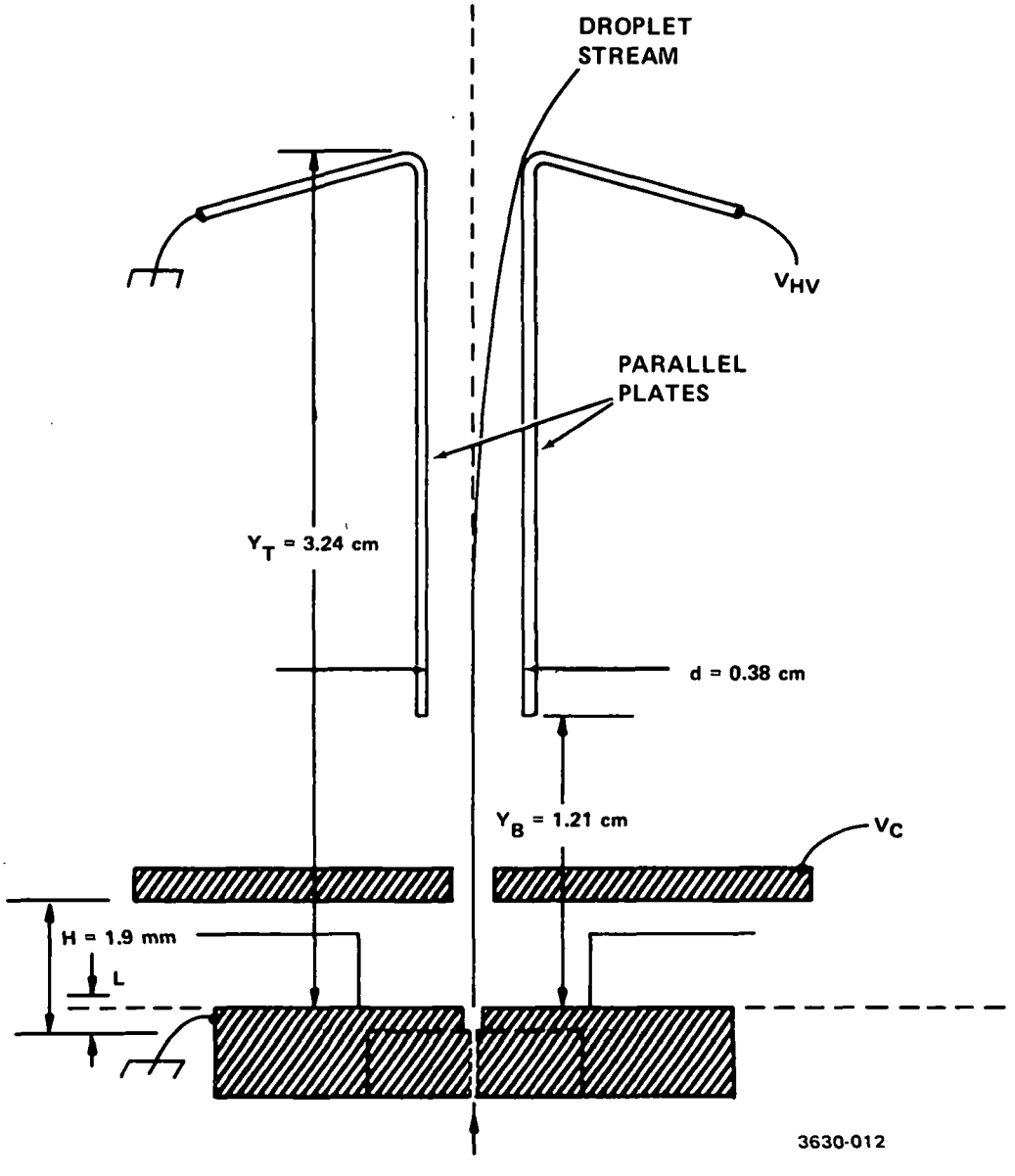


*Figure 21. Charged particle generator orifice region with the parallel plates for charge measurement.*

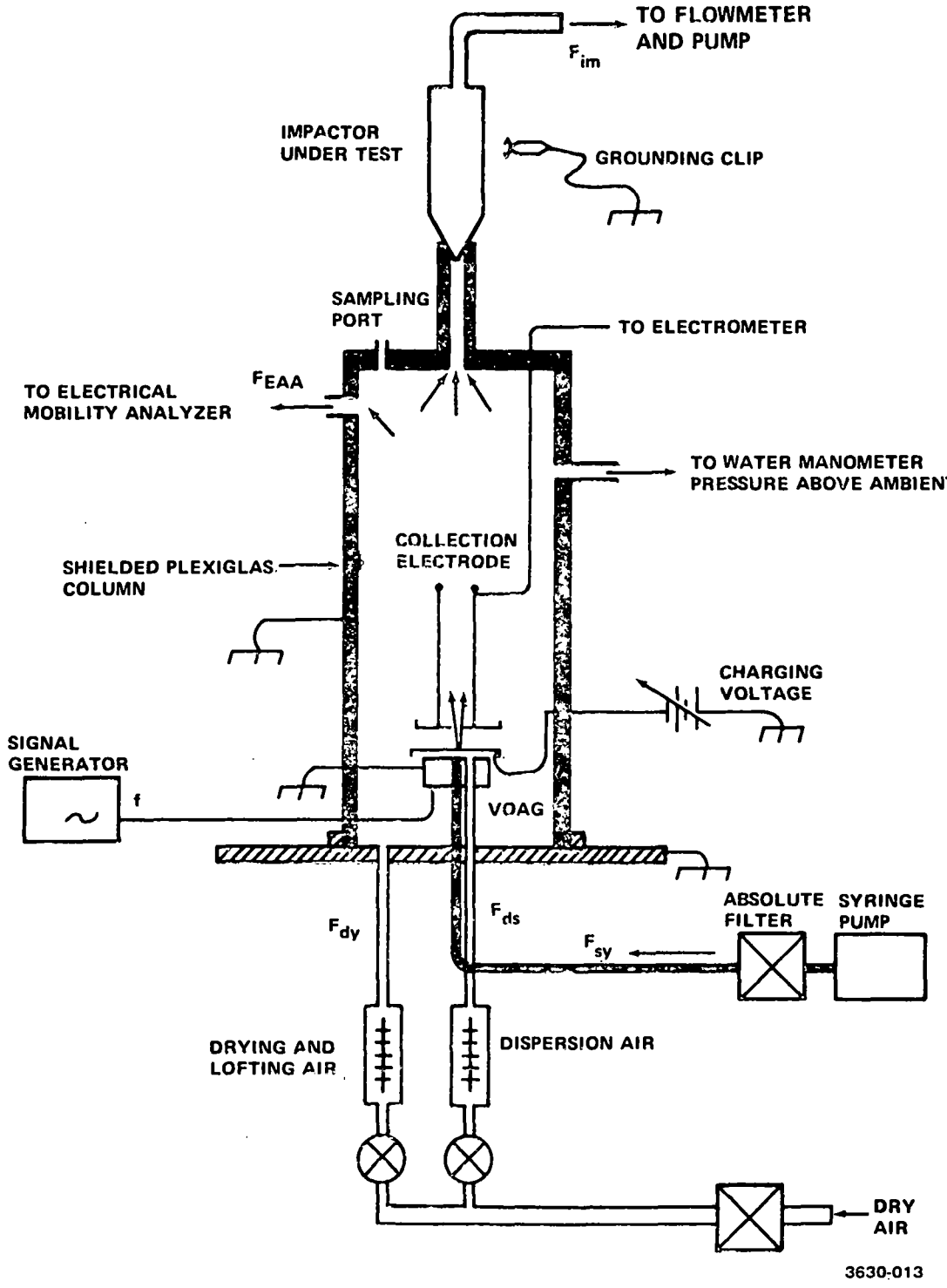


*Figure 22. Schematic of the charged particle generator and sampling arrangement.*

$\alpha$ = constant determined from the geometry of the orifice region = 0.81 for the device shown,

$n_{p_o}$ = charge from spraying process, and

$4\pi\varepsilon_0 a_d$ = capacitance of a sphere.

Equation (3) is based on the model of the spherical droplet immersed in the electric field with a conducting lead (liquid jet) connected to it. This expression has not been verified on an absolute basis; however, the linear dependence of $n_p$ upon $V_c$ was substantiated by Reischl, et al.[12] Thus the measurement of charge was necessary to calibrate the instrument although $a_d$, L, H, $\alpha$, and $V_c$ were measured independently. Comparisons of the predictions of Equation (3) and the charge measurements are given. The most difficult parameter to measure is L. A microscope (125X) allowed visual observation of the jet disturbance at the point of droplet formation and a rough measurement of L. However, this measurement cannot be made accurately without a strobe and camera arrangement.

Reischl, et al,[12] measured the charge on dry particles. No measurements were made of the droplet charge. During a single run no variation in charge per particle could be measured, indicating a variation of less than ±2%. From one run to another, a variation in $n_{p_o}$ and the coefficient of $V_c$ was observed (see Table VII.

## Charge Measurement Methods

In this study four different methods were developed to measure the charge per particle in order to provide independent checks as well as to establish a convenient procedure. Initially two methods were devised to measure charge on the dry particles of ammonium fluorescein: (I) sampling with a commercial electrical mobility analyzer[13] (EAA) and (II) absolute filtering of dried particles on an electrometer electrode. Difficulties were encountered with the EAA due to wall losses and inability to sample high concentrations of dry particles. Method II was time consuming. Because of these difficulties in charge measurement of dry particles, two new methods were then developed and performed which give information about droplet charge: (III) deflection in a uniform field with a parallel plate mobility analyzer, and (IV) collection of undried aerosol droplets on an electrometer electrode. However, there was the question of whether or not the droplet charge is altered while drying. Zung and Snead[14] observed such an effect. In this study a set of measurements were carried out using methods II and IV to evaluate that possibility. These methods are described below, and results and

Table VII. Average Values and Standard Deviations of Charging Parameters Observed by Reischl, *et al*[12]

| Solute | Number of runs | $n_{p_o}$ | Coefficient of $V_c$ in Eq. (2) |
|---|---|---|---|
| Methylene Blue | 12 | -1640 ± 360 | -1830 ± 670 |
| Potassium Biphthalate | 11 | -5540 ± 910 | -2900 ± 700 |
| Sodium | 5 | -2640 ± 160 | -1140 ± 190 |

evaluations are given in the next section. Method IV turned out to be the most suitable one for this project, while the others provide verification and have desirable possibilities for any future work performed in this area.

Method I: Method I employs a Thermo-Systems Model 3030 electrical aerosol analyzer (EAA). This particular device was designed to sample particles with diameters less than one micron. Several modifications were made to eliminate wall losses so that the electrical mobility of larger particles could be measured. With this device $n_p$ is given by

$$n_p = z_p 6\pi\eta a_p / e\ C \tag{4}$$

where C is the slip correction factor,

$a_p$ is the particle radius known from the VOAG operating conditions,

$\eta$ is the viscosity of air, and

$z_p$ is the electrical mobility in m/volt-sec. The mobility is determined by

$$z_p = K/V = 3.98 \times 10^{-4}/V$$

where K is a constant depending upon the flow and geometry of the analyzer, and

V is the applied voltage in the analyzer at which all particles are collected; i.e., removed from the air flow so that the analyzer current goes to zero.

Method II: With Method II the charge on dry particles versus charging voltage was measured with a filtering system in place of the impactor shown in Figure 22. This method employs an filter membrane made of silver and connected to an electrometer. The ammonium fluorescein aerosol is sampled with the filter at the same flow rate as an impactor. An electrometer measures the total charge collected by the filter. After sampling, washing of the filter with an ammonium hydroxide solution and spectrophotometry of the wash solution determines the total mass of ammonium fluorescein collected. In this method $n_p$ is given by

$$n_p = \frac{4\pi}{3} \frac{Q\rho_{AF}}{eM_t} a_p^3 \tag{5}$$

where $Q$ = charge collected,

$\rho_{AF}$ = density of ammonium fluorescein,

$a_p$ = particle radius, and

$M_t$ = total mass collected.

Method III: In Method III the droplet stream passes between parallel plates as depicted in Figure 21. With a high voltage $V_{HV}$ applied between the plates, the charged droplets could be deflected as indicated. The equations of motion for the droplets are:

$$U_y = \left(\frac{mg}{b} + U_{yo}\right) e^{-bt/m} - \frac{mg}{b}$$

$$y = \left(\frac{m^2 g}{b^2} + \frac{mU_{y_o}}{b}\right)\left(1 - e^{-bt/m}\right) - \frac{mg}{b}t \qquad (6)$$

$$U_x = \frac{n_p e\ V_{HV}}{bd}\left(1 - e^{-b(t-t_B)/m}\right)$$

$$x = \frac{n_p e\ V_{HV}}{bd}\left[t-t_B - \frac{m}{B}\left(1 - e^{-b(t-t_B)/m}\right)\right]$$

where $U_x$ and $U_y$ are the horizontal and vertical components of the droplet velocity,

$t$ = time of flight, $t_B$ = elapsed time at the bottom of the plates,

$U_{y_o}$ = initial droplet velocity = $F_{sy}/\pi(\text{orifice radius})^2$,

$m$ = droplet mass = density of liquid x $F_{sy}/f$,

$g$ = acceleration due to gravity,

$b$ = $6\pi a_d \eta$, where $\eta$ is the viscosity of air, and $a_d$ is the droplet diameter, and

$d$ = separation between the plates.

With $V_{HV}$ = 0 (no deflection) and $U_{yo}$ = 793 m/sec, it was found that the droplets rise much higher (y = 15 cm) than the equations predict (y = 5 cm) using the viscosity of air (182.7 x $10^{-6}$ poise) at standard pressure and temperature. The droplets rise higher because of the movement of air along with the droplet stream. Therefore, the droplets experience a lower viscous drag than they would in still air. An effective viscosity of 57 x $10^{-6}$ poise was determined which gives the correct height of the flight with $V_{HV}$ = 0. This value was then used in the determination of $n_p$ with $Y_T$, $Y_B$, $V_{HV}$, and d known. The stream of charged droplets does not spread due to the applied field $V_{HV}$, thus demonstrating a uniformity of the charge per droplet within a few percent.

Method IV: Another method (IV) employed to measure droplet charge collects the droplets onto an aluminum foil electrometer electrode as they pass through the charging plate. The electrode is a hollow cylinder with a hole at the bottom for the droplets to enter. The top of the cylinder is covered with fine mesh metal netting (pore size, 0.16 mm, and 36% open) to allow air to flow through. With this arrangement $n_p$ is given by

$$n_p = \frac{I}{fe}$$

where I = electrometer current,

f = frequency of the oscillator driving the VOAG, and

e = elementrary unit of charge.

The electrode can be inserted and charge measured before and after an impactor sampling run.

Two variations of this method were attempted in search of a measurement method which can be used during impactor runs. An electrode with the same cylindrical shape was formed entirely of fine mesh metal netting. In one variation, a high voltage wire was placed along the cylinder axis. This wire, having the same polarity as the droplets, enhances the collection efficiency of the netting. With the high voltage wire at zero volts a large portion of the charged aerosol passes through the net electrode and is sampled by the impactor. Then, to intermittently measure the particle charge, the voltage on the wire can be increased to collect the aerosol on the electrode. In the other variation of this method, the cylinder, made of metal netting, is used without the high voltage wire. The dispersion and drying air can be varied to give a high collection efficiency for the electrode during charge measurement and then changed to values which reduce the droplet collection of the electrode so

that impactor sampling can proceed. Although both of these variations showed promise, time did not permit sufficient refinement to justify their use in the final analysis of impactor behavior.

## Evaluation of the Charged Particle Generator

The behavior of the charged particle generator has been characterized with the four methods of charge measurement described above. The results are depicted in Figures 23 and 24 where $n_p$ is plotted as a function of charging voltage $V_C$. Figure 23 shows the full range of $V_C$ employed, while Figure 24 gives a better view for small $n_p$.

The open triangle in Figure 23 depicts the charge measured on droplets using Method III. The single point given was determined from the average of three $V_C$-values taken on different occasions with $V_{HV}$ = 2000V. The procedure in this measurement was to vary the charging voltage $V_C$ to deflect the stream to the top of one plate as shown in Figure 21. This value varied by ±6%. The most likely source of error in this calculation is the estimation of the effective viscosity in Equation (6).

The measurements using Method IV, cylindrical electrode made of foil, are depicted by the solid line in Figure 23. This line is a least squares fit to Eq. (3) from 33 measurements obtained in four different runs over a period of two weeks. The fluctuation of measured $n_p$ values from this line were low as judged from the coefficient of determination (= 0.997 where 1.000 is a perfect fit). The value of $n_{p_o}$ is -3050 ±580 and the coefficient of $V_C$ (slope of the line) is 1280 ±20 volt$^{-1}$. These results are comparable to those of Reischl, et al[12] for sodium chloride (see Table VII).

The measurements on dry particles, denoted by open circles, were obtained with the modified EAA. These results are more easily viewed in Figure 24 where the lower quarter of Figure 23 is reproduced. These measurements with the EAA are consistent with the results of the other methods. Although the preliminary results shown in Figures 23 and 24 were obtained by this method, attempts to repeat this measurement were unsuccessful. The problem was that no stable current of any significance (>$10^{-14}$ amps) was produced by charged particles passing through the device. Apparently, the wall losses were too great and the number of particles sampled too small.

The data obtained by Method II for dry particles is depicted by closed circles in Figure 23. Although time consuming, these measurements are important because Zung and Snead[14] observed a

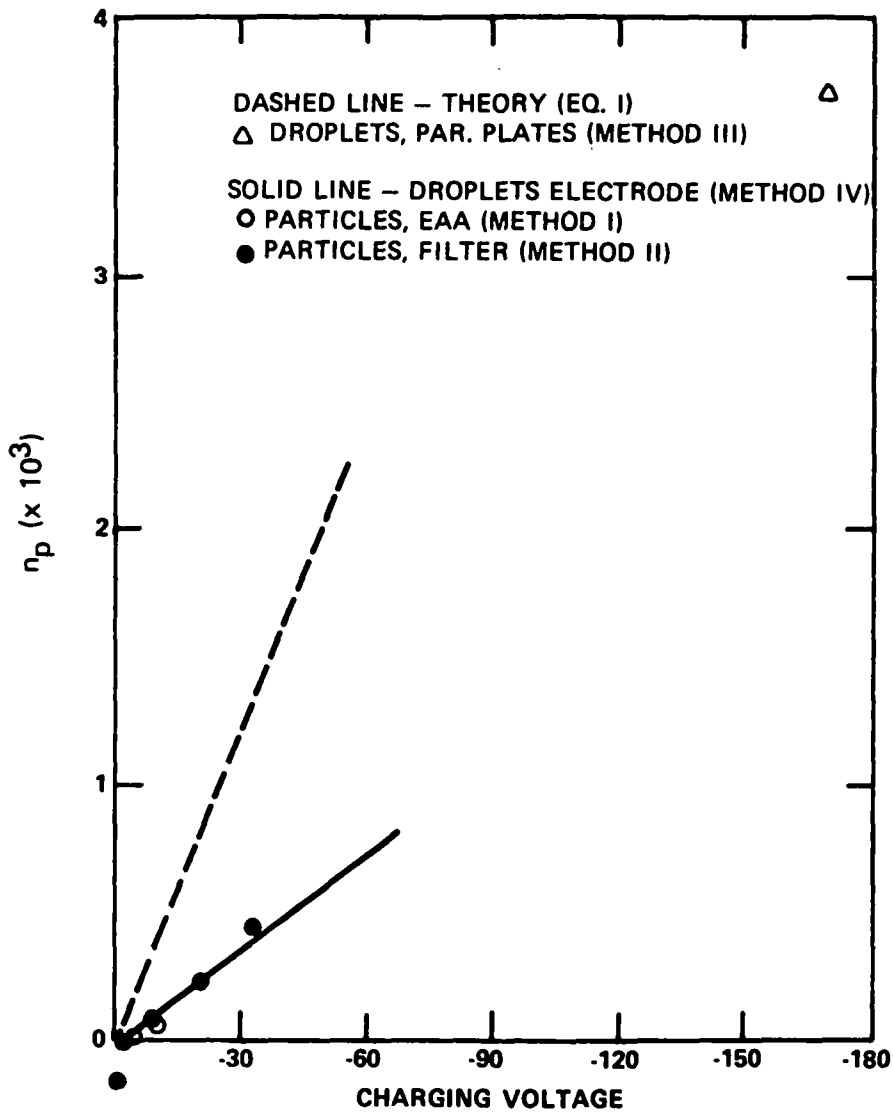


*Figure 23. Particle Charge Versus Charging Voltage as Determined by Methods I – IV. ($a_p$ = 2.6 μm and $a_d$ =23 μm)*

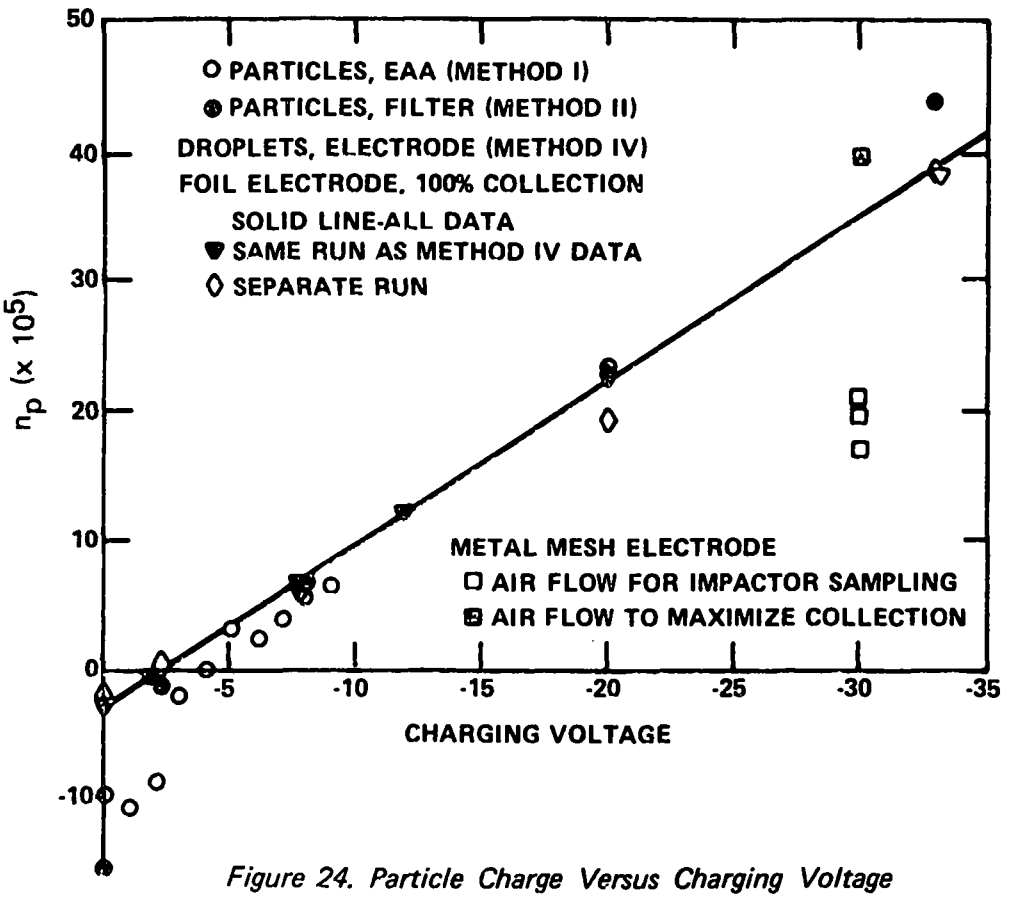


*Figure 24. Particle Charge Versus Charging Voltage*

change in charge of droplets while drying. The agreement between measurements using Methods II, III, and IV eliminate this possibility and thus justify the use of Method II which determines particle charge from the droplet charge measurement.

The dashed line in Figure 23 gives the predictions of Eq. (3) where the parameters L, H, and $\alpha$ were measured independently of $n_p$. Since $n_{po}$, the charge given to particles in the spraying process cannot be predicted, its value in Figure 23 was set as that obtained by Method IV. The length of the jet [L in Eq. (3)] at droplet formation was measured to be $6 \times 10^{-2}$cm ±10%. However, the end of the jet is difficult to locate without high-speed photography. This difficulty causes additional uncertainty in the measurements.

As indicated, Figure 24 gives a more detailed view of the lower part of Figure 23. In addition some data points obtained with Method IV are shown. For the foil electrode one set is shown which was measured in the same run as the Method II data. Another set, obtained in a separate run, is plotted to show the variation one may expect from one run to another.

The data depicted by squares in Figure 23 are presented to illustrate data which may be obtained with the two described variations of Method IV. The data shown as open squares are a result of the metal-mesh electrode with a high voltage wire along the electrode axis. The several values given for $n_p$ at constant $V_c$ are for different levels of this high voltage: 0, 1000, and 2000 volts. The higher $n_p$ values correspond to greater collection efficiencies. Although a 100% collection efficiency was not achieved in this series of measurements, it can be, as shown by the data point depicted by a solid square. This datum was the result of adjusting the dispersion and drying air of the VOAG to maximize the electrometer current with the high voltage wire at zero volts. Data concerning the variations of Method IV is given only to illustrate the possibility for use in further work if the ability to monitor particle charge is important.

The solid line in Figure 24 is being used as the calibration curve for the charged particle generator. Its agreement with Methods I and II and the results of Reisch, et al[12] justify its use. In addition to the calibration, further measurements of particle charge with Method IV were performed before and after most impactor sampling runs.

## Impactor Data

Impactor sampling data are given in Figures 25 through 39 in the form of histograms. Each figure shows data from one

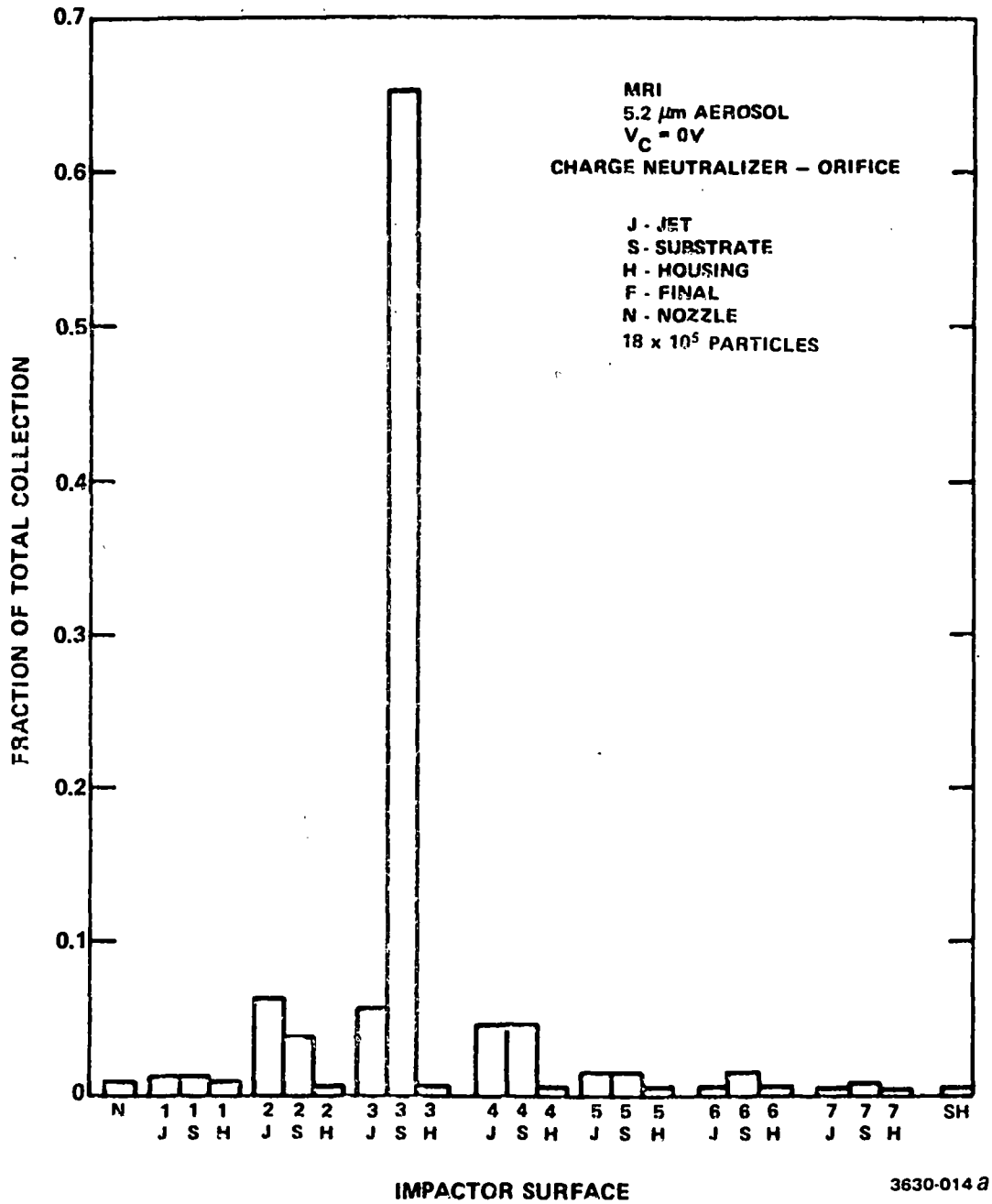


*Figure 25. Control sampling run using MRI-Model 1502 Impactor with no charge.*

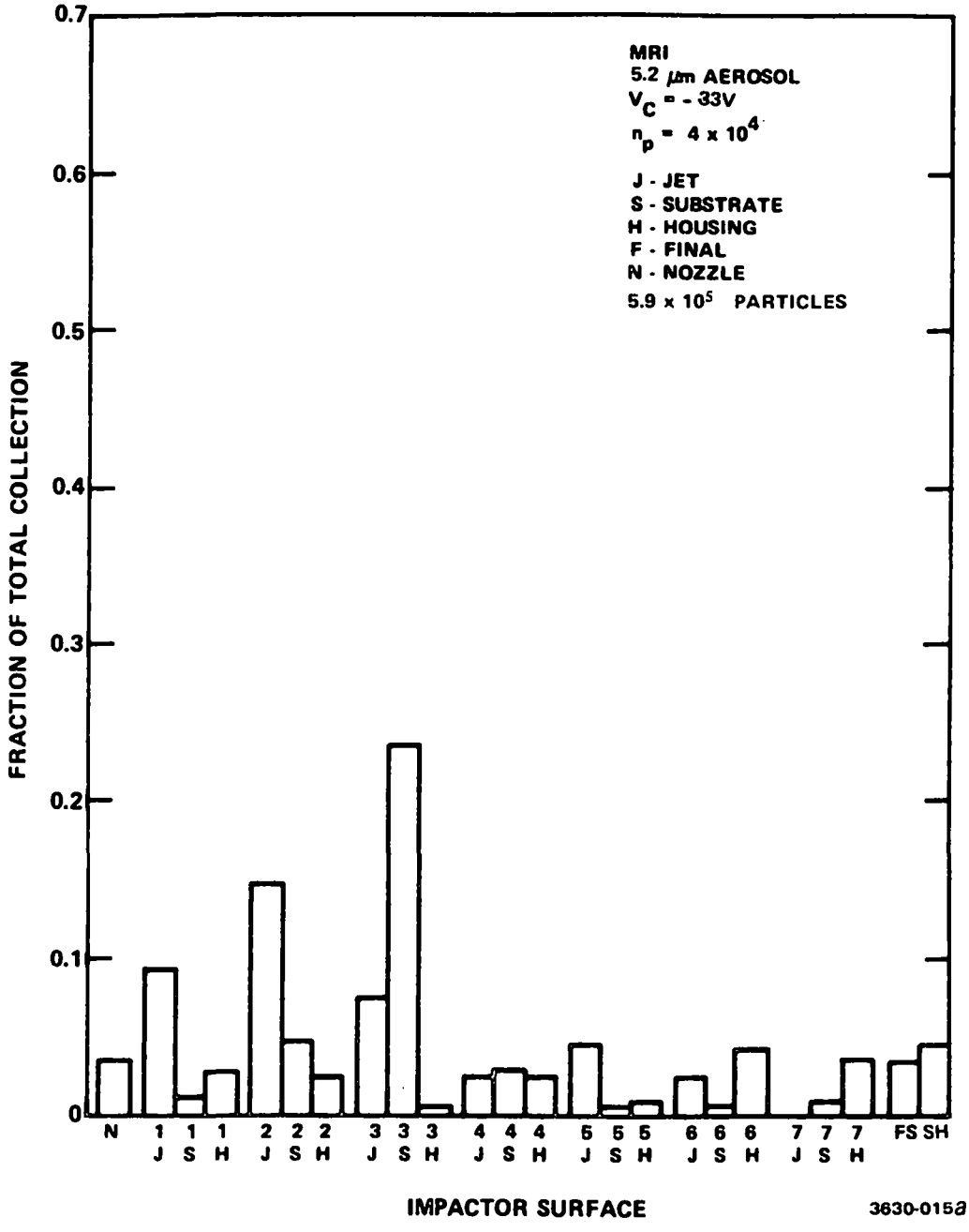


*Figure 26. Sampling charged particles using MRI-Model 1502 Impactor with no grounding wire— high particle charge. (See Figure 25 for comparison.)*

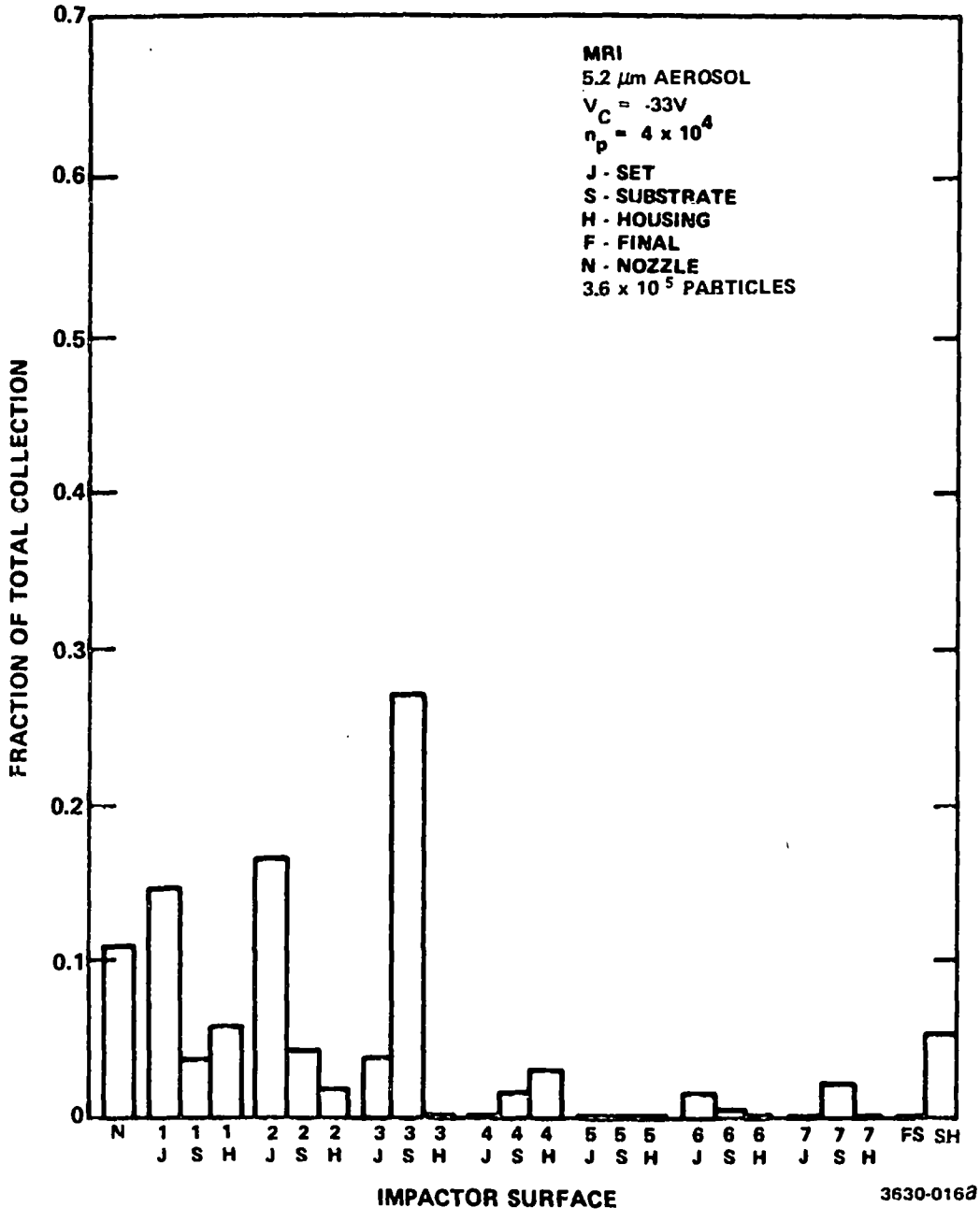


*Figure 27. Sampling charged particles using MRI-Model 1502 Impactor with grounding wire - high particle charge (See Figure 25 and 26 for comparison.)*

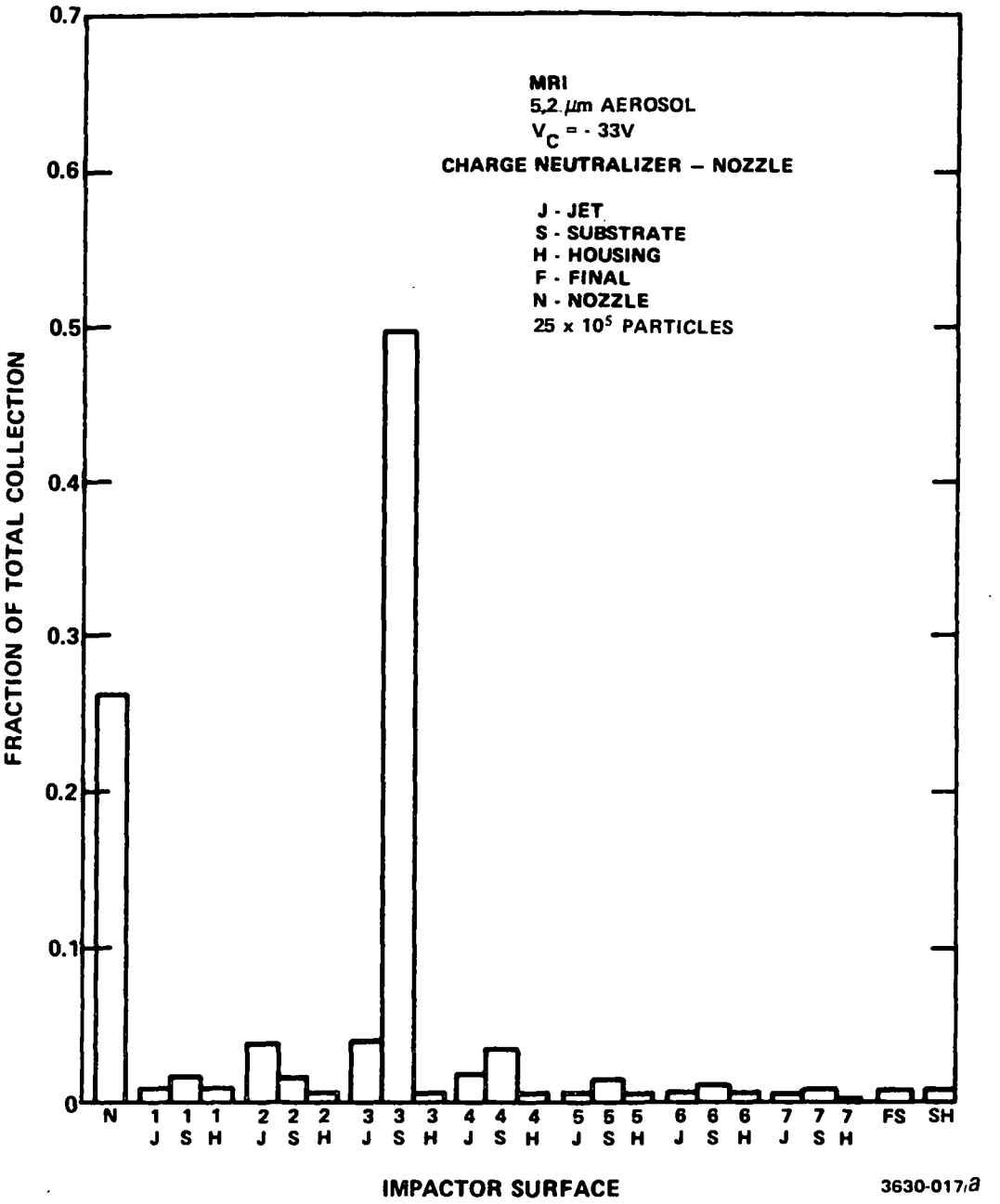


*Figure 28. Sampling charge-neutralized particles using MRI-Model 1502 Impactor with neutralizer at nozzle - $n_p = 4 \times 10^4$.*

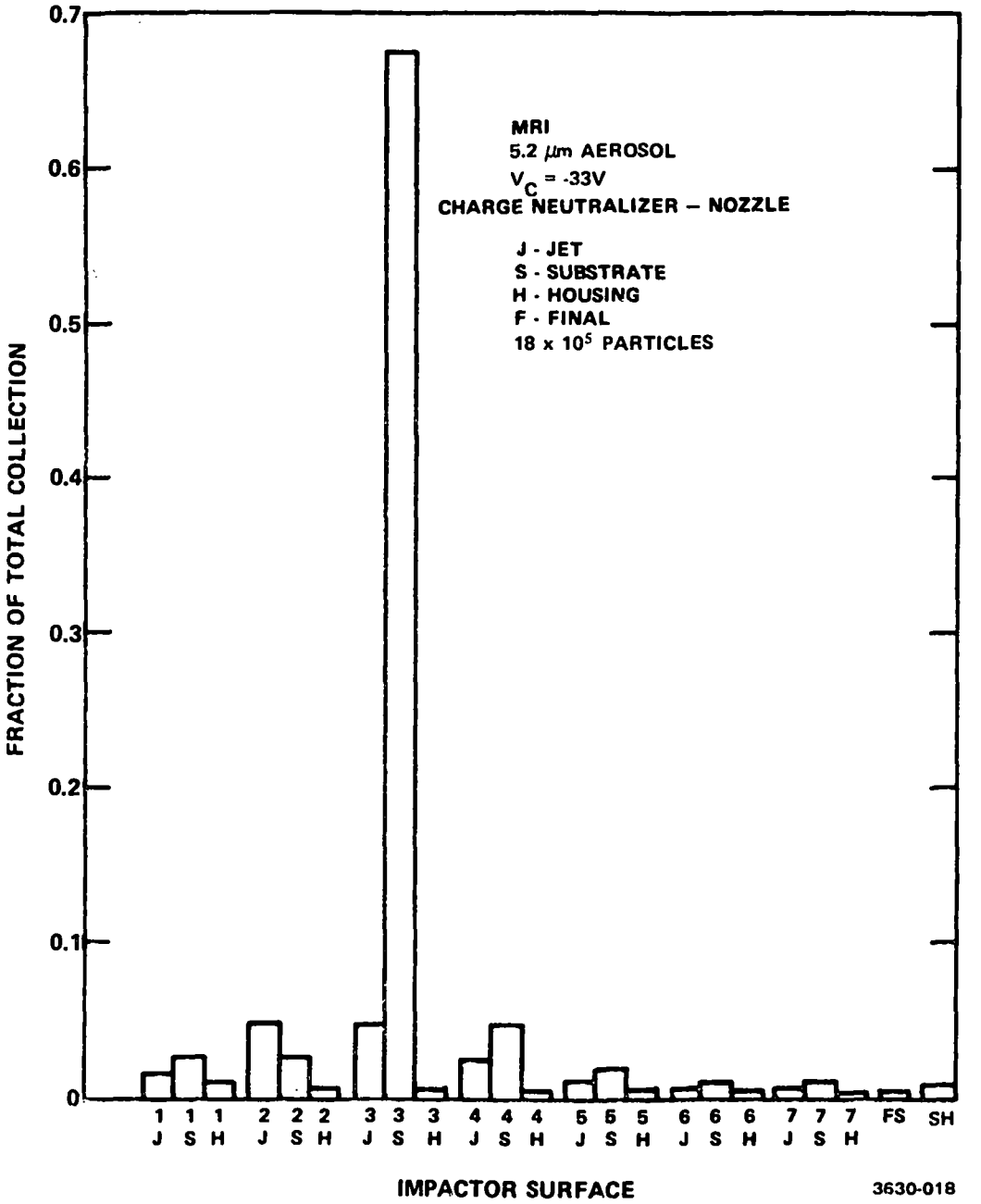


*Figure 29. Sampling charge-neutralized particles using MRI-Model 1502 Impactor with nozzle losses corrected. (Run data identical to Figure 28.)*

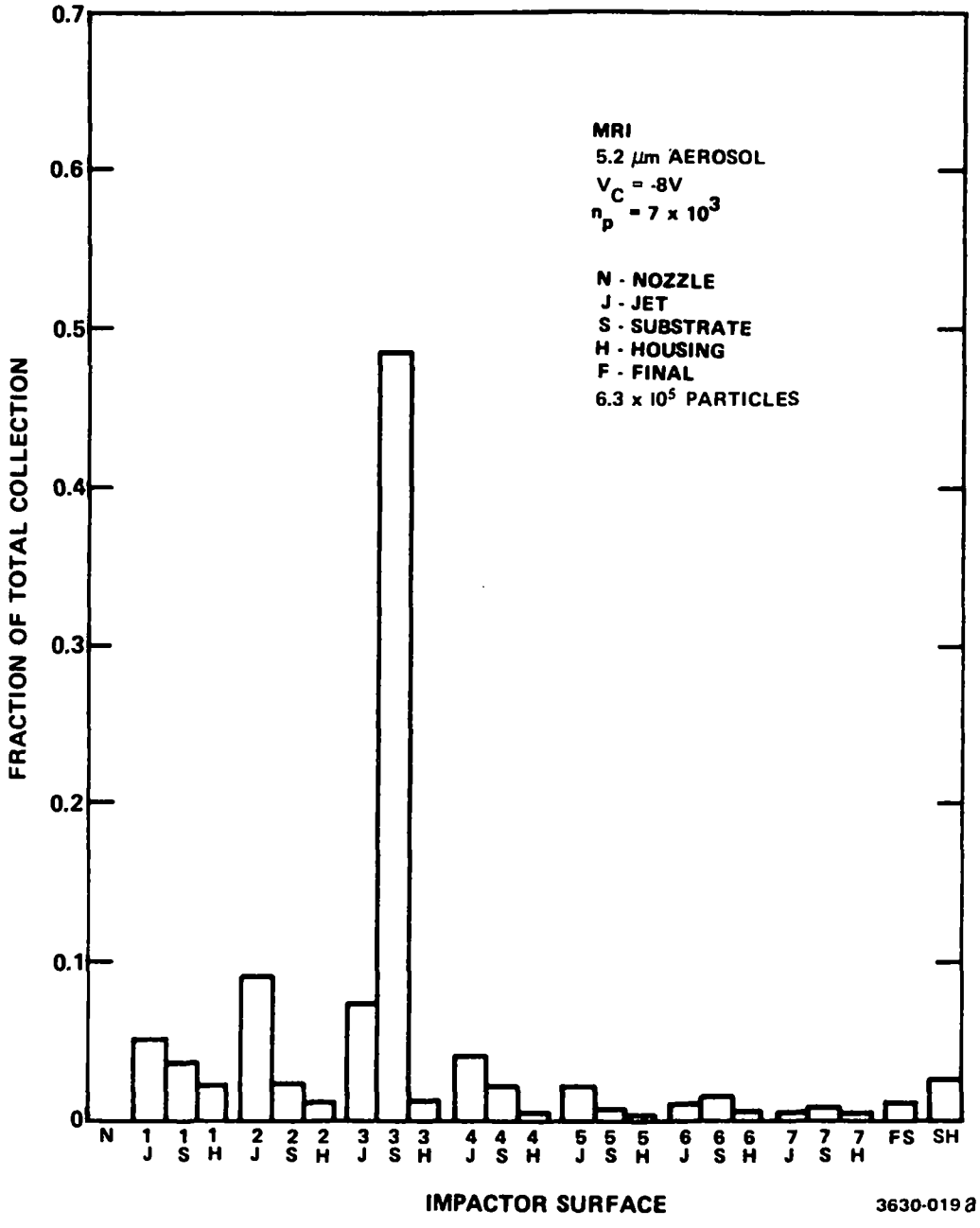


*Figure 30. Sampling charged particles using MRI-Model 1502 Impactor with grounding-wire moderate particle charge. (See Figures 25 and 27 for comparison.)*

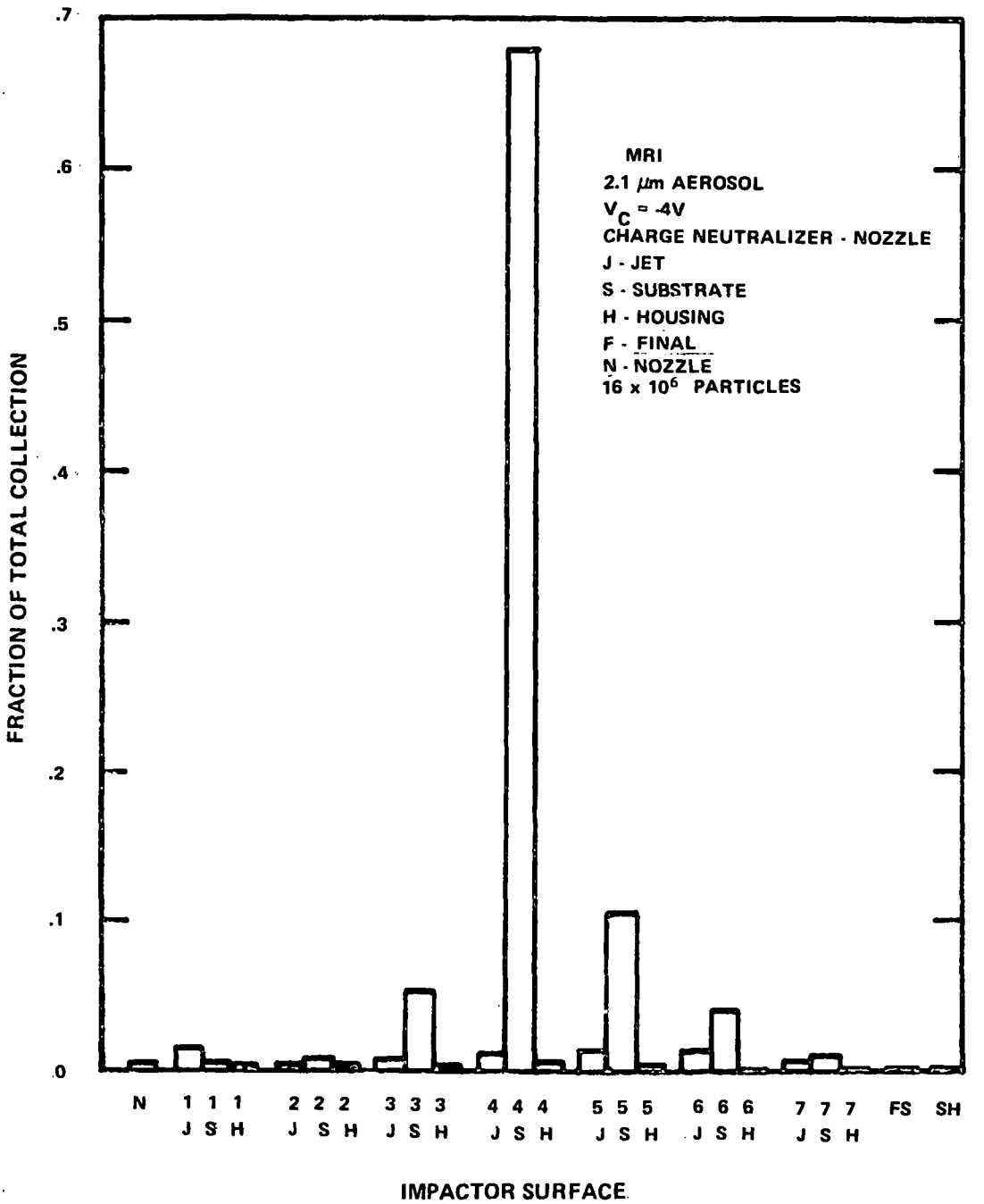


*Figure 31. Sampling charge-neutralized particles using MRI-Model 1502 Impactor with neutralizer at nozzle - $n_p$ = 2.4 x $10^3$. See Figure 29 for comparison with 5.2 μm aerosol data.*

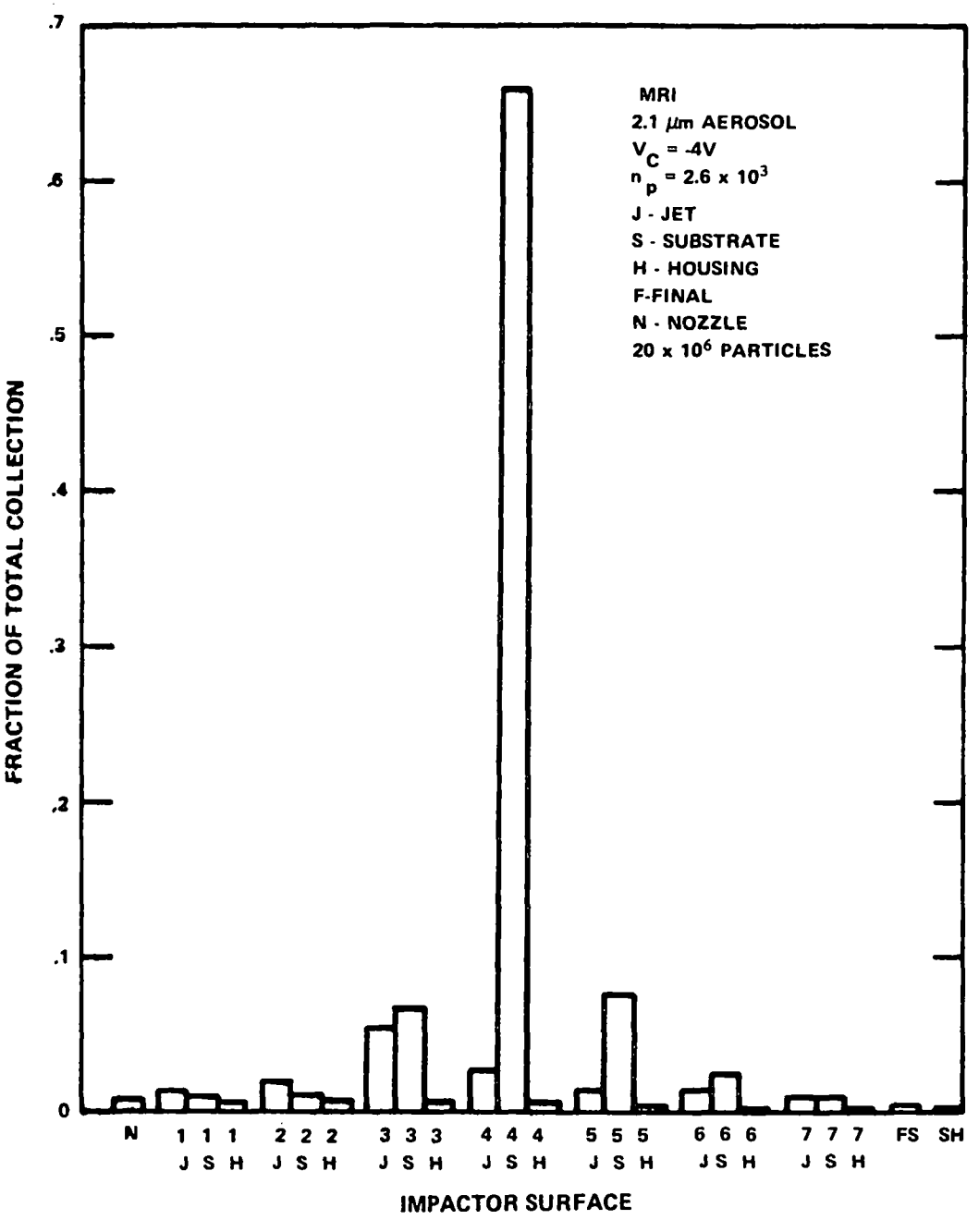


*Figure 32. Sampling charged particles using MRI-Model 1502 Impactor with grounding wire - moderate particle charge. (See Figure 30 for comparison.)*

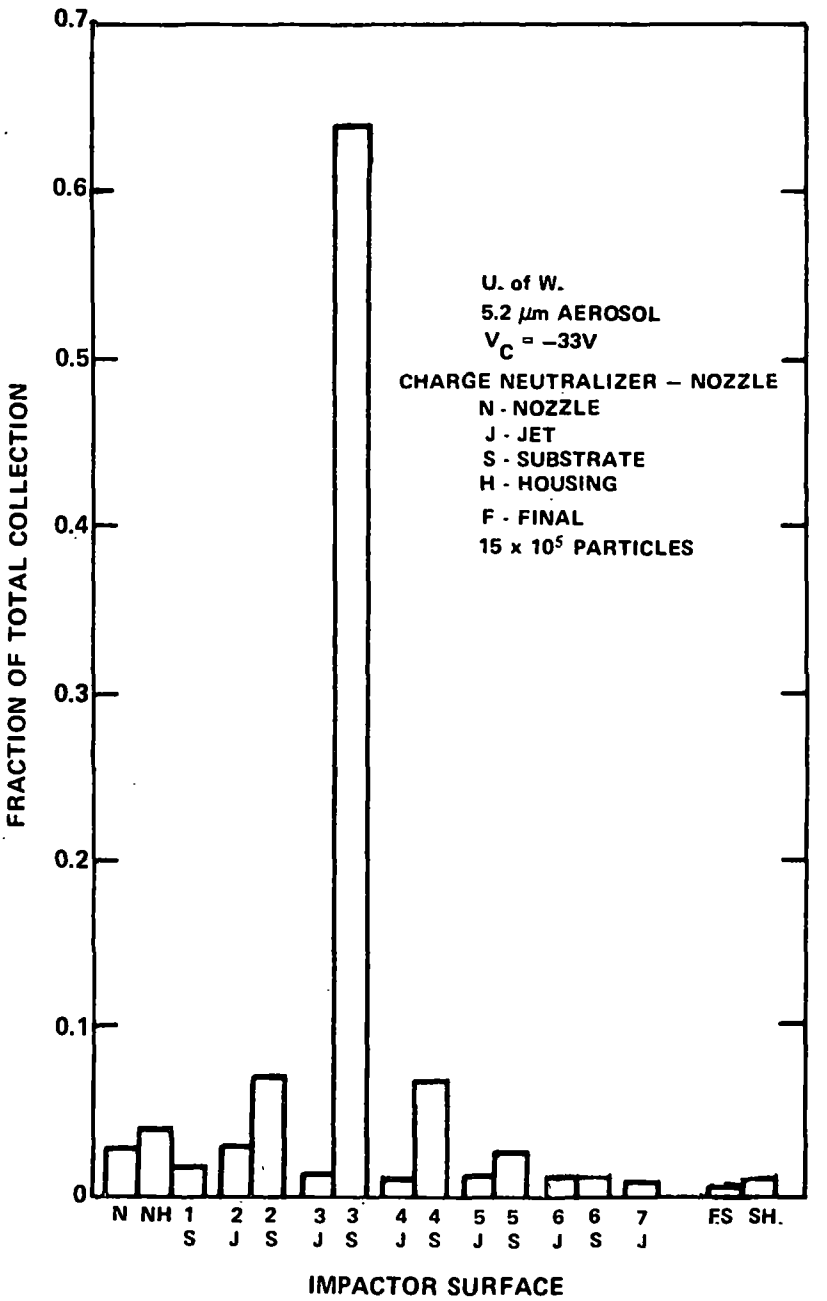


*Figure 33. Sampling charge-neutralized particles using U. of W. Mark III Impactor with charge neutralizer at nozzle - $n_p = 4 \times 10^4$.*

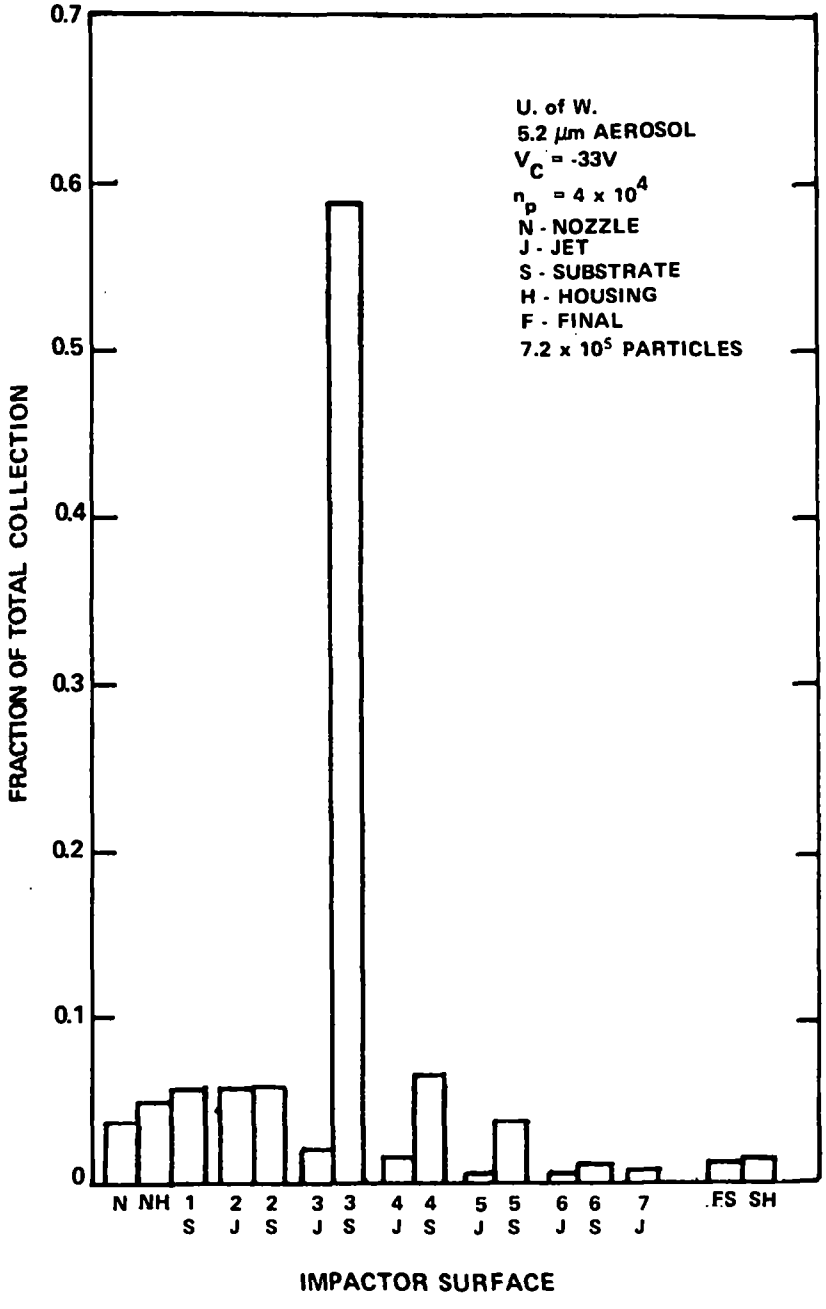


*Figure 34. Sampling charged particles using U. of W. Mark III Impactor with no grounding wire - high particle charge. (See Figure 33 for comparison.)*

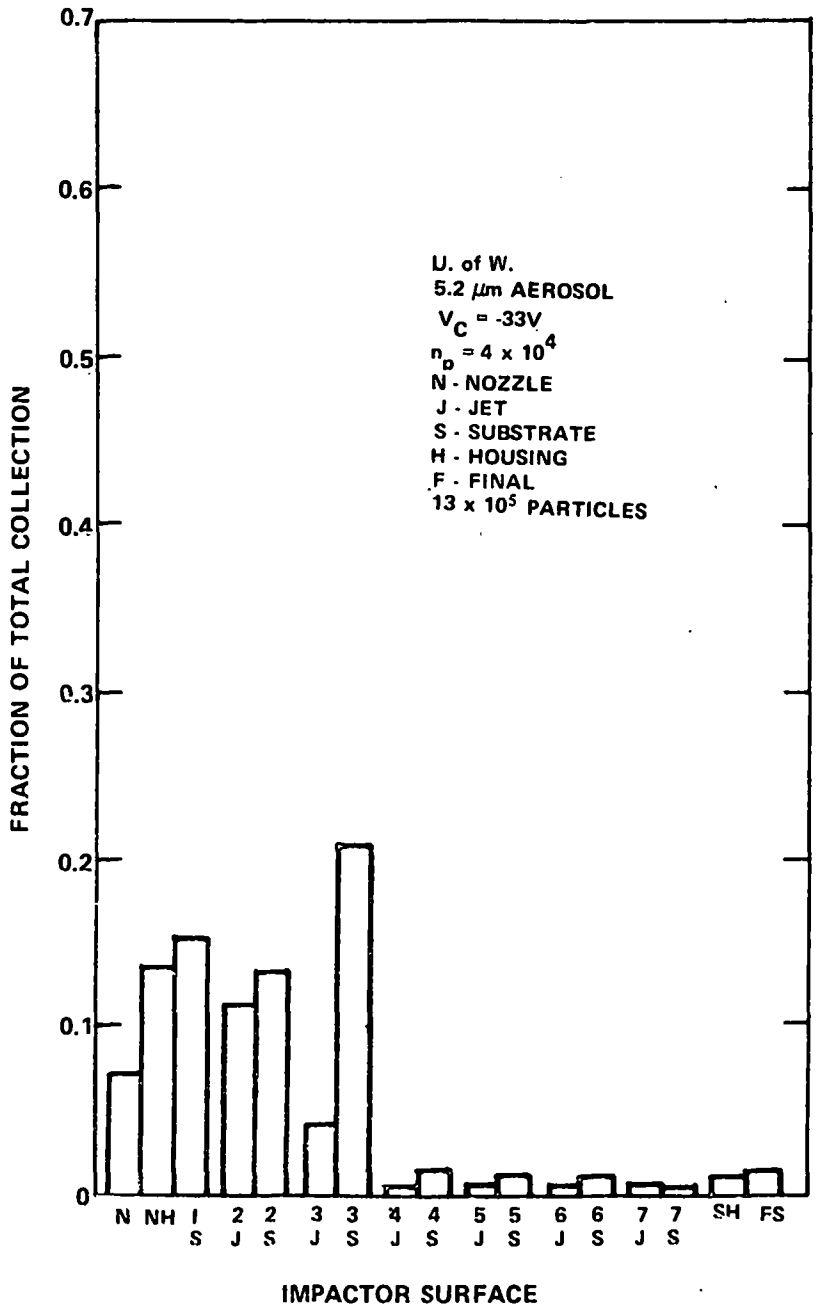


*Figure 35. Sampling charged particles using U. of W. Mark III Impactor with grounding wire - high particle charge. (See Figures 33 and 34 for comparison.)*

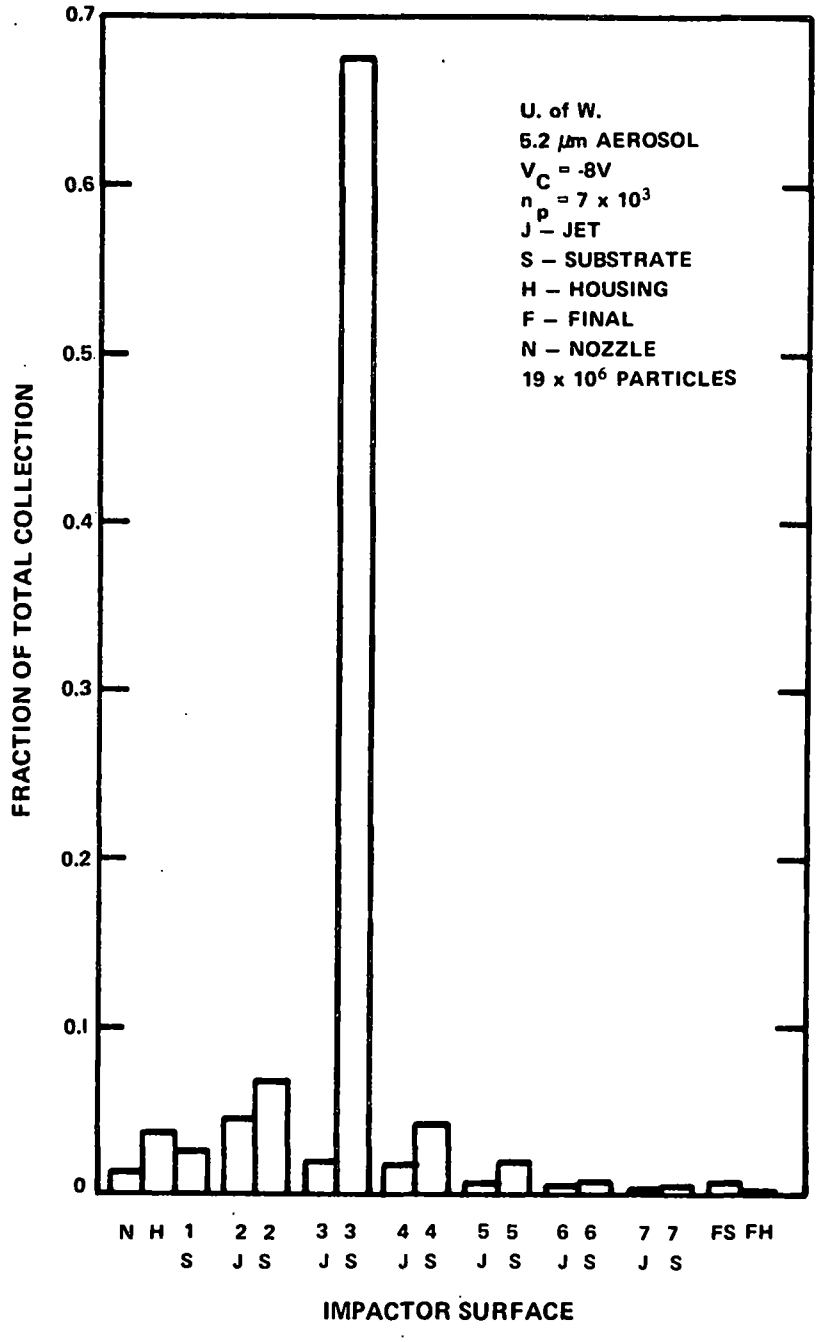


*Figure 36. Sampling charged particles using U. of W. Mark III Impactor with grounding wire - moderate particle charge. (See Figures 33 and 35 for comparison.)*

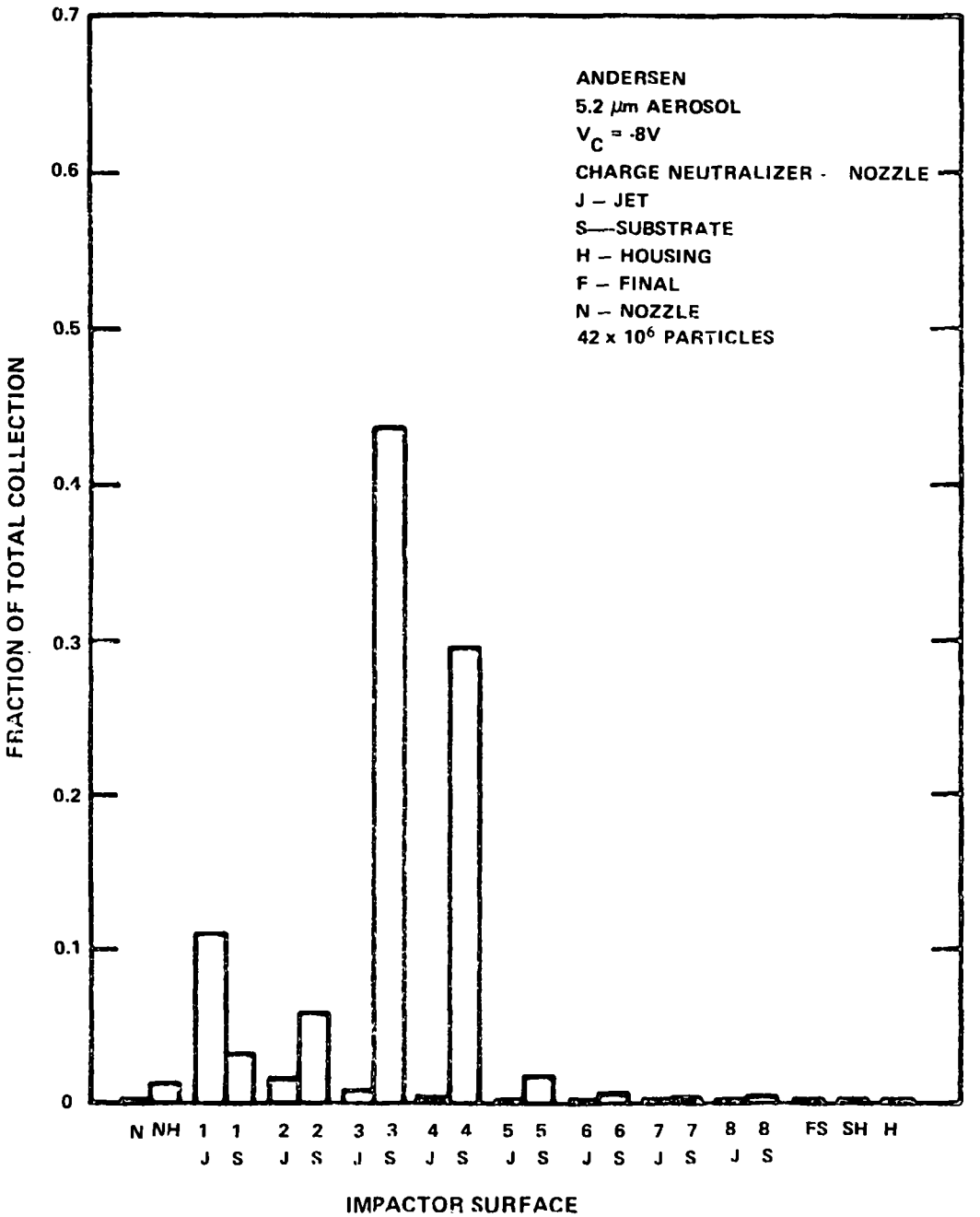


*Figure 37. Sampling charge - neutralized particles using Andersen Mark III Stack Sampler with neutralizer at nozzle - $n_p = 7 \times 10^3$.*

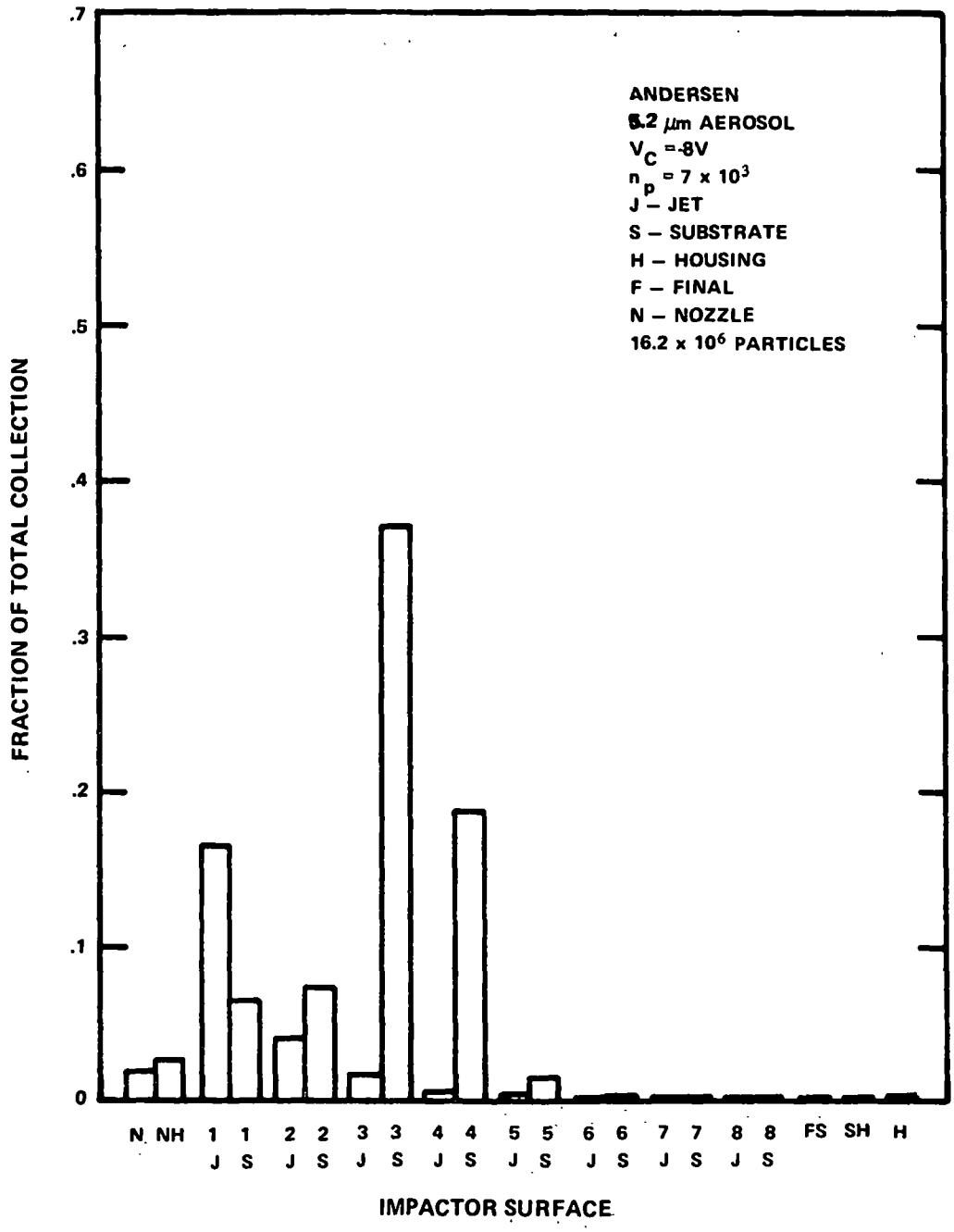


*Figure 38. Sampling charged particles using Andersen Mark III Stack Sampler with grounding wire - moderate particle charge. (See Figure 37 for comparison.)*

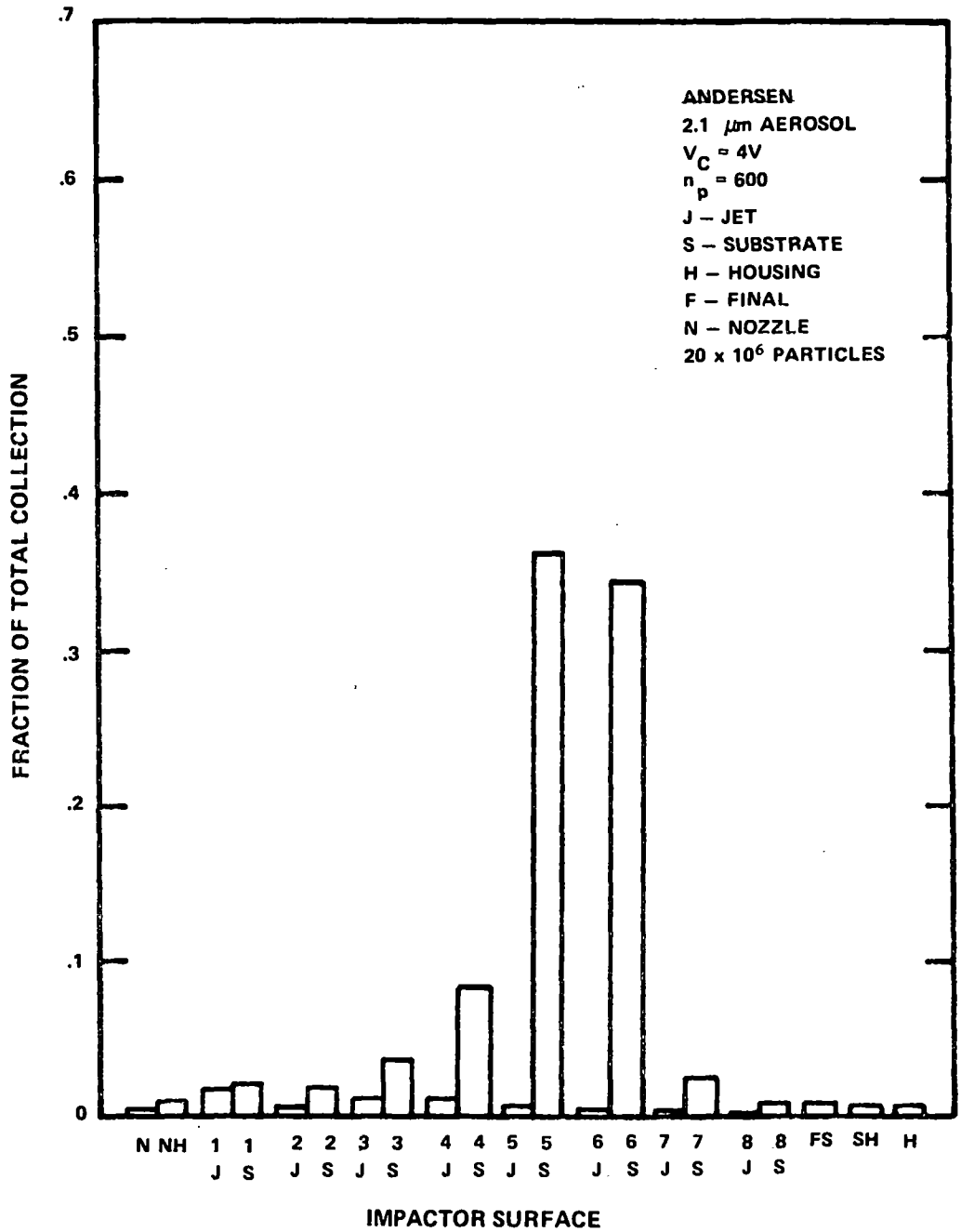


*Figure 39. Sampling charged particles using Andersen Mark III Stack Sampler with grounding wire - moderate particle charge.*

sampling test; the fraction of total particles collected is given for each surface in the impactor starting with the nozzle and ending with the housing of the absolute filter at the exit. The surfaces are distinguished according to nozzle, jet plate, substrate, and housing if separable. Each of these surfaces was washed separately and the mass of fluorescein in the wash water determined with a spectrophotometer.

The parameters varied in these tests were particle size (5.2 μm and 2.1 μm), particle charge, electrical grounding, and the use of a charge neutralizer. The sampling times, varied between one to one-and-a-half hours. However, the total number of particles sampled was smaller for highly charged particles, a result of greater wall losses in the drying chamber.

All sampling tests were performed at ambient conditions with the same flow rate, 14 LPM. The impactor nozzles were 1.27 cm (0.5 in.) in diameter giving a gas velocity of 1.84 m/sec. The stream velocity where sampling occurred was approximately one m/sec. Glass fiber substrates were employed in each test.

MRI Impactor: Figures 25 through 32 show MRI Model 1502 Cascade Impactor data (Figures 25-30 for 5.2 μm diameter and 31-32 for 2.1 μm diameter particles).

Figure 25 shows data for a "reference" run with no particle charge. The data shown in Figure 26 is for particles with about $4 \times 10^4$ charges and an electrically isolated impactor. The increase in the number of particles collected on the nozzle and metal jet plates is quite significant. Also there appears to be a slight increase in the number reaching the stages below number three. Figure 27 repeats the data of Figure 26 with the impactor electrically grounded. The collection efficiency of the nozzle and stage one jet plate (1J) apparently increased. However, only the nozzle and 1J of the MRI can be grounded from the outside due to an anodized coating. In these measurements a grounded wire was wrapped around the threads between 1J and its substrate housing. The resistance between ground and 1J and 2J was measured to be of the order of $10^9$ ohms with the grounding wire and about 15% higher without the grounding wire.

Figure 28 presents a sampling run with identical operating conditions to that of Figure 27 except that a charge neutralizer was mounted upstream of the impactor nozzle. The neutralizer is a polonium 210 strip made by Nuclear Products Company. For use with an impactor it is bent to form a ring and placed at the entrance to the nozzle. In Figure 28 the high collection on the nozzle is thought to be a result of turbulence induced by the charge neutralizer. Collection efficiencies were calculated

excluding the nozzle losses. These values are given in Figure 29. Comparing this figure to Figure 25 shows that indeed the effect of particle charge is eliminated by the ion source neutralizer. After this run the mount was changed to produce less disturbance to the flow.

Figures 26 and 27 show an effect of high particle charge upon impactor behavior. Here, the charge level was higher than encountered in most effluent streams. In the run depicted in Figure 30 the charge per particle is approximately $7 \times 10^3$ elementary charges, approximately that expected in a precipitator. Collection by the stage 3 substrate (3S), is nearly twice that with $4 \times 10^4$ charges/particle (Figure 27) but is still 15% less than with no charge (Figure 25). These data indicate that in sampling 5.2 μm diameter particles exiting a precipitator, approximately 25 percent of the particles collect on surfaces due to their charge and not size. This conclusion is based on the assumption that all particles exiting a precipitator have the level of charge predicted by Eq. (1).

Figures 31 and 32 show the effect of moderate charge on 2.1 μm diameter particles. 3J and 4J again show an increased collection when charged particles are sampled. However, the effect for 2.1 μm particles charged to saturation is much smaller than with the larger particles at saturation.

University of Washington: Figures 33 through 35 show data obtained from the University of Washington Mark III Impactor in sampling 5.2 μm diameter particles with $4 \times 10^4$ charges per particle. Figure 31 shows results with the charge neutralizer and Figures 32 and 33 without the neutralizer. The impactor was grounded electrically in the run depicted in Figure 32 and was not in Figure 33. It is seen that particle charge effects the collection efficiency of the various surfaces. The behavior of the U. of W. impactor is similar to that of the MRI impactor except that the use of a grounding lead appears to produce a greater change in the deposition of charged particles for the U. of W. impactor.

The results obtained with the moderate charge level, $7 \times 10^3$ elementary charges, on 5.2 μm particles are shown in Figure 36. Comparison of these data with those in Figure 33 shows no significant effect due to this charge level on surface collection efficiency.

Andersen: Figures 37 and 38 show data obtained with the Andersen Mark III Stack Sampler when sampling 5.2 μm diameter particles with the moderate charge level. Comparison of these two figures shows a significant difference in the fraction of particles collected upstream of stages three and four. As with

the MRI impactor about 25 percent of the 5.2 μm particles with moderate charge collect on wall and jet surfaces because of their charge rather than size.

Figure 39 shows sampling data for particles with 2.1 μm diameters and moderate charge, 600 elementrary charges. The control run for this data; that is, the sampling of neutral particles with 2.1 μm diameters, had to be discarded because of an apparent syringe pump malfunction. However the agreement of the data in Figure 39 with impactor theory for neutral particles and a previous sampling study[11] shows that no significant effect of charge was present in sampling the 2.1 μm particles.

In the following section the data shown in Figures 25 through 39 are presented in terms of collection efficiency per stage versus Stokes number for different levels of charge.

## Particle Deposition Patterns

The deposition patterns of fluorescein particles on impactor surfaces were observed with ultraviolet light, and in the presence of a water mist to enhance the fluorescence.

Photographs in Figures 40 and 41 show representative deposition patterns of particles on the top and bottom of jet plates and on substrates in the MRI impactor. Most particles, lost to jet plates, are on the downstream side of the plate as shown in these photographs. This pattern is visible with both charged and uncharged particles, but more particles are deposited on the plates in the charged case. Apparently, particles pass in the vicinity of these surfaces whether charged or not. As expected, the U. of W. impactor, with a similar geometry, had deposition patterns similar to these on the MRI.

Collection efficiencies of jet plates in the Andersen impactor were also slightly higher for charged particles than for neutral ones. Also, substantial numbers of charged particles were observed to be deposited on the upper surface around jets as well as the back surface. The photographs in Figures 42-44 illustrate the Andersen deposition data.

## Nonconducting Jet Plates

In an effort to study the effect that jet plates made from an insulated material would have on deposition due to charge on particles, plates 2J, 3J, and 4J were fabricated of plexiglass for the MRI impactor in an attempt to eliminate the effect. The data for this experiment are shown in Figure 45. Comparison with Figures 25 and 30 show two significant differences. First, the stage cut points seem to be shifted to larger sizes. The origin

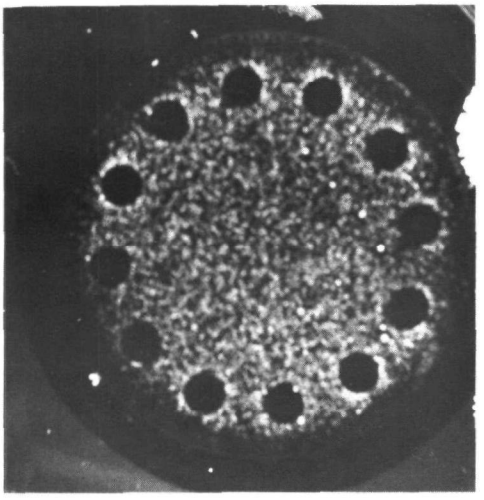

FRONT OF SECOND JET PLATE

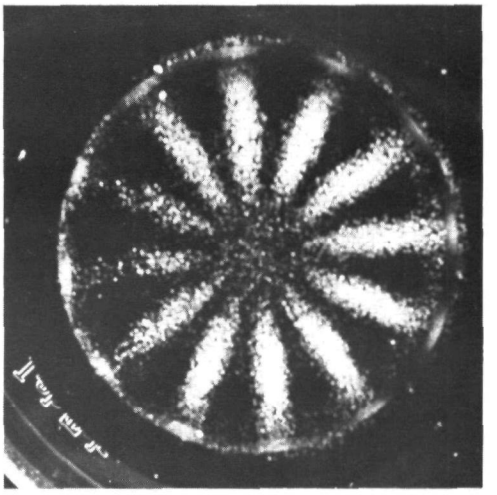

BACK OF SECOND JET PLATE

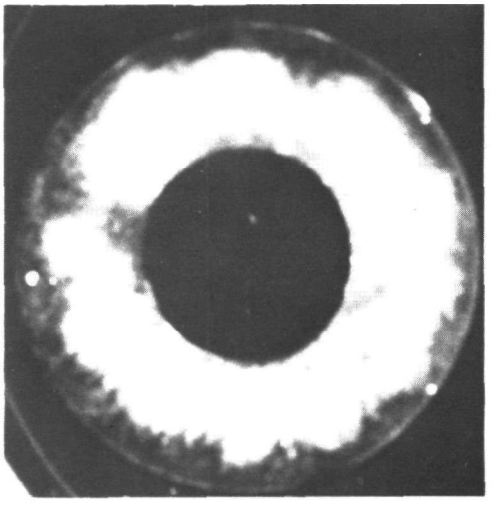

SECOND SUBSTRATE

3630-024

*Figure 40. Photographs of deposition patterns of ammonium fluorescein particles in MRI-Model 1502 Impactor. Particle diameter was 5.2 μm. Sampling test data is in Figure 27.*

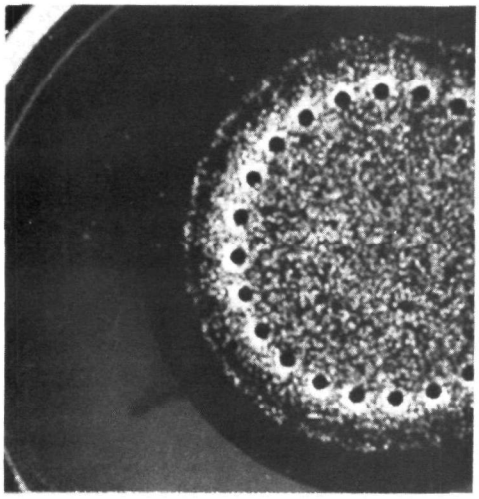

FRONT OF THIRD JET PLATE

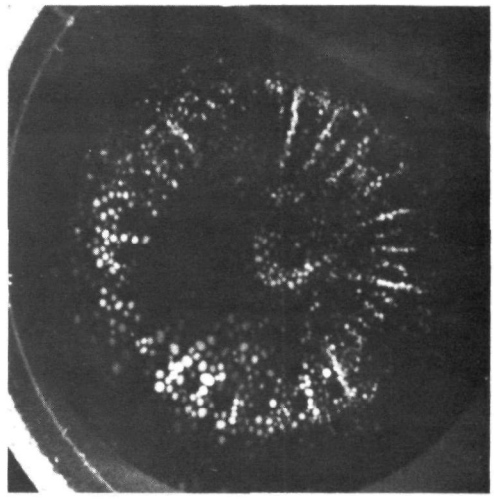

BACK OF THIRD JET PLATE

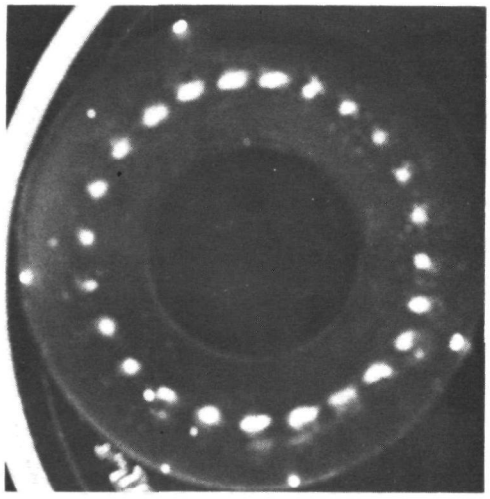

THIRD SUBSTRATE

3630-023

*Figure 41. Photographs of deposition patterns of ammonium fluorescein particles in MRI-Model 1502 Impactor. Particle diameter was 5.2 um. Sampling test data is in Figure 27.*

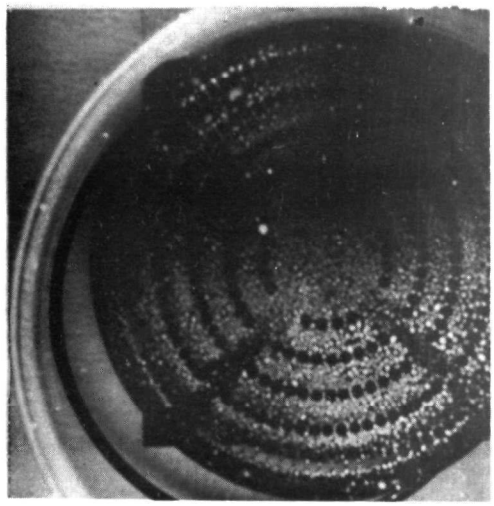

FRONT OF FIRST JET PLATE

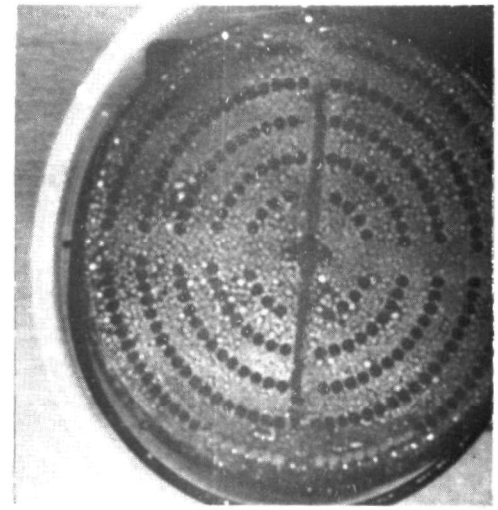

BACK OF FIRST JET PLATE

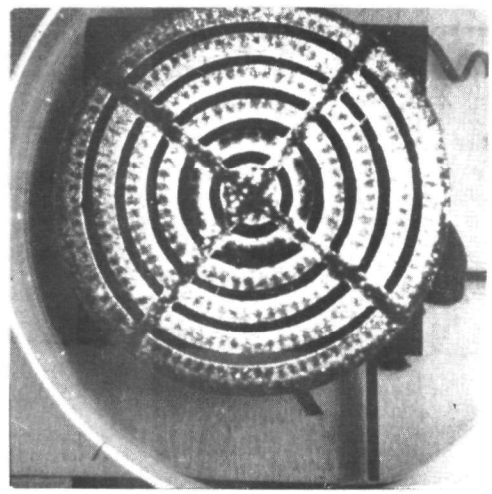

FIRST SUBSTRATE

*Figure 42. Photographs of deposition patterns of ammonium fluorescein particles in Andersen Mark III Stack Sampler. Particle diameter was 5.2 μm. Sampling test data is in Figure 38.*

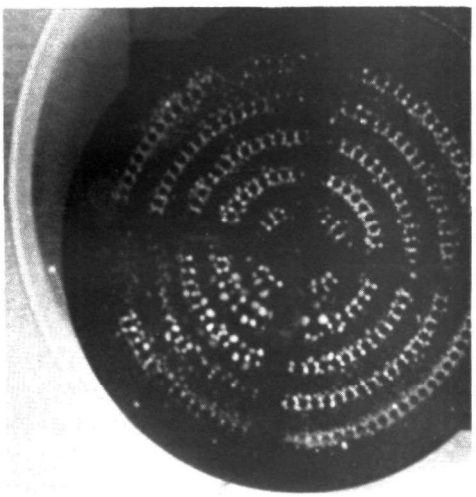

FRONT OF SECOND JET PLATE

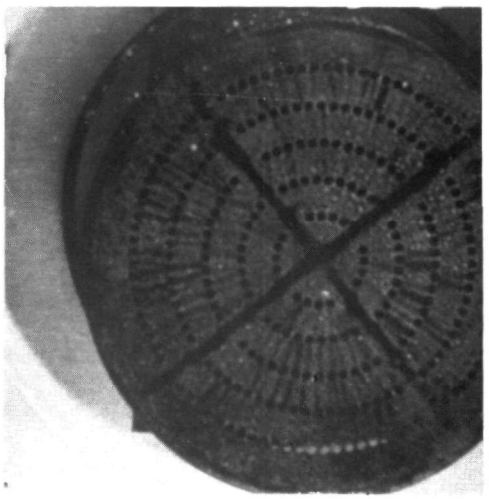

BACK OF SECOND JET PLATE

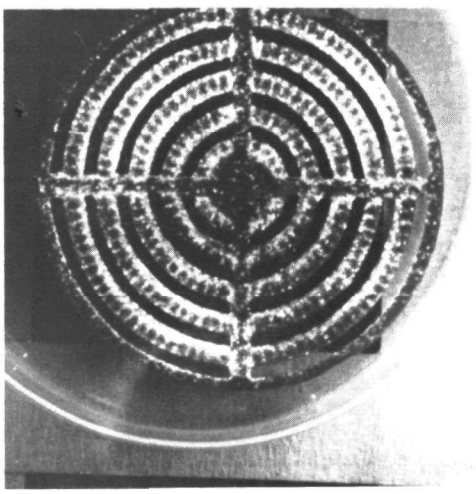

SECOND SUBSTRATE

*Figure 43. Photographs of deposition patterns of ammonium fluorescein particles in Andersen Mark III Stack Sampler. Particle diameter was 5.2 μm. Sampling test data is in Figure 38.*

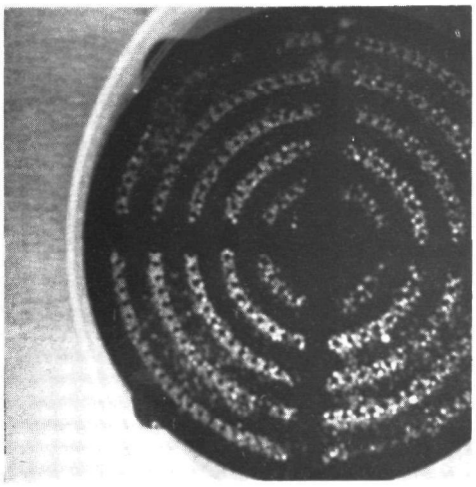

FRONT OF THIRD JET PLATE

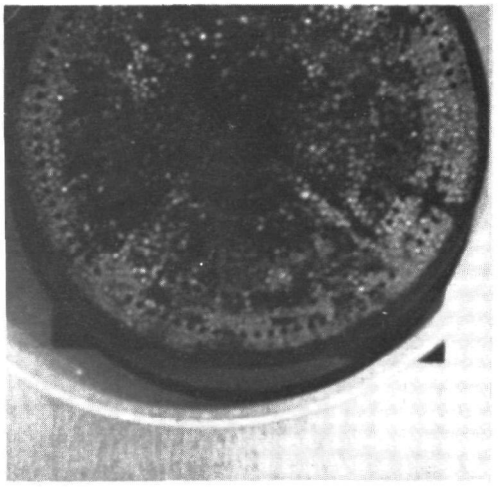

BACK OF THIRD JET PLATE

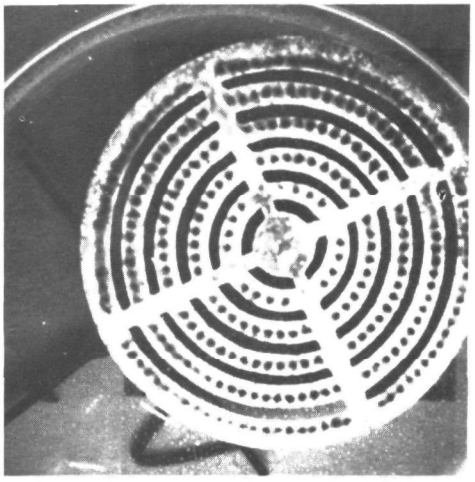

THIRD SUBSTRATE

*Figure 44. Photographs of deposition patterns of ammonium fluorescein particles in Andersen Mark III Stack Sampler. Particle diameter was 5.2 μm. Sampling test data is in Figure 38.*

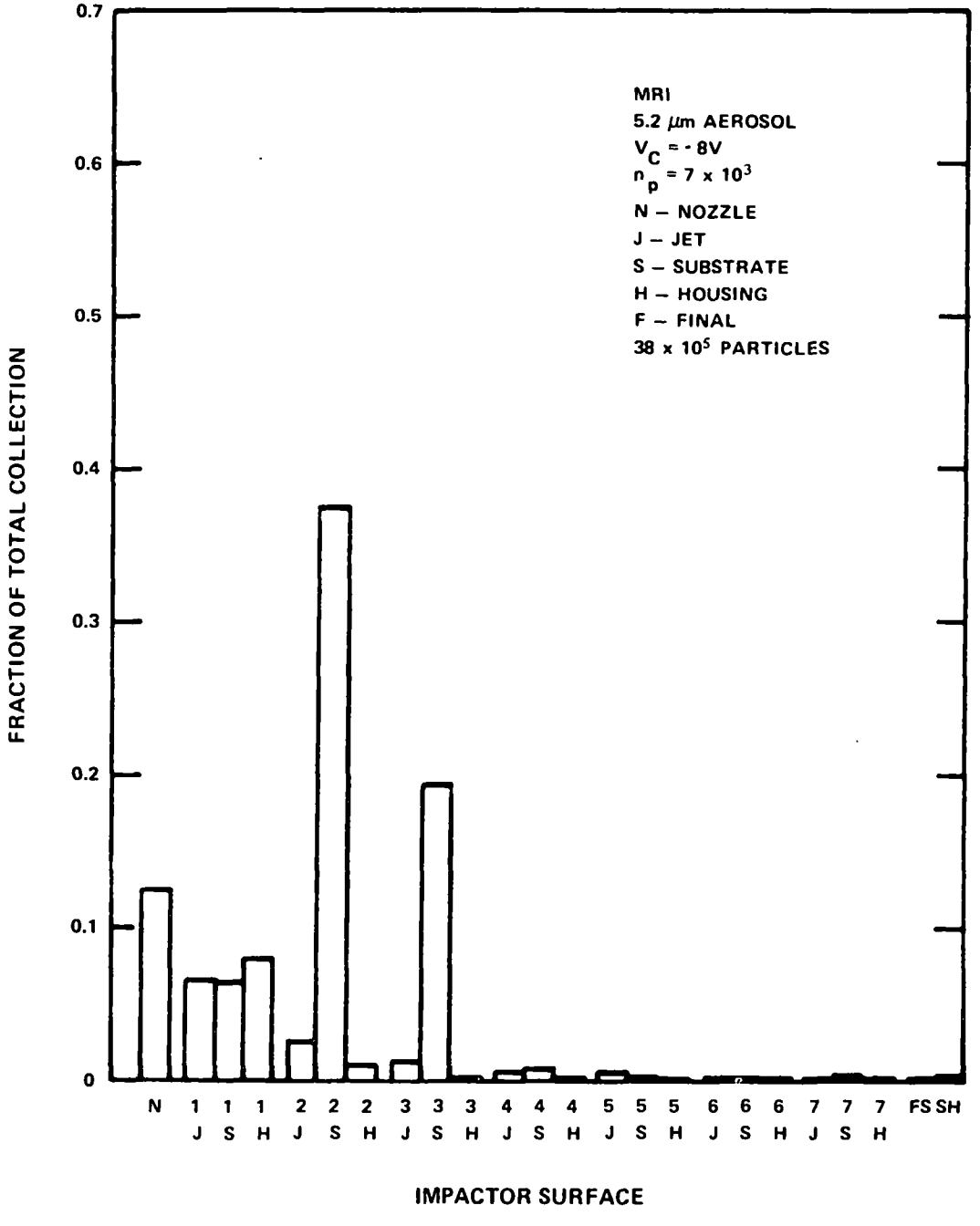


*Figure 45. Sampling charged particles using MRI-Model 1502 Impactor with plexiglass jet plates, 2J, 3J, and 4J. Other conditions are the same as the test depicted in Figure 30.)*

of this behavior is not known. One cause would be changes in the jet hole sizes. However, measurements ruled out this source of discrepancy. Secondly, the collection efficiencies of 2J, 3J, and 4J were reduced.

## Effect of Charge on Efficiency Versus $\sqrt{\psi}$

Figures 25 through 39 depict impactor behavior under various circumstances involving particle charge. As discussed above, a high charge effects the deposition of particles. However, it is not clear from those figures to what extent charge alters the calculated size distribution in a collected sample.

The size distribution inferred from impactor data is based upon stage collection efficiency $E_i$ as a function of the square root of the inertial impaction parameter, $\sqrt{\psi}$. The true collection efficiency is defined as the amount of material of a given size and density collected by a stage divided by the amount incident upon it.

$$\psi = D_p^2 C \rho_p V_o / 18 \eta D_j$$

where $D_p$ = particle diameter (cm),

$C$ = Cunningham slip factor,

$D_j$ = jet diameter (cm),

$\rho_p$ = particle density (gm/cm$^3$),

$\eta$ = gas viscosity (poise), and

$V_o$ = jet velocity (cm/sec).

A representative example of efficiency versus $\sqrt{\psi}$ is given as a solid line in Figure 46. The use of $E_i$ versus $\sqrt{\psi}$ gives the desired stage efficiency as a function of particle size for a range of sampling conditions. In practice a stage is calibrated by experimentally determining efficiency versus $\sqrt{\psi}$ for a particular substrate material to obtain $\sqrt{\psi_{50}}$; that is the value of $\sqrt{\psi}$ at 50% collection efficiency. Then, for particular sampling conditions the effective stage cut diameter $D_{50}$ is obtained from $\sqrt{\psi_{50}}$. It is assumed that all particles caught by an impactor stage are those particles having diameters equal to or greater than the $D_{50}$ of that stage, but less than the cut point of the preceding stage. Therefore, the effect of particle charge upon the calculated size distribution depends on its effect upon $\sqrt{\psi_{50}}$. A more sophisticated deconvolution of impactor data which uses the entire efficiency curve has been proposed,[1,2,3] but use of these techniques is limited to low-noise sampling data.

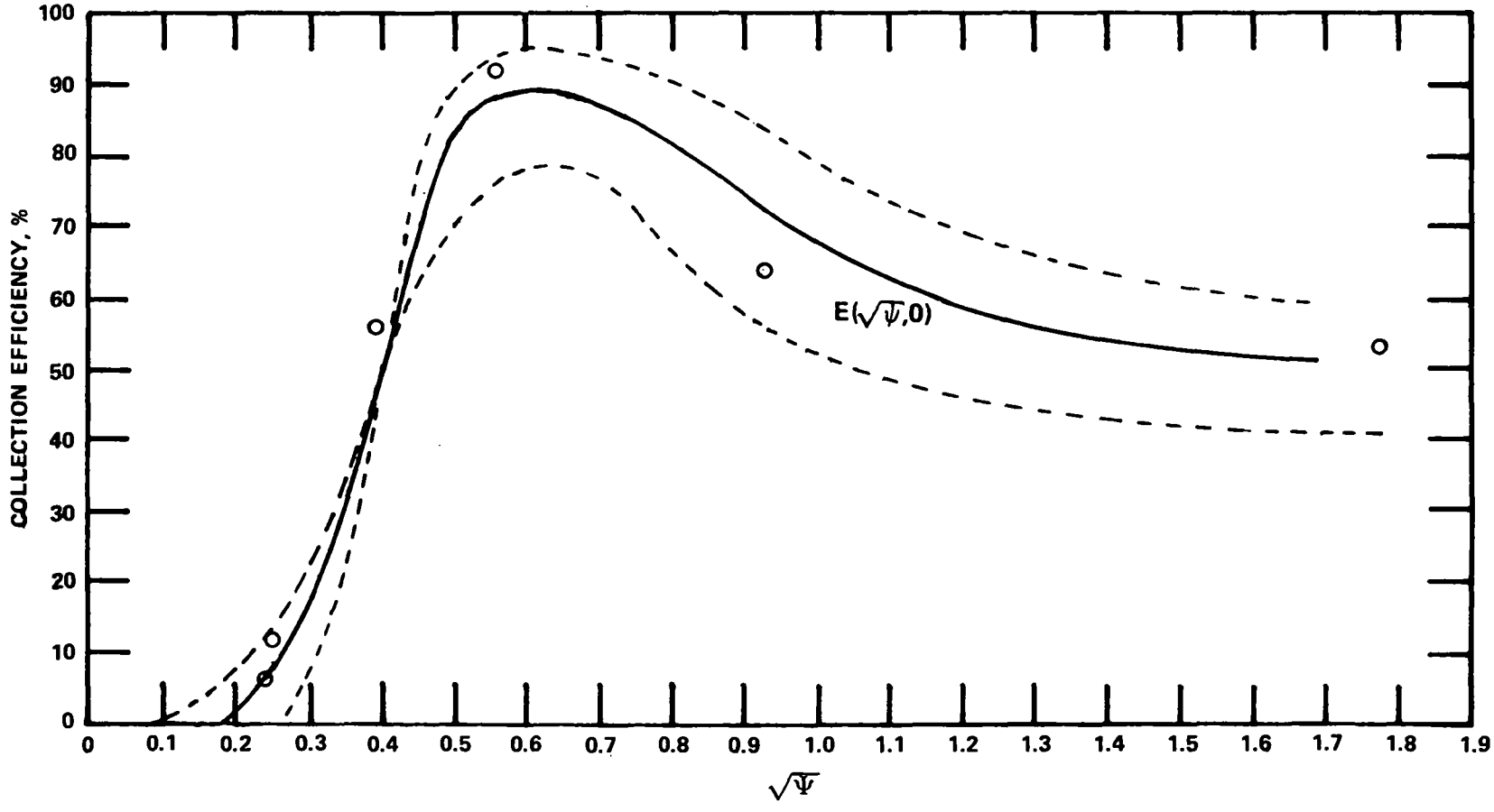


*Figure 46. Reference curve (solid) giving collection efficiency as a function of $\sqrt{\Psi}$ for the Andersen Stack Sampler and neutral particles. The measurements ("O") of this study for neutral particles are plotted by the procedure given in the text. The dashed lines depict the envelope of all stage efficiency curves superimposed.*

In order to completely characterize the effect of particle charge, the function $E_i(\sqrt{\psi},n_p)$; that is, efficiency expressed as a function of the square root of the inertial impaction parameter and charge ($n_p$) for stage i is required. For neutral aerosols, $E_i(\sqrt{\psi},0)$ has been determined in an extensive calibration study[11] for each stage of the Andersen, MRI, and U. of W. impactors at the sampling conditions used here, except that grease substrates were used with the latter two. To a first approximation, $E_i(\sqrt{\psi},0)$ has the same form for all stages with the same substrate material and impactor. The reference curve which we denote by $E(\sqrt{\psi},0)$ in Figure 46 was drawn by superimposing the stage calibration curves of the Andersen from the previous study.[11] Since the major differences in $E_i(\sqrt{\psi},0)$ from one stage to another is not in the shape of the curve, but $\sqrt{\psi_{50}}$, for the purpose of this analysis the calibration curves are normalized so that $\sqrt{\psi_{50}}$ of each coincided at 0.4. The dashed lines in Figure 46 define the envelope of those curves.

The collection efficiency of each stage was calculated for each run from the data given in Figures 25 through 39. These efficiencies were "corrected for wall losses" by combining the particles collected on the various surfaces according to Table VIII. These groupings are based upon the procedure used in field testing and the laboratory observations discussed above concerning deposition on jet plates. In the field, particulate mass on the top of jet plates is combined with the preceding stage, and that on the bottom is combined with the stage below the jet plate. The results for sampling neutral particles with the Andersen are given in Figure 46 as points. For comparison of these data to our reference curve, each measured efficiency is normalized and plotted as described above. The deviations of the data points in Figure 46 from the reference curve is thus a measure of the degree to which impactor calibration data for neutral particles may vary. In Figure 47 the same procedure was followed to relate the measured efficiencies of the Andersen stages with charged particles to its generalized efficiency curve for neutral particles. The dashed curve is the resulting $E(\sqrt{\psi},n_p)$ for moderate $n_p$. The effect of charge is to reduce the sharpness (slope) of the curve at $\sqrt{\psi}$ values below the peak while not changing $\sqrt{\psi_{50}}$ significantly. At $\sqrt{\psi}$ values above the peak the effect of charge reduces the efficiency in a manner similar to particle bounce.

Figures 48 and 49 and Figures 50 and 51 present information about the MRI and U. of W. impactors analogous to that in Figures 46 and 47 for the Andersen. It must be noted that stage efficiency curves of the previous study[11] for neutral particles were obtained using grease rather than glass fiber substrates. Therefore some adjustments in the reference curves had to be made based upon the efficiency data of the present study and

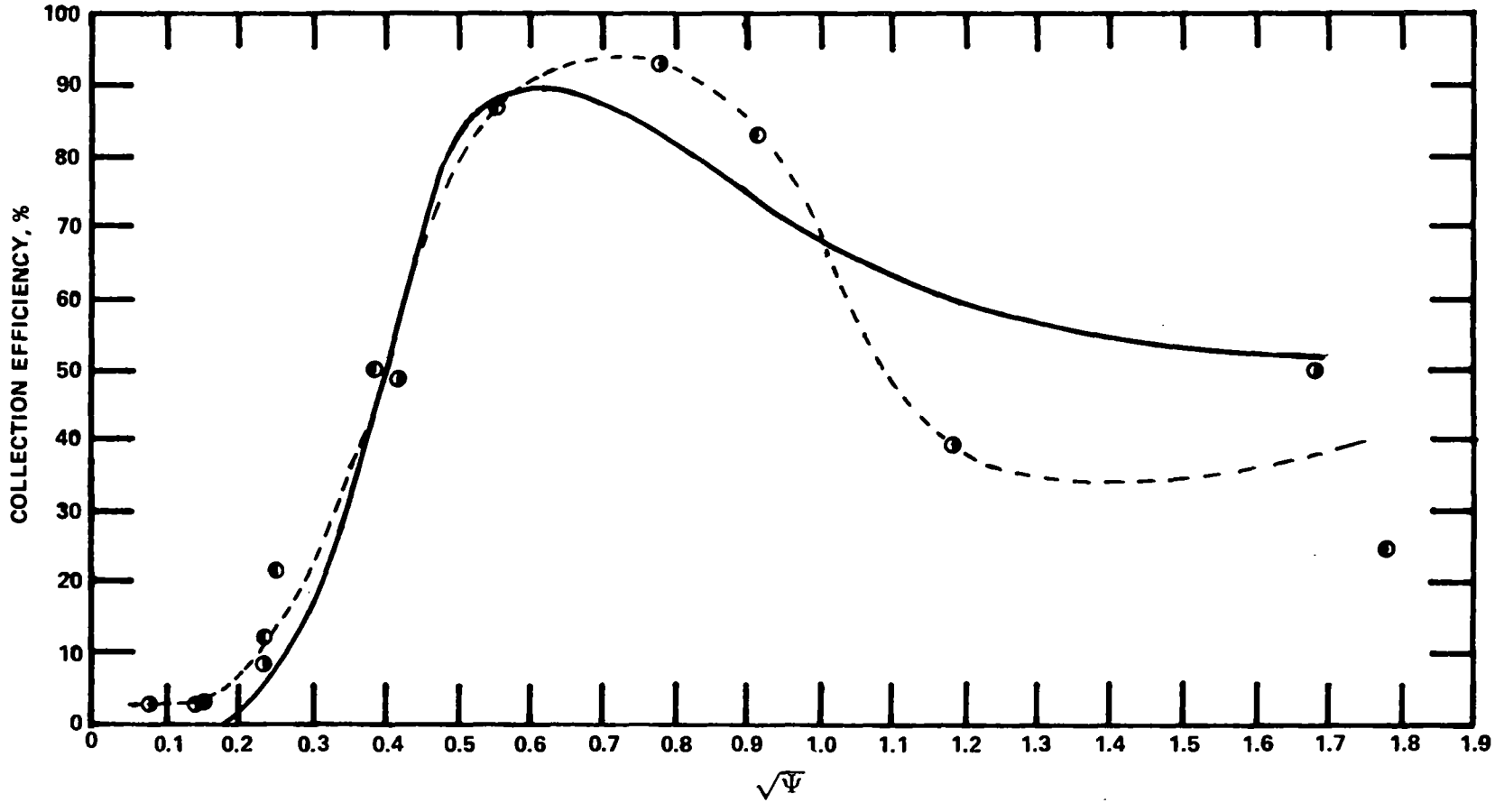


*Figure 47. Efficiency versus $\sqrt{\Psi}$ of stages in Andersen Stack Sampler for neutral particles (solid curve) and moderately charged particles (dashed curve). The measurements of this study for moderately charged particles ("◐" - 5.2 μm and "◑" - 2.1 μm diameter) are plotted by the procedure given in the text.*

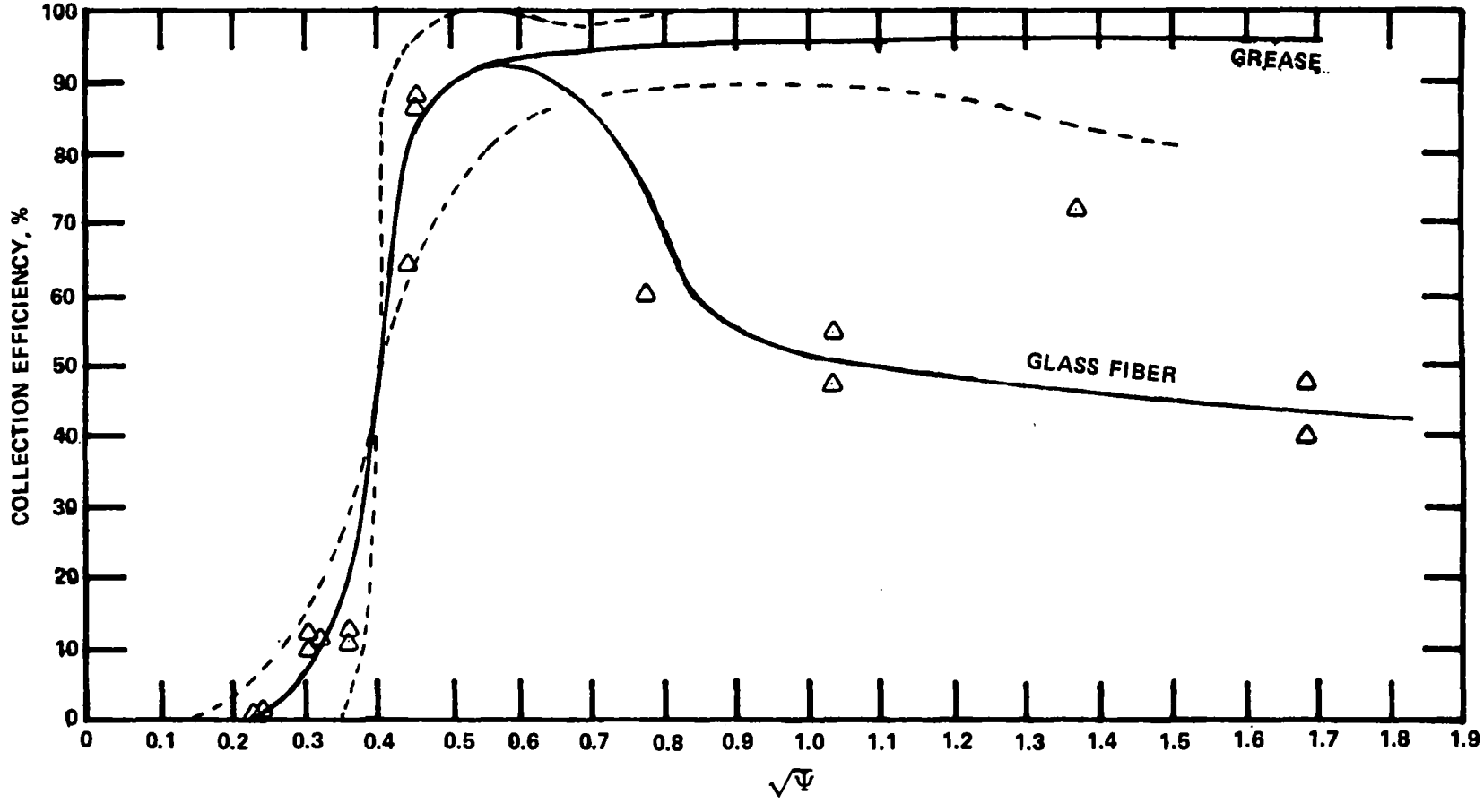


*Figure 48. Reference curve (solid) giving collection efficiency as a function of $\sqrt{\Psi}$ for the MRI-Model 1502 Impactor and neutral particles. The measurements ("Δ") of this study for neutral particles are plotted by the procedure given in the text. The dashed lines depict the envelope of all stage efficiency curves superimposed.*

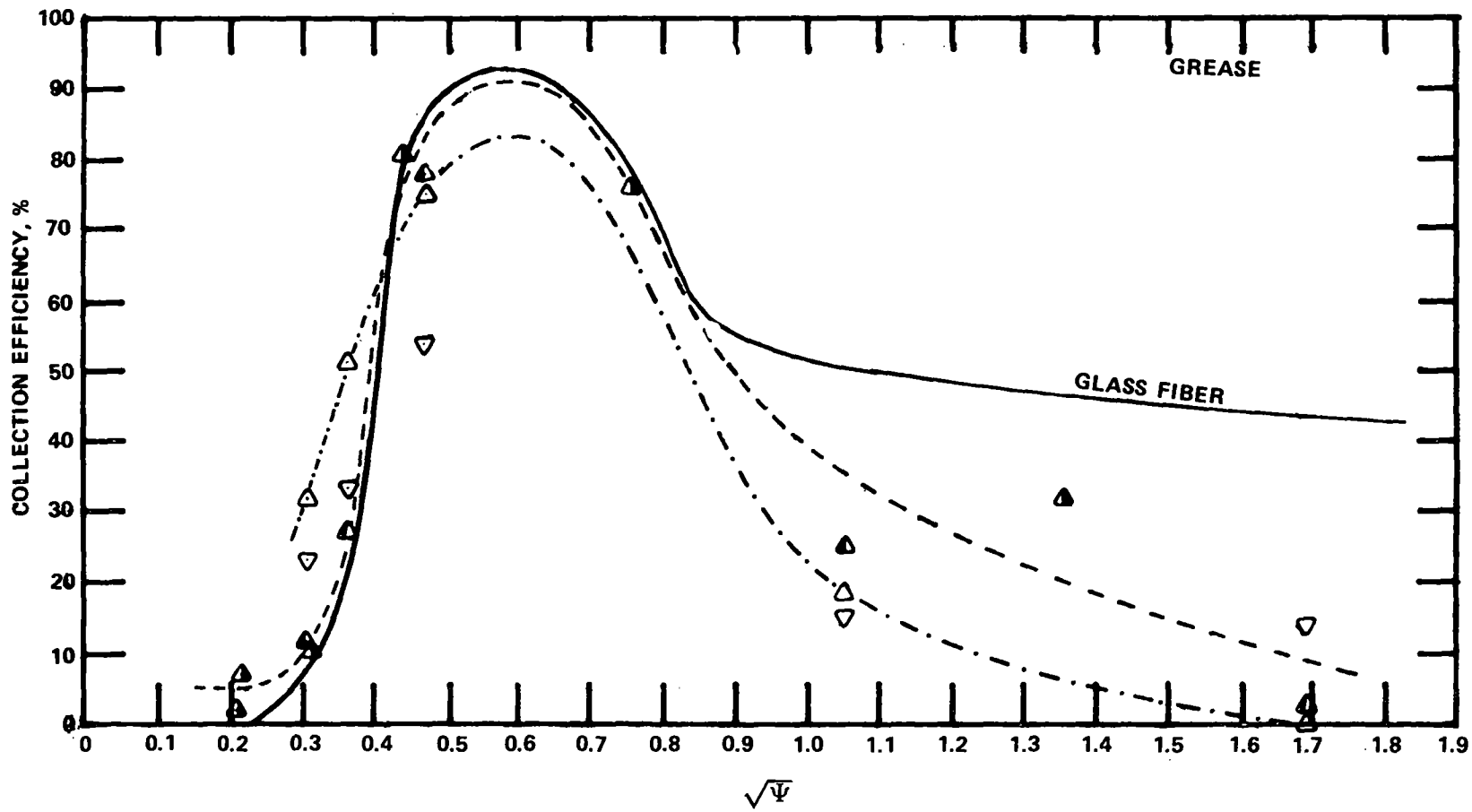


*Figure 49. Efficiency versus $\sqrt{\Psi}$ of stages in MRI-Model 1502 Impactor for neutral (solid curve), moderately charged (dashed curve), and highly charged (-·-·) particles. The measurements of this study for moderately charged ("▲" - 5.2 μm and "▲" - 2.1 μm diameters) and highly charged 5.2 μm diameter ("△" - grounded and "▽" - not grounded) particles are plotted by the procedure given in the text.*

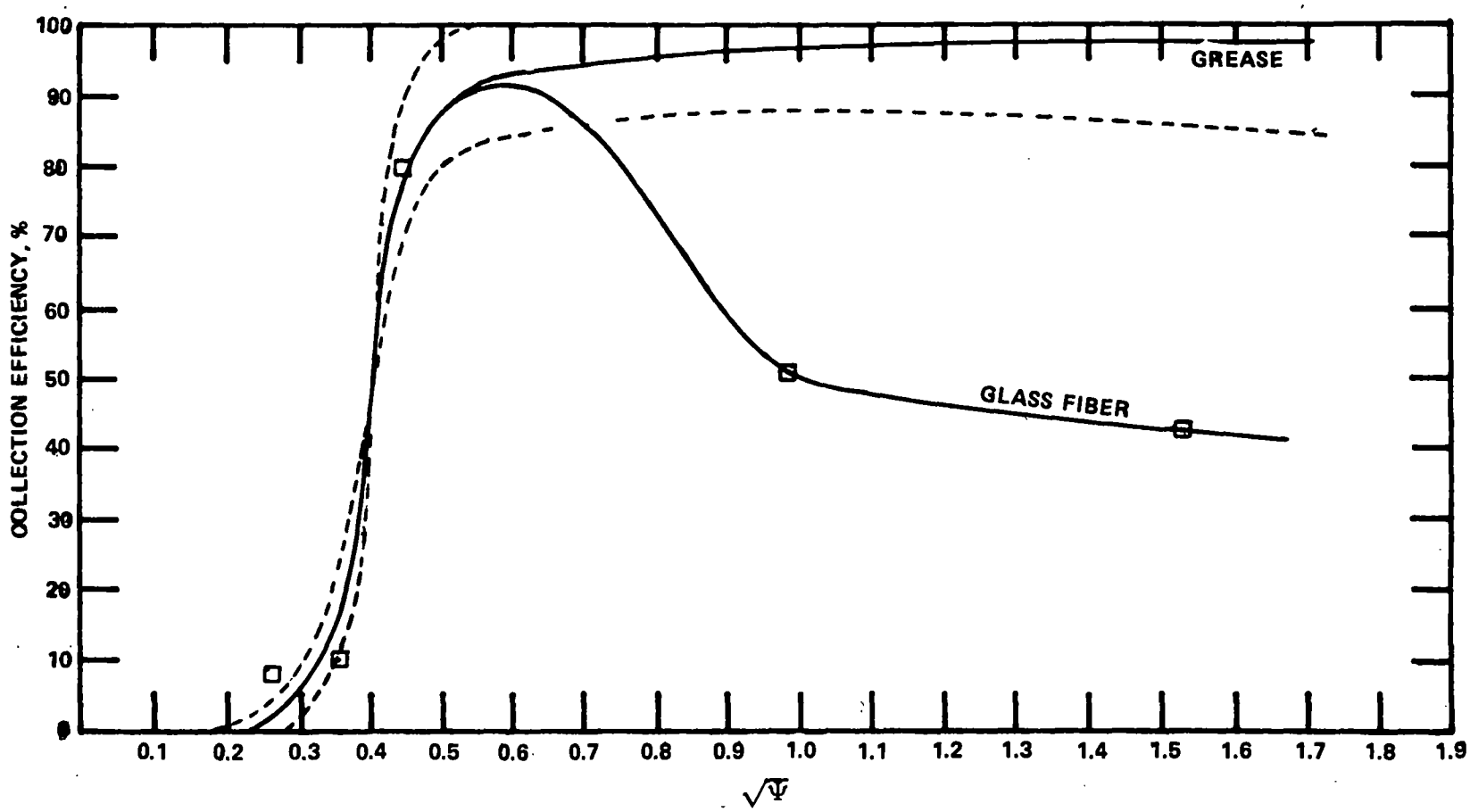


*Figure 50. Reference curve (solid) giving collection efficiency as a function of the $\sqrt{\Psi}$ for the U. of W. Mark III Impactor and neutral particles. The measurements ("□") of this study for neutral particles are plotted by the procedure given in the text. The dashed lines depicted the envelope of all stage efficiency curves superimposed.*

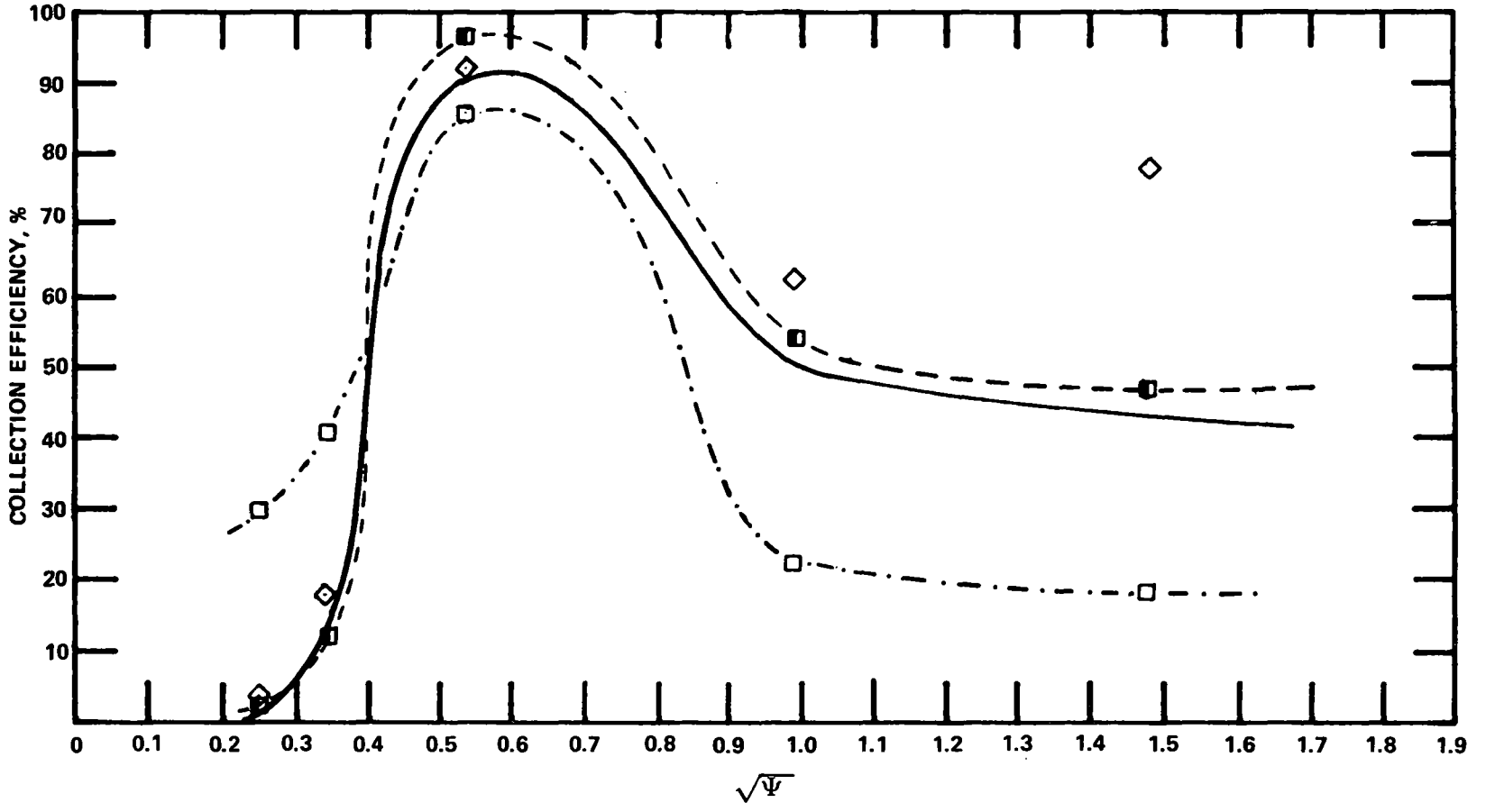


*Figure 51. Efficiency versus $\sqrt{\Psi}$ of stages in the U. of W. Mark III Impactor for neutral (solid curve), moderately charged (dashed curve), and highly charged (-·-·-) particles. The measurements of this study for 5.2 μm diameter particles, moderately charged ("◧") and highly charged ("□" - grounded and "◇" not grounded) are plotted by the procedure given in the text.*

Table VIII. Grouping of Surfaces for the Efficiency of Each Stage

| Stage | Andersen surface | MRI surface | U. of W. surface |
|---|---|---|---|
| 1 | N<br>NH<br>1J<br>1S<br>2J | N<br>1J<br>1S<br>1H | N<br>NH<br>1S |
| 2 | 2S<br>3J | 2J<br>2S<br>2H | 2J<br>2S |
| 3 | 2S<br>4J | 3J<br>3S<br>3H | 3J<br>3S |
| 4 | 4S<br>5J | 4J<br>4S<br>4H | 4J<br>4S |
| 5 | 5S<br>6J | 5J<br>5S<br>5H | 5J<br>5S |
| 6 | 6S<br>7J | 6J<br>6S<br>6H | 6J<br>6S |
| 7 | 7S<br>8J | 7J<br>7S<br>7H<br>FS<br>SH | 7J<br>7S<br>FS<br>SH |
| 8 | 8S<br>FS<br>SH<br>H | | |

comparisons of available efficiencies of another impactor with these two substrates to determine the differences. The resulting reference curve of the MRI impactor is shown in Figure 48. For $\sqrt{\psi}$ values up to 0.5, following the same procedure as in Figure 46, the reference curve of Figure 48 was obtained using MRI efficiency curves for grease substrates. The use of these is justified because in this region the efficiencies for neutral particles measured in this study, do not substantially deviate from this reference curve.

In the region of $\sqrt{\psi}$ values greater than 0.5 glass fiber substrates produce substantial bounce, meaning that efficiency drops to much less than 100%. This is indicated by the low measured efficiencies shown in Figure 48. Therefore in this region a reference curve was determined from experimental data for neutral particles taken in the course of this study.

Figure 49 shows the effect of high and moderate particle charge upon the MRI stage efficiency versus $\sqrt{\psi}$. For moderate charge the effects are similar to those with the Andersen. At the higher charge level however the changes in $E(\sqrt{\psi},n_p)$ are quite large at all $\sqrt{\psi}$ values.

The effect of particle charge upon U. of W. stage efficiency, shown in Figure 51, is small for moderate charge and substantial with high charge. It is interesting that in the "bounce" region, moderate charge appears to increase the efficiency substantially, reducing the effects of bounce. However, data obtained for $\sqrt{\psi}$ values to the right of the peak in efficiency are inherently subject to fluctuation because small numbers of particles are involved. Therefore exceptions to the overall trends in this region are questionable.

Figures 47, 49, and 50 show two obvious effects of particle charge. At low values of $\sqrt{\psi}$ the stage efficiency is increased due to the collection of particles on metal jet plates. At high values of $\sqrt{\psi}$, past the peak, the efficiency is reduced as if repulsive forces of charge are significant. Charge produced very small changes in $D_{50}$.

The foregoing discussion presents the results from an experimental study done with monodisperse aerosols over a limited range of test parameters. A second set of experiments are now being done with polydisperse aerosols. The results of both studies will be analyzed and combined into a single final report.

## Cascade Impactor Substrate Media Study
## (Technical Directive Number 10501)

### Description of Task:

The purpose of this task was to conduct an experimental program to investigate the magnitude of weight changes of cascade impactor substrates when exposed to industrial flue gases. This study determined the causes of these weight changes and investigated all candidate materials to find out which were most stable. Also preconditioning techniques were investigated to stabilize weight changes in those substrates. At the conclusion of this study, a detailed report was written giving the test results and suggesting a protocol for minimizing the impactor substrate weight changes.

### Summary of Progress:

Cascade impactors are widely used to determine particle size distributions in air pollution control device research programs. In these research programs a large variety of flue streams are encountered with temperatures ranging from ambient to around 370°C (700°F). Gas analyses show that many of these sources contain some $SO_x$ components, particularly those associated with fossil fuel fired boilers.

Most impactors have collection stages which are too heavy to allow accurate measurements of the mass of the particles collected in each size fraction. Weighing accuracy can be improved by covering the stage with a lightweight collection substrate made of aluminum foil, teflon, glass fiber filter material, or other suitable lightweight materials, depending upon the particular application. Some manufacturers now furnish lightweight inserts to be placed over the collection stages. With such arrangements it is possible to collect enough material on each stage to make an accurate determination of the mass collected and avoid overloading the stage. If the stage is overloaded, some deposited particulate matter can be reentrained and deposited on another stage or the back-up filter and lead to erroneous results.

Substrate materials may also serve the purpose of changing the surface characteristics from those of a bare metal or plastic to something better suited to holding particles with impact. Thus, various greases are often used, either on bare impactor plates, or, more frequently, on metal foil substrates.

Presented in the published final report are the results of investigations concerning the use of two classes of impactor substrates—greased metal foils, and fiber filter materials. Tests were made under both laboratory and field conditions to evaluate each of several greases and filter materials. The general purpose of this study was to identify specific materials and handling techniques which may be used to improve the accuracy of weight measurements in impactors by reducing uncertainties arising from changes in substrate weights.

Although normal substrate preparation includes baking and desication before the initial weighing, it is frequently found that weight losses can occur when sampling clean air. Previous tests were conducted to investigate this phenomenon in detail.[15] It was found that with careful handling, weight loss per glass fiber substrate for Andersen impactors can be kept below 0.1 mg. This loss is attributed to loss of fibers which stick to seals within the impactor and to "superdrying" when sampling hot, dry air. Weight losses of 0.1 mg are small compared to most stage catches when sampling particulate matter, and this are within an acceptable range for sampling errors.

A more significant problem is excessive weight gain of the glass fiber material itself due to gas phase reactions. These reactions appear to be caused by the $SO_x$ component in flue gases. A series of studies was thus directed toward developing procedures to passivate glass fiber materials against the effect of $SO_x$ components in flue gases.

Although greases offer good impedance to particle bounce on substrates, they are subject to temperature limitations. Sampling clean, hot air while using greased substrates may result in severe weight losses. These losses appear to result from one or more of several mechanisms which may include continued loss of volatile components, erosion of grease by the action of the gas jet in the impactor, and occasional flow of grease from the substrate to other surfaces within the impactor. In addition, chemical reactions may play role in some cases. Occasionally, some of the weight lost on upper impactor stages has been found to reappear on a back-up filter, which is an indication that the grease has been blown off the collection surface or has chemically reacted to form a fine "smoke" which was then collected by the back-up filter.

## Summary of Results of Evaluation of Greases

Upon preliminary screening by static heating tests in the laboratory, six of the nineteen greases tested were found to have acceptable characteristics at elevated temperatures. Among those greases eliminated by these tests, large changes in mass or in consistency had occurred.

In the field tests greases were applied to metal foil impactor substrates and were subjected to a flue gas sampling procedure. Particulate matter was removed by a prefilter so that the effects of the flue gas alone on the greased substrates could be observed.

As a result of the field studies it was concluded that Apiezon H grease performed best of the greases tested. Other greases studied displayed changes in consistency or a tendency to flow under the influence of the gas stream.

Further tests on Apiezon H have demonstrated that this grease is a suitable substrate material for applications where the temperature does not exceed approximately 177°C (350°F).

## Summary of Results of Evaluation of Filter Media

Untreated glass fiber filter materials used as impactor substrates will almost invariably increase in mass when subjected to the hot flue gases normally encountered in field applications. Conversion of $SO_2$ to various sulfates appears to be the cause of mass gains. The various filter materials tested vary widely in the amount of mass change which occurs under a particular set of flue gas conditions.

Preconditioning techniques can be used to force the production of sulfates in a filter medium, leaving a minimal number of sites available for chemical reaction in the flue gas, and hence, providing substrate material for which minimum mass gains occur during use in an impactor. The best results were achieved when substrates were washed in sulfuric acid, baked, and conditioned *in situ*.

Of the filter materials studied, Reeve Angel 934AH was found to be most suitable in all respects for use as cascade impactor substrates.

## Conclusions and Recommendations

Collection stages of most types of cascade impactors are very heavy in comparison with the amounts of particulate material normally collected. It is therefore the usual practice to augment each collection stage with a lightweight substrate to improve weighing accuracy. Generally, two classes of substrates are used—greased metal foils, and glass fiber filter material.

Greased foils provide resistance to particle bounce and scouring effects, but greases tend to be unstable at elevated temperatures. Some tend to harden, and in others the viscosity may become reduced so that they may flow or be blown off the

surface by the high velocity gas flowing through the impactor jets. Of the greases tested, Apiezon H was found to perform most satisfactorily. This grease may be used at temperatures up to approximately 177°C (350°F). No greases were found to be useable at higher temperatures.

Mass gains exhibited by glass fiber filter materials when they are exposed to the $SO_x$ components in flue gas streams pose a complicated problem. Experiments show that these mass gains are caused by formation of sulfates due to a gas phase reaction with $SO_x$. Laboratory and field experiments indicate that the only glass fiber filter material suitable for use as a cascade impactor substrate is Reeve Angel 934AH. When this material is acid treated, according to a procedure given below mass gains caused by flue gas reactions can be kept quite small.

It is recommended that acid washing, baking and in situ conditioning be used whenever large blank mass gains with large standard deviations are expected. In this context, "large" refers to substrate mass gains greater than several tenths of a milligram.

Further research may provide a technique for passivating glass fiber materials to all mass gains. It has been suggested that a high temperature polymer or silicon compound might be developed to coat the glass fibers in much the same way that the Gelman Spectro-Grade material is prepared for use at low temperatures.

The Final Report for this task was published in a document entitled "Inertial Cascade Impactor Substrate Media for Flue Gas Sampling", EPA-600/7-73-060, June 1977.

Procedure for Acid Washing of Substrates

1. Submerge the substrates to be conditioned in a 50-50 mixture (by volume) of distilled water and reagent grade concentrated sulfuric acid at 100°-115°C (230-239°F) for 2 hours. This operation should be carried out in a hood with clean glassware. Any controllable laboratory hotplate is suitable.

The substrates may need to be weighted down to keep them from floating. For this purpose, place a teflon disc on the top and bottom of the substrate stack. The top disc can be held down with a suitable glass or teflon weight.

2. When the substrates are removed from the acid bath they should be allowed to cool to room temperature. They are next placed in a distilled water bath and rinsed continuously with a water flow of 10-20/$cm^3$/min. The substrates should be rinsed

until the pH of the rinse water, on standing with the substrates, is nearly the same as that of the distilled water. The importance of thorough washing cannot be over-emphasized.

3. After rinsing in distilled water the substrates are rinsed in reagent grade isopropanol (isopropyl alcohol). They should be submerged and allowed to stand for several minutes. This step should be repeated four to five times, each time using fresh isopropanol.

4. Allow the substrates to drain and dry. They can be spread out in a clean dry place after they have partially dried (dry enough to handle).

5. When the filters are quite dry to the touch they should be baked in a laboratory oven to drive off any residual moisture or isopropanol. Bake the substrates at 50°C (122°F) for about two hours, at 200°C (392°F) for about two hours, and finally at 370°C (700°F) for about three hours. The substrates are now ready for in situ conditioning.

As a final check, place two substrates in about 50 ml of distilled water, and check the pH. The substrates to be checked for pH should be torn into small pieces, placed in the water, and stirred for about 10 minutes before the pH is measured. If the pH is significantly lower than that of the distilled water, then the filters should be baked out at 370°C (700°F) for several hours more to remove any residual sulfuric acid. The boiling point of sulfuric acid is 338°C (640°F), so high temperatures must be used.

Figure 52 is a flow chart representing the acid wash procedure described in the foregoing paragraphs.

## Calibration and Evaluation of Commercial Impactors (Technical Directive Number 20101)

Description of Task:

Under EPA Contract Number 68-02-0273 the calibration and evaluation of five commercial impactors using ammonium fluorescein aerosols was begun. At the conclusion of this contract the upper stages had been calibrated. Under Contract Number 68-02-2131 the lower impaction stages were calibrated using a Pressurized Collison Nebulizer System and polystyrene latex aerosols. The final report for Contract 68-02-0273 was modified to include these results.

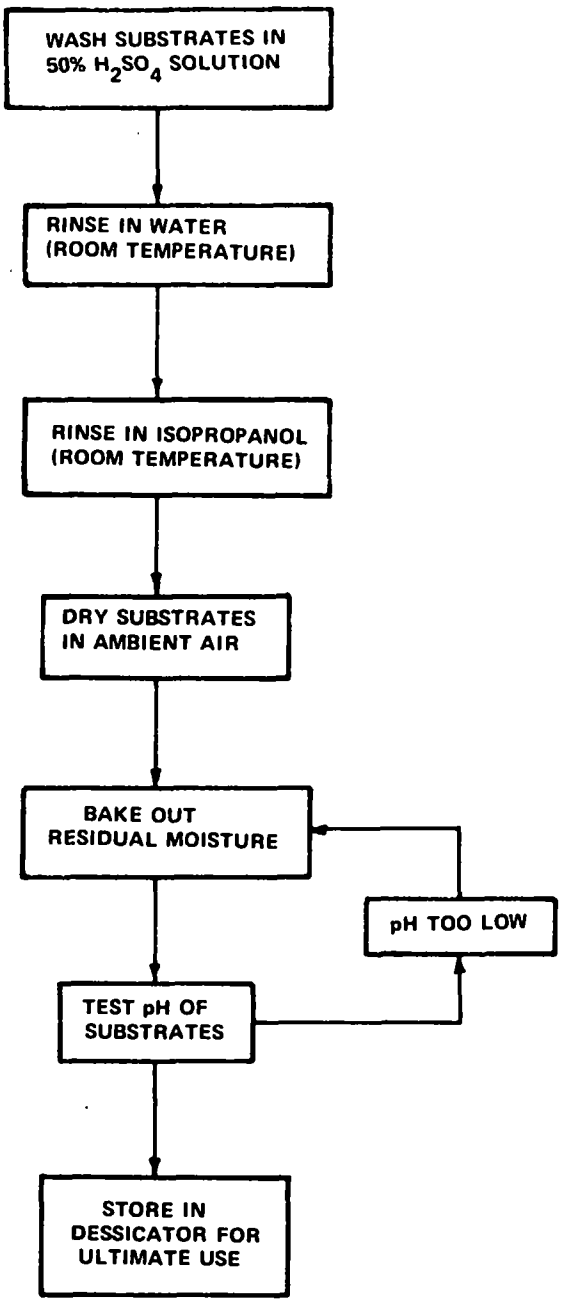


*Figure 52. Flow chart for acid wash treatment of glass fiber filter material.*

Summary of Progress:

This summary presents a brief description of the methods and results of an evaluation and calibration of five commercially available cascade impactors. These cascade impactors and their manufacturers are listed below:

1. Andersen Mark III Stack Sampler (Andersen)
   Andersen 2000, Inc.
   Atlanta, Georgia 30320

2. Brink Model BMS-11 Cascade Impactor (Brink)
   Monsanto Enviro-Chem Systems, Inc.
   St. Louis, Missouri 63166

3. MRI Model 1502 Inertial Cascade Impactor (MRI)
   Meteorology Research, Inc.
   Altadena, California 91001

4. Sierra Model 226 Source Cascade Impactor (Sierra)
   Sierra Instruments, Inc.
   Carmel Valley, California 93924

5. University of Washington Mark III Source Test Cascade Impactor (U. of W.)
   Pollution Control Systems, Inc.
   Renton, Washington 98055

The normal 5-stage Brink impactor was modified to include an inline cyclone pre-collector, a "0" stage, and a "6" stage. Table IX presents the operational parameters of the five cascade impactors. The Andersen impactor was used with glass fiber substrates supplied by the manufacturer. For the Brink impactor a small disc of glass fiber material was tested as well as a thin grease layer (Vaseline). The MRI and U. of W. impactors were tested with thin films of grease (Vaseline) on the collection plates. The Sierra was supplied with pre-cut glass fiber mats.

To the user of an inertial cascade impactor the most important consideration is the degree to which the data that is obtained will duplicate the actual particulate size distribution which is sampled. In order to transform the mass collected by several impaction stages into a size distribution, an accurate knowledge of the relationship between collection efficiency and particle size for each stage is essential.

Theoretically, cascade impactor operation can be described by the theory of impaction from a jet. The end result of such a calculation is impaction efficiency versus particle size.

Table IX. Cascade Impactor Calibration Study
Operational Parameters

Laboratory Conditions - 73°F/22°C 29.5" Hg/750 mm Hg

Aerosol Particles - Ammonium Fluorescein Density - 1.35 $gm/cm^3$
- Polystyrene Latex Density - 1.00 $gm/cm^3$

| Impactor | No. of Stages | Substrate Material | Nominal Sampling Flow Rate |
|---|---|---|---|
| Andersen | 8 | Pre-cut glass fiber filter mats | 0.5 ACFM/ 14.16 LPM |
| Brink (Modified) | 7 | Glass fiber filter inserts | 0.03 ACFM/ 0.85 LPM |
| Brink (Modified) | 7 | Greased collection plates | 0.03 ACFM/ 0.85 LPM |
| MRI | 7 | Greased collection plates | 0.5 ACFM/ 14.16 LPM |
| Sierra | 6 | Pre-cut glass fiber filter mats | 0.5 ACFM/ 14.16 LPM |
| Sierra | 6 | Pre-cut glass fiber filter mats | 0.25 ACFM/ 7.08 LPM |
| U of Washington | 7 | Greased collection plates | 0.5 ACFM/ 14.16 LPM |

Impaction efficiency is defined as the fraction of particles of a certain size in the jet which impact on a collection plate. This value can be obtained theoretically or experimentally under ideal conditions. The collection efficiency of an impactor stage, however, is the ratio of the mass (or number) of particles of a certain size collected on an impaction surface to the total mass (or number) of particles of the same size in a jet impinging on that surface. The collection efficiency is the product of the theoretical impaction efficiency and the adhesion efficiency.[16] The adhesion efficiency is the fraction of the number of particles which adhere to the surface after touching it by the impaction process. This depends in a large part on the surface characteristics of the particle and collection surface. Thus, there will be disagreement between the theoretical impaction efficiency and the experimentally determined collection efficiency in the cases where particle bounce, reentrainment, electrostatic effects, wall losses, and non-ideal geometry have an effect. For this reason, the theory of impaction may not be sufficiently accurate in predicting impactor performance.

The theory of the impaction process has been developed by several researchers[17,18] to a state where the efficiency, E, of impaction can be determined as a function of the particle size ($D_p$), Reynolds Number (Re), jet diameter or width (Dj,W), the jet to plate distance (S), and the jet throat length (T).

$$E = E\ (D_p,\ Re,\ S/D_j,\ T/D_j)$$

It is common practice to relate the particle size $D_p$ to the square root of the inertial impaction parameter, $\sqrt{\psi}$. $\psi$ is the ratio of the particle stopping distance, $\ell$, (the distance a particle will travel in air when given an initial velocity, $V_o$) to the jet diameter or width ($D_j$ or W).

$$\psi = \ell/D_j$$

$$\text{or} \qquad \psi = D_p^{\,2}\ \frac{C\rho_p V_o}{18\ \mu\ D_j}$$

where C = Cunningham Slip Factor,

$D_j$ = Jet Diameter (cm),

$\rho_p$ = Particle Density (gm/cm$^3$),

$\mu$ = Gas Viscosity (poise), and

$V_o$ = Jet Velocity (cm/sec).

The square root of the inertial impaction parameter, $\sqrt{\psi}$, is used in impaction theories as a dimensionless quantity proportional to particle size.

$$\sqrt{\psi} = D_p \left[ \frac{C\rho_p V_o}{18\ \mu\ D_j} \right]^{\frac{1}{2}}$$

The inertial impaction parameter is useful in graphing impactor calibration data because information from all stages of an impactor can be placed on a single graph, and under many circumstances would in theory lie along a common curve. The value of $\sqrt{\psi}$ at 50% collection efficiency, $\sqrt{\psi_{50}}$, defines the impaction stage $D_{50}$, the particle size at which half the particles of that size are collected and half are passed to the next stage. Thus, the $D_{50}$ is used as the effective stage cut diameter.

Recently Marple[18] has been able to construct theoretical impaction efficiency curves for several values of the jet to plate distance, jet Reynolds Number, and jet throat length. Figure 53 shows the results of these calculations for both round and rectangular jet impactors. The value of the square root of the Stokes number used by Marple, $\sqrt{STK}$, differs from $\sqrt{\psi}$ by a factor of $\sqrt{2}$. It can be seen from Figure 53 that for certain ranges of Re, $S/D_j$; S/W, or T/S; T/W, the magnitude of $\sqrt{\psi_{50}}$ is sensitive to these parameters.

## Description of Experimental Procedures

Laboratory evaluation of the cascade impactors involved the use of two types of particle generation systems: A Vibrating Orifice Aerosol Generator (VOAG) and a Pressurized Collison Nebulizer System (PCNS). The VOAG was used to generate monodisperse ammonium fluorescein particles with diameters from 18 micrometers to 1 micrometer. The PCNS was used to disperse three sizes of monodisperse Dow Corning Polystyrene Latex (PSL) spheres: 2.02 micrometers, 0.82 micrometer, and 0.46 micrometer diameter.

The VOAG used in this study was designed and built at Southern Research Institute, although similar devices have been reported by several authors previously,[19,20,21] and a commercial unit is available from Thermo Systems, Inc., St. Paul, MN 55113. Figure 54 is a schematic diagram showing the operating principle of the VOAG. A solution of known concentration (in our case, a solution of fluorescein ($C_{20}H_{12}O_5$) in 0.1 N $NH_4OH$) is forced through a small orifice (5, 10, 15, or 20 μm diameter). The orifice is attached to a piezoelectric ceramic which, under

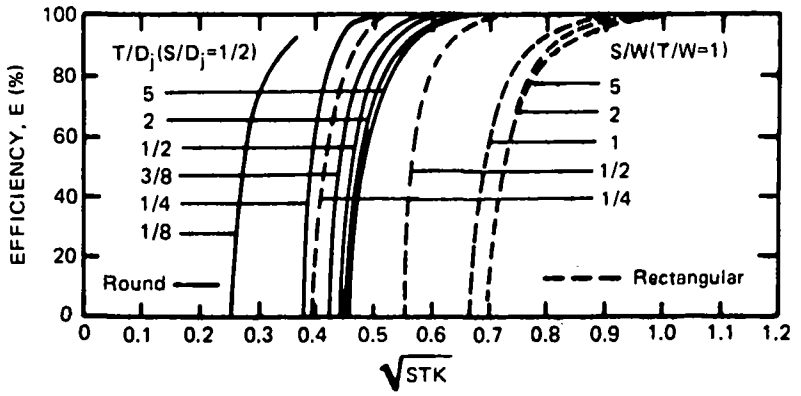


(a) EFFECT OF JET TO PLATE DISTANCE (Re=3,000)

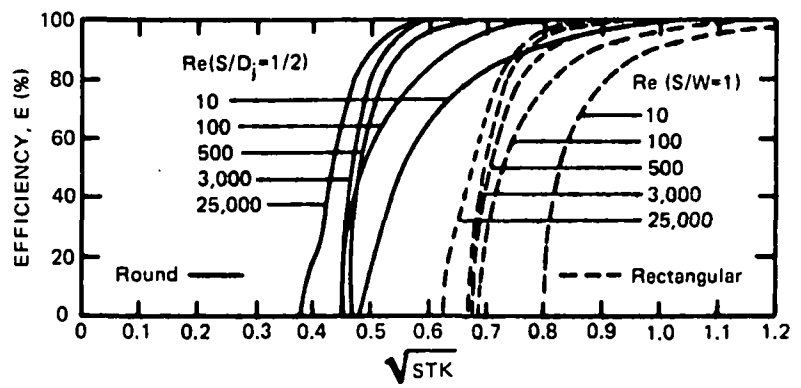


(b) EFFECT OF JET REYNOLDS NUMBER (T/W=1)

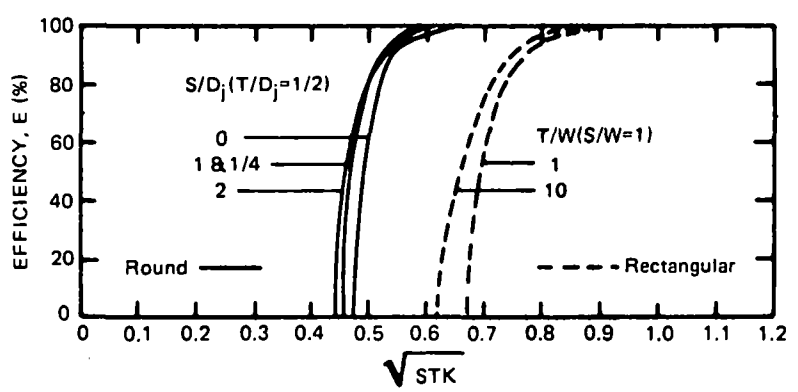


(c) EFFECT OF THROAT LENGTH (Re=3,000)

*Figure 53. Theoretical impactor efficiency curves for rectangular and round impactors showing the effect of jet-to-plate distance S, Reynolds number Re, and throat length T. Note that* $\sqrt{STK} = D_p(C\rho_p V_o/9\ \mu D_j)^{1/2}$, *whereas* $\sqrt{\Psi} = D_p(C\rho_p V_o/18\ \mu D_j)^{1/2}$. *After Marple*[3].

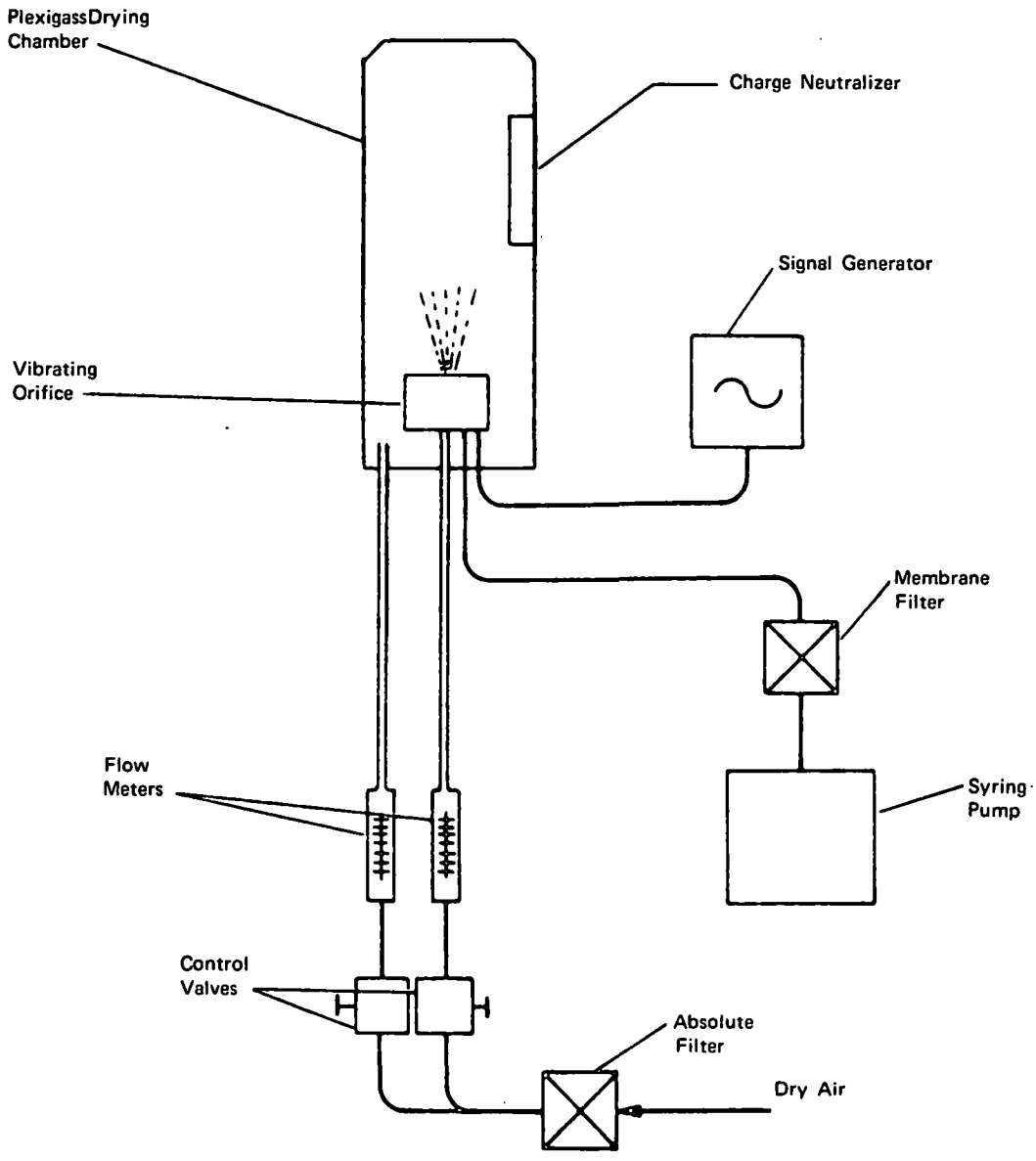


*Figure 54. Schematic representation of the Vibrating Orifice Aerosol Generator.*

electrical stimulation, will vibrate at a known frequency. This vibration imposes periodic perturbations on the liquid jet causing it to break up into uniformly sized droplets of ammonium fluorescein. Knowing the liquid flow rate and the perturbation frequency, the droplet size can be readily calculated. The solvent evaporates from the droplets leaving the non-volatile solute as a spherical residue. The final dry particle size can be calculated from the droplet size through the known concentration of the liquid solution.

During each test, when it had been determined that particles of the correct size were being generated, each cascade impactor was allowed to operate for the required length of time to collect a suitable sample. Except for one impactor, non-isokinetic sampling was performed; however, it was determined by a series of tests that this did not affect the collection efficiency as compared to isokinetic sampling results. It is likely that the nozzle wall losses were influenced, however. After pulling the sample, the quantity of particulate matter on each surface was determined by absorption spectroscopy. With the mass on each plate and surface known, the wall losses and stage collection efficiencies could be calculated.

A Pressurized Collison Nebulizer System similar to that reported by Calvert[22] was assembled as shown in Figure 55. A stream of dry dilution air was mixed with the nebulized suspension to reduce the aerosol concentration and to aid in drying. Valves placed upstream of the impactor allowed variations in the flow rate. Three sizes of PSL particles were used (2.02 μm, 0.82 μm, and 0.46 micrometer diameter). Each impactor stage was tested at three flow rates near the nominal or designed impactor flow rate. Thus nine calibration points were obtained for each stage of each impactor. A Climet Instruments Model 208A Particle Analyzer was used to monitor the impactor inlet and outlet concentrations. Stages of each impactor were tested individually. This system was designed to allow two different air flow strategies depending on whether the impactor flow rate was higher or lower than the Climet inlet flow rate. Because of the limited availability of large PSL spheres, and because these data were supplementary to the ammonium fluorescein data, only the impactor stages for which information could be obtained with sizes of 2 micrometers diameter and smaller were tested. Generally these were the lower 3 or 4 impactor stages. For simplicity and convenience, mass flowmeters were used to measure the critical gas flow rates.

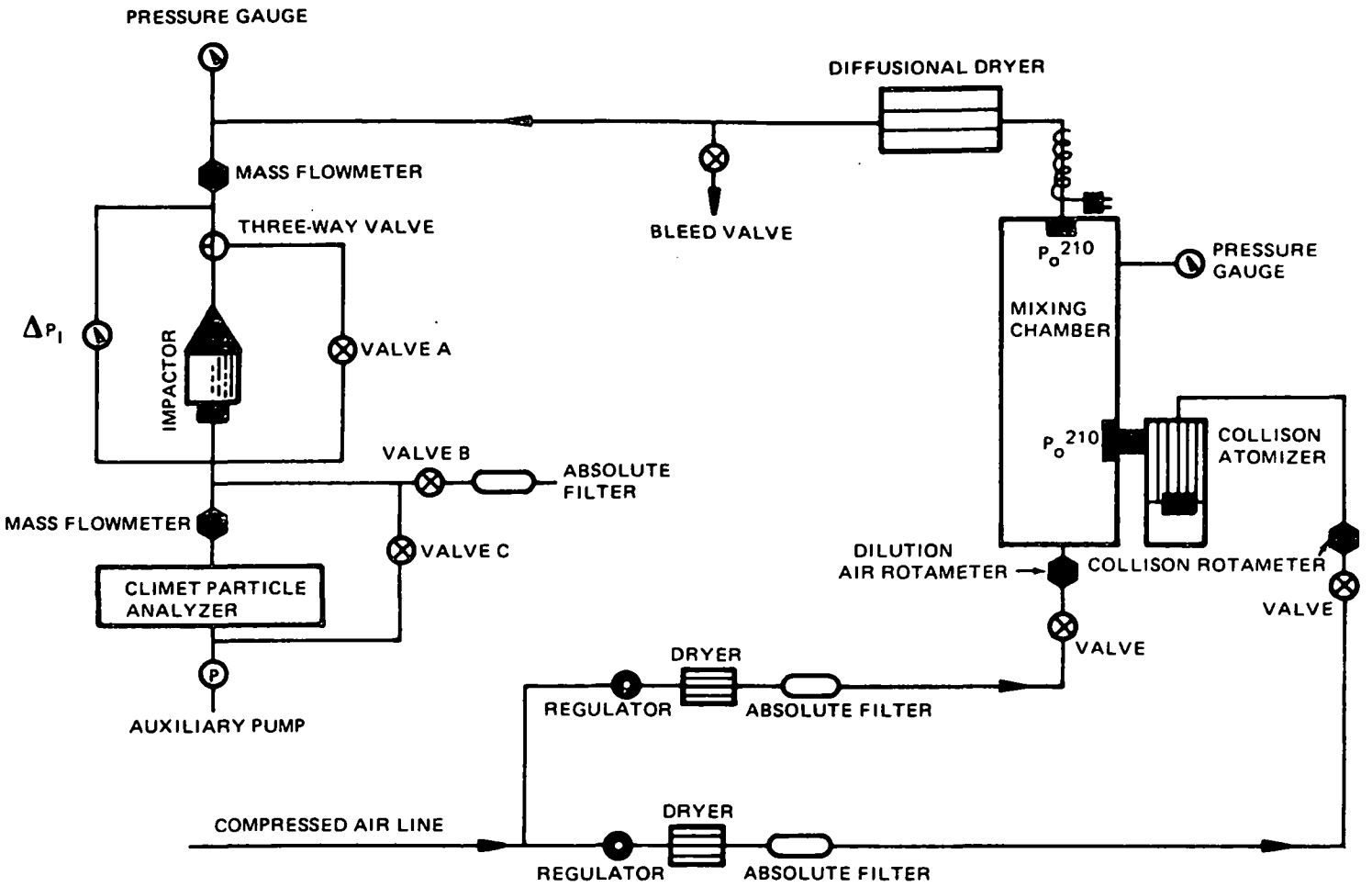


*Figure 55. PSL calibration system for high and low flowrate impactor.*

## Results of the Calibration Study

### Wall Losses:

During the portion of the calibration procedure using ammonium fluorescein aerosols, data on wall losses were tabulated. By washing each cascade impactor surface after sampling a test aerosol, it was possible to obtain information on particle losses occurring in nozzles, inlet cones, jet plates, and other internal surfaces. The total wall loss was calculated as a percentage of the total amount of aerosol entering the impactor.

The results are shown in Figure 56. All wall loss data are based on the results of non-isokinetic sampling, except for the Sierra impactor operated at 7 LPM. The degree to which non-isokinetic sampling influenced the nozzle wall loss contribution is unknown; however, on the average the nozzle wall loss was about 40% of the total wall loss.

In general, wall losses tend to decrease with particle size and are negligible for particles smaller than about 1-2 micrometers in diameter. The majority of the losses occurred in the nozzles and inlet cones.

Wall losses can be attributed to particle settling, diffusion, electrostatic attraction, bounce, and reentrainment. Visual inspection of the nozzles and inlet cones indicate that the losses were predominately due to settling. All impactors except the Brink were run in a horizontal position.

### Calibration Data - Efficiency vs. $\sqrt{\psi}$:

Recall from the Introduction that if two or more impactor stages have the same Reynolds Number, jet to plate spacing, and jet throat length, then according to Marple's theory[18] they should have the same particle collection efficiency for the same magnitude of the square root of the inertial impaction parameter. If these physical parameters differ, or if different collection substrate media are used, then these curves may not be identical. These differences are evident in Figures 57 through 63, which present in alphabetical order the Stage Collection Efficiency Versus $\sqrt{\psi}$ for each cascade impactor configuration. These efficiencies are based solely on the particles actually collected by an impaction surface and those found downstream of that surface. Particles on other surfaces, such as the jet plate surface above the impaction surface, were not included in the efficiency shown in these figures.

The differences in $\sqrt{\psi_{50}}$ for the different impactor stages shown in the foregoing figures require that empirical calibrations

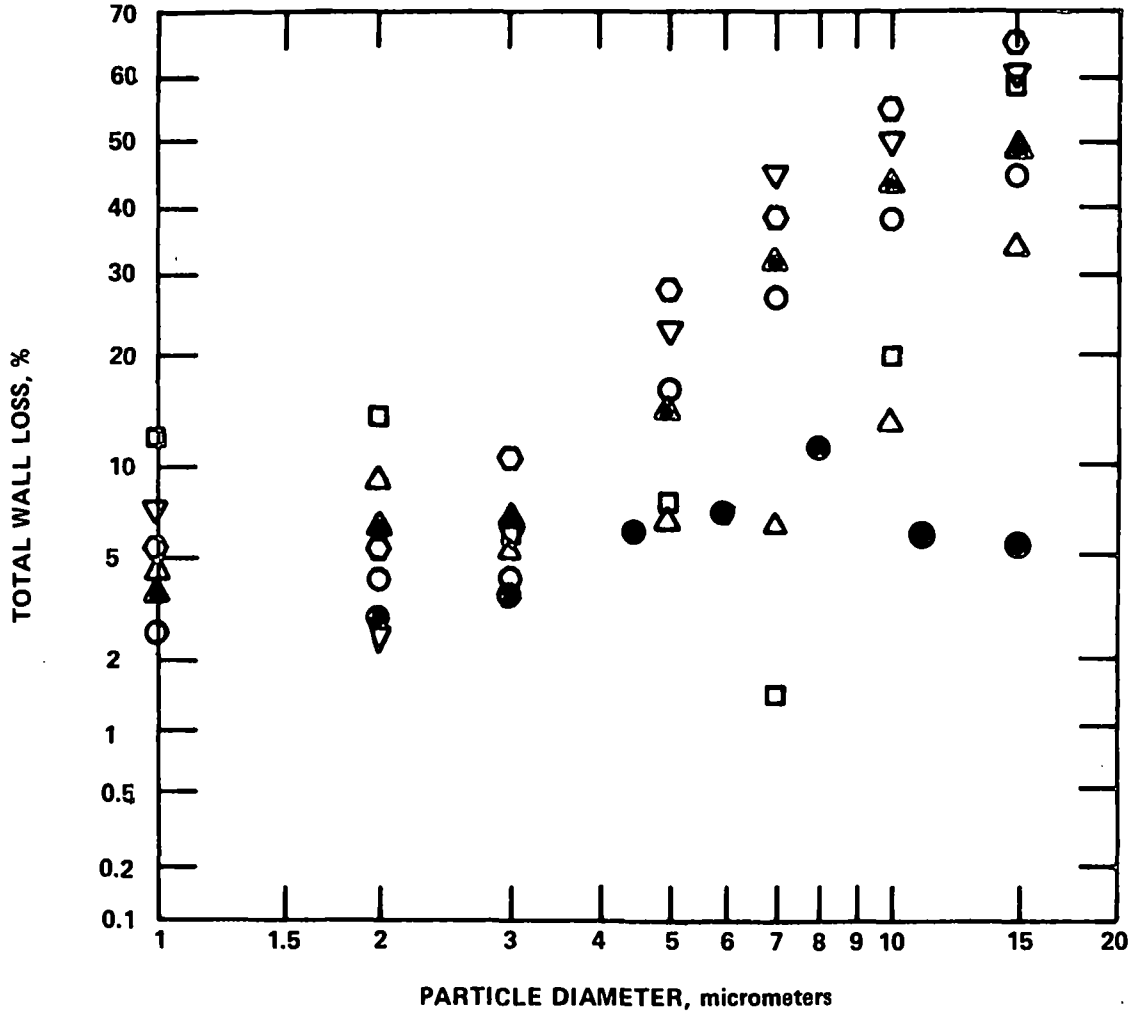


○ ANDERSEN MARK III STACK SAMPLER. NONISOKINETIC SAMPLING.
□ MODIFIED BRINK MODEL BMS-II CASCADE IMPACTOR. GLASS FIBER SUBSTRATES. NONISOKINETIC SAMPLING.
△ MODIFIED BRINK MODEL BMS-II CASCADE IMPACTOR. GREASED COLLECTION PLATES. NONISOKINETIC SAMPLING.
▽ MRI MODEL 1502 INERTIAL CASCADE IMPACTOR. NONISOKINETIC SAMPLING.
⬡ SIERRA MODEL 226 SOURCE CASCADE IMPACTOR. 14LPM. NONISOKINETIC SAMPLING.
● SIERRA MODEL 226 SOURCE CASCADE IMPACTOR. 7LPM. ISOKINETIC SAMPLING.
△ U. of W. MARK III SOURCE TEST CASCADE IMPACTOR. NONISOKINETIC SAMPLING.

*Figure 56. Total wall loss vs. Particle diameter.*

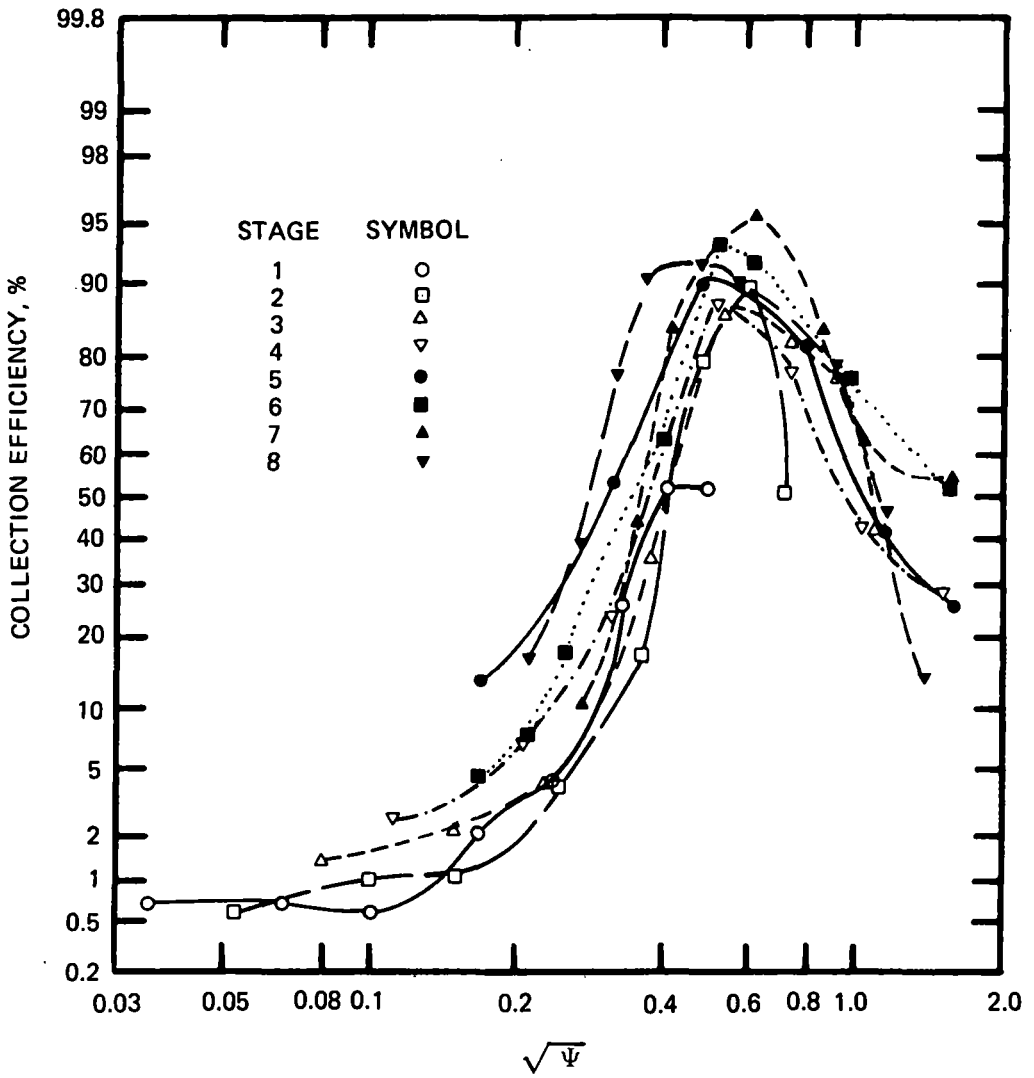


*Figure 57. Collection efficiency vs. $\sqrt{\Psi}$. Andersen Mark III Stack Sampler with glass fiber collection substrates.*

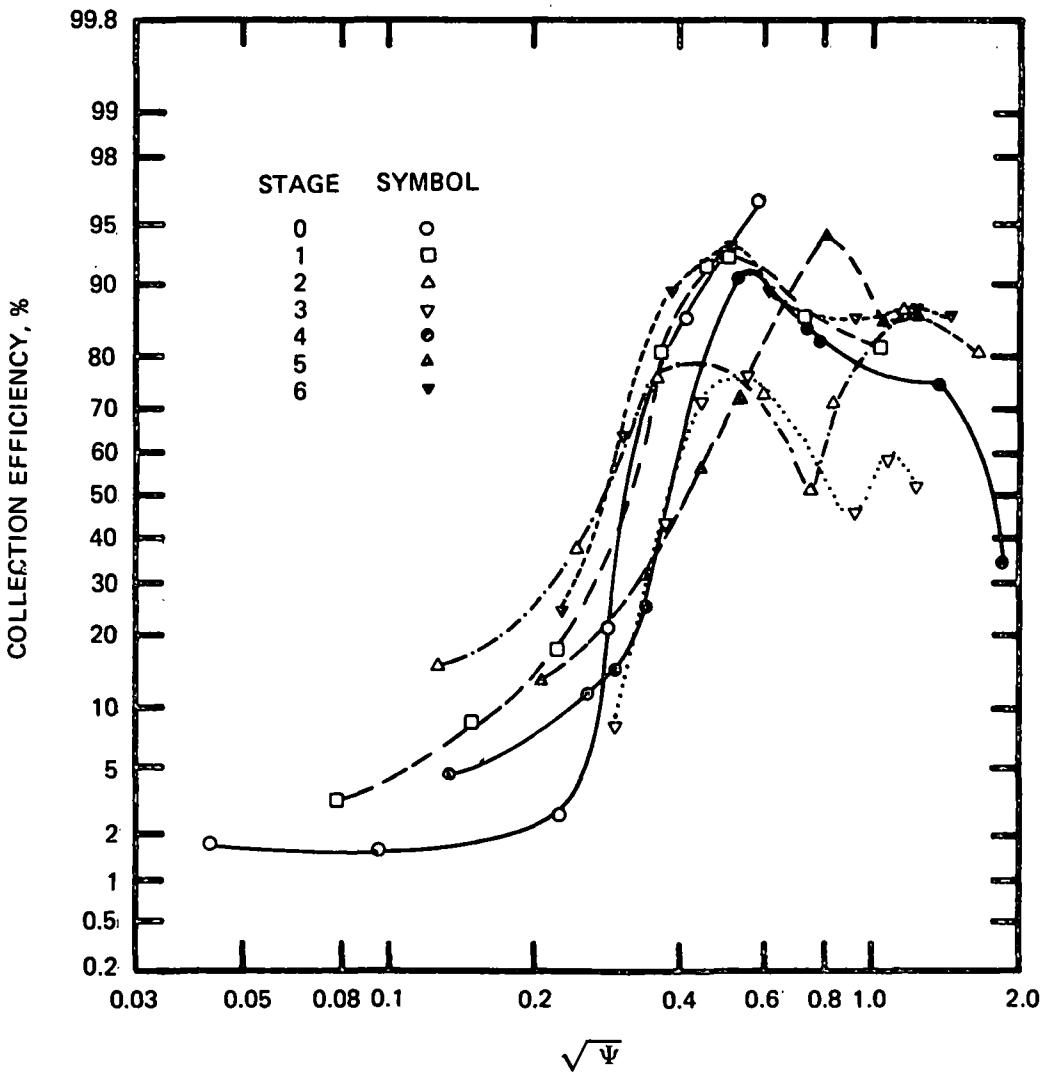


*Figure 58. Collection efficiency vs. $\sqrt{\Psi}$. Brink Model BMS--11 Cascade Impactor with glass fiber collection substrates.*

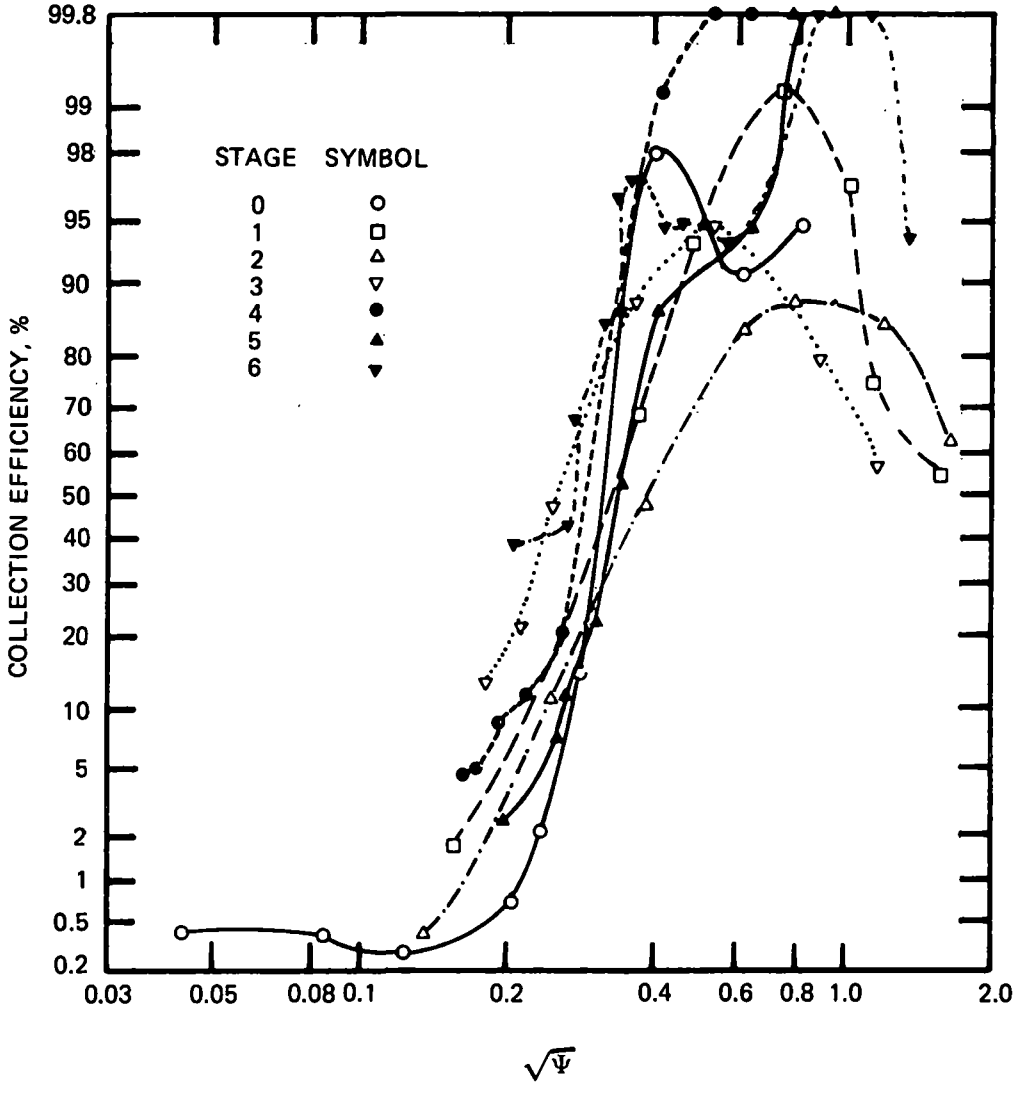


*Figure 59. Collection efficiency vs. $\sqrt{\Psi}$. Brink Model BMS--11 Cascade Impactor with greased collection plates.*

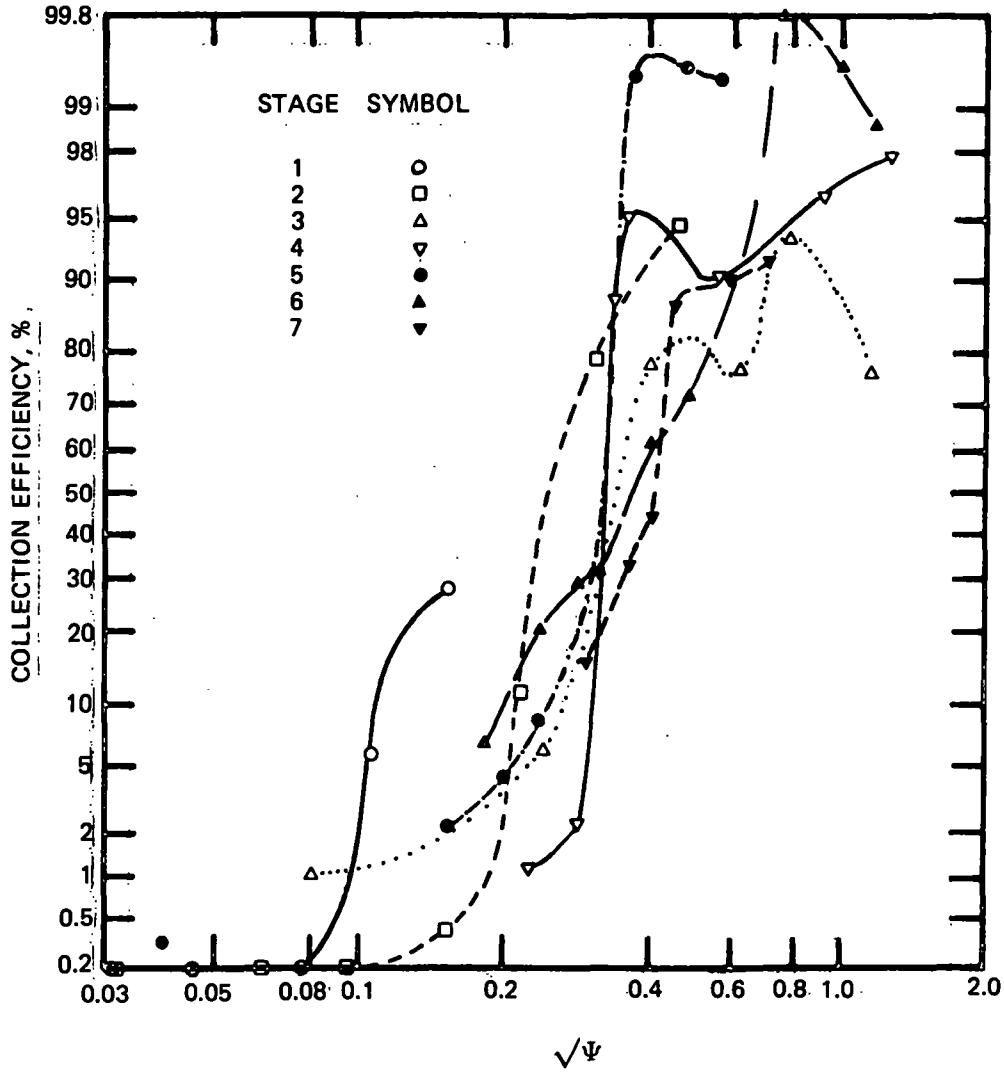


*Figure 60. Collection efficiency vs. $\sqrt{\Psi}$ MRI Model 1502 Inertial Cascade Impactor with greased collection plates.*

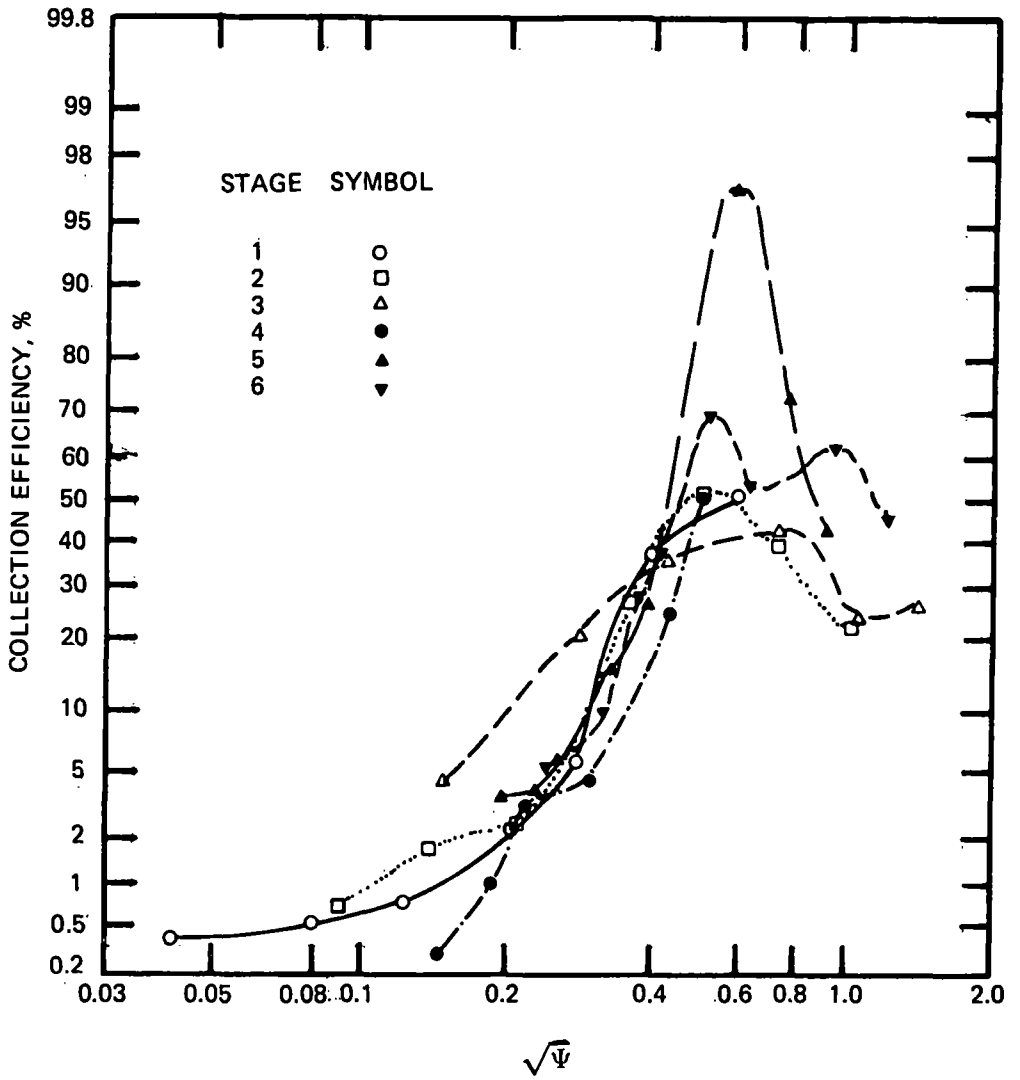


*Figure 61. Collection efficiency vs. $\sqrt{\Psi}$ . Sierra Model 226 Source Cascade Impactor with glass fiber collection substrates. Sampling flow rate is 14 LPM.*

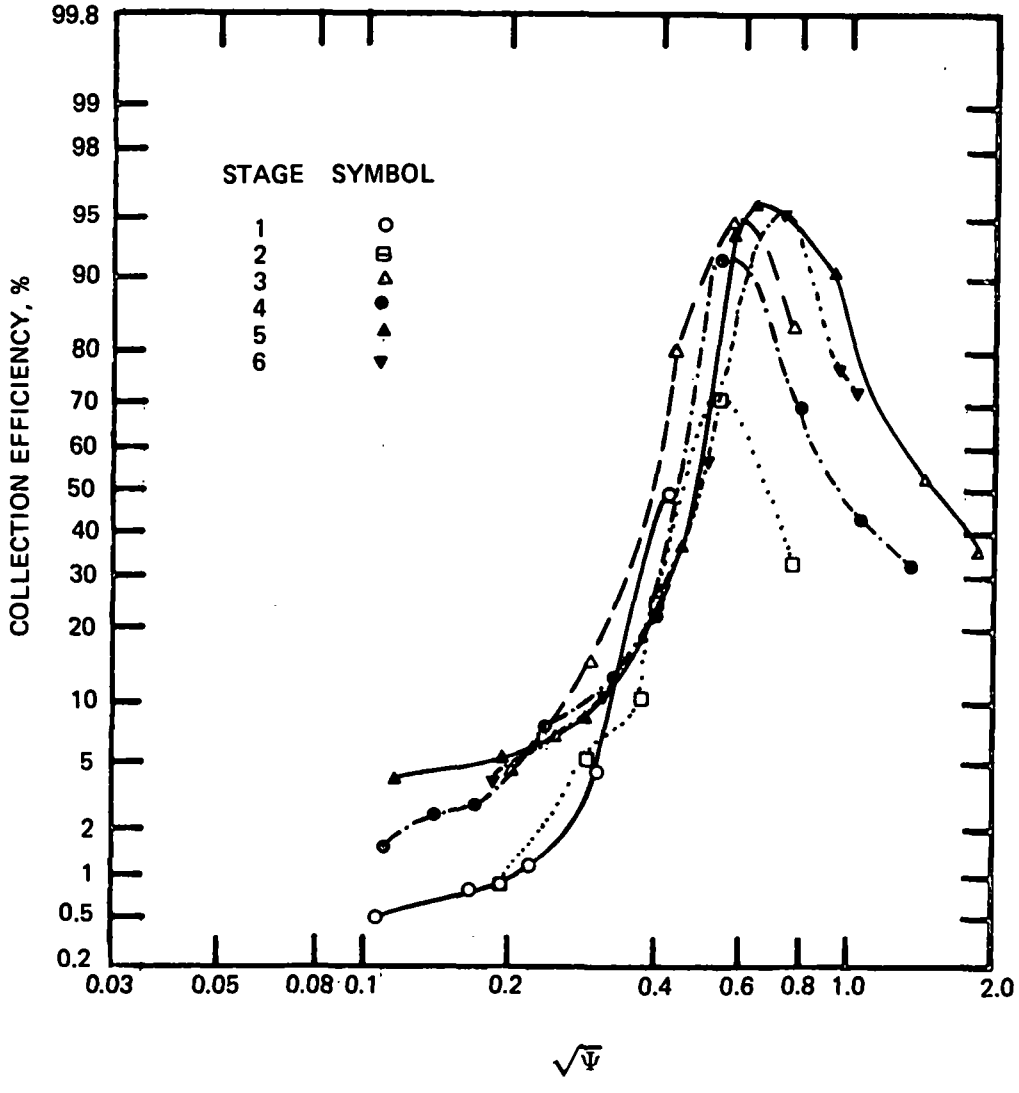


*Figure 62. Collection efficiency vs. $\sqrt{\Psi}$. Sierra Model 226 Source Cascade Impactor with glass fiber collection substrates. Sampling flow rate is 7 LPM.*

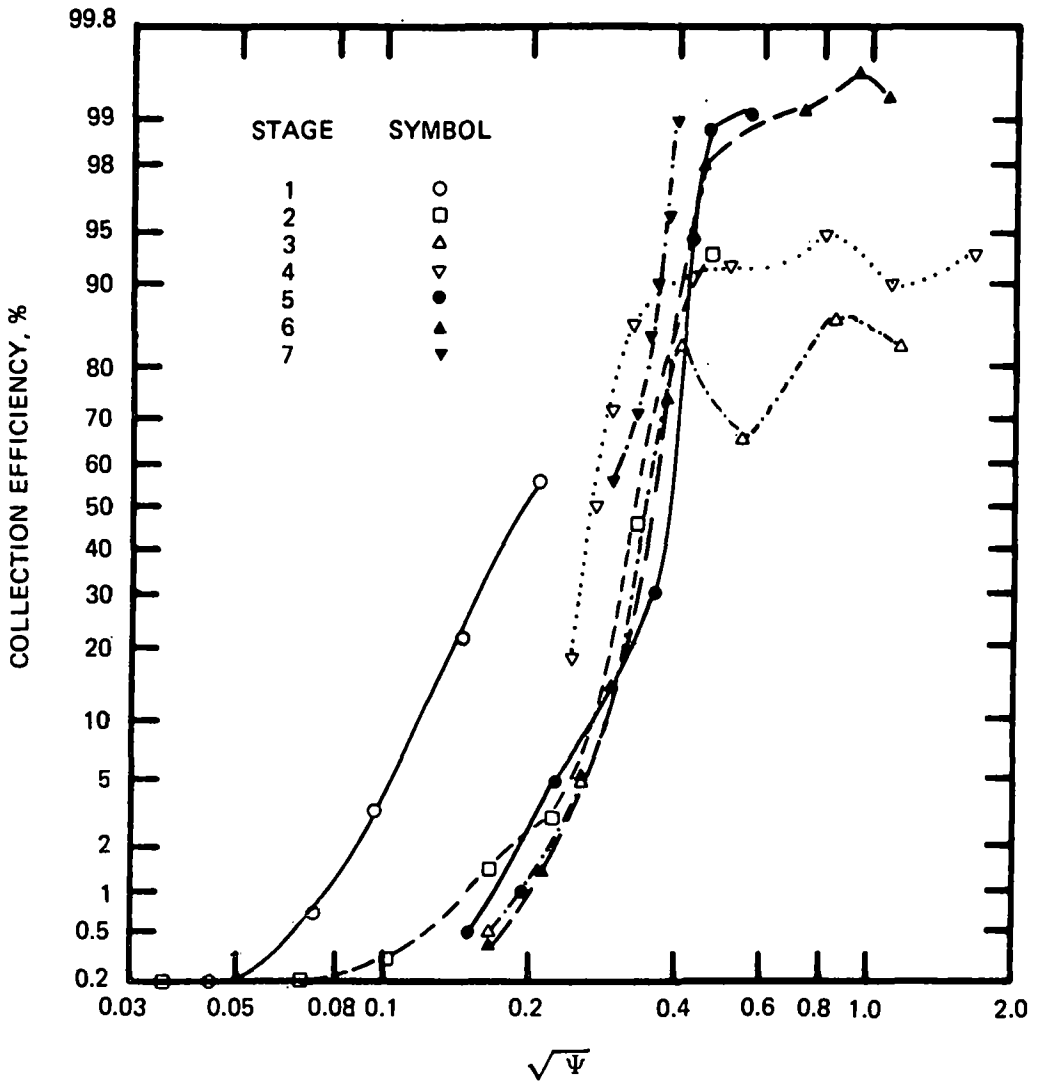


*Figure 63. Collection efficiency vs. $\sqrt{\Psi}$. University of Washington Mark III Source Test Cascade Impactor with greased collection plates.*

be done. No existing theory is comprehensive enough to compensate for the variations in geometry and application techniques for single devices, among different devices, or among different users.

A difference can also be seen between the shapes of the empirical calibration curves and the curves predicted by Marple's theory. The empirical curves show a smooth tail which approaches zero for small values of $\sqrt{\psi}$. Marple's theory, however, predicts a sharp intersection between the efficiency curves and the abscissa. The "tails" are possibly due, at least in part, to the fact that the calibration aerosols cannot be made perfectly monodisperse, and always contain multiplets.[23] Such "tails" are probably unavoidable when using the VOAG, because these devices, at best, produce about 4% doublets at all times.

The graphs also indicate a more severe problem, common to all cascade impactors. On a majority of the stages the collection efficiency does not reach 100% at any value as would be expected theoretically. Also, after reaching a maximum point, the curves fall off to lower efficiencies at higher $\sqrt{\psi}$ values. This means that some large particles will not be collected on upper stages and will be passed through the impactor to lower stages or even the back up filter. An accurate knowledge of this type of behavior is essential to the proper design and application of cascade impactors.

The theoretical data of Marple[18] plotted in Figure 53 show shifts in the square root of the Stokes Number, $\sqrt{\psi}$, which depend upon the jet to plate spacing ratio ($S/D_j$) and the Reynolds Number (Re). The values of $\sqrt{\psi}$ corresponding to a given particle collection efficiency increase for increasing jet to plate spacing ratio and decrease for increasing Reynolds Number.

For the Andersen Mark III the values of the jet to plate spacing ratio change from about 1.5 to 10 between Stages 1 and 8. Theoretically this should cause the $\sqrt{Stk}$ curve to shift to larger values and become much steeper. The Reynolds Number changes from about 45 to 500 between Stages 1 and 8. Theoretically this should cause a shift to the left in the $\sqrt{Stk}$ values as well as causing them to be steeper.

Although it is difficult to pinpoint the exact cause for the shifts in the Andersen data shown in Figure 57, the general shift to smaller $\sqrt{\psi}$ values and the corresponding increase in steepness could be due, in part, to a combination of these effects due to jet to plate spacing ratio and Reynolds Number.

The values of these parameters for the other impactors indicate that the effects would be much more difficult to separate and characterize because of the smaller changes in these values.

## Conclusions

Five commercially available cascade impactors have been calibrated during this study. The method of calibration and the presentation of the results should make this data useful to both the field operator of these devices as well as those interested in the theory of impactor design.

Based on this work, several conclusions can be drawn.

1. The value of $\sqrt{\psi_{50}}$ for each stage of a multiple stage impactor may be different. Prior to the current awareness of the importance of impactor calibration, it was the practice of many cascade impactor manufacturers and users to assume that the value of $\sqrt{\psi_{50}}$ for every stage was identical. In many cases the experimental value determined by Ranz and Wong[17] was used. Attempts to perform calibrations were not comprehensive. The theories of cascade impactor operation at this time do not describe the behavior of cascade impactors accurately enough to make it unnecessary to calibrate each device empirically.

2. The stage collection efficiencies are sensitive to the type of impactor collection substrate which is used. This is evident in the comparison of the Brink Cascade Impactor data using glass fiber collection substrates and greased collection plates. This strong dependence of collection efficiency on stage collection substrate material has also been explicitly illustrated and discussed by Willeke[24] and Rao.[16]

3. In the majority of cases the stage collection efficiency never reaches 100% for any particle size but reaches a maximum value that usually falls between 80% and 95%. This implies that some greatly oversized particles will reach every stage beyond the first stage. Unless suitable compensation can be made for the presence of these oversized particles, their presence will tend to bias the apparent particle size distribution toward higher than actual concentrations of fine particles and reduced concentrations of large particles. These errors probably tend to be more significant for the fine particle end of the distribution.

4. Ideally, an impactor stage should reach 100% collection efficiency for some particle size and stay at that value for all larger particle sizes. In practice, however, this is not the case as demonstrated by this study. In general, the stage collection efficiency reaches a maximum less than 100% and then rolls off and decreases for particles larger than a certain size. This is attributed to the fact that these larger particles strike the plate with appreciable momentum, bounce, and are thus carried to a lower stage. The use of grease on the collection plates as well as a reduction in the impactor flow rate tends to decrease the magnitude of this problem. The Sierra impactor data illustrate the increase in collection efficiency which resulted from a decrease in sampling flow rate and concomitant reduction in bounce and cascading of large particles to lower stages. This study shows that in some cases the maximum efficiency was almost doubled by lowering the flow rate. A discussion of this phenomenon has also been presented by Rao.[16]

A more detailed description of this calibration study and its results has been published in a document entitled "Particle Sizing Techniques for Control Device Evaluation: Cascade Impactor Calibration." EPA 600/2-76-280. NTIS PB-262-849 ($5.00).

## Soviet Impactor-Cyclone Calibration (Technical Directive Number 20201)

Description of Task:

Under a joint U.S.-Soviet Technological Information Exchange Program four Soviet built cascade impactors were sent to Southern Research Institute to be calibrated. The upper stages were calibrated using aerosols generated with a Vibrating Orifice Aerosol Generator. The lower stages were calibrated using polystyrene latex spheres dispersed with a Pressurized Collison Nebulizer System.

Summary of Progress:

Under this task three Soviet cascade impactors and one Soviet impactor/cyclone were calibrated. The three cascade impactors included one twelve stage device and two fourteen stage impactors. The three stage impactor/cyclone had a single impaction stage followed by two cyclonic stages. All four devices had an integral back-up filter holder which uses a plug of glass wool fibers.

A photograph of one of the fourteen stage Soviet impactors is shown in Figure 64. Figure 65 shows the Soviet impactor/cyclone.

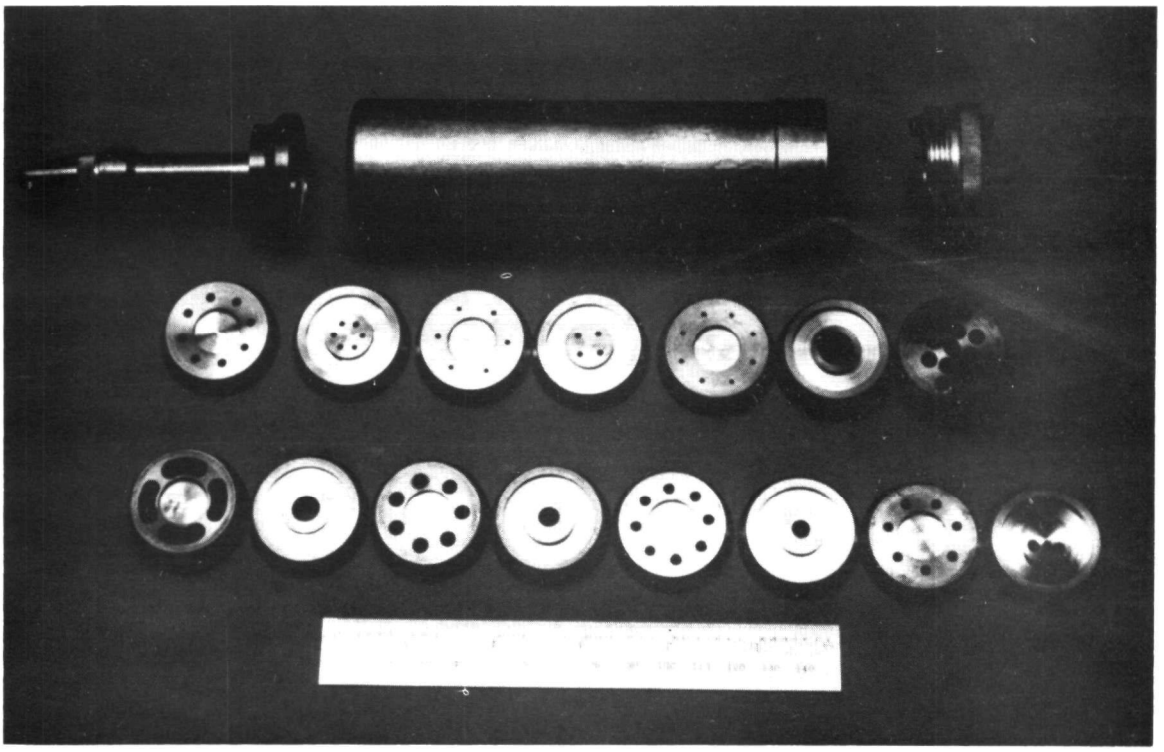

*Figure 64. Soviet 14--Stage Cascade Impactor.*

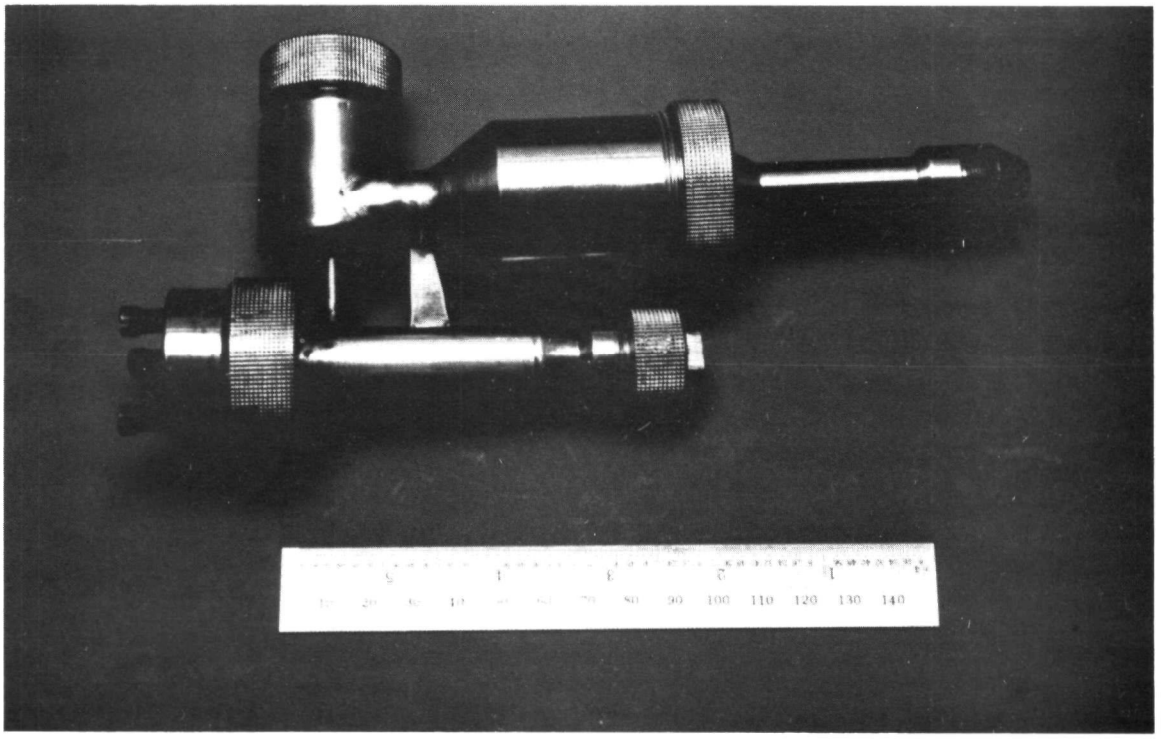

*Figure 65. Soviet 3--Stage Impactor/Cyclone.*

The upper stages of these sizing devices were calibrated using ammonium fluorescein aerosols (20 μm to 2 μm) dispersed by a Vibrating Orifice Aerosol Generator. The lower stages were calibrated using monodisperse polystyrene latex spheres (2.0 μm to 0.46 μm) dispersed by a Pressurized Collison Nebulizer System.

### Soviet Three Stage Impactor/Cyclone

As mentioned above, this instrument consists of a single impaction stage followed by two cyclonic stages. A back-up filter collected all particles passing the last stage. This device was constructed from titanium. A set of nozzles was supplied with the impactor/cyclone. All three stages were calibrated using monodisperse ammonium fluorescein particles with sizes ranging from 18 micrometers diameter to 2.3 micrometers diameter. The ambient pressure was 29.5" Hg, the temperature was 22°C, the particle density was 1.35 $gm/cm^3$, and the sampling flow rate was 10 liters per minute. At these conditions the cut points of the three stages were determined to be 13.5, 6.4, and 2.6 micrometers. The results are presented graphically in Figure 66.

### Soviet 12-Stage Cascade Impactor

This impactor is uniquely designed in that several stages are designed to have identical cut points. Because of this feature, the impactor has seven effective stages. The twelve stages are paired as follows: 1 and 2, 3 and 4, 5, 6 and 7, 8, 9 and 10, 11 and 12. In field use the mass collected by single stages 1 and 2 is combined as the catch for effective stage 1. In a similar manner the mass collected by single stages 11 and 12 becomes the combined catch for effective stage 7. The calibration conditions were an ambient pressure of 29.5" Hg, a temperature of 22°C; the particle density was 1.35 $gm/cm^3$ and the sampling rate was ten liters per minute. Because of the type of construction of this impactor, it was only possible to calibrate it using ammonium fluorescein aerosols between 2 and 20 micrometers diameter. The calibration data are shown by stage both on an individual basis (Figure 67) and on an effective stage basis (Figure 68).

### Soviet 14-Stage Cascade Impactor (Small $D_{50}$'s)
### Soviet 14-Stage Cascade Impactor (Large $D_{50}$'s)

These cascade impactors are similar in design to the Soviet 12 Stage impactor in that their 14 single stages are divided into seven effective stages with a pair of single stages per effective stage. Each member of a pair is theoretically designed to have the same cut point. These seven effective stages are numbered

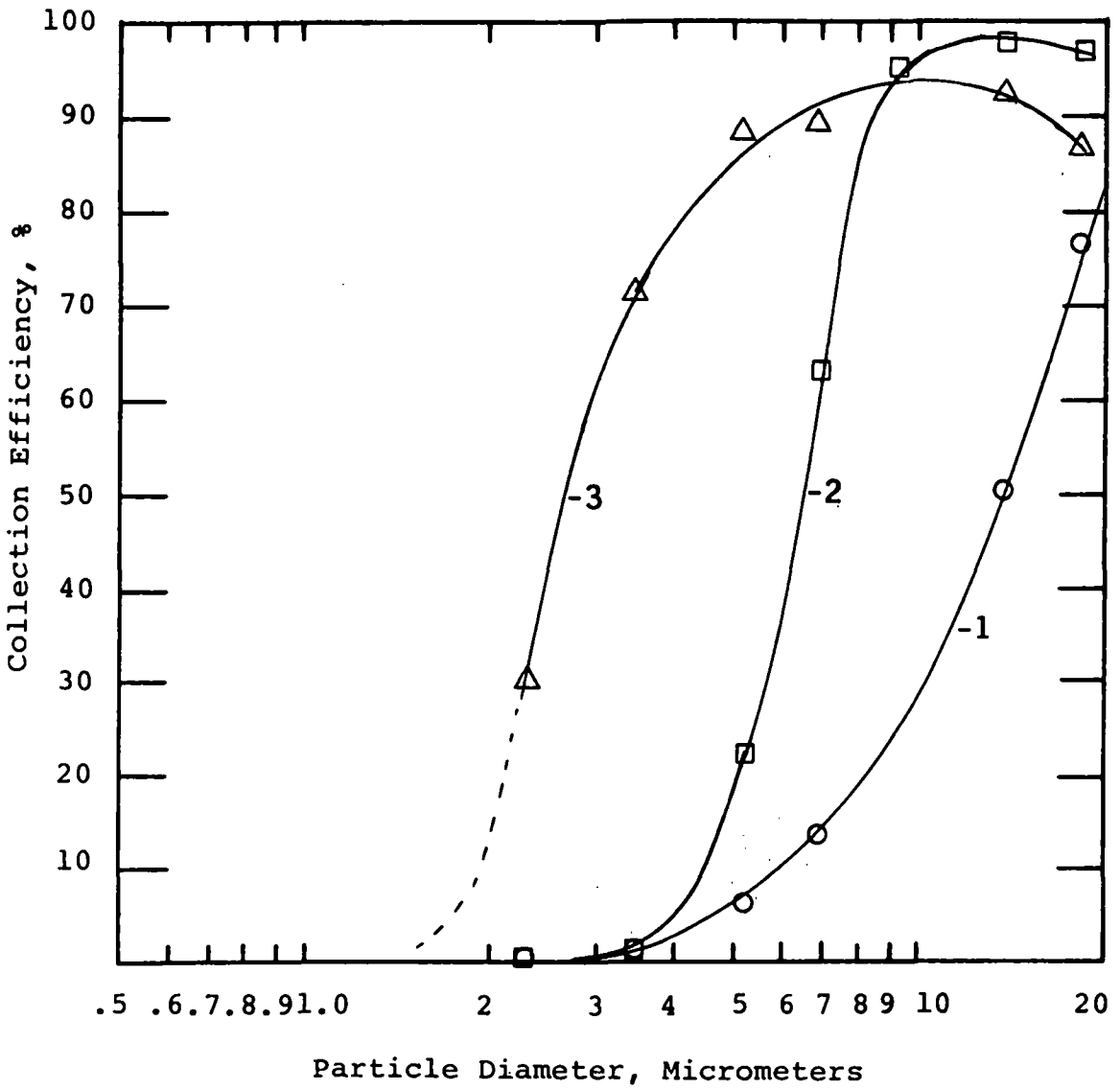


*Figure 66. Collection efficiency vs. Particle diameter. Soviet 12--Stage Impactor/Cyclone.*
*1---Impaction Stage 2---1st Cyclone 3---2nd Cyclone*
*(29.5 in. Hg, 22°C, 1.35 gm/cm$^3$, 10 LPM)*

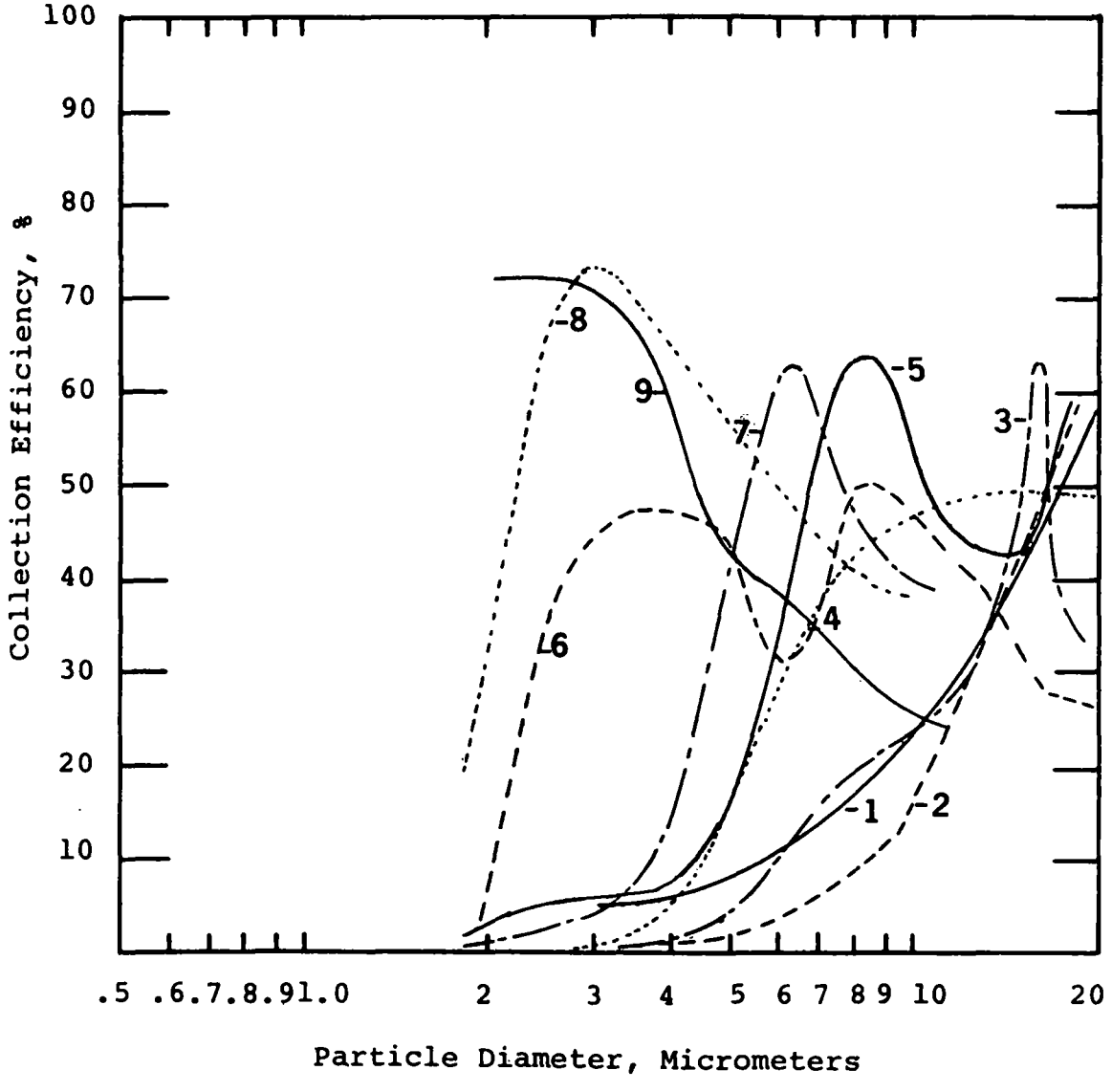


*Figure 67. Collection efficiency vs. Particle diameter. Soviet 12--Stage Cascade Impactor.*
*Data shown for the first nine stages from 2 to 20 microns.*
*(29.5 in. Hg, 22°C, 1.35 gm/cm$^3$, 10 LPM)*

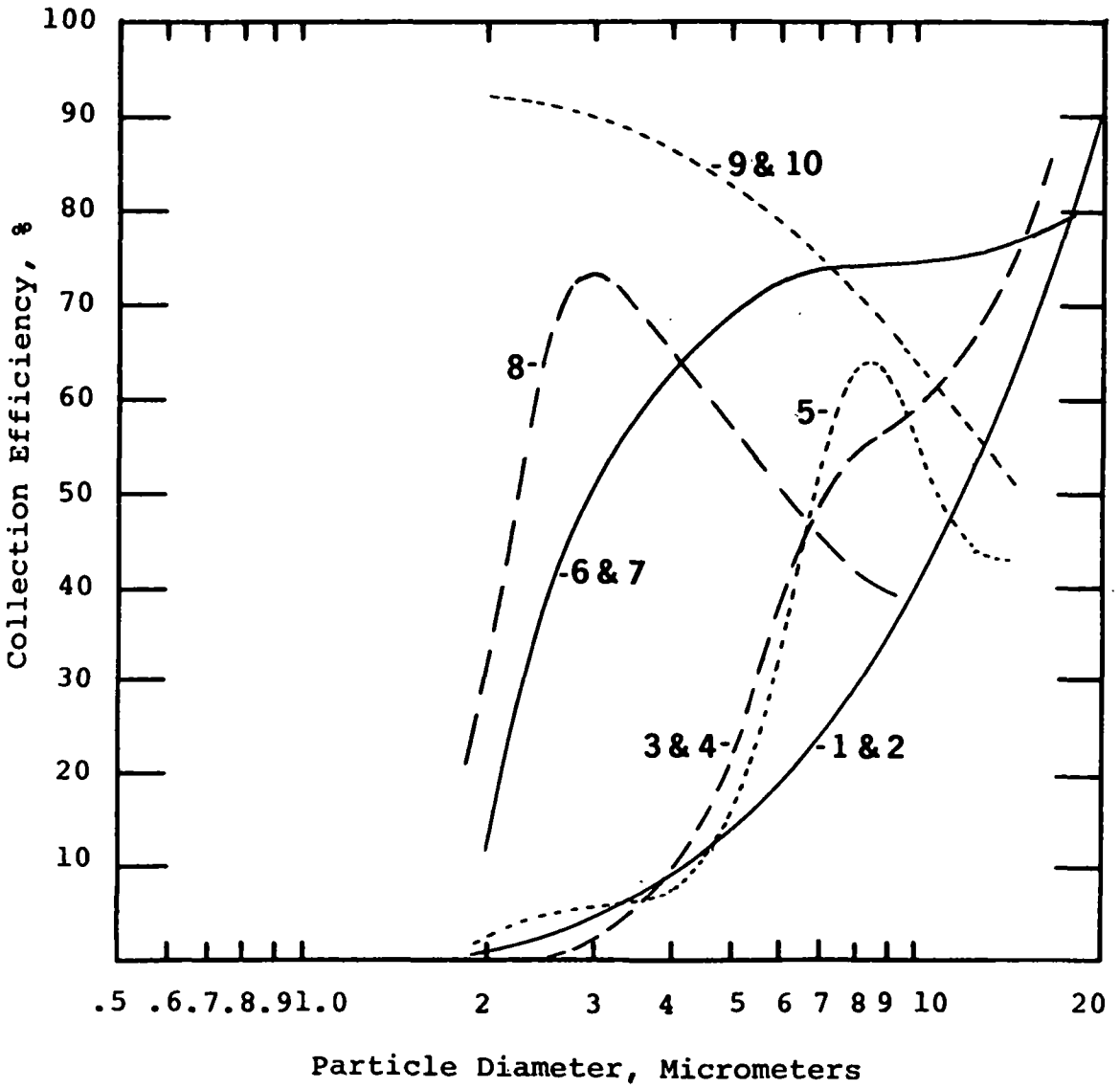


*Figure 68. Collection efficiency vs. Particle Diameter. Soviet 3--Stage Cascade Impactor.*
*Data shown in combined form in the configuration for field measurements.*
*(29.5 in. Hg, 22°C, 1.35 gm/cm$^3$, 10 LPM)*

1.1/1.2, 2.1/2.2, 3.1/3.2, 4.1/4.2, 5.1/5.2, 6.1/6.2, and 7.1/7.2. In practice the mass collected by individual stages 1.1 and 1.2, for example, is combined to give a total mass collected by the first effective stage. This procedure is repeated for the rest of the impaction stages. These two impactors have different cut points but share identical stages on five of the seven effective stages as illustrated in the following chart.

14-Stage Cascade Impactor

| Small $D_{50}$s | | Large $D_{50}$s |
|---|---|---|
| 1.1/1.2 | Same | 1.1/1.2 |
| 2.1/2.2 | | 2.1/2.2 |
| 3.1/3.2 | Same | 3.1/3.2 |
| 4.1/4.2 | Same | 4.1/4.2 |
| 5.1/5.2 | Same | 5.1/5.2 |
| 6.1/6.2 | Same | 6.1/6.2 |
| 7.1/7.2 | | 7.1/7.2 |

Effective stages 1, 2, 3, 4, and 5 of the small $D_{50}$ impactors are identical with stages 1, 4, 5, 6, and 7 of the large $D_{50}$ impactor, respectively. It was possible to calibrate both impactors with ammonium fluorescein and polystyrene latex particles; however, it was not possible to complete the calibration on stages 7.1/7.2 of the small $D_{50}$ impactor since the pressure drop across these stages was greater than our calibration apparatus could maintain. The results of the calibration are depicted graphically in Figures 69 and 70.

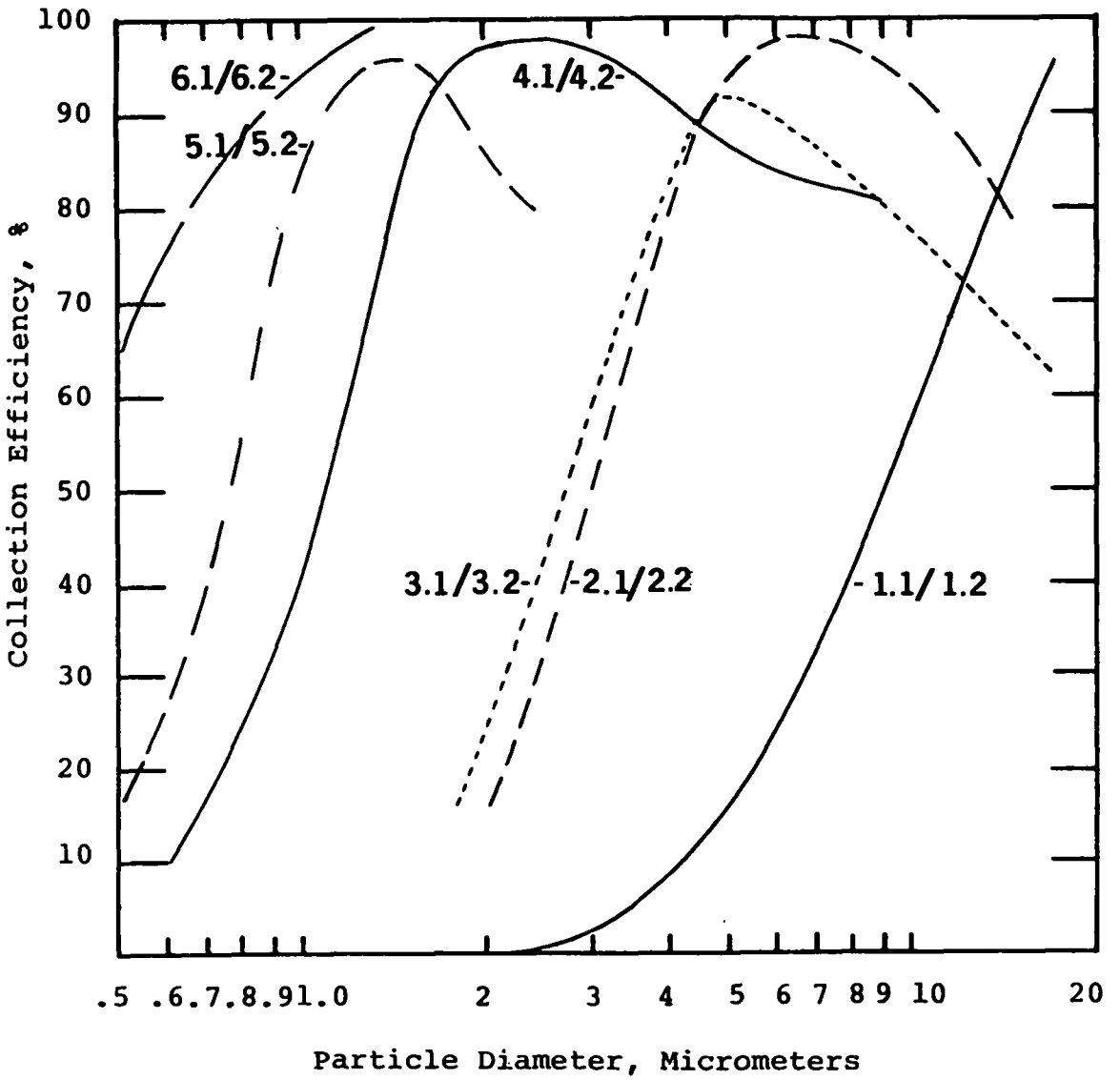


*Figure 69. Collection efficiency vs. Particle diameter. Soviet 14--Stage Cascade Impactor. (Small Cutpoints)*
*Data shown in combined for for the first six of the seven stage pairs.*
*(29.5 in. Hg, 22°C, 1.35 gm/cm$^3$, 10 LPM)*

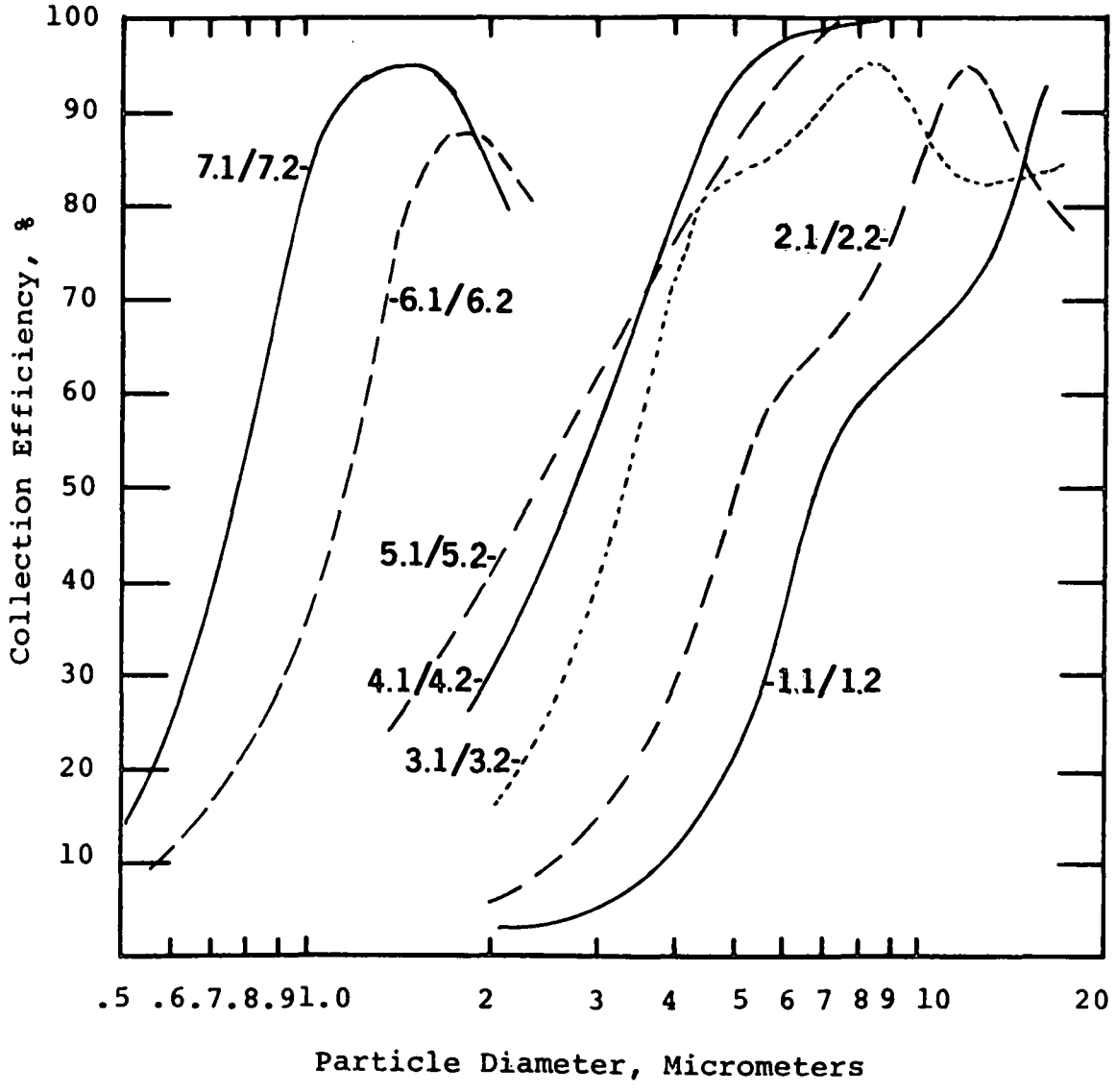


*Figure 70. Collection efficiency vs. Particle diameter. Soviet 14-Stage Cascade Impactor. (Large Cutpoints)*
*(29.5 in. Hg, 22°C, 1.35 gm/cm$^3$, 10 LPM)*

## Task Category - Cyclones

### Develop and Evaluate Five Stage Series Cyclone System (Technical Directive Number 10602)

Description of Task:

Based on the work previously done under Contract No. 68-02-0273, a series cyclone system was designed and constructed. The design goals were 5 cut points and compactness to fit into a four inch port.

1. The cyclones were calibrated using laboratory aerosols. This was done over the range of temperatures expected for field sampling.

2. Minor modifications were made to the prototype and recalibrated.

3. Tests will be performed at a suitable site to compare the performance of the cyclone with cascade impactors.

4. A special report on the design, calibration, evaluation, and operation of the system is being written.

Progress Summary:

A Five Stage Series Cyclone has been designed and a schematic is shown in Figure 71. It has a nominal sampling rate of 472 $cm^3$/sec (1.0 $ft^3$/min). Both a black anodized aluminum and a titanium prototype have been constructed. Preliminary calibration results for the five cyclones are shown in Figure 72.

A more extensive calibration of these cyclones has also been completed. The effect on cyclone behavior due to changes in flow rate, gas temperature, and particle density was studied. The preliminary results are shown in Table X. Work is also in progress on developing a theory of cyclone behavior based on these experimental data.

A complete field test of these prototypes is yet to be performed.

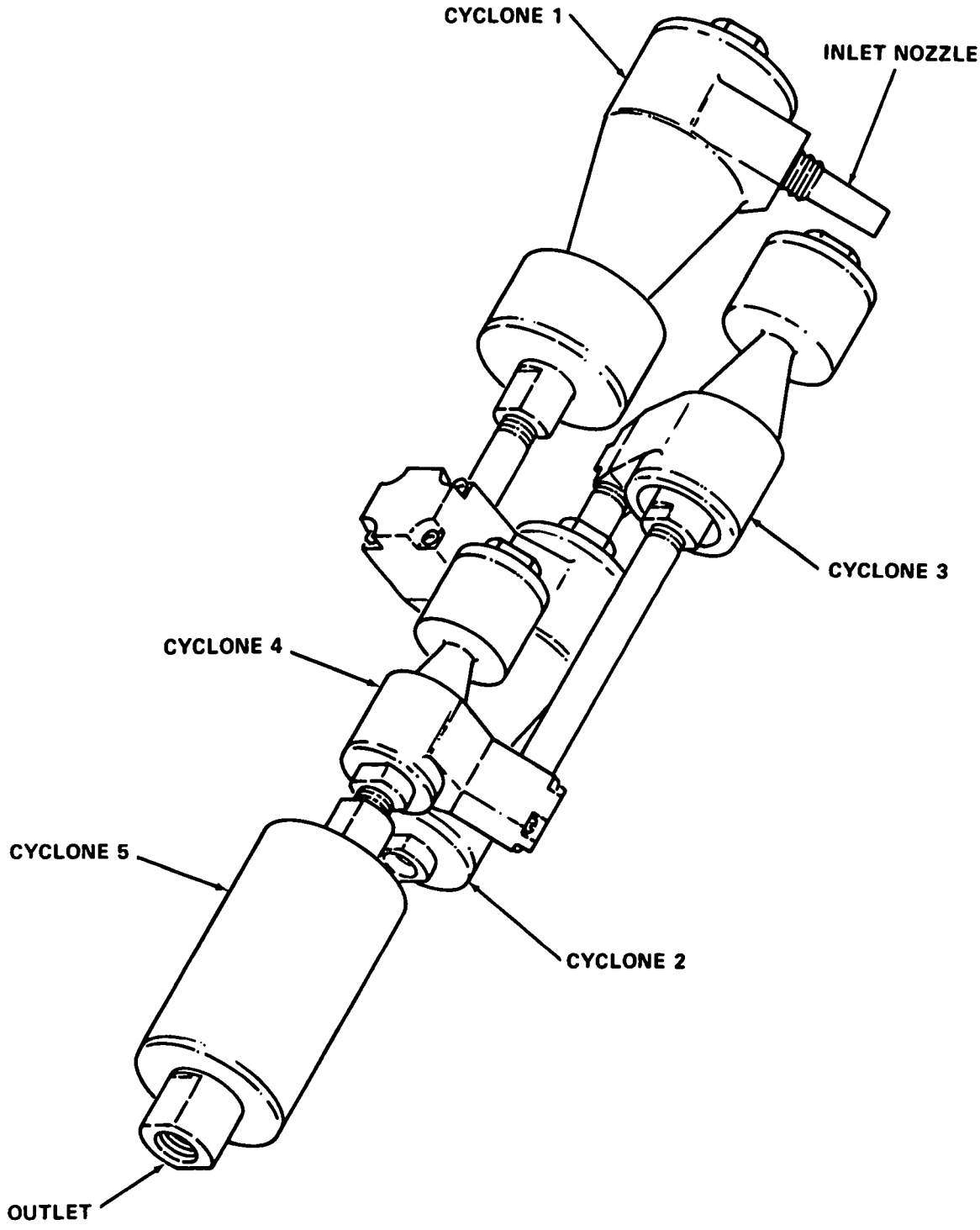


*Figure 71. Five Stage Series Cyclone System.*

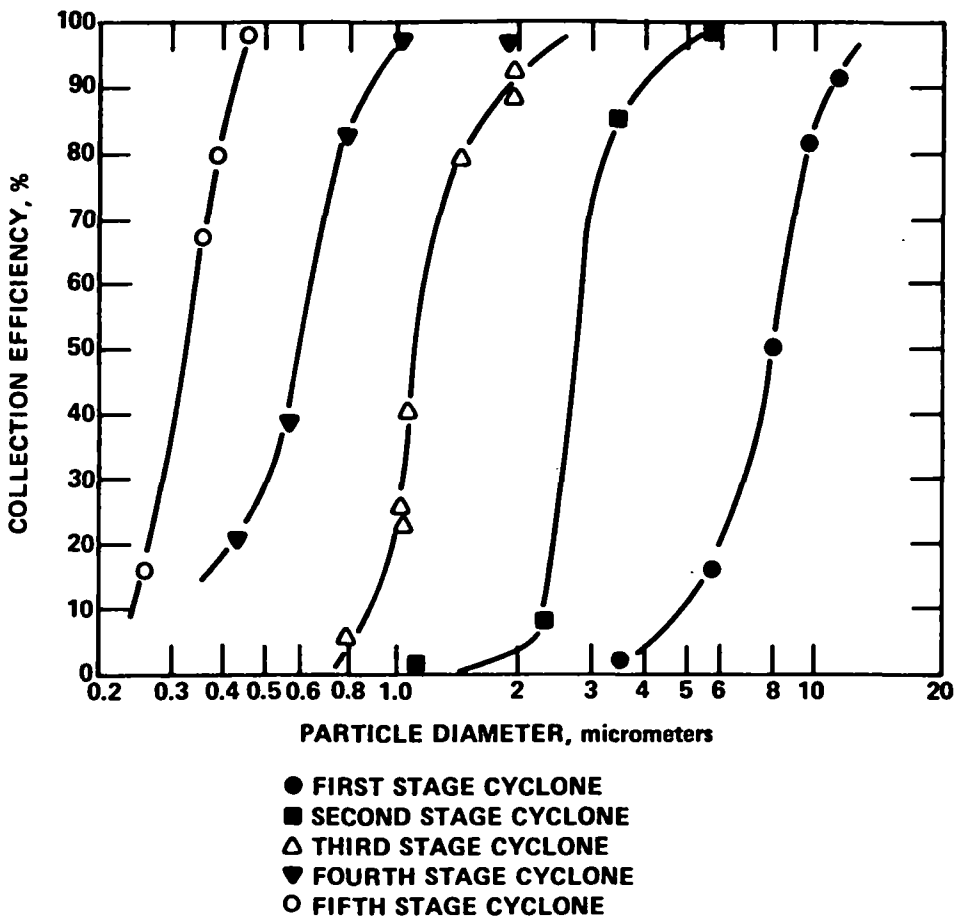


*Figure 72. Laboratory calibration for the Five Stage Series Cyclone System. (472 $cm^3$/sec, particle density—1.0 gm/$cm^3$)*

Table X

Laboratory Calibration of the Five Stage Series Cyclones - Values of $D_{50}$ cut points (in micrometers) for various conditions of sample flow, temperature, and particle density.

| Cyclone | | I | II | III | IV | V |
|---|---|---|---|---|---|---|
| Particle Density ($gm/cm^3$) | | 2.04/1.00 | 2.04/1.00 | 2.04/1.00 | 2.04/1.00 | 2.04/1.00 |
| Flow (LPM) | Temperature (°F) | | | | | |
| 7.0 | 77 | | | | -/2.5 | -/1.5 |
| 14.2 | 77 | 5.9/8.4 | 2.4/3.5 | | 1.0/1.5 | 0.59/0.85 |
| 28.3 | 77 | 3.8/5.4 | 1.5/2.1 | 0.96/1.4 | 0.44/0.63 | 0.22/0.32 |
| 28.3 | 200 | 4.4/- | 2.3/- | 1.2/- | | |
| 28.3 | 400 | 6.4/- | 2.9/- | 1.9/- | | |

## Calibration of the Source Assessment Sampling System Cyclones (Technical Directive Number 20302)

Description of Task:

The purpose of this task was to calibrate the SASS cyclones using both ammonium fluorescein aerosols (20 μm to 2.0 μm) and polystyrene latex spheres (2.0 μm to 0.46 μm). The calibration accuracy was to be sufficient to determine the cut point of the Middle Cyclone (nominally 3.0 μm) to within ±0.5 micrometers diameter.

Summary of Progress:

The three (3) cyclones of the Source Assessment Sampling System (SASS) were calibrated as described below. In the following discussion the terms Large, Middle and Small Cyclone refer to cyclones designed for room temperature $D_{50}$ values of 10 μm, 3 μm, and 1 μm, respectively.

The calibrations of the Large and Middle Cyclones were performed using ammonium fluorescein aerosols generated with Southern Research Institute's Vibrating Orifice Aerosol Generator (VOAG). Monodisperse ammonium fluorescein aerosols with diameters of 2, 3, 4, 5, 7.5, 10.5, and 14.5 micrometers were sampled at flow rates of 4 ACFM and 3 ACFM. These particles have a density of 1.35 $gm/cm^3$. After sampling for a sufficient length of time, each cyclone was washed with a known amount of $NH_4OH$ to dissolve the ammonium fluorescein aerosol. The total mass of the collected aerosol was determined using absorption spectroscopy. The collection efficiency of each cyclone was calculated and plotted versus particle diameter. Figures 73 and 74 present these Collection Efficiency Versus Particle Diameter data for the Large and Middle Cyclones, respectively.

The Small Cyclone was calibrated using Dow Corning PSL spheres dispersed with the Institute's Pressurized Collison Nebulizer System. Using an auxiliary pump, aerosols were pulled through the Small Cyclone at two flow rates, 3.1 ACFM and 1.8 ACFM. A Climet Instruments Model 208A Particle Analyzer was used to measure the number concentration of unit density 0.82 μm, 1.1 μm, and 2.2 μm diameter PSL spheres upstream and downstream of the Small Cyclone. The collection efficiencies were calculated and plotted versus the particle diameter as shown in Figure 75.

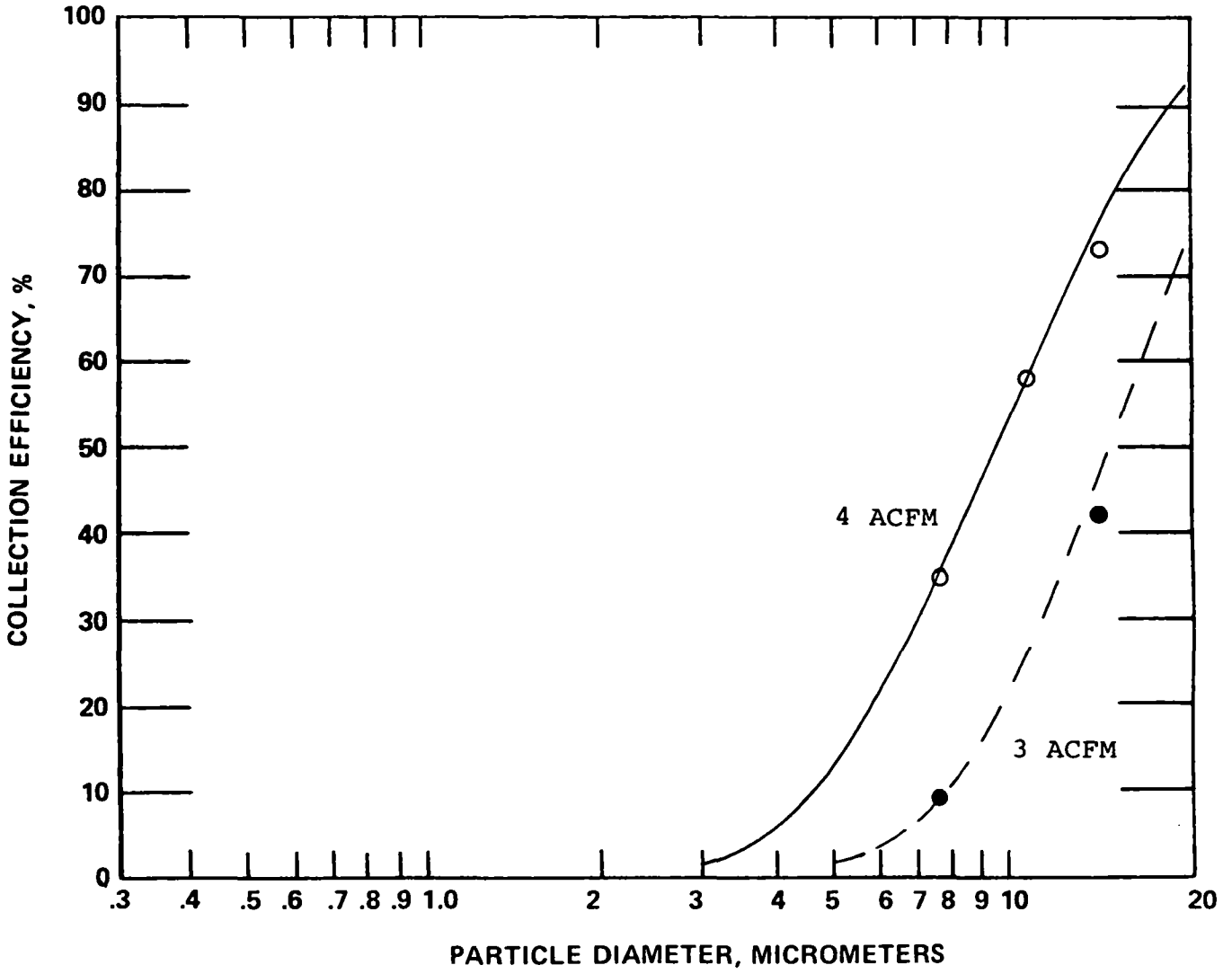


*Figure 73. Collection efficiency vs. Particle diameter. Large SASS Cyclone. Particle Density-----1.35 gm/cm$^3$*

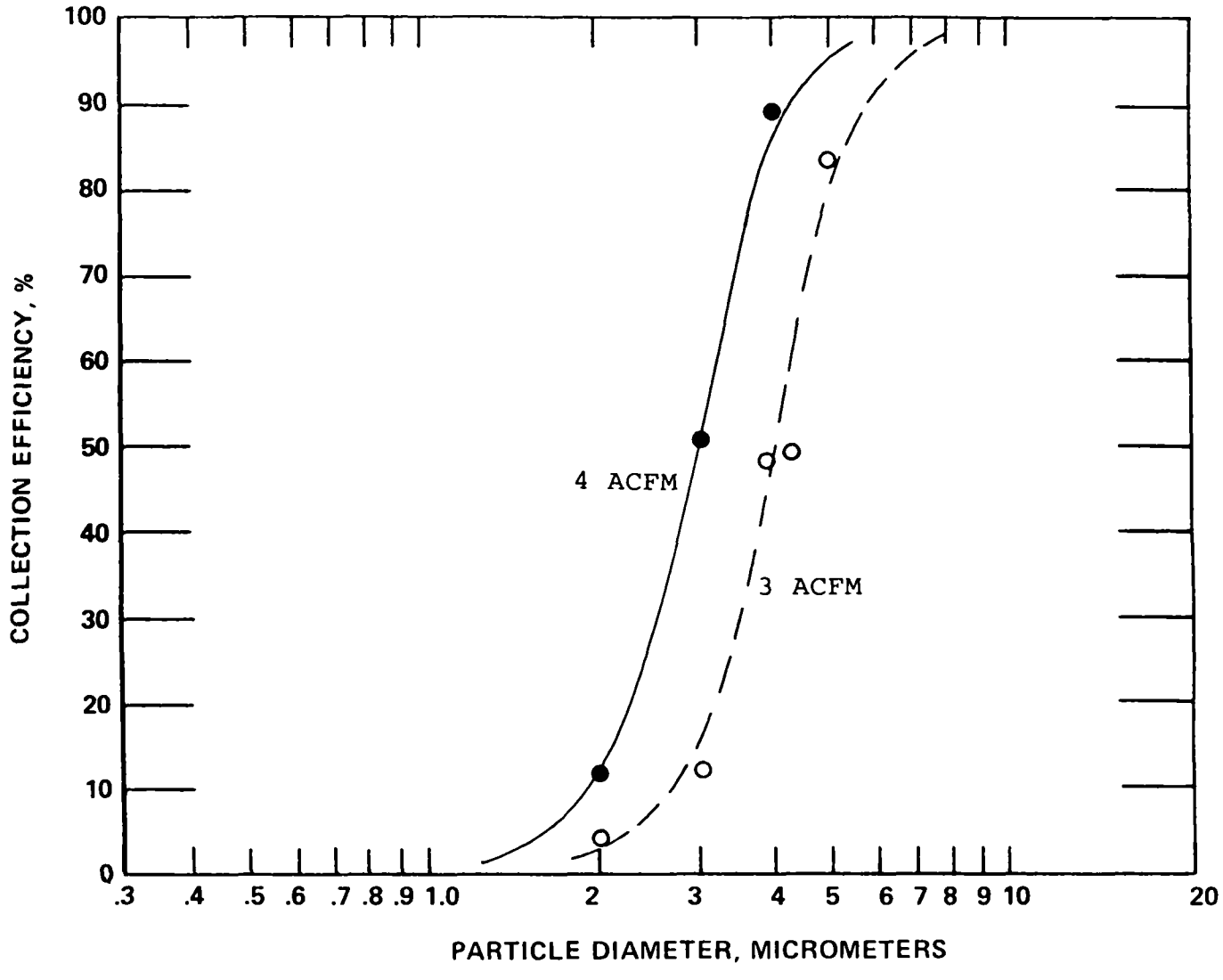


*Figure 74. Collection efficiency vs. Particle diameter. Middle SASS Cyclone. Particle Density-----1.35 gm/cm$^3$*

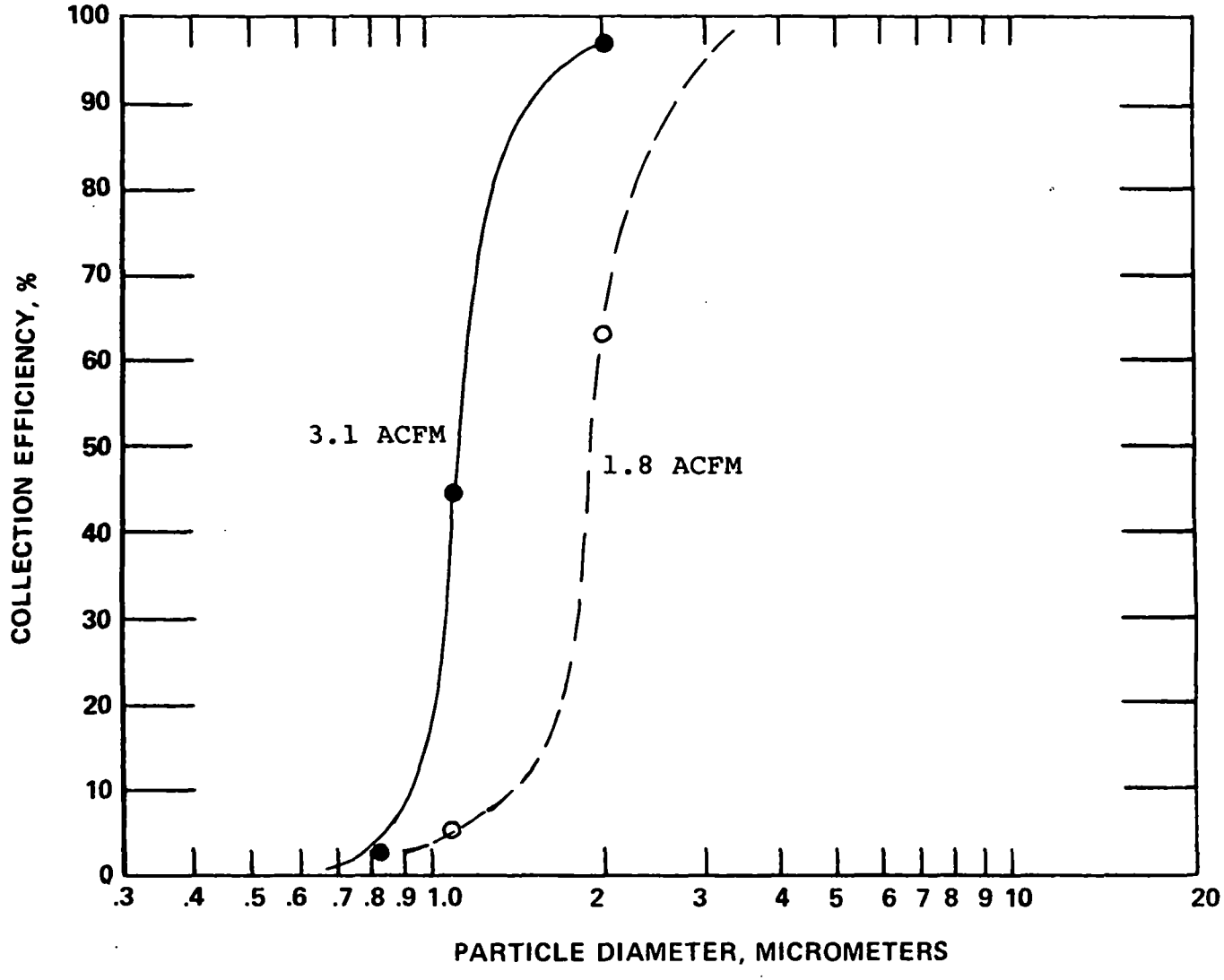


*Figure 75. Collection efficiency vs. Particle diameter. Small SASS Cyclone. Particle Density-----1.35 gm/cm$^3$*

Based on the results of this limited calibration study, it appeared that the cyclone $D_{50}$ cut point varied approximately inversely with the square root of the particle density as predicted by theory.

The specific data obtained in this study were extrapolated to obtain cyclone $D_{50}$'s for four combinations of flow rate and particle density (4 ACFM and 3 ACFM flow rates and 1.00 $gm/cm^3$ and 2.3 $gm/cm^3$ particle densities). The resulting graphs shown in Figure 76 indicate the approximate range of $D_{50}$ cut points which can be expected at temperatures near ambient.

## Recalibration of the Three SASS Cyclones (Technical Directive Number 20402)

Description of Task:

The three Source Assessment Sampling System cyclones were recalibrated at a sampling rate of 4 SCFM and a gas temperature of 400°F. There were two objectives of this task: (1) to establish the cut points of the three SASS cyclones as they presently exist, and (2) to determine what modifications and design parameters were required to achieve cut points of 10, 3, and 1 micrometers at a sampling rate of 4 SCFM and a gas temperature of 400°F.

Summary of Progress:

A recalibration of the three (3) cyclones of the Source Assessment Sampling System (SASS) at 400°F and 4 SCFM was performed. All data presented here have been corrected to unit density aerosols. In the following discussion the terms Large, Middle, and Small Cyclone are used to indicate the nominal 10 μm, 3 μm, and 1 μm $D_{50}$ cyclones, respectively. As reported under Technical Directive Number 20302, the previous calibration at 75°F and 4 ACFM gave approximately 0.86 μm, 3.5 μm, and 11.0 μm $D_{50}$ for the Small, Middle, and Large Cyclones, respectively.

The calibration of the Large and Middle Cyclones was performed using ammonium fluorescein aerosols generated with Southern Research Institute's Vibrating Orifice Aerosol Generator (VOAG). With the cyclones placed in a heated oven and using a heated inlet line, the temperature of the gas stream at the inlet to the Large Cyclone was maintained at 400°F. Particle integrity of the ammonium fluorescein at high temperature was a major problem. It appears that rapid heating of aerosol particles

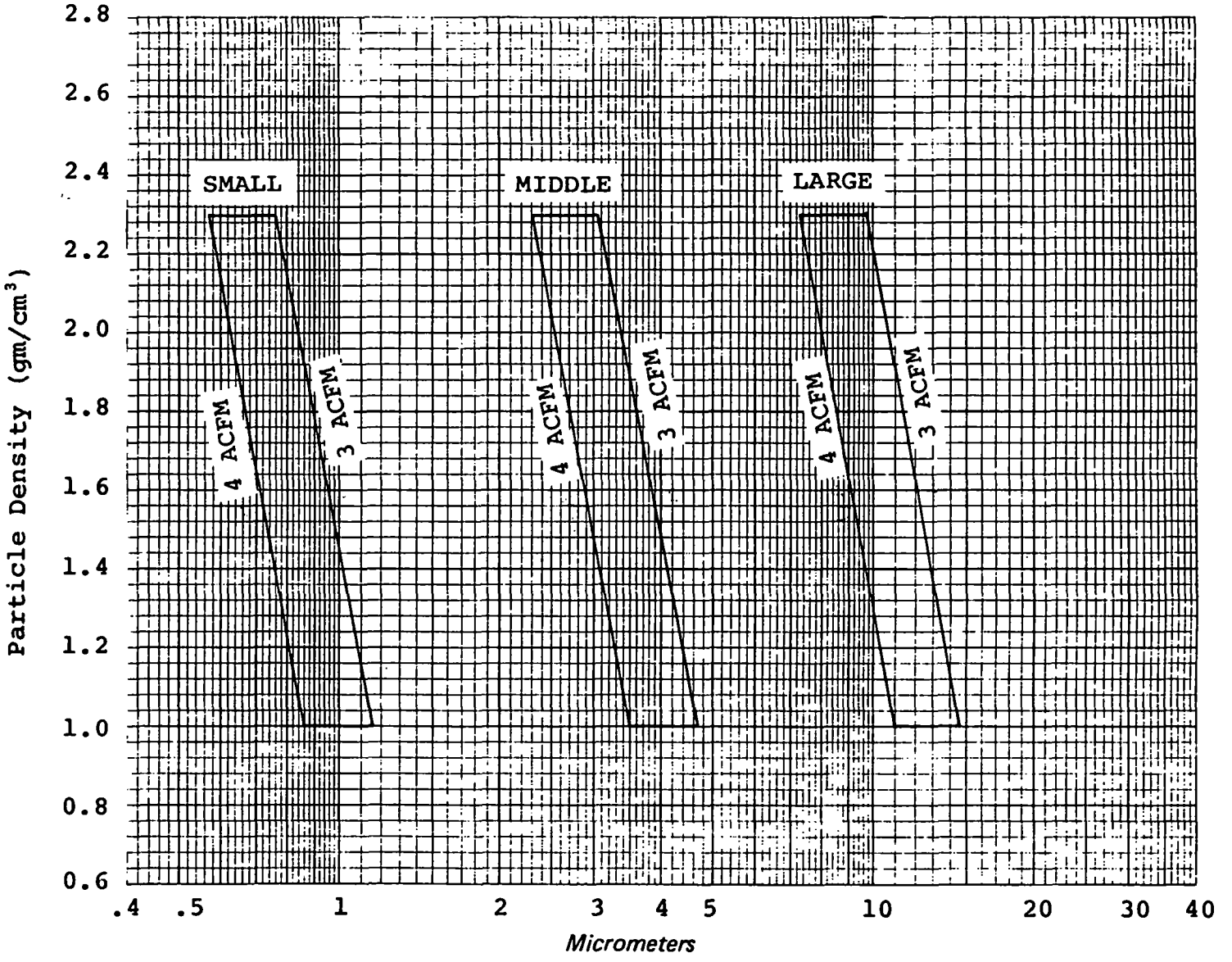


*Figure 76. SASS cyclone cut points. (At 23°C.)*

which had not dried sufficiently after generation caused these particles to explode creating a large concentration of contaminating small particulate matter. This problem was alleviated by allowing the aerosol to come up to temperature more slowly. We also observed a color change in the ammonium fluorescein before and after heating. Microscopic observation also indicated a possible crystalline change, causing us to question the integrity of the dry ammonium fluorescein particles.

The Large Cyclone was modified to try to obtain a $D_{50}$ closer to the desired 10 micrometers. This modification involved the removal of the vortex buster from the Large Cyclone outlet. Unfortunately, there was no apparent effect on the performance of this cyclone. The data for the Large Cyclone is shown in Figure 77.

The Middle Cyclone was also modified in an attempt to obtain a $D_{50}$ closer to the desired 3 micrometers. This was done by reducing the Middle Cyclone inlet diameter from 0.62 inches to 0.53 inches. The effect of this change was minimal as can be seen in Figure 78 and Figure 79 for the Unmodified and Modified Middle Cyclone, respectively.

The approximate $D_{50}$'s for the Large and Middle Cyclones at 400°F and 4 SCFM are 15 micrometers and 4.4 micrometers, respectively.

After considering the data obtained during this recalibration, it was felt that the desired $D_{50}$'s might possibly be obtained by removal of the vortex busters in the collection cups of the Large and Middle Cyclones. The resulting large tangential velocities near the walls of these cups should remove a sufficient number of particles to cause a significant and measurable change in the cut points. However, it was felt that a definitive characterization of the behavior of these cyclones could only be performed if the cyclones were kept for approximately two months. This would allow time for careful consideration of solutions to problems which might arise during the calibration procedure.

On September 14, 1976, a meeting was held at Research Triangle Park to discuss the results of the recalibration of the SASS train cyclones at 4 SCRM and 400°F. It was decided that the results of this study were not sufficiently conclusive to recommend changes in the cyclone construction to obtain the desired cut points of 10, 3, and 1 micrometer at operating conditions of 400°F and 4 SCFM. Data were presented indicating possible physical changes in the ammonium fluorescein aerosol at high temperature. Also the shift in the cyclone calibration curves at these conditions was not expected based on current cyclone operation theories.

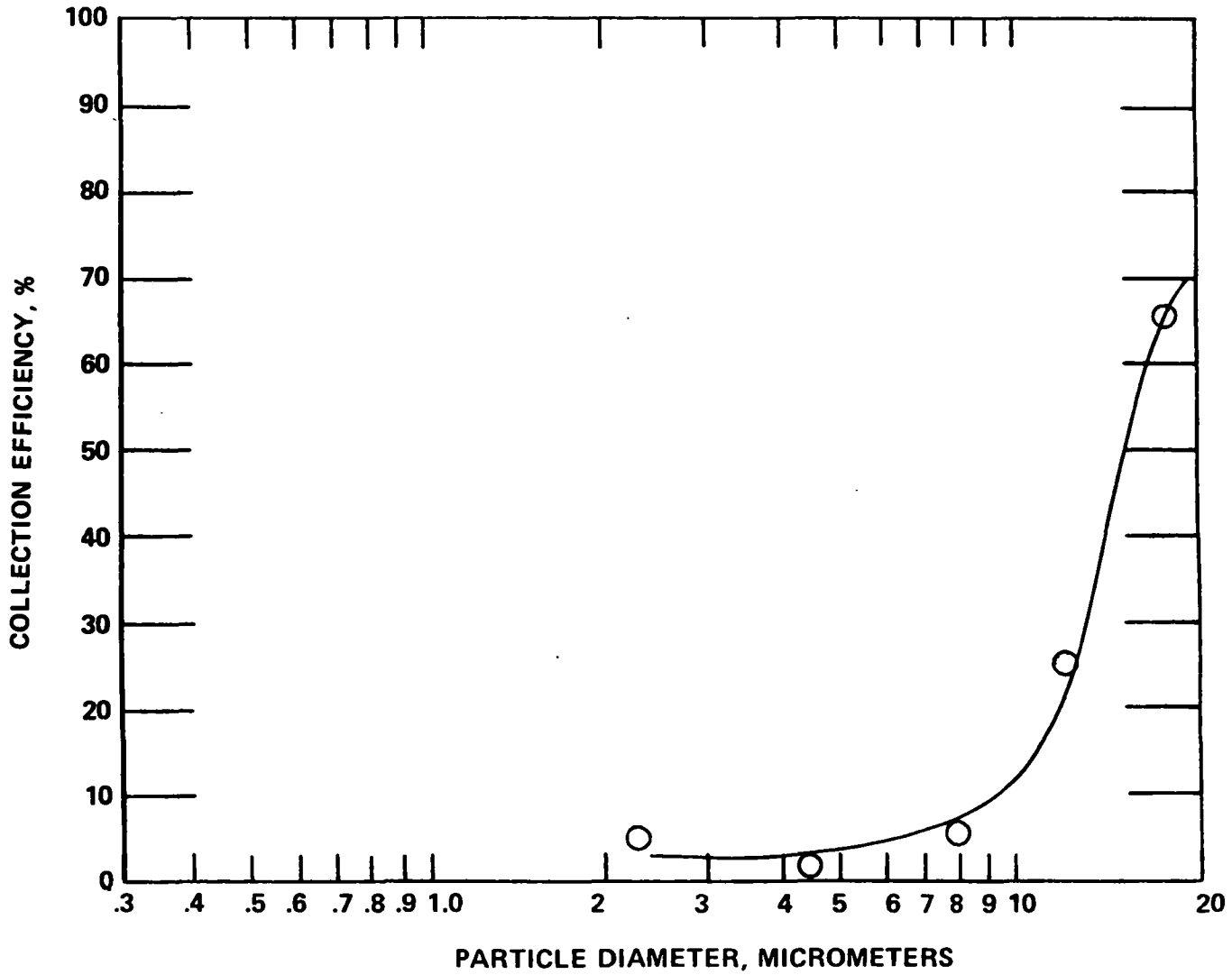


*Figure 77. Collection efficiency vs. Particle diameter. Large SASS Cyclone. (4 SCFM, 400°F, 1.00 gm/cm$^3$)*

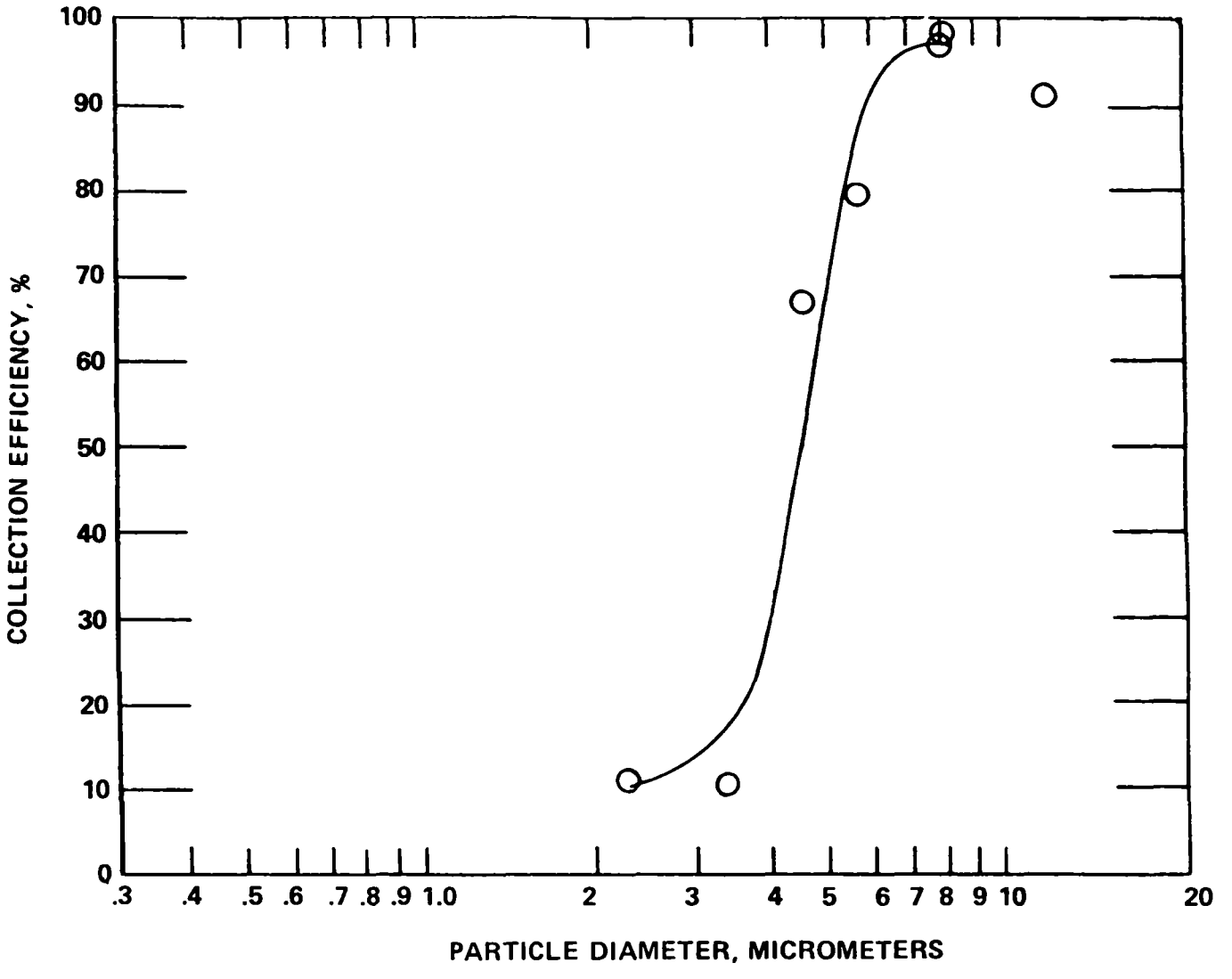


*Figure 78. Collection efficiency vs. Particle diameter. Unmodified Middle SASS Cyclone. (4 SCFM, 400°F, 1.00 gm/cm$^3$)*

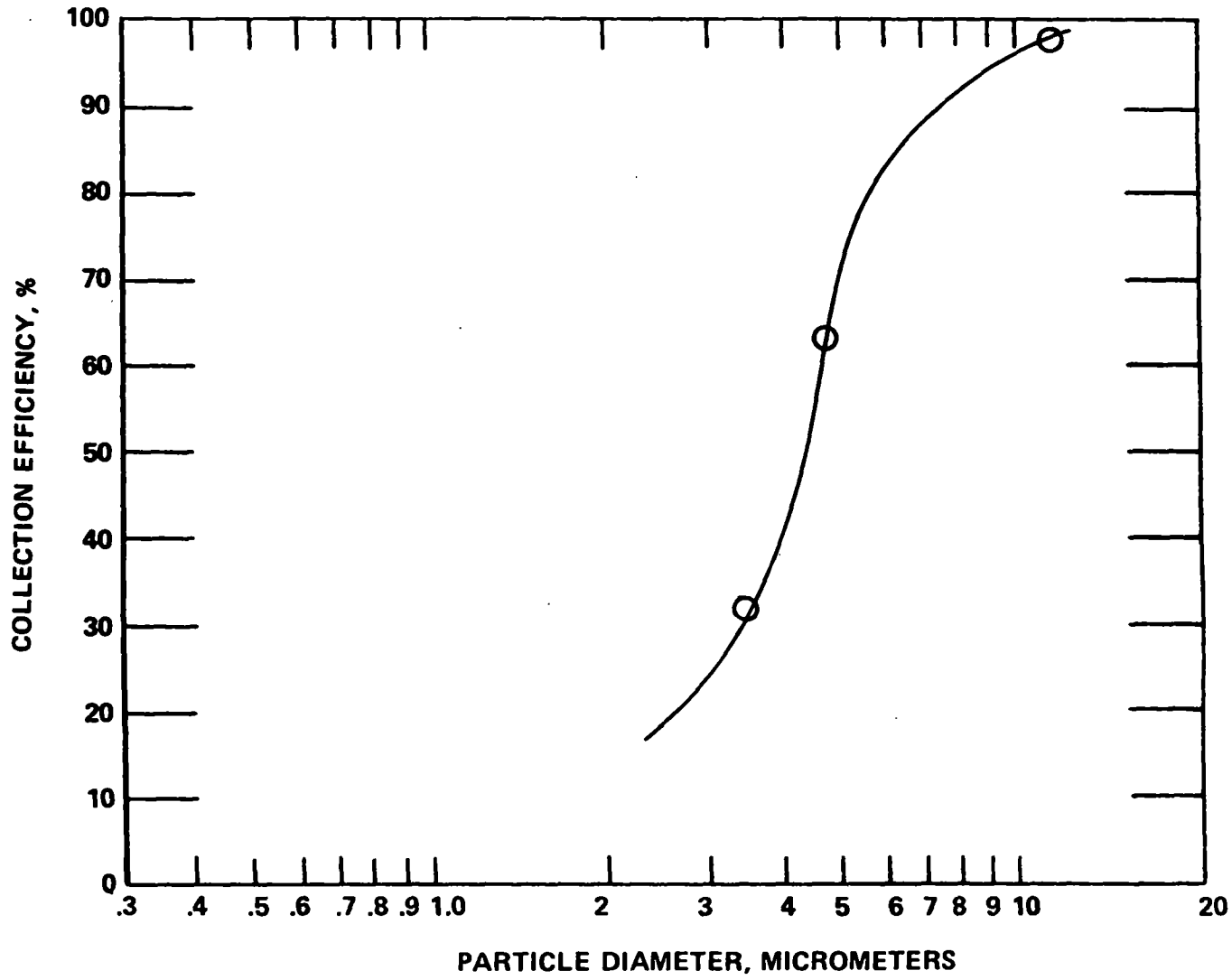


*Figure 79. Collection efficiency vs. Particle diameter. Modified Middle SASS Cyclone. (4 SCFM, 400°F, 1.00 gm/cm$^3$)*

It was concluded that calibration with aerosols which could withstand these high temperatures should take place. Technical Directive Number 20502 was issued to complete this assignment.

## High Temperature Recalibration and Modification of SASS Cyclones (Technical Directive Number 20502)

Description of Task:

The purpose of this task was to determine a material which would be suitable as a high temperature aerosol (400°F). After finding such a material, it was to be used to generate aerosols to be sampled by the SASS cyclones in a calibration procedure. Approximately ten to twelve monodisperse aerosols were to be generated using a Vibrating Orifice Aerosol Generator. After an initial calibration, any necessary modifications would be performed and the cyclones would be retested. The major emphasis was placed on calibration of the Middle Cyclone (3 μm $D_{50}$). If necessary, testing at 75°F, 200°F, and 350°F and extrapolating data to 400°F would be acceptable.

Summary of Progress:

The goal of this task was to calibrate and modify, if necessary, the Source Assessment Sampling System Middle Cyclone so that it would have a 3 ± 0.5 μm $D_{50}$ cut point for 1.00 gm/cm$^3$ particles when operated at 400°F and 4 SCFM. Figure 83 shows the collection efficiency of the SASS Middle cyclone when sampling a turquoise dye (particle density = 2.4 gm/cm$^3$) at the above conditions with and without the vortex buster in the cup. The $D_{50}$ of the cyclone with the vortex buster in place is 3.4 μm for a particle of density 2.04 gm/cm$^3$, or 4.0 μm for a particle of density 1.00 gm/cm$^3$. The $D_{50}$ of the cyclone with the vortex buster removed is 2.5 μm for a particle of density 2.04 gm/cm$^3$, or 3.5 μm for a particle of density 1.00 gm/cm$^3$. Thus, with the vortex buster removed, the cyclone satisfactorily attained the original goal.

### Experimental Procedure

A decision was made to calibrate the Source Assessment Sampling System Middle Cyclone at 400°F and 4 SCFM. Because previous tests have indicated ammonium fluorescein was unstable at 400°F, a search was initiated for an aerosol with some or all of the following characteristics:

Non-toxic
Stable at temperatures up to 500°F or above
Soluble in water or other non-toxic, non-residue forming solvent
Amorphous - dries to form solid, homogeneous spheres when dispersed in solution from a VOAG.
Known or easily measured density
Has a definite, distinct absorption spectrum peak for absorption spectroscopy measurement between 400 NM and 900 NM.

The initial search for such an aerosol was unsuccessful, so, ammonium fluorescein was used to determine the $D_{50}$ cut points of the Middle Cyclone at 70°F, 200°F, and 350°F and 5.45 ACFM and the data obtained from these tests was used to extrapolate to determine the $D_{50}$ cut point at 400°F. This method proved to be difficult when it was found that ammonium fluorescein particles smaller than 4 μm in diameter were unstable at 350°F. Attempts to alleviate this problem were largely unsuccessful. Meanwhile the search for an acceptable aerosol was continued using commercially available dyes.

Of several samples from three chemical companies, du Pont's "Pontamine" Fast Turquoise 8 GLP dye was the first found to satisfactorily meet the requirements listed above. A spectral analysis performed on a dilute water solution of this dye indicated a distinct absorption peak at 622 nanometers. Measurements with a Helium-Air pycnometer gave a density of 2.04 gm/cm . The sample seemed pure and its stability at 400°F was excellent. The expansion problems encountered with small diameter ammonium fluorescein particles were absent. Aerosol particles made from a solution of the dye in distilled water were very nearly, if not perfectly, round.

The calibration of the SASS train cyclones was performed using the Institute's Vibrating Orifice Aerosol Generator (VOAG). The VOAG generated monodisperse ammonium fluorescein particles and turquoise dye particles with diameters from 2 micrometers to 7 micrometers.

Throughout the testing, close watch was kept on the temperature and flow rate of the aerosol stream. Any discrepancies were quickly corrected, and readings of all temperatures were recorded periodically. Therefore repeatability of the tests and test results was insured.

After each test, the cyclone and filter substrate were washed to dissolve and rinse off all the aerosol particles. The wash solutions used were 0.1 N $NH_4OH$ for ammonium fluorescein and a sodium bicarbonate solution for turquoise dye.

A Bausch and Lomb Spectronic 88 Spectrophotometer, calibrated with solutions of known concentration of the aerosol solute (turquoise dye or ammonium fluorescein) was used to measure the absorbance of the wash from the cyclone and the filter. From knowledge of the amount of wash solution, the dilution factor, if any, and the absolute concentration, the mass of particles in the cyclone and on the filter was calculated. With these two masses known, the collection efficiency of the cyclone for that particular particle size was calculated.

## Results

Table XI lists the $D_{50}$ cut points of the cyclone at various conditions. Figure 80 shows the collection efficiency curves of the cyclone when calibrated with ammonium fluorescein particles at 70°F, 200°F, and 350°F. The $D_{50}$'s obtained from these curves and plotted in Figure 81 indicate that the $D_{50}$-gas viscosity relationship is linear. This does not correspond to Lapple's[25] prediction that $D_{50}$ would vary directly with the change in the square root of the gas viscosity.

Figure 82 shows the collection efficiency of the cyclone for ammonium fluorescein particles and turquoise dye particles when collected under similar conditions. The relative differences between the two aerodynamic $D_{50}$ cut points derived from the two curves differ from the prediction of Lapple's equation by only 7%.

Figure 83 shows the collection efficiency curves of the cyclone when calibrated with turquoise dye particles with and without the vortex buster in place. It was determined using Lapple's equation that the $D_{50}$ cut point of the cyclone with the vortex buster removed is 3.5 μm for 1.00 $gm/cm^3$ particles, which is within the acceptable range.

## Calibration of SASS Cyclones for HERL (Technical Directive Number 21002)

Description of Task:

Exxon Research and Engineering Corporation has used a Source Assessment Sampling System at a coal-fuel power boiler in Kentucky to size the particulate effluent. This work was performed for the Health Effects Research Laboratory. Southern Research Institute

Table XI

Five-Stage Cyclone Calibration Data

| Material | Vortex Buster | Temperature | Flow Rate ft.$^3$/min Actual/Standard | $D_{50}$ Physical Micrometers | $D_{50}$ Aerodynamic Micrometers |
|---|---|---|---|---|---|
| Ammonium Fluorescein | IN | Ambient | 5.37/—— | 2.8 | 3.3 |
| Ammonium Fluorescein | IN | 200°F | 5.41/—— | 3.5 | 4.0 |
| Ammonium Fluorescein | IN | 350°F | 5.46/—— | 4.2 | 4.9 |
| Turquoise Dye | IN | Ambient | 5.42/—— | 2.2 | 3.1 |
| Turquoise Dye | OUT | 400°F | 6.50/4.00 | 2.5 | 3.5 |
| Turquoise Dye | IN | 400°F | 6.50/4.00 | 3.4 | 4.9 |

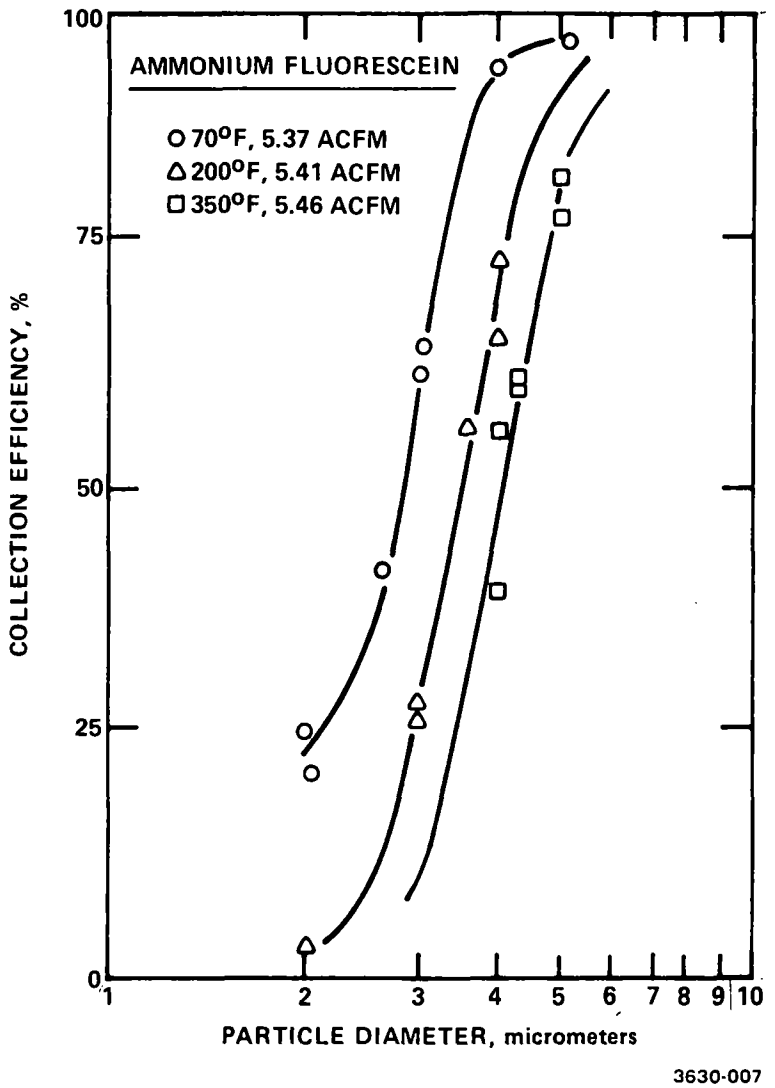


*Figure 80. Collection Efficiency - Temperature Relationship*
*SASS Middle Cyclone*
*Ammonium Fluorescein*
*Particle Density = 1.35 gm/cm$^3$*

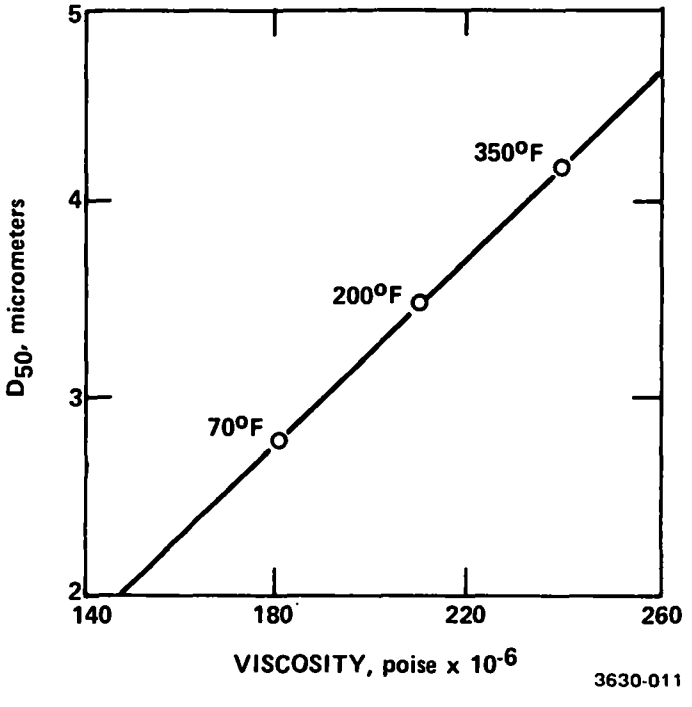


*Figure 81.* *$D_{50}$ - Viscosity Relationship*
*SASS Middle Cyclone*
*Ammonium Fluorescein*
*Particle Density = 1.35 gm/cm$^3$*

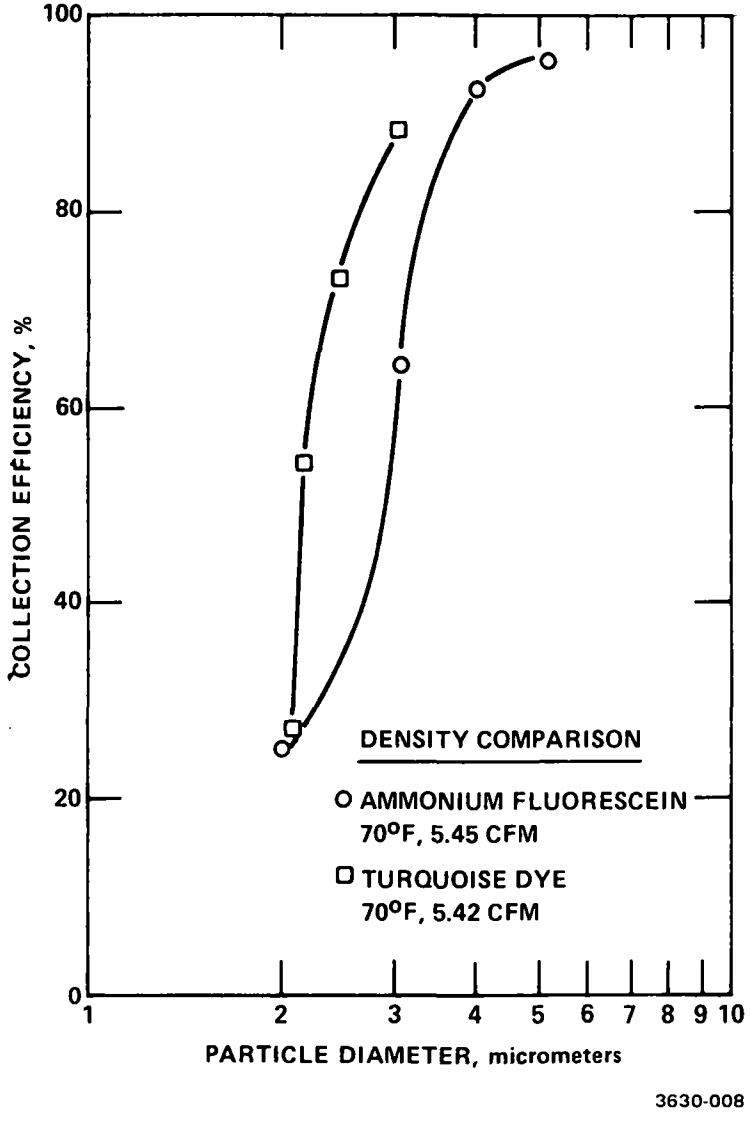


*Figure 82. Collection Efficiency - Particle Density Relationship*
*SASS Middle Cyclone*
*Ammonium Fluorescein Particle Density = 1.35 gm/cm$^3$*
*Turquoise Dye Particle Density = 2.04 gm/cm$^3$*

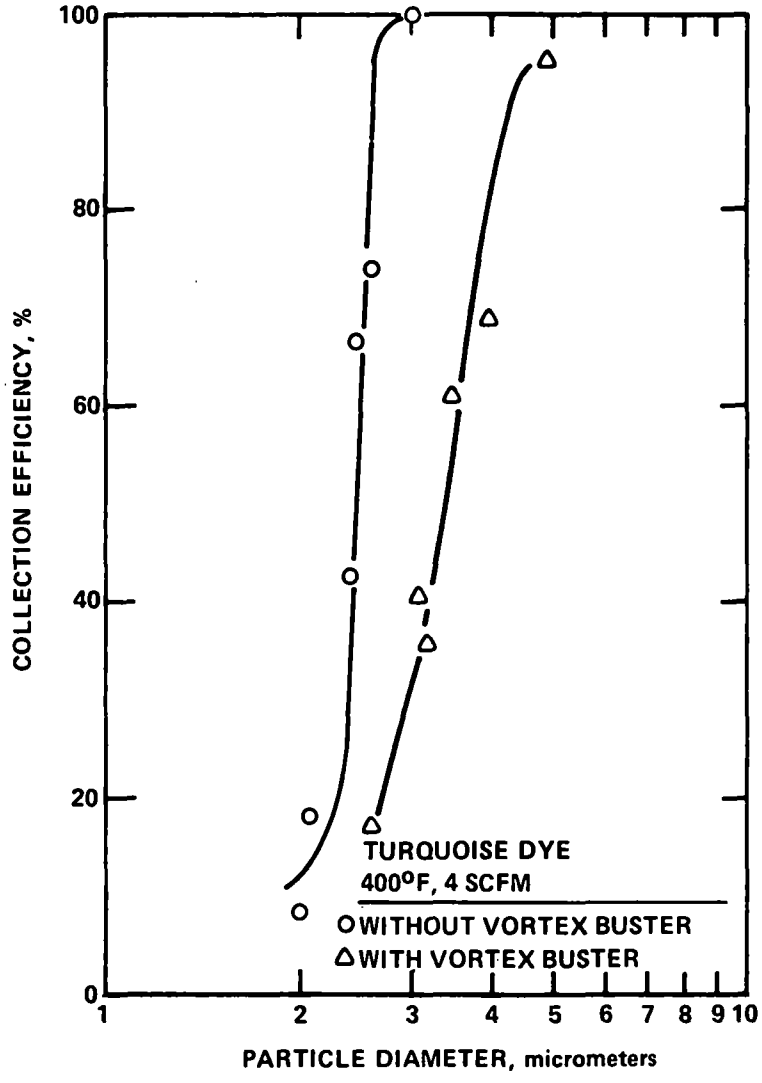


*Figure 83.* *Collection Efficiency at 400°F, 4 SCFM*
*SASS Middle Cyclone*
*Turquoise Dye*
*Particle Density = 2.04 gm/cm$^3$*

calibrated the Middle SASS cyclone used by Exxon. The cyclone was to be calibrated at the actual run conditions as operated by Exxon test personnel.

Summary of Progress:

This report contains the results of the Exxon-SASS Cyclone system calibration. Exxon used the following sampling conditions.

- 600°F inlet gas temperature to the oven
- Oven temperature 375°F
- No filter element in the filter housing in the heated oven
- Pump flow wide open with filter on pump inlet and muffler on pump outlet
- Vacuum measured ahead of pump filter - 14 inches vacuum under sampling conditions
- Stack moisture 8%
- Gas temperature in middle cyclone unknown
- Vortex busters in the collection cups of the Large and Middle cyclones.

These conditions and those of the calibration system were not completely compatible. The inlet gas temperature was 450°F, the constraint being the temperature limit of the calibration aerosol. The oven temperature was 375°F. The humidity of the air was not measured.

No probe was supplied with the cyclones; however, a telephone conversation revealed that Exxon used an Aerotherm probe which was twelve feet long. The sampling line of this probe is one-half inch O.D. Stainless Steel tube. The heat loss through this probe in our lab was unacceptable, and the particle loss would probably be quite high. Also a filter had to be used in the filter holder so that all the mass would be caught for collection efficiency determinations. Therefore, the flow rate at the inlet of the large cyclone had to be determined. The field set-up was duplicated as closely as possible and the flow was measured to be 13 ACFM at an oven inlet temperature of 399°F. Then the probe was removed and a glass fiber filter was added to the filter holder. The flow was adjusted so that the inlet flow to the cyclones was 13 ACFM. There was a definite but unknown amount of water in the air.

A note should be made as to the conditions of the cyclones when they arrived. There were a few dents in the cup and the inlet of the Middle cyclone was bent such that the air stream did not enter the cyclone strictly tangentially. The only modification made to the cyclones by S.R.I. was replacement of some teflon gaskets which were badly deformed.

The calibration system used was a vibrating orifice aerosol generator with du Pont "Pontamine" Fast Turquoise 8 GLP dye as an aerosol. The collected particles were washed off the cyclones and filter with a sodium bicarbonate solution and their mass determined with a spectrophotometer.

For a temperature of 450°F, a flow of 13 cfm, and a particle density of 2.04 $gm/cm^3$, the $D_{50}$ cut points of the large and middle cyclones were 7.6 μm and 2.13 μm respectively (see Figure 84). For a particle density of 1.00 $gm/cm^3$ and the same conditions, the $D_{50}$ cut point of the large and middle cyclones would be 11 μm and 3.0 μm respectively.

Estimation of $D_{50}$ of Middle Cyclone at 600°F

The $D_{50}$ cut point for the Middle cyclone is 3.0 μm for a temperature of 450°F, a flow rate of 13 CFM, and a particle density of 1.00 $gm/cm^3$, with the vortex buster in place. Experimental work with the middle cyclone has indicated the following may be obtained by extrapolating the $D_{50}$ vs. viscosity curve.

| Flow Rate | $D_{50}$ | Temperature | Particle Density |
|---|---|---|---|
| 5.4 CFM | 5.0 μm | 375°F | 1.00 $gm/cm^3$ |
| 5.4 CFM | 5.8 μm | 450°F | 1.00 $gm/cm^3$ |
| 5.4 CFM | 6.2 μm | 600°F | 1.00 $gm/cm^3$ |

Assuming that the $D_{50}$ cut point will increase at the same rate with increasing temperature at flow rates of 5.4 and 13.0 CFM, the following relationships are obtained.

$$\frac{D_{50}\ (600°F;\ 13\ CFM)}{D_{50}\ (450°F;\ 13\ CFM)} = \frac{D_{50}\ (600°F;\ 5.4\ CFM)}{D_{50}\ (450°F;\ 5.4\ CFM)}$$

and

$$\frac{D_{50}\ (375°F;\ 13\ CFM)}{D_{50}\ (450°F;\ 13\ CFM)} = \frac{D_{50}\ (375°F;\ 5.4\ CFM)}{D_{50}\ (450°F;\ 5.4\ CFM)}\ .$$

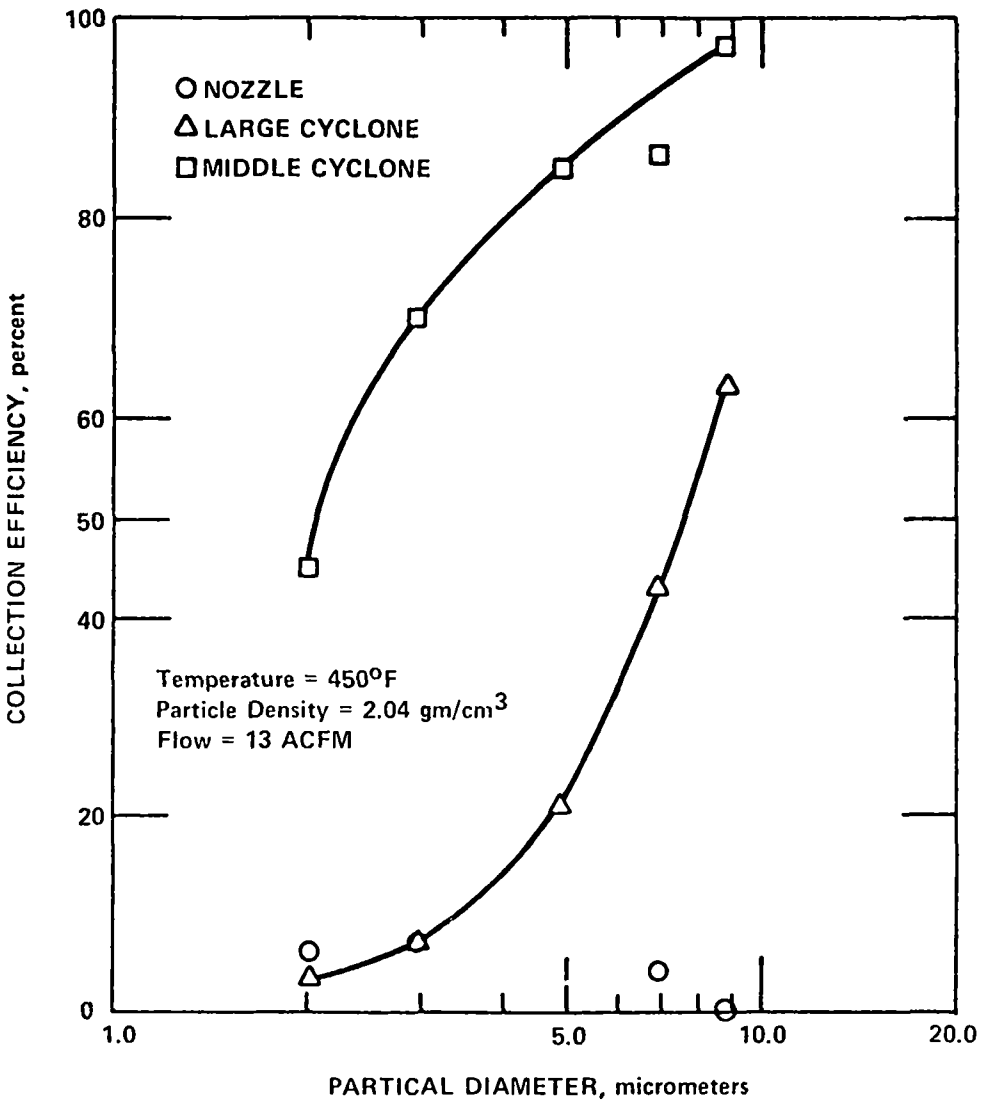


*Figure 84. Exxon SASS Cyclones*

Thus,

$$D_{50}\ (600°F,\ 13\ CFM) = 3.0 \times \frac{6.2}{5.8} = 3.2\ \mu m.$$

and

$$D_{50}\ (375°F;\ 13\ CFM) = 3.0 \times \frac{5.0}{5.8} = 2.6\ \mu m.$$

Therefore, the $D_{50}$ cut points of the middle cyclone for a flow rate of 13 ACFM are estimated to be 2.6 μm for a temperature of 375°F, and 3.2 μm for a temperature of 600°F.

Estimation of $D_{50}$ of Small Cyclone at 600°F

The small cyclone has previously been calibrated at two flows:

| Flow | $D_{50}$ | Temperature | Particle Density |
|---|---|---|---|
| 1.8 ACFM | 1.88 | 77°F | 1.00 $gm/cm^3$ |
| 3.1 ACFM | 1.11 | 77°F | 1.00 $gm/cm^3$ |

Using this relationship $D_{50} = KQ^N$ from Chan and Lippmann[26]

$$\frac{D_{50}\ (1.88)}{D_{50}\ (1.11)} = \frac{K\ (1.8)^N}{K\ (3.1)^N}$$

$$N = -0.97$$

So

$$D_{50} = KQ^{-0.97}$$

or

$$1.88 = K\ (1.8)^{-0.97}$$

$$K = 3.32$$

Assuming the $D_{50}$ vs. Q relationship above holds at Q = 13 ACFM,

$$D_{50} = 3.32Q^{-0.97}$$

$$= 3.32(13)^{-0.97}$$

$$= 0.277\ \mu m.$$

Recent experimental work with the Five Stage Series Cyclone II (which has identical dimensions as the SASS small cyclone except for the width and depth of the cup) has indicated the following

| Flow | $D_{50}$ | Temperature | Particle Density |
|---|---|---|---|
| 1 CFM | 2.30 μm | 77°F | 1.00 $gm/cm^3$ |
| 1 CFM | 5.21 μm | 600°F | 1.00 $gm/cm^3$ |
| 1 CFM | 4.11 μm | 375°F | 1.00 $gm/cm^3$ |

Assuming that the $D_{50}$ cut point will increase at the same rate with increasing temperature at flows of 1 and 13 CFM, we obtain the following relationships:

$$\frac{D_{50}\ (600°F;\ 13\ CFM)}{D_{50}\ (77°F;\ 13\ CFM)} = \frac{D_{50}\ (600°F,\ 1\ CFM)}{D_{50}\ (77°F,\ 1\ CFM)}$$

and

$$\frac{D_{50}\ (375°F;\ 13\ CFM)}{D_{50}\ (77°F;\ 13\ CFM)} = \frac{D_{50}\ (375°F;\ 1\ CFM)}{D_{50}\ (77°F;\ 1\ CFM)}$$

Thus, the $D_{50}$ cut points of the small cyclone for a flow of 13 ACFM are estimated to be 0.49 μm for a temperature of 375°F and 0.63 μm for a temperature of 600°F.

Task Category - E.S.P. Back-Up

Develop an E.S.P. Back-Up for Sampling Systems
(Technical Directive Number 10703)

Description of Task:

Southern Research Institute was to develop and test an electrostatic precipitator to be used in lieu of a conventional filter for back up to high volume sampling systems. This was to be a high efficiency, low pressure drop system.

Summary of Progress:

The design of an electrostatic precipitator to be used in lieu of a conventional back-up filter for high volume particulate mass sampling systems has been completed and a prototype has been constructed. A modified disc-cylinder geometry was selected as the design after an evaluation of wire-cylinder and disc-cylinder configurations indicated that the disc-cylinder would provide a higher collection efficiency per unit length of cylinder. In addition, the disc electrode would have greater endurance than a wire electrode.

The fact that a laminar flow is obtained in the disc-cylinder geometry allowed a straightforward calculation of the length of cylinder required for 100% collection of 0.5 μm diameter particles. In order to maximize the efficiency of collection with a minimal overall precipitator length, it was necessary to increase the area of the collection surfaces. This was done by using a concentric cylinder configuration with alternate high voltage and grounded cylinders (see Figure 85). Such a modification would not be possible in conventional wire-cylinder precipitators.

At this time the prototype precipitator is being evaluated using submicron aerosols.

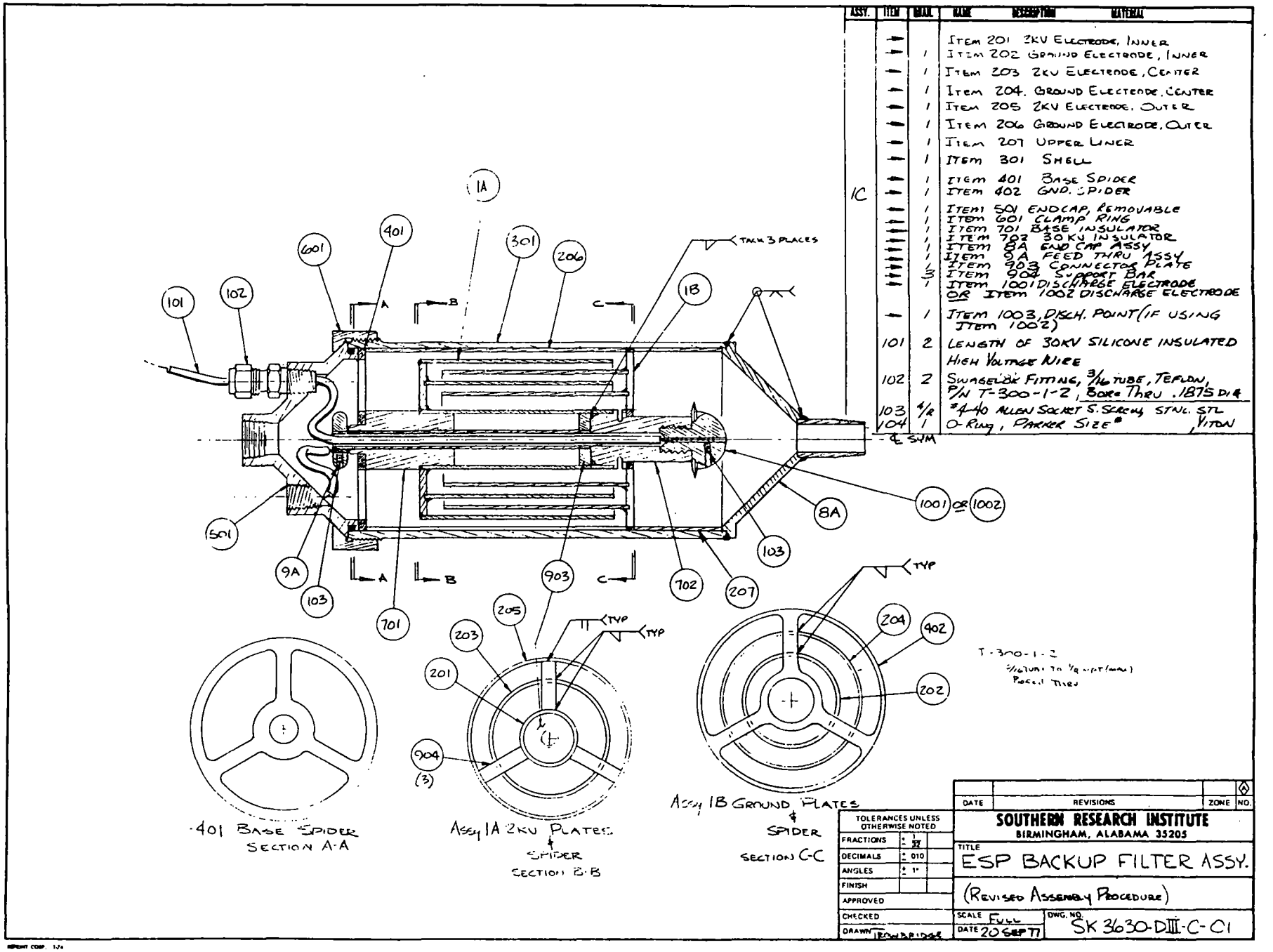


Figure 85. A sketch of the electrostatic precipitator design.

Task Category - Guidelines, Manuals

## Guideline for Particulate Sampling and Annotated Bibliography (Technical Directive Number 10804)

Description of Task:

The purpose of this task is to generate a guideline document which will be a concise survey of the methods and instruments used in sampling gaseous process streams for particulate matter. Briefly describe the considerations involved in setting up and carrying out a particulate sampling program. Also describe the devices currently in use for making sizing and non-sizing measurements. Include a condensed "where to learn more" bibliography keyed to each topic discussed to provide more extensive coverage.

This document will essentially be an executive summary of the document generated under Technical Directive Number 10904. It will be a complete, concise discussion aimed at Program Managers.

Summary of Progress:

Work has been initiated on this task with a completion date set for early 1978.

## Technical Manual on Particulate Sampling (Technical Directive Number 10904)

Description of Task:

A comprehensive document is to be written which will be a technical survey of the methods and instruments used in sampling effluent gaseous process streams for particulate matter. This document should include information on how to set up and carry out a particulate sampling program on industrial and energy process streams and on control devices such as electrostatic precipitators, scrubbers, and fabric filters. Information on the devices currently in use for making sizing and non-sizing particulate measurements, along with descriptions of their theory of operation and use should be included. To provide further reading, a comprehensive bibliography keyed to each topic is to be included.

Summary of Progress:

Requests for information were sent to 110 manufacturers of sizing and non-sizing particulate measurement instruments. To date responses have been received from approximately eighty companies. This material is currently being reviewed and the text of the manual is being drafted. The final draft is expected by the end of December, 1977.

Procedures Manual for Electrostatic Precipitator Evaluation
(Technical Directive Number 20604)

Description of Task:

A procedures manual for the evaluation of electrostatic precipitators was written. This document gave specific methods for collecting data on precipitator design and operating parameters, flue gas composition, particulate mass sampling, and methods for particle sizing and fractional efficiency determination.

Summary of Progress:

A procedures manual for evaluating electrostatic precipitators has been published under the title "Procedures Manual for Electrostatic Precipitator Evaluation", EPA-600/7-77-059, June 1977. The purpose of this procedures manual was to describe methods to be used in characterizing the performance of electrostatic precipitators for pollution control. A detailed description of the mechanical and electrical characteristics of precipitators is given. Procedures are described for measuring the particle size distribution, the mass concentration of particulate matter, and the concentrations of major gaseous components of the flue gas-aerosol mixture. Procedures are also given for measuring the electrical resistivity of the dust. A concise discussion and outline is presented which describes the development of a test plan for the evaluation of a precipitator. Several appendices contain detailed information on testing methods as well as a listing of the Federal Stationary Source Performance Standards and Federal Source Testing Reference Methods.

## Task Category - Review of Documents

### Review Documents and Reports Furnished by EPA (Technical Directive Number 20705)

Description of Task:

The following three documents furnished by the Project Officer were critically reviewed. A list of corrections and suggestions was submitted to the Project Officer.

1. Cascade Impactor Operation and Calibration Guideline
2. Sampling Protocol to Minimize Errors Due to Source Fluctuations
3. Level 1 Assessment - EPA/IERL

Summary of Progress:

All items in this task have been completed.

## Task Category - Consulting Services

### Participate in U.S.A. - Soviet Information Exchange Program (Technical Directive Number 20806)

Description of Task:

For this task, personnel at Southern Research Institute were to participate as consultants on particle sizing in the Soviet-U.S.A. Information Exchange Program. Equipment was to be prepared and shipped to the U.S.S.R. for field tests. One of the Institute staff members was to go to the Soviet Union to supervise the test program, and reports as required were to be written.

Summary of Progress:

Field testing equipment was shipped to the Soviet Union during July, 1976. Field testing on a scrubber at a metallurgical plant in Russia took place during August, 1976. No results have been published to date.

### EPA/IERL/PMB Exhibit Booth at the 1977 APCA Meeting (Technical Directive Number 20906)

Description of Task:

The purpose of this task was to coordinate the arrangements for the EPA/IERL/PMB exhibit at the 1977 Air Pollution Control Association in Toronto, Canada, June, 1977. This exhibit displayed the research and development efforts of the IERL Task Level of Effort contractors. Certain pieces of hardware and software from those contractors were displayed.

Summary of Progress:

On June 21, 22, 23, 1977 the Process Measurements Branch of IERL/RTP supported an exhibit booth at the 70th Annual Air Pollution Control Association Meeting in Toronto, Ontario, Canada. This 10' x 20' booth used a color scheme of dark blue booth back wall and side walls, light blue carpet, and green draped tables. Three tables along the back wall were used for document display. Two tables, one on each side, were used to display hardware. On the white 1' x 20' header board in black letters was printed the following title:

United States Environmental Protection Agency
Industrial Environmental Research Laboratory - RTP
Process Measurements Branch

On either side of the title was an EPA LOGO in color.

On the back wall were hung six 3' diameter discs which briefly described the research and development efforts of the six Task Level of Effort contractors for the PMB. These six contractors are Acurex/Aerotherm, Arthur D. Little, Inc., Research Triangle Institute, Southern Research Institute, The Research Corporation, and TRW, Inc.

The hardware on display included a complete Source Assessment Sampling System, a KLD Droplet Analyser, and the Five Stage Series Cyclone and Advanced Sampling System.

Approximately 200 copies of twenty-one documents were distributed on a first come first serve basis to the 4200 registrants at the meeting.

The following is a list of the documents which were available for distribution:

HP-25 Programmable Pocket Calculator Applied to Air Pollution Measurement Studies: Stationary Sources. EPA-600/7-77-058, June 1977

Procedures Manual for Electrostatic Precipitator Evaluation EPA-600/7-77-059, June 1977

Industrial Environmental Research Laboratory - RTP Annual Report 1976

Flow and Gas Sampling Manual. EPA-600/2-76-203, July 1976

IERL-RTP Procedures Manual: Level 1 Environmental Assessment. EPA-600/2-76-160a, June 1976

Selection and Evaluation of Sorbent Resins for the Collection of Organic Compounds. EPA-600/7-77-044, April 1977

Technical Manual for Measurement of Fugitive Emissions: Upwind/Downwind Sampling Method for Industrial Emissions. EPA-600/2-76-089a, April 1976

Technical Manual for the Measurement of Fugitive Emissions: Roof Monitor Sampling Method for Industrial Fugitive Emissions. EPA-600/2-76-089b, May 1976

Technical Manual for Measurement of Fugitive Emissions: Quasi-Stack Sampling Method for Industrial Fugitive Emissions. EPA-600/2-76-089c, May 1976

Technical Manual for Process Sampling Strategies for Organic Materials. EPA-600/2-76-122, April 1976

Technical Manual for Analysis of Organic Materials in Process Streams. EPA-600/2-76-072, March 1976

Particulate Sizing Techniques for Control Device Evaluation: Cascade Impactor Calibrations. EPA-600/2-76-280, October 1976

Inertial Cascade Impactor Substrate Media for Flue Gas Sampling. EPA-600/7-77-060, June 1977

Operating and Service Manual: Source Assessment Sampling System. Acurex/Aerotherm Report UM-77-81, March 1977

Environmental Assessment Sampling and Analysis: Phased Approach and Techniques for Level 1. EPA-600/2-77-115, June 1977

Procedures for Cascade Impactor Calibration and Operating in Process Streams. EPA-600/2-77-004, January 1977

Technical Manual for Inorganic Sampling and Analysis. EPA/2-77-024, January 1977

Development and Trial Field Application of a Quality Assurance Program for Demonstration Projects. EPA-600/2-76-083, March 1976

HP-65 Programmable Pocket Calculator Applied to Air Pollution Measurement Studies: Stationary Sources. EPA-600/8-76-002, October 1976.

Process Measurements Branch: Report Listing, June 1, 1977

Pollution Control Technology and Environmental Assessment: Prochure Describing the Research and Development Efforts of the Six PMB Contractors.

At the conclusion of the exhibit all of the reports had been given out, except for a few HP-65 booklets. Reaction to the exhibit by the attendees at the meeting was quite favorable.

Task Category - Advanced Concepts - Mass and Size

Evaluation of a PILLS IV Particle Sizing Instrument
(Technical Directive Number 11007)

Description of Task:

The contractors shall perform a detailed evaluation of the theory and operation of the PILLS IV particle sizing instrument. This evaluation shall consider the following:

1. Verify the validity of the theoretical principle.

2. Evaluate or interpret existing experimental data.

3. Investigate problems of obtaining representative samples. Generate a test aerosol and look at response vs. dilution, sample velocity, particle sizing, and purge effects.

4. Investigate the possibility of multiple scattering as an interference.

5. Attempt to measure the beam dimensions and view volume.

6. Investigate the differences in response to scattering of broad or narrow plane waves.

7. Investigate the cumulative effects of 4 and 6.

Summary of Progress:

Laboratory evaluation of the PILLS-IV is complete and a final report is being written.

## References


1. Cooper, Douglas W. and John W. Davis, "Cascade impactors for aerosols: Improved data analysis," Amer. Ind. Hyg. Assoc., p. 79, 1972.

2. Cooper, Douglas W. and Lloyd A. Spielman, "Data inversion using nonlinear programming with physical constraints: Aerosol size distribution measurement by impactors," Atmospheric Environment, Vol. 10, pp. 723-729, 1976.

3. Picknett, R. G., "A new method of determining aerosol size distributions from ministage sampler data," Aerosol Science, 1972.

4. McCain, J. D., K. M. Cushing, and W. B. Smith, "Methods for determining particulate mass and size properties: Laboratory and field measurements," J. APCA 24(12): 1172-1176, December 1974.

5. Rao, A. K., "An experimental study of inertial impactors," Ph.D. Dissertation, University of Minnesota, Minneapolis, Minnesota, 1975.

6. Dzubay, T. G., L. E. Hines and R. K. Stevens, "Particulate bounce errors in cascade impactors," Atmospheric Environment, Vol. 10, pp. 229-234, 1976.

7. Natusch, D. F. S. and J. R. Wallace, "Determination of airborne particle size distributions: Calculation of cross-sensitivity and discreteness effects in cascade impaction," Atmospheric Environment, Vol. 10, pp. 314-324, 1976.

8. Cushing, K. M., J. D. McCain, and W. B. Smith, "Experimental determination of sizing parameters and wall losses of five commercially available cascade impactors," in Proceedings of the 69th Annual Meeting of the Air Pollution Control Association, Portland, Oregon, 1976, paper No. 76-374.

9. Lundgren, D. A. (1967). "An aerosol sampler for determination of particle concentration as a function of size and time," J. APCA 17, pp. 225-229.

10. Smith, W. B., and J. R. McDonald. Development of a Theory for the Charging of Particles by Unipolar Ions. J. Aerosol Sci., 7(2): 151-166.

11. Cushing, K. M., G. E. Lacey, J. D. McCain, and W. B. Smith. Particle Sizing Techniques for Control Device Evaluation: Cascade Impactor Calibration. EPA-600/2-76-280, U.S. Environmental Protection Agency, Research Triangle Park, North Carolina, 1976. 79 pages.

12. Reischl, G. P., W. John, and W. Devor. Uniform Electrical Charging of Monodisperse Aerosols. J. Aerosol Sci., submitted for publication May 17, 1976.

13. Particle Technology Laboratory. In the Performance of the Electrical Aerosol Analyzer. No. 237, Mech. Eng. Dept. University of Minnesota, Minneapolis, MN 55455. 15 pages.

14. Zung, J. T., and C. C. Snead. Evaporation Kinetics of Liquid Droplets. U.S. Dept. of Army, Edgewood Arsenal-DAAA-15-67-C-0151, Field Evaluation Division, Edgewood Arsenal, Maryland 21010, 1968. 116 pages.

15. Smith, W. B., K. M. Cushing, and G. E. Lacey. Andersen Filter Substrate Weight Loss Study. Special Report under EPA Contract No. 68-02-0273, Research Triangle Park, NC 27711.

16. Rao, A. K. Sampling and Analysis of Atmospheric Aerosols. Particle Tech. Lab. Publ. No. 269, Department of Mechanics Engineering; University of Minnesota, Minneapolis, Minnesota 55455, June 1975.

17. Ranz, W. D., and J. B. Wong. Impaction of Dust and Smoke Particles, Ind. and Eng. Chem., 50, No. 4 (April, 1958).

18. Marple, V. A. A Fundamental Study of Inertial Impactors. Ph.D. Thesis, Mechanical Engineering Department, University of Minnesota, Minneapolis, Minnesota 55455, 1970.

19. Berglund, R. N., and B. Y. H. Liu. Generation of Monodisperse Aerosol Standards. Environmental Science and Technology, Vol. 6, No. 2, 1973.

20. Lindblad, N. R., and J. M. Schneider. Production of Uniform-Sized Liquid Droplets. J. Sci. Instru., Vol. 42, 1965.

21. Strom, L. The Generation of Monodisperse Aerosols by Means of a Disintegrated Jet of Liquid. Rev. Sci. Instr., Vol. 40, No. 6, 1969.

22. Calvert, S. Cascade Impactor Calibration Guidelines. EPA-600/2-76-118, U.S. Environmental Protection Agency, Research Triangle Park, NC, 1976.

23. Jaericke, R., and I. H. Blifford. The Influence of Aerosol Characteristics on the Calibration of Impactors. Journal of Aerosol Science, 5(5): 457-464, 1974.

24. Willeke, K. Performance of the Slotted Impactor. Am. Ind. Hygiene Assoc. J., 683-691, September 1975.

25. Lapple, C. E. Process Use Many Collector Types, Chem. Eng., 58, pp. 144-151 (1951).

26. Chan, Tai and Morton Lippmann. Particle Collection Efficiencies of Air Sampling Cyclones: An Empirical Theory, Envir. Sci. and Tech., Vol. 11, No. 4, pp. 377-382 (377), 1977.

## TECHNICAL REPORT DATA
*(Please read Instructions on the reverse before completing)*

| | | |
|---|---|---|
| 1. REPORT NO. EPA-600/7-78-009 | 2. | 3. RECIPIENT'S ACCESSION NO. |
| 4. TITLE AND SUBTITLE Particulate Sampling Support: 1977 Annual Report | | 5. REPORT DATE January 1978 |
| | | 6. PERFORMING ORGANIZATION CODE |
| 7. AUTHOR(S) K.M. Cushing, William Farthing, L.G. Felix, J.D. McCain, and W.B. Smith | | 8. PERFORMING ORGANIZATION REPORT NO. SORI-EAS-77-661 |
| 9. PERFORMING ORGANIZATION NAME AND ADDRESS Southern Research Institute 2000 Ninth Avenue, South Birmingham, Alabama 35205 | | 10. PROGRAM ELEMENT NO. EHE624 |
| | | 11. CONTRACT/GRANT NO. 68-02-2131 |
| 12. SPONSORING AGENCY NAME AND ADDRESS EPA, Office of Research and Development Industrial Environmental Research Laboratory Research Triangle Park, NC 27711 | | 13. TYPE OF REPORT AND PERIOD COVERED Annual; 11/76-10/77 |
| | | 14. SPONSORING AGENCY CODE EPA/600/13 |

15. SUPPLEMENTARY NOTES IERL-RTP project officer is D. Bruce Harris, Mail Drop 62, 919/541-2557.

16. ABSTRACT The report describes the activities supporting the particulate sampling efforts of EPA/IERL-RTP during FY 1977. Twenty technical directives were issued in seven categories: cascade impactors (7), cyclones (5), sampling electrostatic precipitators (1), guidelines and manuals (3), document review (1), consulting services (2), and advanced concepts (1). Significant results of the 12 completed tasks are presented.

17. KEY WORDS AND DOCUMENT ANALYSIS

| a. DESCRIPTORS | b. IDENTIFIERS/OPEN ENDED TERMS | c. COSATI Field/Group |
|---|---|---|
| Air Pollution | Air Pollution Control | 13B |
| Dust | Stationary Sources | 11G |
| Sampling | Particulate | 14B |
| Impactors | Cascade Impactors | |
| Cyclone Separators | | 07A |
| Electrostatic Precipitators | | |

| | | |
|---|---|---|
| 18. DISTRIBUTION STATEMENT Unlimited | 19. SECURITY CLASS *(This Report)* Unclassified | 21. NO. OF PAGES 174 |
| | 20. SECURITY CLASS *(This page)* Unclassified | 22. PRICE |

EPA Form 2220-1 (9-73)